UNIVERSITY OF SOUTHAMPTON

FACULTY OF ENGINEERING AND THE ENVIRONMENT

School of Engineering Sciences

Periprosthetic Fluid Flow, Particle Distribution Modelling and the Implications for Osteolysis in Cementless Total Hip Replacements

by

Hamidreza Alidousti

Thesis for the degree of Doctor of Philosophy

June 2012

UNIVERSITY OF SOUTHAMPTON
FACULTY OF ENGINEERING AND THE ENVIRONMENT
SCHOOL OF ENGINEERING SCIENCES

Doctor of Philosophy

PERIPROSTHETIC FLUID FLOW, PARTICLE DISTRIBUTION MODELLING AND THE IMPLICATION FOR OSTEOLYSIS IN CEMENTLESS TOTAL HIP REPLACEMENT

by Hamidreza Alidousti

ABSTRACT

When there is debonding at a bone-implant interface, the difference in stiffness between the implant and the bone can result in micromotion, allowing existing gaps to open further or new gaps to be created during physiological loading. It has been suggested that periprosthetic fluid flow and high pressure may play an important role in osteolysis development in the proximity of these gaps. It has also been suggested that the periprosthetic flow may facilitate migration of wear polyethylene particles to the periprosthetic bone, which can also cause osteolysis. To explain these phenomena, the concepts of 'effective joint space' and 'pumping stem' have been cited in many studies. However, there is no clear understanding of the factors causing, or contributing to these mechanisms.

It is likely that capsular pressure, gap dimensions and micromotion of the gap during cyclic loading of an implant as well as factors such as biological osteolysis threshold, the rate of wear generation and the degree of particle clogging in the periprosthetic tissue, play defining roles in periprosthetic flow, particle migration and osteolysis generation. In order to obtain a better understanding of the above mechanisms and factors, steady state and transient 2D computational fluid dynamic models of the lateral side of a stem-femur system including the joint capsule, a gap in communication with the capsule and the surrounding bone were studied. First, fluid velocities and pressures in the periprosthetic tissue were investigated. Then, particles were introduced to the continuum fluid at the gap entrance as a discrete phase and their migration to the bone was analysed. Lastly, the models were further refined by introducing algorithms and factors developed to simulate particle clogging and permeability variation caused by the fibrous tissue generation in osteolytic lesion and particle clogging in the periprosthetic tissue throughout postoperative periods.

Simulations without particles showed that high capsular pressure may be the main driving force for high fluid pressure and flow in the bone surrounding the gap, while micromotion of only very long and narrow gaps can cause significant pressure and flow in the bone. At low capsular pressure, micromotion induced large flows in the gap region; however, the flow in the bone tissue was almost unaffected. The results also revealed the existence of high velocity spikes in the bone region at the bottom of the gap. These velocity spikes can exert excessive fluid shear stress on the bone cells and disturb the local biological balance of the surrounding interstitial fluid which can result in osteolysis development. High capsular pressure was observed to be the main cause of these velocity spikes whereas, at low capsular pressure, gap

micromotion of only very long and narrow gaps generated significant velocity spikes in the bone at the bottom of the gaps.

Simulations with particles also showed that capsular pressure is the main driving force for particle migration to periprosthetic tissue. In contrast to common belief, the models showed that implant micromotion pumped out, rather than sucked in the particles to the interfacial gaps, except in long gaps in which, even at low pressure, particles that made it to the bottom region migrate to the bone tissue as a result of micromotion. Particles entered the periprosthetic tissue along the entire length of the gap with higher concentration at proximal and distal regions. However, particles mainly accumulated with an increasing concentration at the bottom of the gap because of the presence of the fluid spikes in this region. Therefore, focal osteolysis is more likely to develop in the gap bottom region, whereas linear osteolysis, which requires less particle concentration, is more likely to develop along the entire gap length. It was also shown that risk of osteolysis development was higher for shorter gaps since they experience higher particle concentration. In addition, the models showed that for osteolysis to develop, a constant supply of particles, as well as an access route to the endosteal bone must be available.

When a particle clogging model was included, it was shown that the depth of particle penetration into the surrounding tissue reduced, leading to increased particle concentrations. Particle clogging and accumulation initially occurred at distal and proximal gap regions in the stem proximity. However, as time elapsed, this accumulation extended along the entire interface. The rate of particle accumulation was a function of particle wear generation. Accumulation of particles at the interface caused changes in the tissue permeability and periprosthetic flows. Partial clogging and particle accumulation in the gap bottom region caused increases in fluid spikes in that region. Once this region was completely clogged, the magnitude of fluid spikes reduced. In addition, there was a complementary relationship between particle concentration and the reduction of permeability; regions with lower permeability tended to experience higher particle accumulation.

Models developed to simulate fibrous tissue generation in osteolytic lesions, presented this tissue by regions with increased permeability. It was showed that, as time elapses, particle concentrations become higher than the osteolytic threshold which leads to increased periprosthetic tissue permeability. In general, for lower osteolysis thresholds, regions with increased permeability progresses faster at the bottom of the gap. This results in increased permeability having a linear pattern along the interface and a focal pattern at the bottom of an interfacial gap. Higher osteolysis thresholds, generally, result in only a linear pattern of increased permeability along the gap except for the cases with high wear generation rates in which a focal pattern at the bottom of the gap can still be seen.

Contents

List of Figures

List of Tables

DECLARATION OF AUTHORSHIP

I, **Hamidreza Alidousti**, declare that the thesis entitled:

"Periprosthetic Fluid Flow, Particle Distribution Modelling and the Implication for Osteolysis in Cementless Total Hip Replacements"

and the work presented in the thesis are both my own, and have been generated by me as the result of my own original research. I confirm that:

- this work was done wholly or mainly while in candidature for a research degree at this University;
- where any part of this thesis has previously been submitted for a degree or any other qualification at this University or any other institution, this has been clearly stated;
- where I have consulted the published work of others, this is always clearly attributed;
- where I have quoted from the work of others, the source is always given. With the exception of such quotations, this thesis is entirely my own work;
- I have acknowledged all main sources of help;
- where the thesis is based on work done by myself jointly with others, I have made clear exactly what was done by others and what I have contributed myself;
- parts of this work have been published (listed in Appendix A).

Signed: .....
Date: .....

Acknowledgements

Blessed is the gambler
who has lost everything
except the desire
to gamble
once more
(Rumi)

I thank Him for letting me to taste the gamble of life, and to sail through the stormy waters and to not lose the faith to see the calm. I could not write these words when I started this journey. It has been a long way and, indeed, without the support of the great people around me I could not have made it. My parents whose words and actions of encouragement have always been a light to illuminate the dark path. My supervisor, Dr Neil Bressloff, who is the main reason of me being here today. When all the doors were closed, he graciously opened one to me. The trust he put in me was life changing and I will benefit from it in the years to come. It was only by his great and in-depth supervision that this work came to existence. I also thank my other supervisor, Professor Mark Taylor, whose great help and advice have given direction to this project. I thank Professor Martin Browne, who truly supported me during the difficult times. He is one of those people who will always stay in my mind. I thank Professor Phillippa Reed who patiently listened to me and did all she could to help me. I thank Dr Gary Coleman whose critics of the work were constructive. I would also like to acknowledge DePuy Ltd for partially funding this project.

And of course, my great appreciation goes to friends who never stopped caring for me. I thank Amirmohmmad who always took my attention to important matters in life. He is a true brother to me. Pramod who's been beside me all the way along. I greatly appreciate his friendly supports and the great amount of time he spent on proofreading my work. I thank Hatice for being such a good friend to me. I never forget our after work conversations in the office. Aida, who has been a source of great support and encouragement all the way along. Asieh, for always being there and being such a good listener to me. I never forget her support when I was getting towards the end. Sanjay, without his intellectual help many of the things achieved in this work would not be possible. I would like to thank all my friends since having them around me during this time was a gift and encouragement, but it is not possible to name each in the short space here.

Glossary

Anastomosis	Recoonection or branching off of two or more blood vessels.
Arthritis	Inflammation of a joint, usually accompanied by pain, swelling, and stiffness resulting from infection, trauma, degenerative changes, metabolic disturbances, or other causes.
Aseptic loosening	Loosening of prosthesis in absence of osteolysis and infection, with the proviso that bacteria may be present.
Avascular necrosis	Is a disease where there is cellular death (necrosis) of bone components due to interruption of the blood supply.
Bone cement	Usually an acrylic compound used in fracture repair and positioning of bone pins.
Cancellous bone	Otherwise known as trabecular bone, which is made of a network interconnected bony rods and plates known as trabeculae.
Cartilage	Firm, rubbery tissue that cushions bones at joints.
Cortex	Outer portion of an organ.
Cortical	Having to do with the cortex.
Cortical bone	Otherwise known as compact bone, is the dense and solid bone that constitutes the outer layer of all bones as well as the shaft of the long bones.
Finite Element Analysis or Method	Numerical technique for finding approximate solutions of partial differential equations (PDE) as well as of integral equations.

Micromotion	Amplitude of the cyclic relative implant-bone displacement for a load cycle.
Periprosthetic	Associated with regions around a prosthesis.
Osseointegration	Growth action of bone tissue, as it assimilates surgically implanted devices or prostheses to be used as either replacement parts or anchors.
Osteoarthritis	Degenerative joint disease abnormalities involving degradation of joints, including articular cartilage and subchondral bone.
Radiolucency	Regions with greater transparency in radiographs which may indicate the presence of soft tissue .
Rheumatoid arthritis	Is an autoimmune disease that causes chronic inflammation of the joints.
Stress shielding	Osteopenia (reduction in bone density) occurring in bone as the result of removal of normal stress from the bone by an implant.
Synovial fluid	A clear, viscid lubricating fluid secreted by membranes in joint cavities, sheaths of tendons, and bursae.

Nomenclature/List of Symbols

Nomenclature

CAD	Computer Aided Design
CFD	Computational Fluid Dynamics
CT	Computerised or Computed Tomography
DPM	Discrete Phase Model
HA	Hip Arthroplasty
FEM	Finite Element Method
NHS	National Heath Services
OA	Osteoarthritis
ODE	Ordinary differential equation
RA	Rheumatoid arthritis
SEM	Scanning Electron Microscopy
SIMPLE	Semi-Implicit Method for Pressure-Linked Equations
THR	Total Hip Replacement

List of Symbols:

p	Capsular pressure (kPa)
l	Gap length (mm)
w	Gap width (μm)
d	Gap displacement (μm)
k	Intrinsic permeability (m^2)
ϕ	Porosity
Np_f	Final number of particles after a particular postoperative year
Np_d	Desired number of particles in a postoperative year
Np_{inj}	Total number of particles injected to the model
c_f	Clogging factor (%)
s_f	Scaling factor (years)
p_d	Degree of the scaling factor
o_s	Osteolysis threshold (number of particles per gram of tissue)

Chapter 1

Introduction

1.1 Background

Joint problems can affect the quality of life significantly as they limit the level of activity in patients. Millions of people suffer from joint complications and therefore treatments that can offer functional restoration and pain elimination can significantly improve the quality of life of those suffering. One of the widely used procedures is Hip Arthroplasty (HA). In this procedure the damaged bearing surfaces of a hip joint are replaced with artificial ones. Over 65,000 primary hip replacement procedures undertaken in England and Wales 2009 compared to around 30,000 between 2003 and 2004. The number of procedures is increasing every year according to the National Joint Registry [1]. The demand for hip joint replacement is increasing as the age population of patients undergoing this procedure is decreasing. This means that the long term performance of the implants in younger patients is now expected to be sufficiently high to avoid revision surgery during their life time. Revision surgery is indeed a difficult and costly procedure with inferior results. More than 7,000 revision procedures were performed alone in 2009 in England and Wales, which places a considerable financial burden on the National Health Service (NHS) [1]. Cementless implants were introduced to reduce the revision rates due to bone loss around the implants, otherwise known as osteolysis. Nevertheless, clinical observations show that osteolysis still occurs, sometimes at higher rates, in this type of implant, indicating that there is a need to better understand the mechanisms of failure in cementless implants.

Despite much research to investigate the causes of osteolysis, the factors involved in its initiation and progression has not been completely understood. The most commonly accepted explanations for the causes of osteolysis are adverse tissue reaction to wear particles and bone resorption due to high periprosthetic fluid pressures and/or velocities. However, mechanisms involved in high fluid pressure/velocity generation at the bone-implant interface and transport of particles to the periprosthetic tissue are

not clearly understood and there is a lack of studies investigating these mechanisms in the literature. Information gained by such studies can be used to improve future implant designs.

The research questions to be addressed in the current work are: "what are the main contributors to facilitate fluid flow and wear particle migration leading to osteolysis in the periprosthetic tissue?" and "what is the extent of the influence of each contributing factor?" The hypothesis is that joint capsular pressure, interface gap micromotion, fibrous tissue generation, patient sensitivity to wear particles and the rate of wear generation may contribute to the periprosthetic fluid flow and wear particle migration, which influence osteolysis generation.

1.2 Aims and objectives

While significant research is being undertaken to investigate the causes of osteolysis, computational models can also provide a powerful means to investigate osteolysis generation. The aim of the current study is to develop computational models which can be used to simulate periprosthetic fluid flow, particle migration and the potential for osteolysis generation. Such models may provide insights into the role played by different parameters involved in osteolysis. The advantage of these models is that they provide a tool to simulate and measure in vivo conditions which are experimentally difficult to perform. To achieve this aim, the objectives of the current study are:

- To devise computational models to simulate periprosthetic fluid flows.
- To study the effect of capsular pressure, gap dimensions and micromotion of the gap during cyclic loading of an implant on periprosthetic flows.
- To simulate particle migration to the periprosthetic tissue by the joint fluid.
- To simulate the effect of particle clogging at the bone-implant interface on periprosthetic flow and particle accumulation in long postoperative periods.
- To simulate osteolysis generation and to study the effect of different parameters on its progression.

In should be noted that the new models presented in this thesis are intended to provide general insights into the problem and do not represent patient-specific models and data.

1.3 Outline of the thesis

In Chapter 2 an overview of hip anatomy and physiology and an introduction to the total hip replacement (THR) is given. This introduction reviews failure of THRs and explains the role played by wear particles and high fluid pressure/velocity in causing periprosthetic osteolysis. In addition, likely causes of high fluid pressure/velocity generation and particle migration are discussed. A detailed review on periprosthetic bone tissue, its properties and fluid flow within its constituents is also presented. Chapter 3 describes methodologies to develop the models and presents the verification studies. This chapter also includes additional methods and models developed to define a permeability value for the periprosthetic tissue based on available experimental data in the literature. Chapter 4 includes the study of periprosthetic fluid flows. In this chapter the fluid flows and pressures as a result of high capsular pressure and implant micromotion are studied in detail during a gait cycle. Chapter 5 includes the models simulating particle migration to the periprosthetic bone as a result of high capsular pressure and implant micromotion in a short term represented by 50 gait cycles. In Chapter 6, the particle migration models are refined by including mechanisms to induce particle clogging at the interface tissue to model long postoperative periods. In addition, permeability increase because of high particle concentrations to represent fibrous tissue filling the osteolytic lesions, is simulated. This may demonstrate osteolysis generation and progression in the periprosthetic tissue. Chapter 7 presents the conclusions and contributions of the this study and suggestions for future work.

Chapter 2

Literature review

2.1 Hip joint anatomy and physiology

The hip is an articulating multi-axial ball and socket joint that anchors the bony pelvis to the proximal end of the femur or thigh bone. The hip joint transfers the upper body weight to the lower limb and facilities body motion. It consists of acetabulum, femur and the surrounding soft tissues that create the joint capsule.

2.1.1 Acetabulum

The articulation surface on the pelvic side of the hip joint is a large cup-shaped region where the three components of the pubis, the ilium and the ischium, fuse to create the acetabulum (c.f. Figure 2.1). The acetabulum provides stability for the joint by almost accommodating the entire articular surface of the femoral head. The surface of the acetabulum consists of articular and nonarticular parts. The nonarticular part, called the acetabular fossa, is a rough depression situated in the central and inferior region of the cup. The articular surface of the acetabulum, called the lunate surface, is a crescent-shaped hyaline cartilage that surrounds the acetabular fossa. It is broadest in the superior region of the cup where most of the body weight is transmitted from the bony pelvis to the femur.

2.1.2 Femur

The femur is the longest bone in the body which consists of a long cylindrical shaft (diaphysis) that is joined to the distal cartilage-covered bone (epiphysis) through a cone-shaped shaft just beneath the growth plate (metaphysis) (c.f. Figure 2.2). The cartilage-covered bearing surface of the femoral head is approximately spherical and articulates against the acetabulum . Its proximal region consists of the femoral neck and the greater and lesser trochanters. The femoral neck is a superomedial projection that

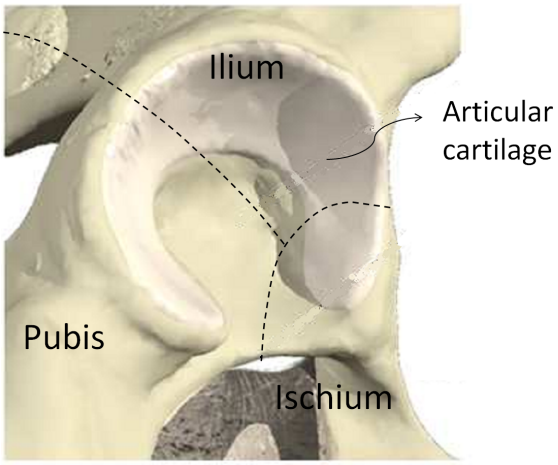

Figure 2.1: The acetabulum.[1]

connects the femoral shaft to the head. The femoral neck and its orientation provide more space between the shaft and head and therefore a greater range of movement in the hip joint. The greater and lesser trochanters are projections between the femoral shaft and neck that provide regions for muscle and ligament attachments around the hip joint [2]. The diaphysis consists of cortical bone whereas the epiphyses and metaphyses contain mostly cancellous bone that is covered with a thin layer of cortical bone. The subchondral bone near the joint is covered by hyaline cartilage. The outer layer of the femur is covered by periosteum, a tight and stiff connective fibrous tissue.

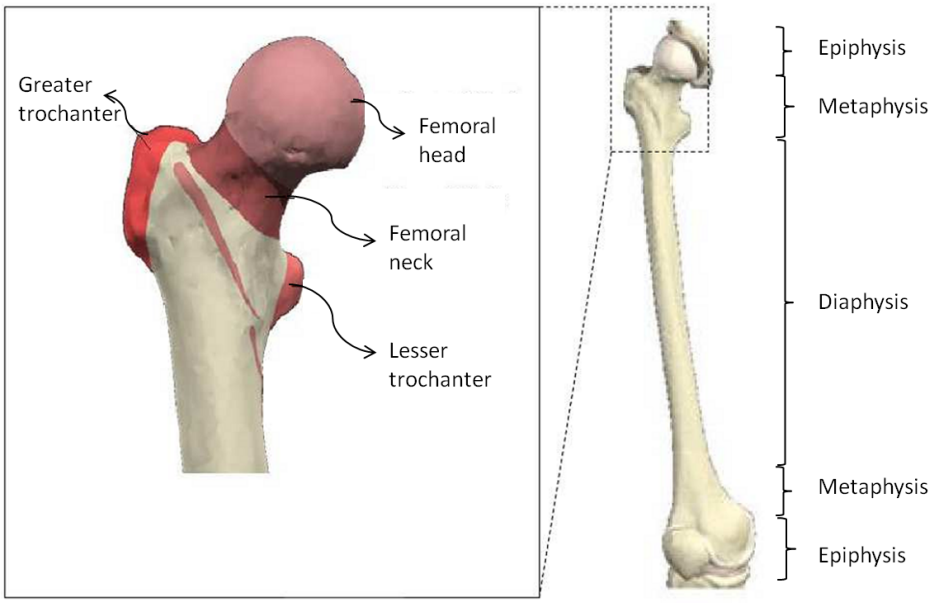

Figure 2.2: The Femur.[2]

[1]Constructed from Anatomy TV (www.anatomy.tv)
[2]Constructed from Anatomy TV (www.anatomy.tv)

2.1.3 Synovial membrane and the joint capsule

The synovial membrane originates from the margins of the articular surfaces of the femoral head and acetabulum. From its attachment to the rim of the articular surface of the femoral head, the synovial membrane extends distally to cover the femoral neck (c.f. Figure 2.3). It folds back at the end of the neck and extends to the margin of the acetabulum. It also forms a tubular covering around the ligament of the head of the femur. The synovial membrane blocks any access of the joint fluid to bone tissue [3]. External to the synovial membrane there is a strong and generally thick fibrous membrane that encloses the hip joint and seals the joint capsule from its surroundings. The joint is further stabilised by three other ligaments that reinforce the external surface of the fibrous membrane. The fibres of these ligaments are oriented in a spiral pattern around the hip capsule providing more resistance and tightness when the joint is extended. Joint capsule is the combination of these soft tissues surrounding the hip joint. The joint space accommodates synovial fluid and facilitates its access to the bearing surfaces of the joint for lubrication and nutrition, with iliopectineal bursa acting as the fluid reservoir (c.f. Figure 2.3). Under high loads, when the pressure within the joint is excessive, the synovial fluid egress from the joint space to this reservoir [4]. When the pressure within the joint falls below that of reservoir the flow is reversed. This mechanism maintains the pressure approximately constant in normal and healthy joints during physical activity. In healthy joints the pressure is considered low and it only rises less than a few kPa above the atmospheric pressure [5]. However, high pressure, which is experienced in some problematic joints, is considered as a pressure above the normal pressure and can reach up to 69 kPa in some cases [6].

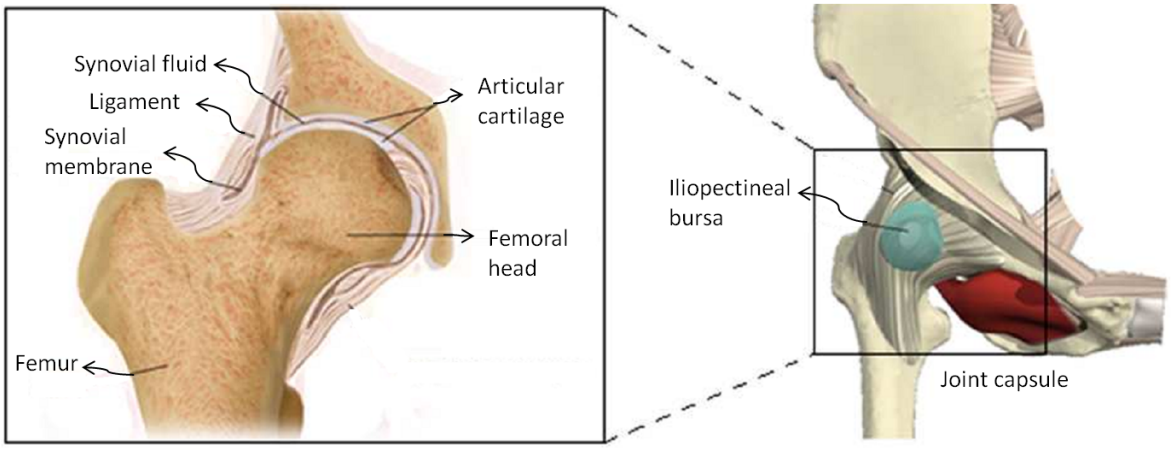

Figure 2.3: Joint capsule (right) and its cross-sectional view (left) showing the capsular space, the surrounding bone and soft tissue in healthy joints. Figure shows regions filled with synovial fluid and iliopectineal bursa which acts as a fluid reservoir for this fluid.[3]

[3]Left image from: www.ohsu.edu. Last checked May 2012 . Right image constructed from Anatomy TV (www.anatomy.tv)

2.1.4 Kinematics of the hip

The organisation of the ligaments around the hip joint as well as the shape of the joint provides a structure that requires minimum muscle force to facilitate standing and joint movement. Movement of the hip joint include flexion, extension, abduction, adduction, internal and external rotations and circumduction which is a combination of all the other motions (c.f Figure 2.4). This range of motion can be impaired for patients with joint problems.

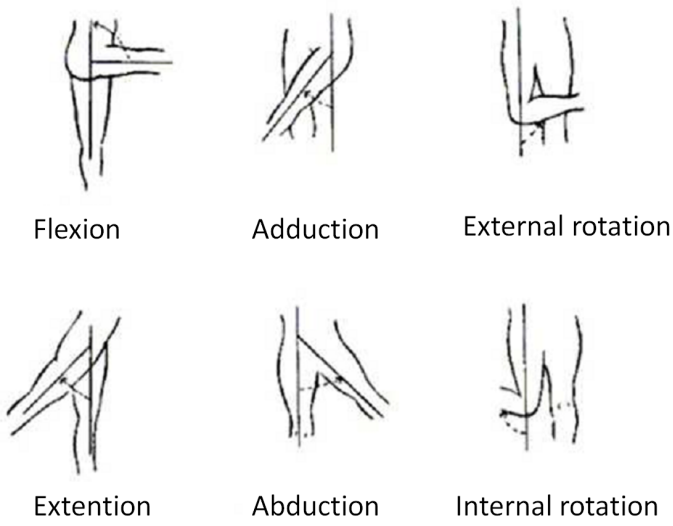

Figure 2.4: Hip range of motion.[4]

2.2 Total hip replacements

2.2.1 Introduction

Replacing a malfunctioning part of the body to restore function has always been sought by physicians since modern science has emerged. Some of the attempts culminated with astonishing outcomes. An exemplary of this success is the THR or in a more general term, hip arthroplasty, in which the diseased and dysfunctional hip joint is replaced with an artificial one. The joint complications which require THR for treatment and their prevalence are shown in Table 2.1 . The main diagnosis is osteoarthritis which involves degeneration of the joint including articular cartilage and the subchondral bone adjacent to it.

[4]Image from: http://dwd.wisconsin.gov/dwd/publications/wc/wkc-7761-p.htm. Last checked May 2012.

Table 2.1: Number of primary THRs per diagnosis. [7]

Diagnosis	Share (%)
Primary osteoarthritis	77.7
Fracture	11.1
Inflammatory arthritis	4.0
Idiopathic femoral head necrosis	2.8
Childhood disease	1.8
Secundary osteoarthritis	0.7
Tumor	0.5

2.2.2 A brief history

This surgical procedure has gone through a long journey to reach its current state. Initially, reduction of pain rather than functional restoration in the diseased joint was the primary objective of the treatment [8]. Early attempts included bone fusion (arthrodesis), bone resection (osteotomy), nerve division and joint debridement which could successfully offer pain reduction but at the expense of immobility [9]. In order to restore mechanical functionality of the joint, physicians and surgeons employed many biocompatible materials ranging from muscles, fat, chromatised pig bladder to glasses, gold, ivory, magnesium and zinc which all resulted in failure in terms of restoring functionality. Jean and Robert Judet were the first to design a practical prosthesis to resurface the femoral head using an acrylic ball which provided a smooth surface on the articulating components (c.f. Figure 2.5 a). However, their design was not able to cope with the intensive mechanical loads within the hip joint tended to fail soon after replacement.

Frederick R. Thompson and Austin T. Moore developed mechanically stronger prostheses consisting of a metallic Vitallium stem with a distinctive flared collar which was inserted into the femoral cavity connected to a metal ball (c.f. Figure 2.5 b). Their device did not replace the diseased acetabulum and, therefore, articulation of the metal surface against the cartilage resulted in arthritic destruction of the socket. The first THR in which the acetabular articulating surface was also replaced was introduced by Philip Wiles using metal-on-metal ball and socket stainless steel components which were fixed to the bone of the femur and acetabulum with screws and bolts. However, the results were not completely satisfactory because of the lack of stability of these prostheses. To overcome the problem of instability and fixation, Edward J. Haboush and Kenneth McKee suggested dental acrylic cement for prosthetic fixation [9]. However, the success of hip replacement did not reach its climax until Sir John Charnley, an innovative surgeon from England, fixed both femoral and acetabulum components into the surrounding bone tissue using a polymeric material, polymethylmethacrylate (PMMA, or bone cement). He first used Teflon for the articulating surfaces, which

(a) (b) (c)

Figure 2.5: a) Judet acrylic femoral prosthesis b) Thompson prosthesis c) Charnley polyethylene cup THR.[5]

was not successful. Subsequently, he used polyethylene against the metallic bearing surface which is still the gold standard for current joint arthroplasties. By 1961, Charnley was performing hip replacement procedures successfully with predictable long-term outcomes. Despite the great success of THR, there are still complications associated with this course of treatment meaning that not all the THRs serve the patient with satisfactory long-term results. A problematic THR often requires revision surgery to replace the failed implants with new ones. This is a difficult procedure with inferior outcomes compared to the primary hip replacement. Currently, hip arthroplasty is carried out around the world and the number of procedures carried out increases every year. In the next section different types of HA currently used are introduced.

2.2.3 Types of hip joint replacements

Since the introduction of this procedure, different implant designs have been pioneered to overcome the complications. As a result, different designs of hip implants are categorised according to the type of fixation and the biomaterial used. Implants, fixed into the bone using PMMA or bone cement, are called cemented implants (c.f. Figure 2.6a). It is currently one of the most common procedures carried out by surgeons with good long term results, particularly for older patients. The Swedish Hip Registry [10] shows that the majority of patients undergoing cemented procedures were above the age of 70.

[5]Images taken from: a) www.maitriseorthop.com, b) www.bone-implants.com and c) www.totaljoints.info. Last checked June 2011

Bone cement is liquid at the time of surgery when it is inserted into the bone. After implant insertion the polymeric chain reaction starts resulting in a solid but brittle substance providing a bed for the implant. The quality of bone cement depends on many factors including method of manufacture and mixing of the powder and liquid components [11], the cure time [12], method of insertion [13], surgeon skills, the thickness of the cement between bone and implant [14]. There are, however, complications with regard to cemented prostheses. The polymerisation of PMMA is accompanied by heat generation and volumetric shrinkage that may, respectively, cause tissue damage at the time of implant insertion or establish residual stresses within the cement. The accumulated damage, crack and debris generation under cyclic loading have been recognised as the main shortcomings of cemented implants [15].

To eradicate these shortcomings, surgeons turned towards designs that relied on bone growth on the surface of the implant rather using bone cement to facilitate fixation. These types of implant are called cementless or uncemented implants (c.f. Figure 2.6b). They consist of entirely or partially roughened or porous surfaces on which the bone tissue can ingrow. Partially porous implants have porous surfaces either on the proximal region circumferentially or they have patches of porous surface at the proximal region leaving the rest of the implant with a smooth surface. In some designs a bioactive coating called hydroxyapatite is applied on the porous surface to promote bone generating cells to migrate to the implant-bone interface and deposit bone to achieve faster and stronger bone-implant interlock. These type of implants are becoming more popular particularly for younger patients with better bone quality to ingrow and higher physical activity which may cause accumulative damage and failure in otherwise cemented implants.

In England and Wales, compared with previous years, there has been a reduction in the percentage use of cemented THR procedures and corresponding increase in the use of cementless interventions. Cemented procedures dropped from 53% in 2004 to 38% in 2008, while cementless surgeries rose from 21% in 2004 to 33% in 2008 [1]. Despite improvements in cementless design the rate of failure has not improved in comparison with cemented implants, which means more in-depth research is required to investigate the causes of failure in this type of implants [16].

As mentioned earlier, revision surgery for failed implants is a difficult procedure with inferior results. Implants often become loose and sometimes painful and need to be replaced because there is loss in the surrounding bone to support the implant. This lack of bone to fix and secure the new implant in place is one of the main problems associated with revision surgery. To overcome this problem, surgeons and orthopaedic engineers pioneered the concept of hip resurfacing (c.f Figure 2.6c). In this procedure, at the femoral site, only the proximal cartilaginous surface of the femoral head is removed

and replaced by an artificial metallic one. The rational is to conserve the bone stock in the proximal femur for the later probable total hip replacement revision. This will considerably increase the success rate of the revision surgery as well as increasing the time that a patient can have a functional joint after revision [17]. One of the downsides of this procedure is the high risk of femoral neck fracture [18]. 8% of hip arthroplasties performed in England and Wales in 2008 were hip resurfacing [1].

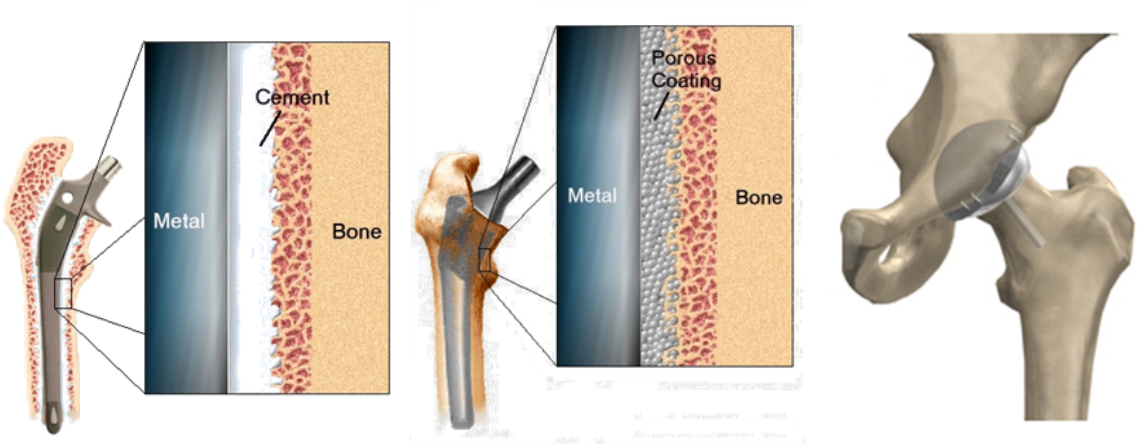

(a) (b) (c)

Figure 2.6: a) cemented b) uncemented hip replacement c) hip resurfacing.[6]

It is also a common practise amongst the surgeons to use different fixation techniques in a joint to secure the implant in the acetabular and femoral sites. This type of implantation is called hybrid arthroplasty. This is because different designs, cemented or uncemented, perform differently in the acetabulum and femur. This has encouraged surgeons to use a cemented component in one part along with an uncemented component in another. The choice of component combination depends on surgeons experience, the brand and history of the prostheses and manufacturer recommendation. According to the Swedish Hip Registry [7], procedures using cemented components in both acetabulum and femur represent a decreasing proportion of the total number of THR. From 2001 to 2006 , the relative proportion decreased from 91.7% to 80.3%.

2.2.4 Failure of total hip replacement

The current designs of THR do not generally last for the life time of patients particularly in the younger population who undergo this procedure. Table 2.2 shows that the most common causes of failure in hip arthroplasty is aseptic loosening [7]. Aseptic loosening is diagnosed when one or two components of an implant become loose in the absence of infection. This can result in pain and loss of mobility and has always been the main

[6]Images taken from: a) http://www.the-health-pages.com, b) http://www.the-health-pages.com c) www.eorthopod.com. Last checked June 2011

cause of implant revision since Charnley's implants. In England and Wales, in 2008, 54% of cases underwent revision surgery because of aseptic loosening [1]. Despite all the new designs and modifications the chance of failure due to aseptic loosening becomes higher as postoperative years increase. Even for recent implant designs (implanted after 1995) more than 5% of the THRs require a revision surgery (c.f. Figure 2.7) [7].

Table 2.2: Causes of THR revisions and their distribution [7].

Causes of revision surgery	Share (%)
Aseptic loosening	59
Deep infection	10
Dislocation	14
Fracture	8
Technical error	2
Others	7

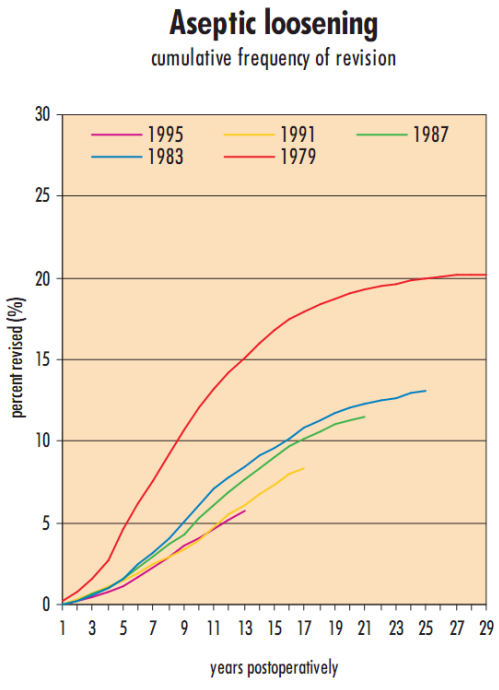

Figure 2.7: Percentage of revised THRs at 13 (red), 16 (yellow), 21 (green), 25 (blue) and 29 (pink) years, postoperatively [7].

High prevalence of aseptic loosening has resulted in enormous effort to understand this phenomenon. Aseptic loosening has been described as a multi-factorial and cumulative damaging process that proliferates to disrupt the bonding between the bone and implant which eventually results in gross loosening [19]. The main causes of aseptic loosening are associated with osteolysis in the periprosthetic tissue [10]. However, the percentage of failure due to osteolysis in unknown and aseptic loosening is not always due to osteolysis. Other proposed mechanical causes for aseptic loosening include stress

shielding, interface debonding as a result of fatigue or accumulated damage [19, 20]. These causes are not independent from each other and they may occur sequentially. The main hypotheses explaining the origins of osteolysis are particle reaction and high fluid pressure and/or velocity. A particle based theory postulates that wear debris generated from bearing and other interacting surfaces are responsible for bone resorption due to adverse biological reaction to the debris. A high fluid pressure/velocity theory considers adverse tissue reaction due to elevated high pressures/velocities experienced in the replaced joint during physical activities as the main cause of osteolysis. These theories will be reviewed in depth in section 2.3 while other causes of aseptic loosening will be reviewed briefly in this section.

2.2.4.1 Implant bone debonding

Sufficient tissue ingrowth, osseointegration and biological bonding at the implant surface are essential prerequisites to establish the fixation of a cementless implant. If the initial bonding and fixation is not achieved gaps at the interface between implant and bone will result in implant loosening. Even after the initial bonding is achieved debonding may occur as a result of fatigue at later postoperative stages. It is an established fact in engineering practice that repetitive loading may cause mechanical damage to the structure under load even when the loads are less than those to cause failure in a single load application. Implants, and in particular the interface between bone and cement are not an exception to this fact. In the case of uncemented prostheses the damage to the implant-bone interface depends strongly on the nature of the bone-implant interlock, bone tissue and its growth to the surface of the implant. The detailed mechanism of fatigue damage to the cement in cemented implants is not discussed here since it is outside the scope of the present study. In the case of uncemented implants the local stresses may exceed the strength of the bone-implant bond throughout repetitive loading. Once this damage accumulates in different regions of the bone-implant interface, the micromotion of the implant in the bone cavity starts to occur. This leads to more damage and subsequent increased micromotion and eventually the formation of fibrous tissue and gaps at the interface. The pattern and the nature of the stresses generated at the interface are very important in determining the mechanism of interface gap generation and fatigue or accumulative damage. The stress patterns associated with load transfer in hip prostheses depend on mechanical factors, such as stem shape and material properties, interface bonding characteristics, bone mechanical properties and hip-joint loading [19]. In addition, the difference between bone and implant stiffness results in different degrees of deformation in these two materials when the stem is under mechanical loading. This may consequently lead to interface gap generation and opening during physical activity.

2.2.4.2 Stress shielding

Stress shielding is a phenomenon that occurs when the normal pattern of load transmission in bone is distorted. Bone resorption as a result of stress shielding takes place in the femoral component where load-shearing between bone and implant depends on the implant shape and especially relative stiffness of the bone and implant. A stiffer-than-bone stem tends to take a higher share of the load and transmit it to the distal portion of the stem, whereas a more compliant stem will take a lower share of the load and will concentrate it in the proximal region of the femur or metaphysis. According to Wolff's law which states bone remodels and adapt itself to the applied loads and strains [21], the portion of the bone that is experiencing less than normal stresses undergoes bone resorption. However, it should be noted that bone resorption caused by stress shielding is different in nature from that of osteolysis in which inflammatory response plays a great role.

In most currently used implants with higher stiffness than bone, loss of bone substance is evident in the proximal femur. Stress shielding was recognised by Oh and Harris [22] using strain gauges mounted on the cortex of implanted cadaver femora. They showed that the pattern of strain in the proximal part of the femur was reversed compared to that of an intact femur. The maximum strain occurred around the tip of the prosthesis accompanied by a massive decrease in stress in the proximal femur. Considering this phenomenon, which is usually evident in radiographs after two years postoperatively [23] (c.f. Figure 2.8), as a sign or mechanism of initiation of failure is debatable. There are patients who experience stress shielding, but they have no symptoms of loosening [20]. Nevertheless, it may be considered as an initiating process for loosening or osteolysis by weakening the support for the stem which can resulting in earlier implant-bone debonding or reducing periprosthetic tissue permeability for easier wear particles migration. Stress shielding has also an impact on revision surgery and may result in a lack of bone stock to secure the new implant. It is more pronounced in cementless prostheses where there is no soft bed of bone cement and there is sharp change in stiffness at the bone-implant interface. The extent of bone density loss varies with different implant designs but can reach levels of 30% or more in certain periprosthetic regions [24]. To overcome this problem, new designs attempt to transmit the load to the cortex near the metaphysis by confining the porous ingrowth to the proximal part the implant leaving the distal portion relatively smooth as opposed to coating the entire implant. In addition, inadequate proximal fit, as the result of over-reaming of the bone, the use of an undersized stem or subsidence of the stem into the bone medullary, may transmit the load to the distal region and cause proximal bone loss [19].

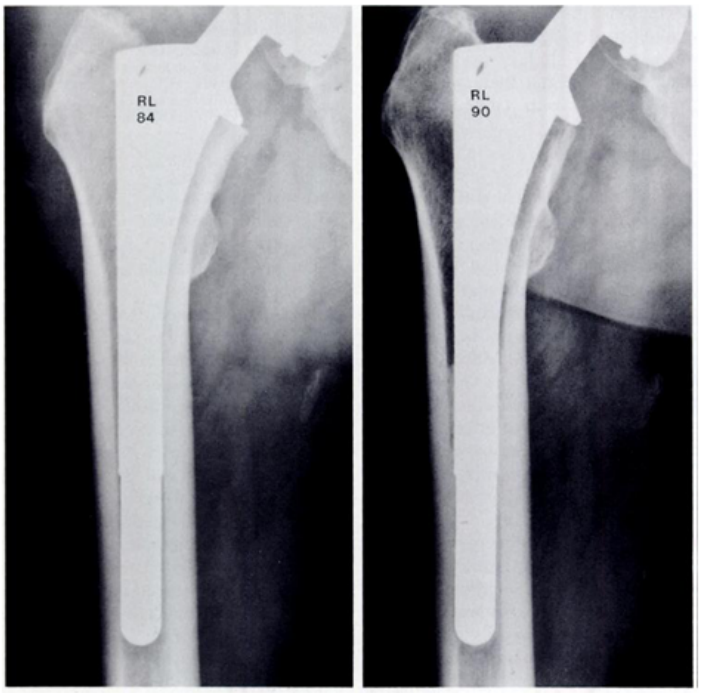

Figure 2.8: Radiographs showing bone immediately after surgery (left) and decrease in bone substance because of stress shielding (right) at the time of the death of the patient [23].

2.3 Osteolysis

In radiographs, osteolytic lesions can appear as focal scallop shaped radiolucencies at parts of the interface or as linear radiolucencies that extend along the edge of an implant [25] as shown in Figure 2.9. In hystological examination linear osteolysis appears as a connective tissue layer between the implant and bone that can be sometimes up to 5-6 mm thick [26]. Focal osteolysis is accompanied by aggressive granulomatosis which is a condition of localised, tumour-like bone resorption appearing on the radiograph as ovoid cysts around the stem, in the definite absence of infection [27]. Linder et al. [26] described osteolysis progression as a soft tissue front that moves from the interface outward. To better explain the periprosthetic environment in which osteolysis is generated, the concept of the effective joint space, introduced in the next section, has been proposed.

2.3.1 The concept of effective joint space

The environment around a THR is different from that of a normal joint. Due to tissue sectioning and scars left from the surgical procedure the joint capsules takes a new shape and the fluid in the capsule has access to the regions that were previously sealed from its access. To describe this situation the concept of the effective joint space (c.f. Figure 2.10), which includes all periprosthetic spaces and tissues in communication

Figure 2.9: linear and focal osteolysis.[7]

with the joint fluid has been proposed [28]. The limits of the effective joint space are determined by the intimacy of the contact between the prosthesis and the bone and the variability of bone-implant contact within a given reconstruction. This variability determines the access routes for the joint fluid and particles, to and along various interfaces as well as the periprosthetic bone and soft tissues. In this effective space, joint fluid flows into the path of least resistance according to the associated pressure gradients.

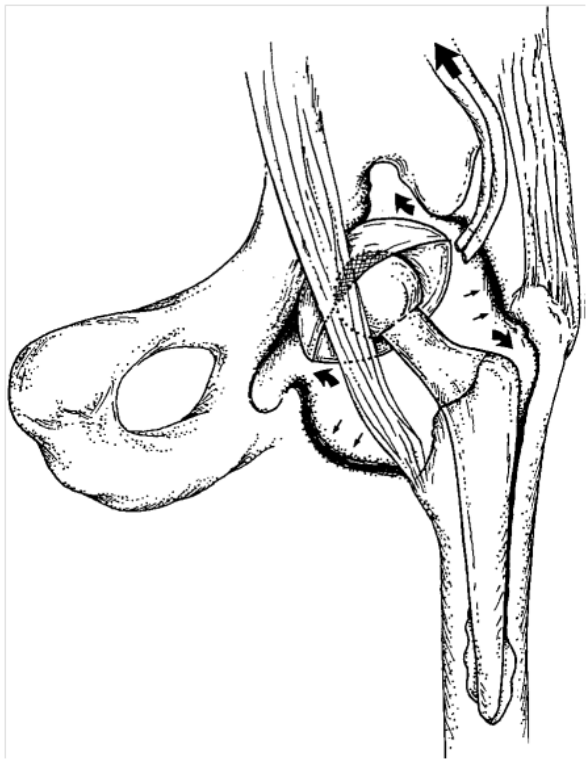

Figure 2.10: Diagram showing the access of joint fluid to the effective joint space [28].

[7]Image from: www.radiologyassistant.nl. Last checked April 2011

2.3.2 Temporal characteristics of osteolysis development

To understand osteolysis development it is important to gain insight into its temporal progression. Tanzer et al. [29] followed twenty patients who developed femoral osteolysis after a none-circumferentially porous cementless THR. Osteolysis was defined as endosteal erosion along the component that was not identifiable on the immediate post-operative radiograghs. They observed that osteolysis was first noted radiographically at twelve to sixty-six months in loose femoral components and between twenty-four and sixty-six months in stable implants. Implants were considered stable if there was no evidence of migration (subsidence of the stem into femoral cavity) or loosening at the time of surgery. The stability of an implant may indicate that the micromotion experience at the interface is less than that of loose implants. Osteolysis was more severe in cases in which the components were loose than those in which it was stable. However, they did not mention the rate and extent of the progression in their studies. In addition, they found no relationship between the detection of the onset of osteolysis and the onset of femoral loosening. Donnelly et al. [30] also showed that osteolysis appears after twenty four months in implants with smooth surfaces. Maloney et al. [31] showed that osteolysis in association with stable cemented implants appears after forty months. Comparing their findings with Tanzer er al. [29] shows that, in general, the onset and progression of osteolysis is earlier and faster in cementless prostheses than cemented ones. Similarly, Zicat et al. [32], in a study investigating the patterns of osteolysis in both cemented and uncemented implants, showed that the rate and frequency of osteolysis was greater in cementless implants. The above clinical observations suggest that it takes at least twelve to twenty months for osteolysis to be observable in clinical examination.

2.3.3 Regional characteristics of osteolysis

It is a common practise to evaluate the location of osteolysis around a femoral stem by dividing the bone around it into seven zones, as described by Gruen et al. [33]. These zones are shown in Figure 2.11 and the same regional definition is used in the current study. Tanzer et al. [29], who studied stems with non-circumferential coating (only patches of proximal porous coating), reported that osteolysis occurred more frequently in distal regions and the medial and lateral regions were involved almost twice as often as the anterior and posterior regions (c.f Figure 2.11 a). They observed that osteolysis was in form of a single focal, multifocal or linear lesions. As can be seen in Figure 2.11 a, zone three and five were the most frequently involved, and zone one and seven were rarely affected by osteolysis. They reported that no lesion initiated from zone four and those lesions seen in this region were an extension from zone two or five. Maloney et al. [34] also suggested that in cementless implants with non-circumferential porous coating,

osteolysis often occurred in distal regions. However, Zicat et al. [32] demonstrated that a circumferential porous coating is able to prevent osteolysis generation in the distal regions. They observed that in these implants, instead of distal regions, osteolysis developed in the bone adjacent to the capsule beneath the collar of the prosthesis (upper zone seven), behind the shoulder of the prosthesis (upper zone one) and in greater the trochanteric region (c.f. Figure 2.11 b). The size of the lesions they observed ranged between 0.7 to 3.3 cm and focal lesions tended to develop more frequently in younger patients. They also reported that osteolysis appears to extend away from the bone-implant interface. Willert et al [35] also reported that in the presence of bone cement, which creates a seal at the proximal interface, osteolysis mainly began in the sections neighbouring the joint cavity including the greater or lesser trochanter. Donnelly et al. [30] studied the appearance of osteolysis in radiographs in different types of cementless implants. They compared implants which had proximal smooth and ridge surfaces, to those with proximal hydroxyapatite coating. They showed that the incidence of linear osteolysis was significantly higher for the implants with smooth surfaces after five postoperative years. High incidence of focal osteolysis was seen in implants with smooth surfaces after two postoperative years, whereas there was no focal osteolysis in stems with hydroxyapatite coating. Their results show that osteolysis, particularly in focal form, occurs more frequently in distal regions far from the joint capsule in smooth implants in which there may not be an intimate contact between the bone and implant (c.f. Figure. 2.11 c). However, in the presence of a strong contact generated by the HA coating, no osteolysis appears at the interface (c.f. Figure. 2.11 d). In summary, the above clinical observation suggests that, when there is not an intimate contact between the stem and the bone, such as those seen in smooth implants, osteolysis tend to occur in distal regions remote from the joint capsule.

2.3.4 High pressure theory

There are studies in the literature suggesting that fluid pressure and flow play a key role in periprosthetic osteolysis. Van Der Vis et al. [36], used an experimental implant model, in which high fluid pressure could be exerted on a sealed surface of rabbit tibia bone by means of an expander filled with saline. They exerted a constant fluid pressure of 20 kPa on the bone for two weeks and observed that osteolysis similar to that of clinical prosthetic loosening occurred in all animals exposed to high fluid pressure. A similar experiment [37] was carried out with pressure oscillating between 9.3 kPa and 20 kPa with a frequency of 0.1 Hz exerted two hours per day for two weeks. In this experiment, which more realistically represents the in-vivo situation, osteolysis was seen to still occur even during short periods of oscillating pressure. However, in these two animal experiments, external nonphysiological saline solutions were used to induce

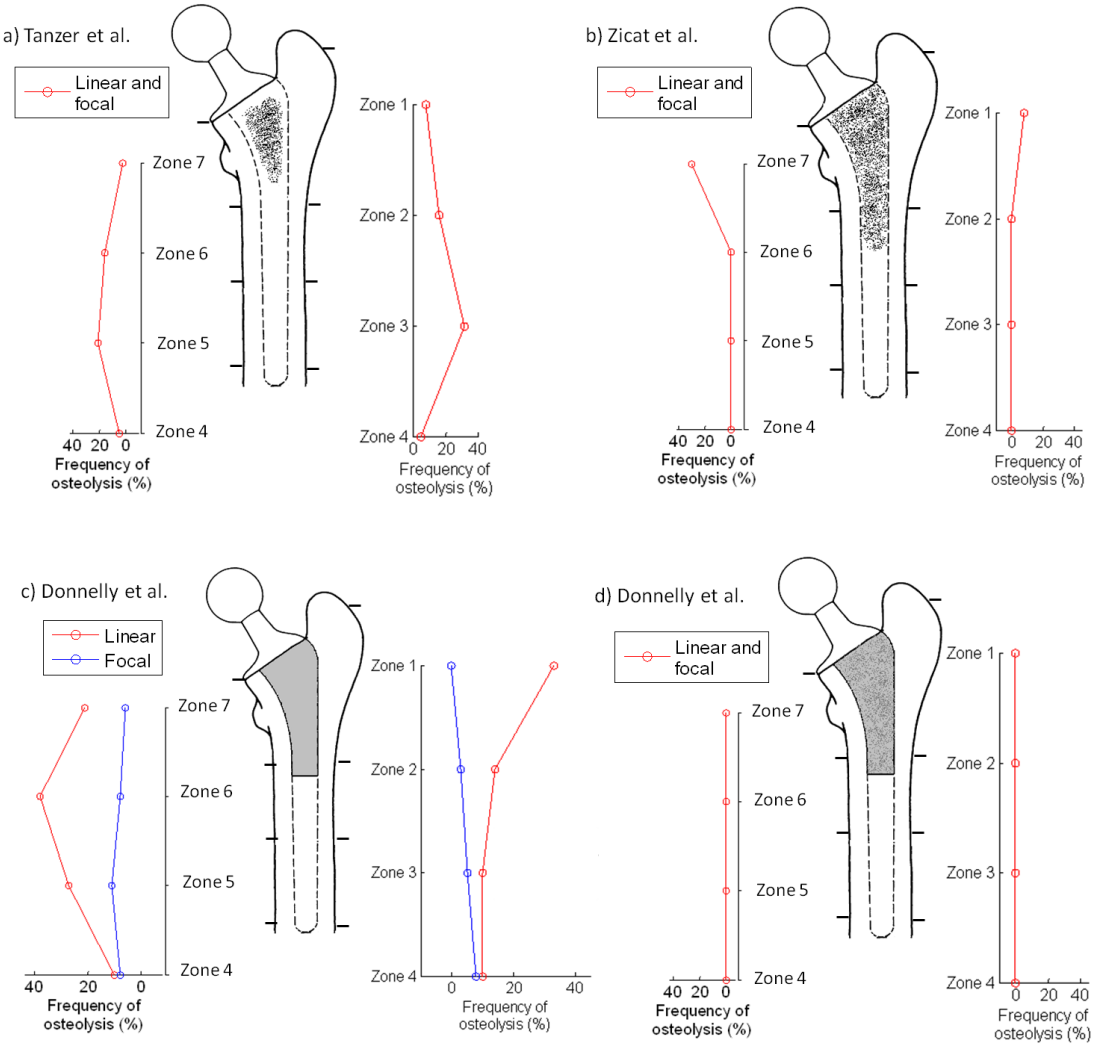

Figure 2.11: Frequency of linear and focal osteolysis occurrence gathered from different sources in the literature. a) It can be seen that frequency of osteolysis is higher in distal regions when the porous coating only consists of local patches leaving other proximal regions smooth [29]. b) It can be seen that when the entire proximal region is coated, osteolysis tend to occur in proximal periprosthetic tissue [32] c) It can be seen that a shot-blast smooth surface cannot prevent osteolysis generation at distal regions. The blue and red line show the frequency of focal and linear osteolysis, respectively. It can be seen that the frequency of osteolysis is higher at distal regions [30]. d) It can be seen that a strong bone contact caused by hydroxyapatite coating prevents osteolysis in both distal and proximal regions [30].

high pressure on the bone tissue. In theory, this could cause osteolysis by altering the chemical environment regardless of the pressure. To circumvent this shortcoming, Skripitz and Aspenberg [38] devised an experiment in which the hydrostatic pressure was exerted on the bone through body fluids. To do so, they designed an implant which allowed generation of a soft tissue membrane containing body fluid on rat tibia in a sealed environment. The soft tissue was then compressed by applying load via a piston located over it (c.f. Figure 2.12). Cyclic pressure of 600 kPa was applied to this tissue by twenty cycles twice a day with a frequency of 0.17 Hz for five days. They observed dramatic osteolytic lesions in pressurised bones. However, the load used in this study is significantly higher than what has been clinically observed and it is applied to a biphasic material. Therefore, the exact value of fluid pressure, which depends on the poroelastic properties of the soft tissue covering the bone is unknown in this study. In addition, it is unclear if the resorption was caused by pressure changes or the resulting fluid flow in the bone (i.e high fluid velocity generated due to high pressure). Fahlgren et al. [39] conducted the same rat experiment to describe the three-dimensional distribution of osteolytic lesions, in order to elucidate the roles of pressure and flow. They used a pressure transducer to measure the actual fluid pressure beneath the fibrous tissue. This pressure was recorded to be approximately 93 kPa, which is a more clinically relevant magnitude. They observed that there was a correlation between bone resorption and pressures recorded; as bone was resorbed, the pressure decreased. After 14 days of pressurisation there was 52% decrease in bone volume fraction. They estimated the fluid velocity to be 26 mm/s initially, 23 mm/s after five days of pressurisation and 19 mm/s after 14 days of pressurisation. Once a pathway was opened to the marrow cavity beneath the cortical bone, the pressure was levelled out and decreased significantly. They also used tracer particles to detect fluid displacement during a 10-min pressure cycle in the controls. Most of the particles were found in cavities and canals within the bone at the periphery of the pressurised area, which are likely to have high fluid flow velocity, but somewhat less fluid pressure than the directly pressurised area under the piston. Osteolysis generation started in these areas, which may suggest that velocity of fluid flow, in addition to pressure, may be a crucial causative factor in osteolysis generation.

High fluid pressure responsible for bone resorption is also seen in joints without implants. Landells et al. [40] was the first to suggest that osteolytic bone cysts can form by intrusion of synovial fluid under pressure into the substance of the bone. However, it was suggested that exposure of the bone to pressurised synovial fluid has to be long enough to cause bone resorption. This observation was not on periprosthetic tissue with particles present, but on subchondral bone tissue, which was in communication with the joint fluid as a result of cartilage loss. Later, Jayson et al. [41] were able to correlate larger cysts with high fluid pressure by showing that larger bone loss was found in

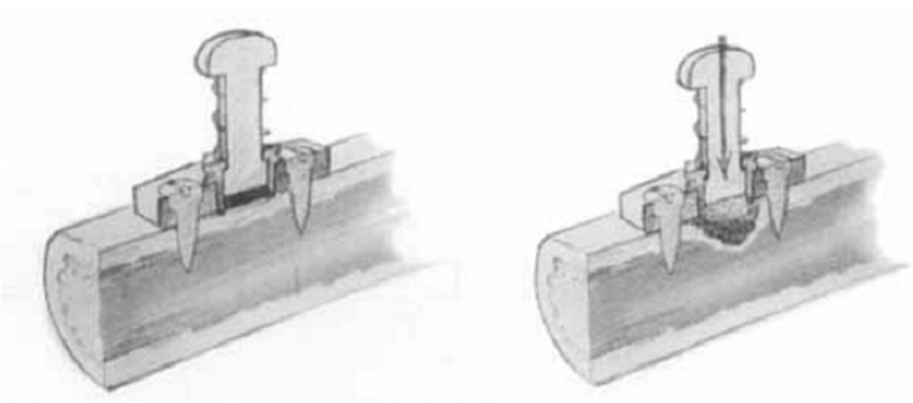

Figure 2.12: Schematic of the pressure chamber developed by Skripitz and Aspenberg [38] to exert pressure on rat bone via a piston. a) shows a soft tissue layer between piston and bone at the beginning of the experiment. b) shows bone resorption after applying hydrostatic pressure.

those individuals generating higher pressures in their joint by doing the hardest manual work. They supported their hypothesis experimentally by simultaneously measuring the pressure inside the cyst using an inserted needle and the intracapsular pressure. The pressure in the cyst and joint capsule were the same and increased identically during a movement. Not only did the pressure not drop to its original level after removing the load, but further manoeuvres would result in higher pressure accumulation. In a parallel study on the healthy joints of dogs they showed that the pressure in the subchondral tissue did not change with pressure changes in the joint space during joint movement when there was no communication between the cysts and the capsular cavity.

The relationship between high fluid pressure and osteolysis can also be established by the relation between thigh pain and high capsular pressure. Well-localised thigh pain corresponding exactly to the sites of osteolytic lesions has been reported [42]. Haversian canals and bone marrow trabeculae are innervated [43] and it is possible that the high pressure exerted to the endosteal surface of the bone produces pain by stimulating nociceptors [37]. Thigh pain is reported to appear when the fluid pressure is high in the joint capsule [6]. This shows that high fluid pressure in the joint has direct influence on osteolytic lesions.

Different theories explaining the causes of osteolysis have been postulated. Van Der Vis et al. [37] suggested that fluid pressure can induce osteolysis by causing bone cell death. Cell death can be caused by the high pressure/velocity interference with the vascular supply or by the flow disturbing the local composition of the interstitial fluid. In addition, it is generally accepted that fluid flow within the bone matrix plays an important role in a strain sensing mechanism involved in bone adaptation response,

otherwise known as mechanosensation. In this mechanism, the fluid flow is sensed by osteocytes, which signal the bone cells to increase bone formation [44]. High fluid pressure, or the resultant high velocities, may disturb this mechanism by prohibiting bone formation or encouraging bone resorption [45].

Johansson et al. [46] developed a computational model to simulate the osteolysis generation because of high fluid pressures and velocity in bone tissue. Their model which was based on the experimental setup developed by Fahlgren et al. [39] showed that fluid velocity is a more likely cause for osteolysis generation.

2.3.5 Particle theory

2.3.5.1 Particles and their relation to osteolysis

In cementless THRs which have a polyethylene acetabular cup, both metallic and polyethylene wear particles can be found in the tissue. The majority of the metallic particles are generated from the relative motion between the stem and the bone. In addition to these particles, cement debris can also be found in cemented implants. The association between particles and osteolysis can also be demonstrated by histological examination of the periprosthetic tissue retrieved from revision surgeries or autopsies. Schmalzried et al. [47] carried out histological examination on periprosthetic tissues obtained from revision surgery and autopsy of thirty four cemented and uncemented hips which had developed linear or focal osteolysis. In all cases, wear debris were found inside or outside the macrophages in osteolytic regions. Polyethylene particles were present in all hips and were dispersed widely in the effective joint space. The degree of bone resorption had a direct relationship to microphages that were laden with polyethylene debris. Similarly, Maloney et al. [34] observed the presence of polyethylene in areas of osteolytic lesions in patients undergoing revision surgery. Willert et al. [35] found large amounts of polyethylene debris in areas of massive bone resorption around the femoral stem, whereas metallic and cement particles were either completely absent or occurred in only very small amounts. Their study showed that metal and cement debris were not phagocytised at all or were stored in granulomas in only very small amounts. The findings of these studies suggests that, amongst particulate debris found in the periprosthetic tissue, polyethylene particles may play the primary role in causing bone resorption. In the above studies, the polyethylene cup was considerably worn due to extensive surface abrasion, which indicates the relationship between the degree of wear rate and the severity of osteolysis. This relationship is discussed in the following section.

2.3.5.2 The rate of wear generation and osteolysis

The amount of wear and the number of particles released into the joint capsule is indeed related to the number of loading cycles that a hip implant experiences. Schmalzried et al. [48] estimated that an implant experiences around 1 million loading cycles on average each year and in extreme cases active patients can subject it to about 3.2 million cycles per year. Wear from the bearing surfaces can be measured by either depth of penetration of the stem ball into the polyethylene cup (linear wear), or the volume of material loss from the polyethylene cup (volumetric wear). Jasty et al. [49] and Sychterz et al. [50] measured mean annual rates of wear of 35 mm^3 and 39.8 mm^3, respectively, for well functioning THRs. Orishimo et al. [51] confirmed that both linear and volumetric wear rates significantly affected the prevalence and risk of osteolysis. Their analysis revealed that increases in linear and volumetric wear rates escalates the prevalence of osteolysis. They also observed that each 40 mm^3 per year increase in volumetric wear raised the risk of osteolysis by about three times. Dowd et al. [52] also showed an overall relationship between the rate of polyethylene wear generation and the prevalence of osteolysis. However, details of this relationship describing the extent of osteolysis as a function of the wear rate was not presented.

2.3.5.3 Particle concentration and osteolysis threshold

It has been shown that the mere presence of particles within the bone tissue is not a sufficient cause for osteolysis development. More importantly, the concentration of particles plays a key role for osteolytic lesion initiation and progression. Revell et al. [53] showed that polyethylene particle concentration retrieved from different periprosthetic sites ranged between 5.2×10^8 and 9.17×10^{10} particles per gram of tissue. Sites containing more than the critical value of approximately 1×10^{10} particles per gram of tissue had developed focal osteolysis. This critical threshold was also confirmed by Kobayashi et al. [54]. However, Elfick et al. [55] reported a lower threshold of 1×10^9 particles per gram of tissue for osteolysis generation. Koseki et al. [56] showed, by counting particles in retrieved tissues from 35 patients undergoing revision surgery with an average of 16.4 years of implant in service, that the particle concentration in the focal osteolytic lesions (lesions greater than 5 mm in radiographs) was 2.10 $\times10^9$ particles per gram of tissue, and in linear lesions (lesions less than 5 mm in radiographs) was 2.91 $\times10^8$ particles per gram of tissue. The concentration in focal lesions was significantly greater than the linear ones. However, there are patients with high wear generation rates who did not develop osteolysis [49]. This may suggest that the biological threshold for osteolysis generation may be patient specific. Ise et al. [57] observed a correlation between the ratio of osteolysis in radiographic images and patient sensitivity to polyethylene particles. They showed that the point at which

osteolysis occurred and the speed of its development varied in each individual. The speed of progression was faster for patients who were more sensitive to polyethylene particles.

2.3.5.4 Particle size and osteolysis

Green et al. [58], who cultured murine microphages in the presence of polyethylene particles, showed that not only the concentration, but the size of the particles is a critical factor for macrophage activation, with the most biologically active particle size range being 0.3 to 10 μm. They showed that both the smallest (0.21 ± 0.07 μm) and the largest (88 ± 29 μm) particles did not stimulate the macrophages to produce bone damaging cytokines. This phenomenon is evident in retrieved studies in which most of the particles found in osteolytic regions were in the biologically active range. It has been shown that approximately 90% of the particles in cells from total hip replacement patients were less than 1 μm with mean diameter of 0.83 ± 0.45 μm [59, 56, 53]. Similarly Schmalzried et al. [47] observed polyethylene particles ranging from 100 μm to less than one micrometre with a majority of particles in the submicron range.

2.3.5.5 Periprosthetic particle distribution

The presence of particles in periprosthetic tissue has been described by many authors. However, there is a lack of descriptive detail on the extent of particle penetration into and their distribution pattern in the periprosthetic tissue. Large amount of particles have been observed to find their way deep into the bone adjacent to an implant [53] and remote osteolytic lesions containing particles, in some cases as far as 10 cm below the tip of the implant, have been reported [47]. Willert et al. [35] also observed that particles and granulomatous tissue infiltrated the marrow cavities of cancellous bone as well as the Haversian canals of cortical bone. Particles projected from the interface border deep into the bone canals and marrow spaces of the femur, partially extending into its outer periosteal surface. Bauer et al. [20] mentioned that biopsies obtained several millimetres away from the implant showed the presence of particles in close proximity to vessels or perivascular spaces. The presence of particles at the interface and the bone marrow adjacent to it after four weeks has also been observed by Lalor et al. [60] who injected polyethylne particles into implanted rabbit joints

A study by Massin et al. [61] on cemented implants showed that particles are more prone to accumulate in the cancellous bone in the metaphysis region as well as in the distal extremity of the stem. Particles were present in the bone marrow of cancellous bone, between the trabeculae and, to a lesser extent, in Haversian canals of the cortical bone. Table 2.3 shows the average number of particles they recorded per 0.6 mm^2 of interface tissue in 50 μm thick sections of the femur at proximal metaphysis, distal

metaphysis, diaphysis and distal femur. This table shows that particle concentration around stem is higher in distal and proximal regions. They performed their analysis on three femoral cemented stems retrieved from autopsy with no sign of loosening. Therefore, the number of particle in the bone tissue recorded by them is not comparable to those studies mentioned earlier in which particle concentration was presented by the number of particles per gram of tissue in loose and osteolystic implants. Unfortunately, such a study describing wear distribution in the tissue around stem does not exist for cementless prostheses.

Table 2.3: Average number of particles per 0.6 mm^2 at different cross-sectional regions along the femoral stems of well-functioning implants after nine postoperative years [61].

Interface section	Average number of particles at cement-bone interface
Proximal metaphysis	324
Distal metaphysis	541
Diaphysis	198
Distal femur	695

2.3.5.6 Periprosthetic particle migration

Particle migration to the periprosthetic tissue is evident. However, it has not yet been completely understood how the particles migrate to the periprosthetic bone and osteolytic lesions and what factors influence such migration and transportation. Two possible transport mechanisms of diffusion (i.e hydraulic transfer) and cellular transport have been suggested by Elfick et al [55]. In the former, particles are carried with the fluid flow in the bone as the result of hydrodynamic forces generated by pressure differences. In the latter, macrophages act to remove foreign bodies by transporting them to lymphatic system for disposal.

If diffusion is the main driving force for particles, it is possible to assume that particles flow through the path of least resistance. In smooth surfaces of non-circumferentially coated stems where there is no interlock between the bone/fibrous tissue and the metal surface of the implant, or in regions where there is a debonding because of mechanical failure, gaps are created and opened during physical activity. These gaps may serve as a path of least resistance to facilitate particle migration to the interface bone.

Bobyn et al. [62] observed that polyethylene debris (1×10^8 particles twice a week) injected in the joint migrated easily along the smooth surfaces of cylindrical implants implanted into the distal femur and proximal tibia of dogs. Such migration was not observed along porous surfaces which had an intimate interlock with the surrounding bone. They characterised the gaps by a distinguishable space between the bone and implant measuring as much as 50 micron in thickness that was filled with fibrous tis-

sue as time elapsed. After 10 weeks of injection and 10 weeks of rest, they observed osteolytic lesions, some of which were expansile and 1.5 mm wide, appearing as radiolucencies along smooth surfaces of implants in radiographs. They observed that during this time particles penetrated the intratrabecular spaces up to approximately 2 mm. Although they proposed that fibrous tissue provided the pathway of least resistance as a ready conduit for the migration of particles, it is more likely that the lack of interlock between the fibrous tissue and the smooth implant surface had resulted in generation of gaps when the joint was deformed and/or capsular pressure raised under physiological loading. The incapability of fibrous tissue to transport particles has been already shown by Yuan et al. [63] who developed an FE model of fibrous tissue between bone and implant. They demonstrated that particles hardly penetrate the fibrous tissue.

The findings of Von Knoch et al. [64] show that the path of least resistance for distal migration is provided by the interfacial gaps and not through the porosity of the bone and fibrous tissues. They demonstrated that in cementless prostheses with wear rate above 100 mm^3 per year, adequate proximal interlock between the femoral stem and bone could prevent distal migration of polyethylene wear debris along the bone implant interface in both bone grown and fibrous-encapsulated implants. In these cases of sealed interface, they observed osteolytic lesions in the greater trochanter above the shoulder of the prostheses and in the upper Gruen zone one and seven that did not progress distally. However, with incomplete or non-circumferential porous surface femoral stems, in which an interlock between tissue and stem is not achieved and an interfacial gap may exist, osteolytic lesions could be seen in the proximal-stem, middle-stem and distal-stem levels. They also showed that fibrous tissue ingrowth to the porous surface appeared adequate to prevent distal particle migration, despite the lack of solid bone fixation. The importance of seal interface has also been emphasised by Coathup et al [65] who confirmed this fact by showing that if the interface is sufficiently sealed from the joint capsule, using hydroxyapatite coating on a porous stem, osteolysis did not occur in sheep joints even in continuous generation and high concentrations of submicron polyethylene wear particles. A similar observation has been made by Zicat et al. [32] who demonstrated that a circumferential porous coating is able to prevent osteolysis generation in distal regions. Histological examination of distal regions of these implants failed to demonstrate particle presence in these regions. In summary, the above clinical observations show that for particles to migrate to distal regions there must be a gap in communication with the joint fluid.

2.3.5.7 The effect of particle size in their migration

Elfick et al. [55] suggested that the ability of particles to migrate away from their point of origin to be inversely proportional to their size. However, they did not present any evidence for this claim. However, there are a few other studies suggesting that the size

and shape of particles influences their migration to different regions of the effective joint capsule. Mabrey et al. [66] showed that polyethylene particles from the capsular tissue were different in terms of their size and shape from those in the synovial fluid and the interface tissue adjacent to stem. Particles taken from interface at femoral bone tissue tended to have a smaller size (0.697 $\pm$ 0.009 μm) and more globular shape (decreasing elongation) compared to particles taken from the hip capsule. Although the particles from the femoral tissue were smaller compared to those from the synovial fluid, this difference was not statistically significant. Revell et al. [53] also reported that only smaller particles which tended to be rounder could be found in the surrounding tissue. The observation by Zolotarevova et al. [67] that smaller wear particles (ranging between 0.1 to 10 μm in size) were more evenly distributed between the granuloma and the surrounding periprosthetic tissue than larger particles (>10 μm) can also support the hypothesis of easier migration of small particles than large ones. Certainly, more studies are required to establish the definitive size and shape distributions at different anatomical sites. However, the above clinical observations may suggest that, in the presence of an interfacial gap, the majority of biologically active particles flow distally to the interface, which in turn, leads to higher probability of osteolysis generation at the interface tissue rather than in the proximal periprosthetic tissue in the vicinity of the capsule.

2.3.5.8 Particle supply and clearance

The existence of a biological threshold for osteolysis in terms of particle numbers implies that for an osteolytic lesion to initiate and progress, sufficient concentration of particles has to be maintained for a long enough period of time. For such a condition to occur a continuous and sufficient wear generation, a permanent route for migration of generated wear to a particular site and an insufficient drainage system for particle elimination from that site is required. Kim et al. [68] demonstrated the importance of wear generation continuity and dosage dependence of osteolysis development. Their in-vivo rat knee model showed that only a continuous injection of 8 $\times 10^5$ of polyethylene particles per day over a period of four weeks and longer could cause inflammation and osteolysis. In fact, a study carried out by Massin et al [61] shows that the periprosthetic tissue particle drainage is an insufficient mechanism in THRs. They studied tissues retrieved from autopsy of a patient who died for unrelated reasons three months after a revision surgery. In these tissue samples they could still observe particles remained from the first implantation, which suggest that clearance of particles is rather a slow process and is incapable of clearing particles in the period of three months. In another study, investigating the leakage of radioactively labelled particles from synovial joints of rabbits, Nobel et al [69] showed that the mean leakage from the joint for inert carbonised microspheres of size 10 and 15 μm, the phytate collide (average size, 0.7

μm), and gold collide (0.03 μm) were 0.3 ± 0.05, 0.08 ± 0.09, 1.21 ± 0.20 and 2.02 ± 1.49 per cent of the injected dose after twenty four hours, respectively. The overall trend suggested that the leakage is reduced as particle size increases. This study also shows a very low rate of drainage of particles from the joint capsule even for very small particles. In a replaced joint, where particles are constantly being released to the joint capsule, this means a high rate of accumulation of particles in the effective joint space. It is possible to assume that, since large particles have a lower rate of drainage, they may reside in the periprosthetic tissue and clog the path of smaller particles and reduce the drainage rate even further.

Despite the slow rate of the drainage system, there exists evidence for the dissemination of wear debris to the lymph nodes, liver and spleen. This suggests that one way for wear debris transportation may be via the lymphatic system [70]. However, the sites, routes and efficiency of this drainage mechanism is not clearly known. Jell et al. [71] showed the presence of lymphatic capillaries in the whole periprosthetic tissue in six out of ten patients undergoing revision surgery. However, in the close proximity of the bone-implant interface, there were relatively few lymphatic vessels (3.4% of total vessels). They observed that, in those who still had lymphatic vessels at the interface, these vessels could provide a route for particle dissemination to distal regions. However, in the majority of cases, as the concentration of particles increased in a site, no lymphatic vessel could be observed. This suggests that high particle concentration may impair generation of lymphatic vessels and reduce the particle and interstitial fluid drainage rate even further. Potentially, growth factors generated by macrophages may impair the generation of lymphatic vessels. This, in turn, may perpetuate inflammation and bone resorption by inhibiting removal of interstitial fluid. Impairment in interstitial fluid drainage from a bone-implant interface may also increase the hydrostatic pressure which has been shown to cause bone resorption [38]. They also suggested that wear particles may block the lymphatic capillaries and impair further generation. In another study, Edwards et al. [72], using specific markers to detect lymphatics in periprosthetic tissue obtained from 26 patients undergoing revision surgery, showed that lymphatics were only present in the hip capsule after arthroplasty and not in the femoral bone-implant interface. This finding indicates that particles cannot be completely cleared from the interface via the lymphatic circulation which may lead to rapid accumulation of particles at this site.

2.3.6 Synergistic effect of particles and high fluid pressure/velocity

Despite the fact that the potential roles of particles and high fluid pressure/velocity in generating osteolysis is hypothesised, it is not clearly understood how the combination of these factors may influence the periprosthetic tissue. Aspenberg and Herbertsson

[73], using the same experimental setup as Skripitz and Aspenberg [38] explained in section 2.3.4, demonstrated that fluid pressure/velocity was the prime cause of bone loss while presence of particles at the interface only preserved the osteolysis that has been previously generated by a fluid pressure/velocity. However, De Man et al. [74] improved the animal experimental model of Skripitz and Aspenberg [38] to a more realistic loading condition which could generate both tension and compression in the fibrous tissue. Their model produced micromotion and high fluid pressure in the bone while particles were administered. In contrast to Aspenberg and Herbertsson [73], their model showed that there was no synergistic effect and both stimuli could cause bone resorption by fibrous and cartilaginous tissue generation.

2.4 Mechanisms involved in high pressure/velocity generation and particles migration

So far, the potential causes of osteolysis have been discussed. It has been established that particles and high fluid pressure/velocity may play an important role in osteolysis generation. However, mechanisms involved in generating high fluid pressures/velocities and transporting particles into the periprosthetic tissue have not been described in detail. Both high pressure/velocity generation and particle migration are dependent on periprosthetic flow. In other words, periprosthetic conditions can distribute high pressures/velocities to the periprosthetic tissue, or can facilitate particle migration to it. A postulated source for periprosthetic flows at the interface is the elevated capsular fluid pressure during physical activity [6, 3, 75]. Another postulated source is the interface gap micromotion which acts as a pump to cause periprosthetic flow [76]. However, how this mechanism are involved in generating periprosthetic flow and the extent of the role played by each mechanism are not clearly understood. Simulations in this study attempt to elucidate the effect of these mechanisms on periprosthetic flow. These mechanisms are discussed in detail in the following sections and are investigated in detail in Chapters 4 and 5, respectively.

2.4.1 Capsular pressure

2.4.1.1 Joint capsule and pressure in healthy joints

As mentioned in section 2.1.3, the hip joint is sealed from the surrounding tissue. This results in an isolated space where there is a direct relationship between the volume and the pressure. Wingstrand et al. [5] showed that in healthy joints pressure hardly changes within the normal range of passive rotation. However, there is no study measuring capsular pressure in healthy hips when it is under load during physical activity.

Nevertheless, such measurements have been carried out on knee joints and it has been shown that during a gait cycle fluid pressure drops to subatmospheric pressure of 2.6 kPa with the foot on the ground (foot-stance phase in a gait cycle) and it only rises less than 0.5 kPa above atmospheric pressure when the foot is not on the ground (swing phase). The authors showed that the drop to subatmospheric pressure in the joint was due to quadriceps muscle contraction in the foot-stance phase. At this phase the soft tissue appeared sucked in between the tendon bands. This contraction enlarged the joint spaces and creates negative pressure. The slight subatmospheric pressures in the hip at passive rotation could also be seen in the results obtained by Wingstrand et al. [5]. It seems, in addition to the surrounding muscles and ligaments, subatmosperic pressure is an important mechanism to stabilise synovial joints. It is possible to assume that in normal hips, similar to the knee joint, pressure does not increase significantly under physiological loading.

The vascular supply of the proximal femur is unique in that its vessels travel along the length of the femoral neck between the bone and the capsule. Therefore, any high capsular pressure maintained for long enough could result in blood supply blockage to the femoral bone and cause necrosis. Therefore, it is possible to assume that in healthy joints capsular pressure does not rise above the local blood pressure which is approximately 5 kPa (c.f. section 2.5.2) for that otherwise it would create bone tissue necrosis.

2.4.1.2 Joint capsule and pressure in THR

The hip joint capsule in a normal hip is very elastic and can be stretched up to 55% without any plastic deformation [77]. The prerequisite for this is the hyperboloid shape of the capsule that allows volumetric changes in the capsule to maintain appropriate intracapsular pressures (c.f. Figure 2.13). If this hyperboloid shape is distorted toward a more cylindrical shape due to any kind of pathological changes, the intracapsular pressure may be altered. After THR, despite incision and resection of bone and soft tissue during THR surgery, an articular space or so-called pseudo-capsule space filled with fluid still exists. However, its properties are significantly different from those of a normal joint. Arthrograghs studied by Cone et al. [78] clearly demonstrated the existence of an articular closed space. However, they showed that the volume of this cavity varies for individual patients depending on the degree of scarring around the prosthesis.

However, it was shown that in problematic joints and THRs diagnosed for revision the joint pressure can be higher than the normal situation and it can even increase dramatically during joint movement and physical activities. Goddard and Gosling [79] measured a mean value of 5.76 kPa at resting position for 50 hips before undergoing THR surgery diagnosed with osteoarthritis and rheumatoid arthritis. They showed

that the resting pressure could rise to almost twofold in medial (internal) rotation and in extension (c.f. Figure 2.4 for hip range of motions), and that it decreased slightly in mid-abduction and at about 20°of flexion. They also found that resting pressure was higher in young patients with osteoarthritis with more mobile and painful hips. Robertsson et al. [75] demonstrated that intracapsular pressure is usually elevated in a hip joint with loose prosthetic components at different positions of the hip in the supine position. However, they did not measure pressure changes during physical activities. Their measurements are shown in Table 2.4. Hendrix et al. [6] were the only ones to measure hip joint pressures in THRs during different physical activities using a catheter connected to the hip capsule in patients who were asked to perform different manoeuvres while the pressure was measured. The patients had symptoms of loosening and underwent revision surgery after the experiment. Their results, shown in Table 2.4, show strikingly high pressures up to 69 kPa in stair climbing and standing up manoeuvres. High pressures also occur in other problematic body joints. Jayson et al. [41] showed that, in rheumatic knee joints, muscle contraction in quadriceps setting, a manoeuvre in which the lying patient with legs straight tightens the quadriceps muscle and pushes the back of the knee to the bed, can rise the intracapsular pressure from rest at 4.7 kPa to up to 52 kPa.

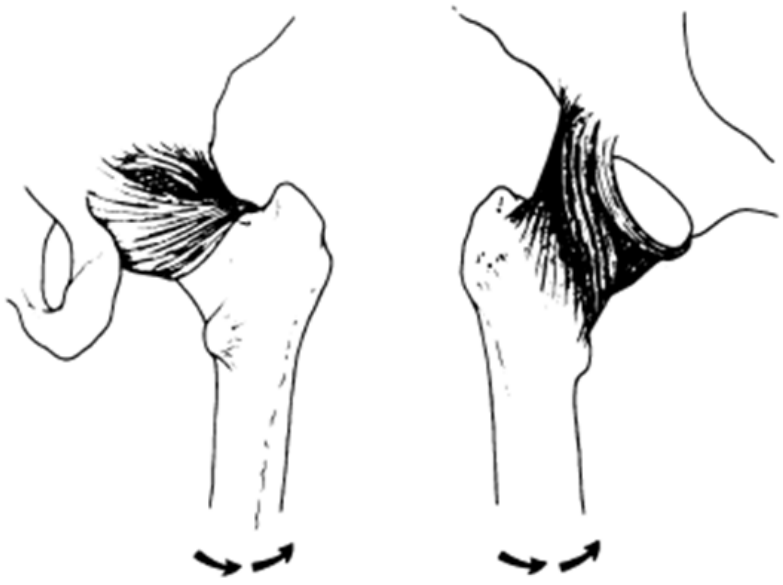

Figure 2.13: Shape of the joint capsule when it is relaxed (right) and when it is tightened (left) [79].

There is no study indicating how long the increased pressures are maintained if the hip is immobilised in a position. However, Vegter et al. [80] showed that high pressure generated in the capsule does not fall after five minutes of holding the position that caused high pressure. This may demonstrate the inefficiency of the surrounding

fluid drainage mechanism in the body to drain the excess joint fluid causing the high pressure, at least within the short period of five minutes.

Table 2.4: The summary of the intracapsular pressure measurements (kPa). Presented by the mean values and the range of measurements which are shown in parenthesis.

Position	Hendrix et al. [6]	Robertsson et al. [75]	Cone et al. [78]
Standing	13.7 (0 -16)		
Sudden changes in direction	48 (21-96.5)		
Stair climbing, sitting down, or standing up from a sitting position	69 (48 - 103.4)		
Extension in supine position		3 (0-8)	
Extension and inward rotation in supine position		21.2 (3.2-37.3)	
Extension and outward rotation in supine position		4 (0.4 - 8.9)	
At rest			0.96 (0.5 - 1.6)

2.4.1.3 Causes of high capsular pressure

Lloyd-Robers [81] showed that, in patients with osteoarthritis, synovial membrane and the capsule tissue undergo progressive fibrosis and thickening and in some cases shortening and calcification which results in loss of tissue elasticity and compliance. They also discovered that the hip capsule became taut in positions of extension with slight internal rotation which correlate with positions in which intracapsular pressure increases to its maximum as mentioned previously. Capsular tissue fibrosis and thickening which leads to loss of elasticity may continue to exist even after a THR procedure. Robertsson et al. [75] were able to demonstrate that there is a positive correlation between the increase in intracapsular pressure in extension and inward rotation and the extent of thickening of the capsular tissue. Despite the small amount of joint fluid in these joints, the pressure could still be as high as 37 kPa. The above findings suggest that the loss of elasticity in the capsular tissue is an important factor in increasing the capsular pressure. Inflammatory reaction to wear particles can also cause loss of elasticity in the capsular tissue. Joint capsule thickening of several centimetres as a result of excessive

wear was observed by Willert et al. [35].

Excessive effusion, which is commonly seen in loose THRs [6], may be another factor influencing the fluid pressure within the joint. Wingstrand et al. [5], by using cadaver hip specimens mounted in a test rig, showed that excessive effusion plays an important role in high capsular pressure generation. In normal hips, in which there was no increase in intracapsular pressure within the normal range of rotation, injection of 36 ml of saline to mimic in vivo effusion, increased the pressure up to approximately 6.6 kPa. However, the significance of joint effusion becomes apparent when a joint is in motion. It was shown that under this effusion, joint rotation as small as 25°could increase the pressure up to approximately 53 kPa. At lower amounts of saline injections the jump in pressure as a result of joint rotation was smaller. These findings suggest that excessive effusion stretches the spirally oriented capsular tissue wrapped around the joint and, therefore, limits the elastic range of joint deformation. As a result, the capacity for volumetric change in the capsule is reduced and any small joint deformation leads to high pressure build-up.

While loss of capsular tissue elasticity and excessive joint effusion can both alter the intracapsular pressure, the presence of both in a hip joint can exacerbate the situation. Tarasevicius et al. [82] showed that, in 31 patients diagnosed for hip arthroplasty, as capsular elasticity decreased, smaller amounts of fluid effusion were needed to cause high capsular pressure (c.f Figure 2.14). In very stiff hips, fluid effusion as small as one ml could cause high pressures of up to 41 kPa. Soto-Hall et al. [83] showed that in patients with problematic hips only 12 to 15 ml of fluid could be introduced into the hip joint before the pressure increased significantly, while, by contrast, in apparently normal cadaver hips, as much as 35 to 40 ml of fluid could be injected into the joint with a syringe, using moderate force before pressure raised significantly. These findings show how the loss of capsular elasticity results in stronger effects for joint effusion. In summary, the literature suggests that properties of the hip joint capsule including elasticity of the capsule and joint effusion are the factors causing high capsular pressure.

2.4.1.4 Hydrostatic communication between capsular pressure and osteolytic regions

It is important to know whether high capsular pressures are transmitted to other regions of the effective joint space. Jayson et al. [41] observed that, in the knee and wrist joints at rest, the pressure in the osteolytic regions is identical to that of the joint capsule and it rises identically during muscle contraction in both the capsule and the osteolytic lesion. Anthony et al [84] observed that contrast agent for arthrograms injected to the capsule had penetrated to the osteolytic regions in Gruen zone six after a patient had walked for 45 minutes after injection, which suggests the existence of fast communication between the capsule and the osteolytic lesions. The existence of

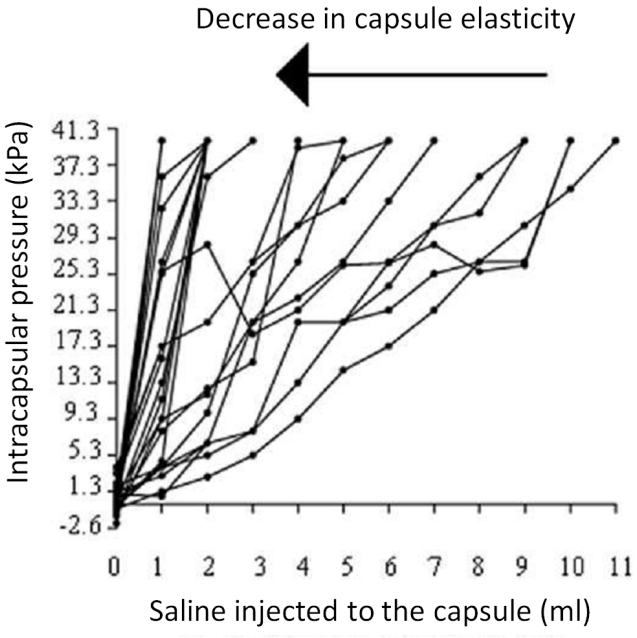

Figure 2.14: Each line of data in the graph represents a patient (n=31). The graph shows that in capsules with lower complacency even a small amount of fluid injection (as low as 1 ml) can result in high pressure generation during hip motion [82].

this communication route was also observed during the revision surgery. In another case they also observed that as little as 15°of passive flexion and extention of the hip was associated with immediate fluctuations of up to 26 kPa in fluid pressure in the osteolytic lesion. They suggested that the forces involved in generating these pressure changes in vivo under physiological loading could be much higher than those associated with gentle passive movement of the hip. Cone et al. [78] showed that for the injected contrast agent to the capsule to flow to the an osteolytic defect, at least a mean value of 24 kPa pressure was required. This suggests that a high capsular pressure is necessary for the joint fluid to flow to interfacial spaces in the effective joint space.

In summary, the above clinical observations suggest that, in problematic THRs, the capsular pressure can rise up to an average value of 60 kPa when the joint is under physiological loading. The excess of joint fluid and the low compliance of the capsule may subject the bone-implant interface to extreme hydraulic pressures.

2.4.2 Micromotion of interfacial gaps

As mentioned previously, gaps may be generated at the bone implant interface. When a stem is under physiological loading, the difference between bone and metal stiffness causes different degrees of deformation in these two materials, which in turn leads to micromotion at the interface. This micromotion may cause the interfacial gaps to open or close during physical activity, which may pump the joint fluid into and out of the

gap region. In order to understand and describe gap micromotion, the forces exerted to a stem are described in the next section. Then, the likely links between applied force and gap motion are described.

2.4.2.1 Forces in the hip joint

Forces directly acting on an implant stem are complex since they are resultants of forces from the patient's weight and different muscles groups, each acting at a different point with different directions. Bergmann et al. [85] established the physiological loads acting on the head of a femoral stem by telemtric measurements for daily activities such as walking and stair climbing. Hip contact forces with magnitude F and the components F_x, F_y and F_z were measured (c.f. Figure 2.15). The force F causes implant moments M_x, M_y and M_z around the insertion point of shaft and neck axes of the implant. Figure 2.16 shows the magnitude of these forces as a percentage of body weight for a gait cycle which lasts approximately one second. The plot showing the magnitude of moments is similar to that of forces for the same activity. Fast walking or stair climbing generated the highest forces and moments in the hip joint.

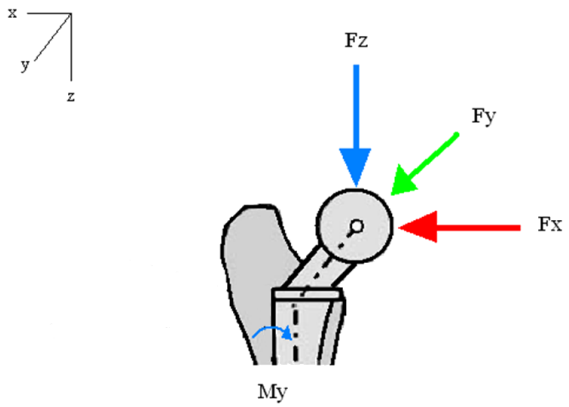

Figure 2.15: Schematic diagram showing forces acting on the hip joint.[8]

Muscle forces acting on a hip implant in these activities have been estimated by numerical models [86]. In this study, the muscles acting on the proximal femur were simplified to groups of abductor and adductor, ilio-tibial tract, tensor fascia latae and vastus muscle groups. Figure 2.17 shows for these muscle groups and their point of action on the femur. While muscles act on P1, P2 and P3 locations, the hip contact force acts on P0. Table 2.5 shows the maximum value of the hip contact and muscle forces acting on these points at the proximal femur during walking. The instances of maximum loading during walking and stair climbing are characterised by the strong activity of the abductors group and the quadriceps muscles (not shown in Figure 2.17

[8]Image from: www.dwd.state.wi.us/.../wc/images. Last checked April 2011

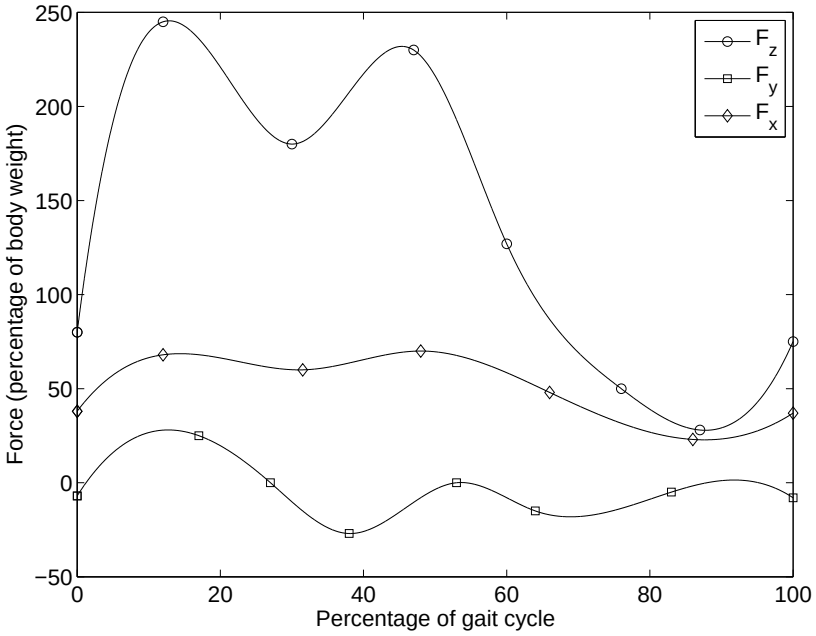

Figure 2.16: Forces acting on the hip joint during a normal walking gait [85].

because they have no attachment to the proximal femur). However, during these instances of maximum loading, hip contact force is still higher and more dominant than muscle forces (c.f. Table 2.5). The resultant of hip contact and muscle forces acting on an implant is an important factor influencing micromotion experienced at the interface. For instance, the momentum M_y acting around the implant insertion point, generated by the hip contact force F_z, causes an implant rotation (c.f Figure 2.15) which may lead to implant bone detachment and gap opening at the lateral interface, whereas the abductor and adductor muscle groups may tend to close the gap at the same time. The effect of these forces are discussed in section 2.4.2.4.

Table 2.5: Forces acting on the hip joint in percentage of body weight [86]

Force (%BW)	x	y	z	Acts at point
Hip contact	-54.0	-32.8	-229.2	P0
Abductor group	58.0	4.3	86.5	P1
Tensor fascia latae, proximal part	4.2	11.6	13.2	P1
Tensor fascia latae, distal part	-0.5	-0.7	-19.0	P1
Vastus lateralis	-0.9	18.5	-92.9	P2

2.4.2.2 The dimension of interfacial gaps

There is no study in the literature measuring the length and width of interfacial gaps. However, it is possible to estimate the length of interfacial gaps by studying the range in which radiolucent lines are seen along the femoral stem in radiographs [87]. These radiolucent lines are observed to extend to proximal regions (representing short gaps)

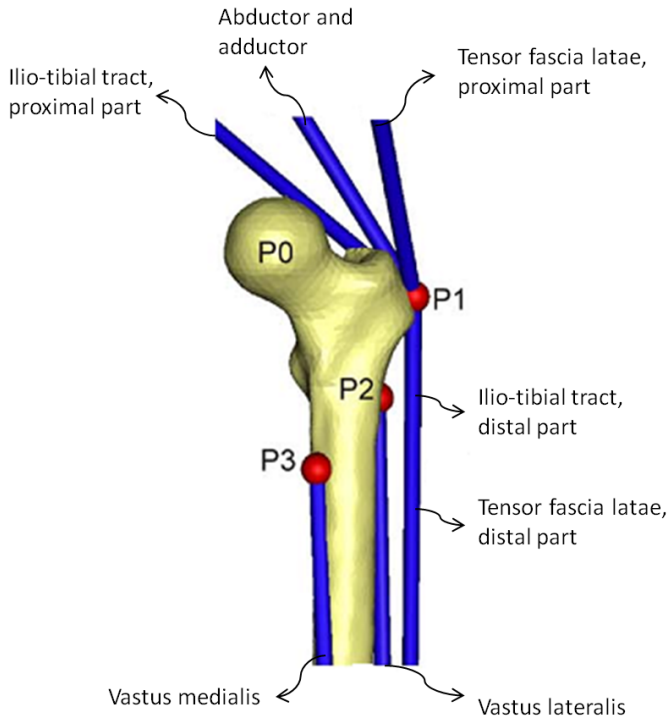

Figure 2.17: Muscle groups acting on the femur. The point of action for these muscle are shown by P. P0 is where hip contact force acts [86].

or to regions near the tip of the stem (representing long gaps).

There is no direct measurement of the gap width in the literature. Howard et al. [88] used CT images to show that only 43.6% to 57.7% of the femoral stem was in direct contact with the surrounding bone after implantation. This demonstrates the high probability for the existence of gaps in communication with the joint capsule in the proximal region. They chose a threshold of 500 μm to detect the existence of interfacial gaps using Computer Tomography (CT) scans. However, they did not present a range or distribution frequency for the width of the gaps, neither had they reported on the smaller gaps that may exist at the interface. In addition, the study by Park et al. [89] indicated that choosing a gap threshold larger than 500 μm (for instance 1000 μm) for gap detection would result in detection of no gap at the interface. This indirectly shows that there is a lower chance of having larger than 500 μm gaps at the interface. This may establish an upper limit for the width of the interfacial gap. However, there is no study in the literature reporting on the dimension of very narrow gaps to establish a lower limit for gap width.

2.4.2.3 The temporal and regional development of interfacial gaps

It is important to understand when and where, in the life of the implant, these pathways (gaps) become functionally available. Park et al. [89], using composite bones under cyclic loading showed that an average of 67% of the stem was in contact with the bone,

and interfacial gaps were mostly present on the proximal lateral side of the stem after implantation. Howard et al. [88] also showed that interfacial gaps were mainly located and largest in proximal lateral aspects in different stem designs. Interfacial gaps may also appear at the interface of implants long after implantation as the result of fatigue and bone resorption [19].

2.4.2.4 Interface micromotion

There is no direct measurement of gap opening and closing experimentally and computationally. However, it is possible to correlate micromotion measurements at bone-implant interface to interfacial gap generation. Gap opening and closing at proximal posterior and anterior aspects of the stem has been demonstrated by Glyn-Jones et al. [90] using a finite element (FE) model including hip contact and major muscle forces shown in Figure 2.17. Abdul-Kadir et al. [91] demonstrated that in a loading condition in which hip contact and abductor forces as well as the complacency of the cancellous bone at the trochanter region were included, micromotion occurred in proximal lateral regions for different implant designs in both stair climbing and walking activities. In FE micromotion studies, micromotion is defined as the displacement of the stem relative to the endosteal surface of the bone. This displacement is the resultant of implant sliding into the bone cavity and implant separation from the endosteal bone. In the proximal region, however, as demonstrated by Bruke et al. [92] who included both abductor muscle group force and hip contact forces in their in vitro study of micromotion in cementless implants, there is no significant sliding micromotion occurring in the proximal region and the micromotion in that region is thus of a separation (gap generating) nature. They reported a micromotion range between 13 μm to 280 μm in the proximal region during stair climbing. Harman et al. [93] applied 700 N load to the stem head in an interior to posterior direction to assess the primary stability of cementless prostheses. The applied load created a moment about the femoral axis and internal rotation of the axis. An extensometer was used to measure interface micromotion between the proximal medial stem and femur. They measured micromotion ranging between 88 to 366 μm. The same phenomenon has been observed in FE models developed in our research group that have not yet been published. These observations confirm that gaps in the proximal lateral region still open during physical activity even when the abductor load, which tends to close the gap, is taken into account. The same can be concluded from studies measuring in vivo hip contact forces using telemetric hip stems. In such measurements hip contact forces are measured while the abductor load effects are in place [85]. Under such a condition, it can still be seen that hip contact force acting on the stem head in the superior-inferior direction (F_z) and a moment acting on the stem around the anterior-posterior direction (M_y) are the dominant force and moment in vivo throughout a walking cycle (c.f Figure 2.16 and Table 2.5 in section

2.4.2.1). F_z and M_y both cause the gaps in the posterior lateral direction to open.

2.4.2.5 High fluid pressures and flows caused by interface micromotion

It has been suggested that micromotion of the femoral stem may act a pumping mechanism to transport particles to distant sites and generate high fluid pressure/velocities at the interface [84]. Bartlett et al [76] developed a new in vitro model of a smooth surface stem imbedded in bone cement and measured interface fluid pressures under dynamic sinusoidal stem loading. Their experimental model contained a chamber around the implant filled with vegetable oil acting as the synovial fluid. Pressure transducers were placed in different regions around the stem surface to measure the fluid pressure. They observed that the application of dynamic loads to the stems gave rise to a significant pressure response, cycling above and below resting values at all regions along the interface. The average pressure values under the combined loading condition varied between different regions from 5 kPa to 17 kPa. The peak negative pressure occurred at or near either the start or end of the cycle for pure axial loading, when the axial load was at a minimum. Under this loading, pressure developed first near the tip and creating a fluid flow in the proximal direction as axial load approached the maximum value. This flow reversed as the axial load decreased. Their model was able to show that under physiological loads micromotion of the stem can act as a pump generating substantial pressures in the fluid layer present at the interface.

2.5 Bone tissue and its fluid flow

As discussed in section 2.2, after THR the periprosthetic bone may come into direct contact with the joint fluid where there is an interfacial gap. As bone is a porous material, the joint fluid may flow into its matrix and transport wear particles and transmit high pressures and flows generated as a result of high capsular pressure and/or implant micromotion. To simulate such flows in the periprosthetic tissue, an understanding of fluid flows in the bone tissue is necessary. In the following sections, the porous nature of bone tissue and the mechanical properties influencing the flow of fluid through it are explained.

2.5.1 Bone tissue: solid phase

Bone is a hard and rigid tissue that is composed of both fluid and solid phases. Its solid phase consists of 65% minerals and 35% organic matrix, cells and water. 90% of the organic matrix is collagen fibres and the remaining 10% consists of a large variety of non-collagenous proteins. The organic fibres are embedded in minerals and inorganic salts. The hard and rigid structure of bone enables it to support the weight and

maintain the shape of the body as well as providing a framework on which the muscles act to facilitate body movement. It also accommodates the bone marrow within its cancellous and medullar cavities [94].

Bone has the ability to repair and revitalise itself by constantly resorbing and regenerating new bone matrix. Bone generation and resorption is sensitive and adaptive to the surrounding mechanical environment (mechanosensation) as well as the biochemical agents such as cytokines and growth factors. This mechanical and biological adaptation leads to an optimised structure for mineral crystals that serves the function of the bone in a particular region [95].

There are two types of bone in the body: cortical and cancellous. Cortical or compact bone, which contributes 80% of the solid skeletal mass, is the dense bone that provides protection and support for the body. It constitutes the outer layer of all bones as well as the shaft of the long bones such as the femur. In proximal femur the thickness of the cortical shell in metaphysis and epiphysis regions is approximately 1.5 mm and in diaphysis (femoral shaft) region is approximately 4 mm [61].

Cortical bone is an organised structure consisting of 3-7 μm lamellae. Each lamella contains fine fibres that are aligned in the same direction (c.f. Figure 2.18). These lamellae are mainly organized in concentric circular rings around a vertical channel through which nerves, blood vessels and lymphatics pass. This cylindrical system is known as an osteon or Harversian system. A typical osteon is a cylinder with a diameter of 200 to 250 μm. Each osteon is made of 20 to 30 concentric lamellae with the thickness of approximately 70 to 100 μm. Around each osteon, there is a 1 to 2 μm thick mineralised matrix with no collagen fibres known as the cement line. Within the lamellae, there are small cavities known as lacunae that accommodate the bone cells known as osteocytes. Lacunae are connected to each other through several canaliculi, which are small tubular canals filled with long osteocyte processes and interstitial fluid. Osteocyte cells communicate with the adjacent osteocytes as well as the bone lining cells, progenitors, Haversian channels and vasculature through gap junctions at the end of their processes. The Haversian canals are connected to each other vertically by Volkmann's canals. Canaliculi that are open to Haversian and Volkmann's channels and the bone surface provide a root for extracellular fluid transportation.

The remaining 20% of the mass of solid bone in the body is the cancellous bone, otherwise known as trabecular bone, which is made of a network interconnected bony rods and plates known as trabeculae (c.f. Figure 2.19). Cancellous bone fills the end of long bones beneath the cortical shell and its trabeculae are oriented in directions to provide the best mechanical support and load distribution throughout the tissue. The trabeculae consist of parallel sheets of lamellae separated by cement lines, preferentially aligned with the orientation of trabeculae. The epiphysis and metaphysis regions of the femur consist of cancellous bone. When a hip stem is placed in the femur its proximal

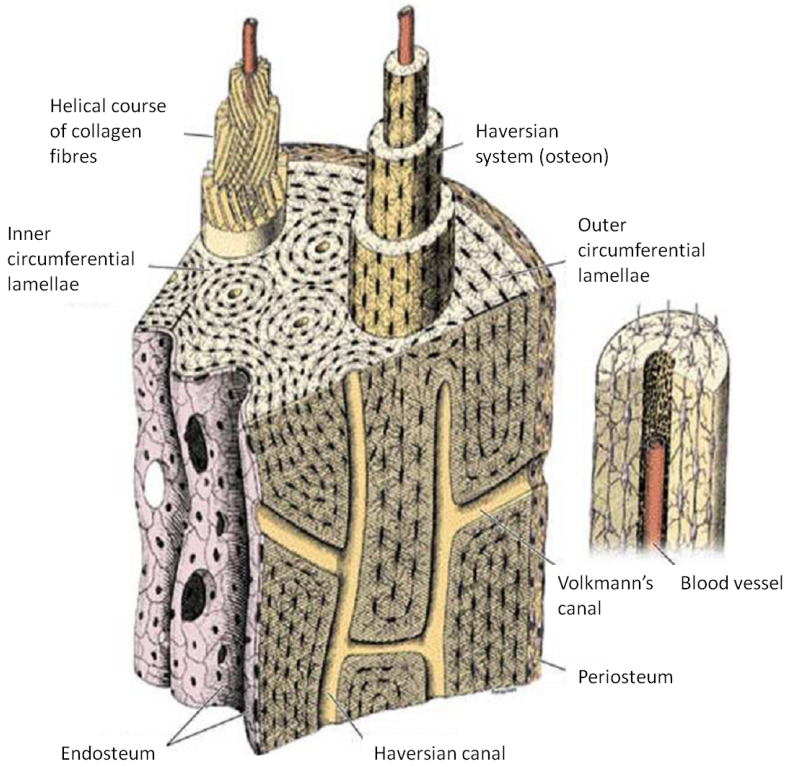

Figure 2.18: Osteon Structure.[9]

region comes into contact with cancellous bone while its distal region is in contact with cortical bone.

2.5.2 Blood supply and lymphatic circulation in the femoral bone

Bone tissue in the femur is highly vascularised. However, the source of blood supply is not the same for different regions of femur. The diaphysis region is mainly supplied by an artery commonly known as the 'principle nutrient artery' that penetrates the femoral shaft distally and branches off in the endosteal cavity [96] (c.f. Figure 2.20). This region is also supplied, but to a lesser extent particularly in younger people, by smaller, but many, periosteal arteries penetrating its outer surface. Epiphysial and metaphyseal regions of the femur are supplied by a great number of small blood vessels encircling and penetrating the external surface of the bone in these regions (c.f. Figure 2.20). Before they reach the bone they must travel almost the entire length of the neck within the capsule. In the capsular region these vessels are covered by loose folds of svnovial membrane which leaves them exposed to the capsular pressure [83]. Churchill and Brooks [97] demonstrated that arterial vessels enter these regions from medial, lateral and superior surfaces. Anastomosis between these penetrating arteries provide

[9]Image from: http://en.wikipedia.org/wiki/File:Illu-compact-spongy-bone.jpg. Last checked on August 2011

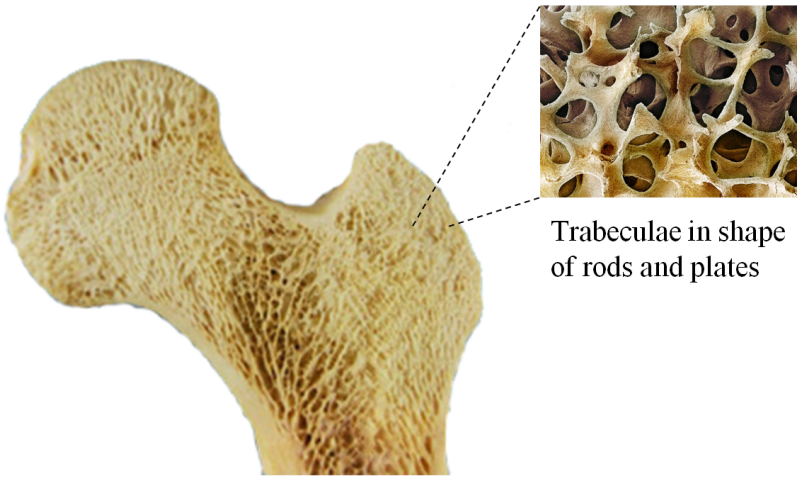

Figure 2.19: Trabecular bone.[10]

a rich vascular network within the cancellous bone in these regions. There is no clear border between the regions supplied by different blood supplies and they often merge with each other by anastomosis. In addition, one source can extend to supply other regions when there is impairment to another. This is indeed the case for an implanted femur in which the femoral cavity is filled with the implant stem. It has been shown that two thirds of the total supply to the bone surrounding the implant is supplied by periosteal, epiphyseal and metaphyseal arteries [98].

Blood is drained from the femur by veins leaving the bone in various locations. It has been suggested that the greater portion of blood in diaphysis is drained from the periosteal surface rather than endosteal [99]. This is supported by the observation that intravascular pressure drops from about 8 kPa to around 2 kPa from endosteum to periosteum surfaces [96]. Blood in epiphyseal and metaphyseal regions drain from numerous veins leaving the bone tissue from its outer surface similar to arterial supply shown in Figure 2.20. This drainage is facilitated by the very thin wall of venous sinuses of bone marrow that provides the ease of fluid exchange between the bone fluid and the vascular system.

As mentioned in section 2.3.5.8, the existence of lymphatic vessels in the bone and bone marrow around an implant is controversial. While Jell et al. [71]were able to demonstrate the existence of lymphatic capillaries in the majority of periprosthetic tissues, Edwards et al. [72] showed that lymphatics were only present in the hip capsule after arthroplasty and not in the femoral bone-implant interface. Whether lymphatic pathways exist in the femoral bone is significant because they would provide

[10]Image from: http://www.answersingenesis.org/articles/am/v4/n4/architects. Last checked on August 2011

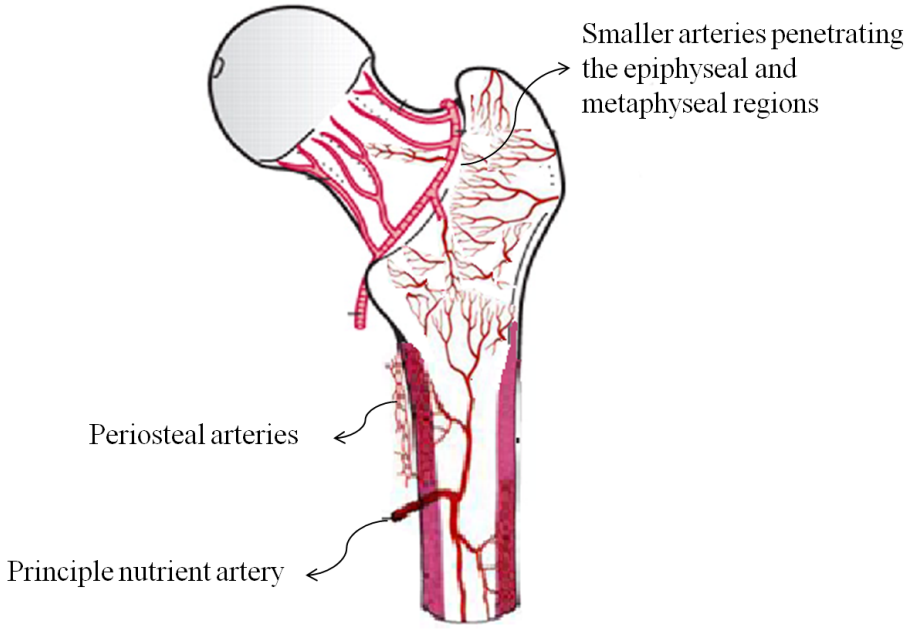

Figure 2.20: Femoral bone blood supply (manually created)

an important mechanism by which wear particles can be transported to different regions or out of the periprosthetic tissue.

2.5.3 Bone tissue: fluid phase

Bone tissue also contains fluid constituents which occupy the porous solid components. Apart from blood which flows in the bone vascular system, other fluids in the bone tissue are interstitial fluid, which is mainly found in cortical bone, and the more viscous bone marrow within cancellous bone.

Interstitial fluid, also known as tissue fluid, fills, and flows within, the spaces of bone mineral matrix and can be considered as the intermediate medium between bone tissue and cells, and the vascular system. It plays an important role in physiological and biological process such as metabolism, growth, repair and adaptation. Its flow within the bone matrix is also important in mechanosensation of bone cells responsible for bone resorption and formation. These cells can detect their surrounding mechanical environment by the hydrostatic and shear stresses imposed on them by the flow of this fluid [100]. Interstitial fluid has ionic composition similar to that of plasma which behaves like a Newtonian fluid [101]. In mathematical modelling of bone as a poroelastic material, interstitial fluid is often modelled with properties of salt water [102].

Bone marrow is usually found to be red or yellow [103]. In the proximal femur which is of the interest in this study, bone marrow is red and highly vascularised (c.f. Figure 2.21). In red marrow, the small vessels are thin walled sinusoids with minimal hindrance

to molecular exchange. They are called sinusoids because of their size which is many times the size of the ordinary capillaries. In the literature, bone marrow is referred to as the whole substance filling the medullar and cancellous cavities. However, this substance is composed of non-fluid constituents including blood vessels, marrow and fat cells and a loose connective framework which maintains the mechanical integrity of the tissue [103] (c.f. Figure 2.21). While the fluid compartment of the marrow may flow in the bone, non-fluid constituents may be stationary and exert resistance to the flow of fluid. In experiments to measure bone marrow viscosity performed by Bryant et al. [103], five bovine samples from sites at the proximal and distal ends of the marrow cavity immediately adjacent to the cancellous bone were obtained. In order to measure bone marrow viscosity, samples were 'broken up' using a glass rod, wormed until liquid, and then filtered through a fine square mesh with aperture size of 0.5×0.5 μm. The amount of marrow obtained in liquid form after filtration of the proximal marrow weighed approximately 70% of the weight of the original mixture. The obtained liquid after filtration was opaque. To remove cell debris, blood and other granular material, this opaque liquid was centrifuged which resulted in a clear yellowish liquid. Viscosity measurements were carried out on both the opaque and clear liquids. Their measurement for bone marrow viscosity at in vivo temperature assuming it as a Newtonian fluid was approximately 0.05 $\mathrm{kgm^{-1}s^{-1}}$ for both liquids. The fact that they had to break up the samples and filter them to obtain marrow in liquid form may confirm the existence of non-fluid constituents in marrow, which can exert resistance to any fluid flowing in the system.

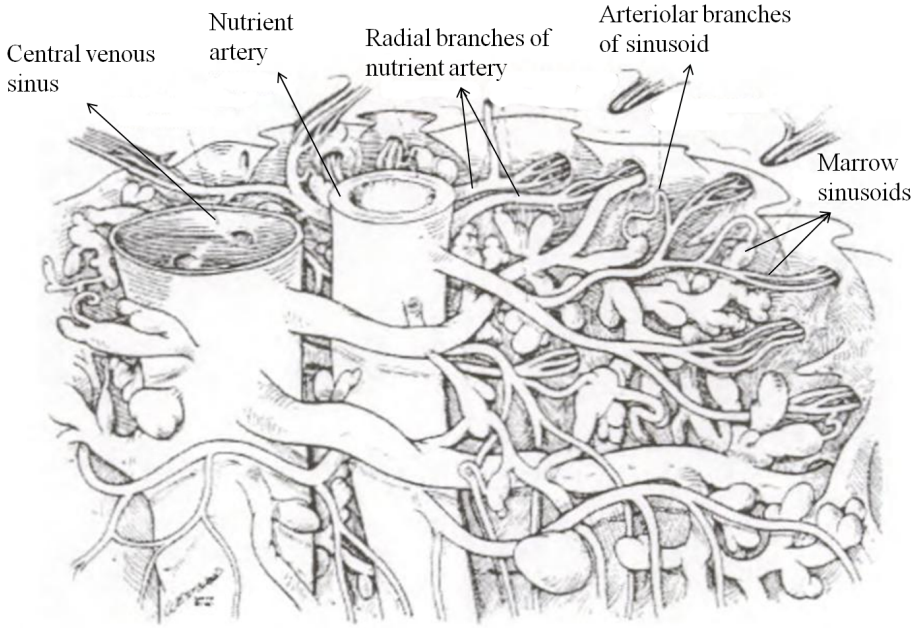

Figure 2.21: Vasculature of the bone marrow. Arterioles and sinusoid branches occupying the space in the marrow tissue [104].

2.5.4 Porosity levels in bone tissue

There are four levels of porosity within the bone tissue to which the mentioned fluids may flow: vascular porosity, the lacunar-canalicular porosity, the collagen apatite porosity and intertrabecular space porosity. Vascular porosity with typical size of 20 μm refers to the cylindrical passageways (osteonal or Volkmann canals) containing vasculature where bone interstitial fluid can freely be exchanged with vascular fluid. The lacunar-canalicular porosity has a much smaller porosity (0.1 μm) and its residing fluid has higher pressure than vascular porosity. Lacunar-canalicular porosity is filled with bone interstitial fluid and glycocalyx which functions as a gel. The intertrabecular porosity is associated with cancellous bone and may be considered as the largest one with pore size up to 1 mm. The pore size, however, decreases at load-bearing surfaces such as the femoral head. In descending order of length scale, the marrow cavity, the vascular porosity and the lacunar-canalicular porosity are all well connected to each other to form a hierarchical system of pore fluid space [105].

Any extra-osseous fluid such as joint fluid that finds its way to the bone tissue flows through this complex system if sufficient pressure gradient is provided and is finally drained out of the system by the lymphatic and venous draining vasculature which leaves the bone tissue mostly from periosteal surfaces [97, 98]. To define this flow, a material property called 'permeability' can be used. Permeability defines the ability of a porous medium to conduct fluid. The permeability of bone tissue for cortical and cancellous bone has been measured and is discussed in the following sections.

2.5.5 Permeability and Darcy's law

Darcy's law describes the flow of fluid through porous media. The original Darcy's equation (Eqn. 2.1) describes the relationship between the averaged volumetric flow rate per unit cross-sectional area (Q_A) of a fluid to a medium, and the pressure gradient necessary to induce such a flow (∇p), as a function of a constant known as 'hydraulic permeability', K (ms^{-1}). Hydraulic permeability is a parameter dependent on both the fluid and porous medium properties.

$$Q_A = K\frac{\Delta P}{\Delta L}. \tag{2.1}$$

However, a more appropriate and generally accepted form of Darcy's permeability is

$$K = \frac{k}{\mu}, \tag{2.2}$$

where, k (m^2) is the 'intrinsic permeability' of the porous medium and μ ($\mathrm{kg.m}^{-1}.\mathrm{s}^{-1}$)

is the dynamic viscosity of the fluid. The advantage of using intrinsic permeability is that it is a parameter independent of fluid properties and a function of the porous meduim only. Therefore, the Darcy's equation in vector form can be written as

$$Q_A = \frac{1}{\mu} k \nabla p \tag{2.3}$$

The permeability values for bone presented in the literature are the intrinsic permeabilities. The permeabilities used in the simulations in the current study are also the intrinsic permeabilities. Thus, from this point intrinsic permeability is referred to as permeability only.

2.5.6 Permeability of cancellous bone

Cancellous bone displays a wide range of porosity even when porosity is measured within a single skeletal (proximal femur) site. The reported permeability values measured for femoral cancellous bone are shown in Table 2.6. Histological examination in these studies show that cancellous bone exhibits no void shape consistency when samples are excised from different anatomical sites. It can be seen that available data for permeability of cancellous bone range over three orders of magnitude and depends on porosity and the anatomical direction of measurements. It has been shown that permeability can vary, even at fixed porosity, by one order of magnitude depending on how aligned the flow direction is with the trabeculae [102].

In all these measurements Darcy's law was utilised to measure the permeability. The specimens were mounted in a chamber and volumetric flow rates as the result of pressure differences from one surface to the opposite were measured while it was ensured that flow remained in a Darcian region (Re <1). All the permeability measurements for cancellous bone, including the ones cited here in Table 2.6, have been performed after removing the bone marrow from the bone tissue which has a considerable effect on the measurements.

Other factors may also contribute to the large variation in data seen Table 2.6. Most of the measurements are carried out using water or saline which are Newotonian fluids. In these measurements the reported permeability is, therefore, independent of the viscosity of the fluid. However, Grimm et al. [106] used linseed oil, which is a non-Newotonian fluid, for their measurements. Since, in non-Newtonian fluids viscosity of the fluid is not constant at different velocities, their permeability value is not entirely a function of the porous medium. In addition, specimens used by Thompson et al [107] were from osteoarthritic bone which may have different porous structural properties than normal bone.

Table 2.6: Reported values of cancellous bone permeability for various anatomical sites and flow directions.

Reference	Anatomic site	Orientation	Permeability ($\times 10^{-10}$ m^2)	Porosity
Nauman et al. [108]	Human proximal femur	Longitudinal	20.76 ± 19.1	0.73 ± 0.06
Nauman et al. [108]	Human proximal femur	Transverse	1.2 ± 1.1	0.73 ± 0.02
Nauman et al. [108]	Bovine proximal tibia	Longitudinal	31.7 ± 10.2	0.75 ± 0.06
Nauman et al. [108]	Bovine proximal tibia	Transverse	7.4 ± 8.3	0.75 ± 0.07
Hui et al. [109]	Porcine proximal Femur	Transverse	0.1 - 0.48	0.28 - 0.65
Hui et al. [109]	Porcine proximal Femur	Longitudinal	0.1 - 12	0.28 - 0.65
Thompson et al. [107]	Human proximal Femur	Longitudinal	1.155 ± 1.2	0.28 ± 0.076
Kohles et al. [110]	Bovine distal Femur	Transverse	2.33 ± 0.5	0.65 ± 0.09
Kohles et al. [110]	Bovine distal Femur	Longitudinal	4.65 ± 1.2	0.65 ± 0.09
Pakula et al. [111]	Human proximal Femur	NA	0.08 - 10.15	0.67 - 0.96

2.5.7 Permeability of cortical bone

Cortical bone has much more compact structure compared to cancellous bone and contains two levels of vascular and lacunar-canalicular porosity, as mentioned in section 2.5.3. Because of its compact nature, which makes experimental measurements difficult, most of the porosity and permeability values for cortical bone are based on theoretical calculations rather than direct experimental measurements. However, there are also a few experimental studies measuring cortical bone permeability.

Li et al. [112] measured the permeability of cortical bone in canine tibia. They demonstrated that the tibial cortex is impermeable in the presence of the 0.5-1 mm thick periosteal tissue. Periosteal tissue consists of collagenous fibres, fibroblasts in the outer layers and multiple layers of bone cells in the inner layer [102]. Once this dense compact layer is removed, a pressure gradient across the bone would result in fluid flow, primarily in the Haversian and Volkmann's canal, and secondarily in the lacunar-canalicular spaces. This hypothesis is consistent with observations by Smith et al. [113] that the bone fluid mainly drains into the Haversian canals. They reported a mean permeability of 5.0 $\times 10^{-15}$ m^2. This permeability corresponds to the vascular level porosity since this porosity provides the path of least resistance for the fluid to flow within the tissue.

Assuming that the permeability of cortical bone is isotropic and can be estimated from ideally closed packed arrays of annularly shaped Haversian system of inner radius of 25 μm and outer radius of 125 μ m, Zhang et al. [105] calculated the porosity of 0.04 for cortical bone, which is the square of inner-to-outer radius ratio of the Haversian system. However, this porosity contains blood vessels (15 μm in diameter) and nervous fibres which are considered as immobile soft tissue. Assuming the central part of the vascular porosity is occupied by this immobile soft tissue, they estimated the effective porosity to be 0.018. Using a model consisting of parallel tubes, they evaluated the bone permeability at vascular level to be $k = 6.35 \times 10^{-13}$ m^2. They also estimated the permeability of a porous medium consisting of only the lacunar-canalicular to be $k = 1.47 \times 10^{-20}$ m^2. A summary of the measured and estimated values for cortical permeability are presented in Table 2.7. When considering cortical bone tissue at large scale, the role of smaller lacunar-canalicular pore spaces is minimised in their contribution to hydraulic fluid flow due to the extreme difference in their relative permeabilities.

2.5.8 Porosity-permeability relation for bone tissue

Various models are used in the literature to describe the porosity-permeability relationship for different porous media. One of them is a hydraulic radius-based capillaric model in which the porous medium is assumed to be hydraulically equivalent to a bed

Table 2.7: Reported values of cortical bone permeability.

Reference	Vascular permeability ($\times 10^{-14}$ m^2)	Vascular porosity	lacunar-canalicular Permeability ($\times 10^{-20}$ m^2)	lacunar-canalicular porosity
Zhang et al. [105]	63.5	0.04	1.47	0.05
Li et al. [112]	0.5	-	-	-

of thin tubes. The most commonly accepted form of radius-based model is called the Kozeny model in which the tubes are assumed to be straight. However, in reality, not all the porous media, including cancellous bone, can be represented by straight tubes. An extension of this model introduces a tortuosity factor that accounts for bends in tubes. Later this model was improved and named the Kozeny-Carmen model to represent media with random pore structure similar to that of cancellous bone. Arramon and Nauman [101] employed this model to obtain a good fit to cancellous bone. They presented the fit in the form of the following equation:

$$k = \frac{c\phi^{\alpha}}{S_v(\phi)^2}, \tag{2.4}$$

where k is the permeability, ϕ is the porosity, c and α are correlation coefficients, and $S_v(\phi)$ is the bone specific surface function. The functional form of the specific surface is a fifth order polynomial in terms of the porosity, ϕ, and was empirically determined from a wide variety of species over a large range of porosity. The appropriate specific surface S_v for bone is given by

$$S_v(\phi) = 323.\phi - 939.\phi^2 + 1340.\phi^3 - 1010.\phi^4 + 288.\phi^5 \qquad (1/\text{cm}) \tag{2.5}$$

The fit constants for permeability-porosity experimental data obtained by Arramon and Nauman [101] are $c = 2.592 \times 10^{-2}$ and $\alpha = 4.668$. This permeability-porosity relationship is shown in Figure 2.22.

2.5.9 Hydraulic resistance of the whole bone structure

As mentioned in previous sections, the porous medium surrounding the interfacial gap is a complex system including bone marrow confined in the trabeculae of cancellous bone, the soft tissue consisting of vasculature, cells and a loose connective framework which maintains the mechanical and functional integrity of the marrow, porous cancellous bone, the cortex of cortical bone and the relatively impermeable layer of periosteum tissue. Therefore, the resistance to flow in this system is a function of local organization of hard and soft tissue. All permeability measurements in the literature are carried

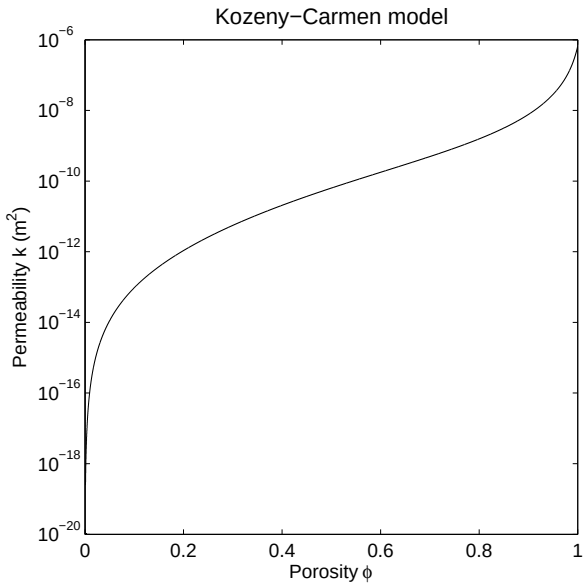

Figure 2.22: The best fit empirical Kozeny-Carmen model relating permeability and porosity for human, bovine and porcine cancellous bone at different anatomical sites obtained by Arramon and Nauman [101].

out on individual specimens from cancellous bone without marrow or from specimens of cortical bone without the periosteal layer. There is not a realistic value in the literature for the hydraulic resistance of this system. However, there is one study from Simkin et al. [114] in which the hydrostatic resistance in such a system is established by recording the hydrostatic pressure response to transchondral injections of saline into the cancellous region of canine humerus when the cortical cortex was and was not in place. In their experiment, a hole was drilled into the humeral head and then a 14 gauge aspiration needle was inserted at the same site to a depth of 9 mm. The injection liquid was coloured with blue dye to facilitate detection of possible leakage through the needle track as well as detection of drainage paths. A pump was connected to the needle which was run to establish a level intraosseous pressure response to each individual flow rate. The pressure was then recorded for each saline flow rate. After completion of this experiment, the needle was left in place and the surrounding bone was removed creating four vertical cuts at right angles to each other and 5 mm away from the injection needle. The needle was left in this rectangular block of trabecular bone and then a horizontal cut was made 7 mm beneath the tip of the needle. Another series of pressure-flow measurements was carried out for these cubes. They calculated the hydraulic resistance of the injection site as the slope of pressure against flow rate plots. The average value for the pressure-flow measurements and their slope for fourteen specimens of whole humerus and humeral cubes are shown in Figure 2.23 in appropriate units for the current study. The hydraulic resistance values presented here are used to calculate permeability of the bone-marrow system in the next chapter.

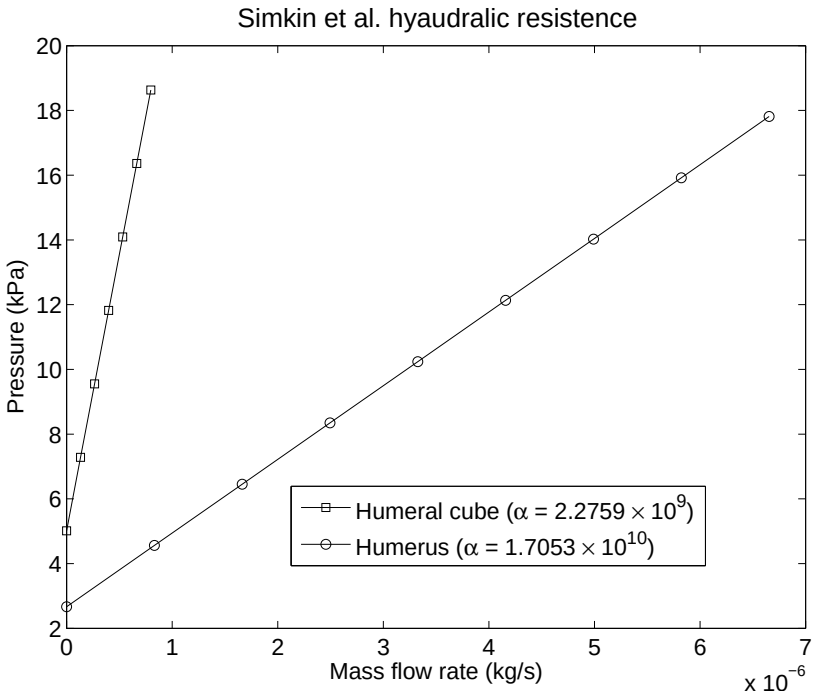

Figure 2.23: Mean hydraulic resistance represented as the slope of pressure vs. mass flow rate in bone of canine humerus before and after 'cubing' by removal of surrounding bone [114].

2.6 Summary

In this chapter, the potential causes of osteolysis in THRs, including high fluid pressure/velocity and wear particles, were addressed. It was mentioned that periprosthetic flow, distributing high fluid pressure/velocity and particles in the effective joint space, may originate from high capsular pressure and/or interfacial gap micromotion. However, there is no clear understanding on how these mechanisms cause or affect the periprosthetic flow. In the following chapters, it is attempted to shed a light on how capsular pressure and gap micromotion contribute to periprosthetic flow and particle migration to the interface tissue using computational simulations. In addition, the effect of particle clogging and fibrous tissue generation due to high particle concentrations and their implication on osteolysis generation and progression are addressed in the simulations.

Chapter 3

Modelling methodology and verification studies

3.1 Introduction

Having established the key elements contributing to the periprosthetic flow, this chapter describes the development and verification process for the primary computational models that can be employed to simulate the periprosthetic flow, particle migration, particle clogging and changes in local permeability due to high particle concentrations representing the fibrous tissue present in osteolytic lesions.

3.2 Model construction

3.2.1 The geometry

The geometry constructed for simulations was obtained from a cross-sectional cut of a developed realistic 3D model of an implanted femur and the surrounding joint capsule. To develop the 3D model, all solid body operations were carried out in Solidworks (Dassault Systèmes, Vélizy, France), which included positioning a commonly used cementless femoral stem (Summit stem, DePuy, Warsaw USA) in the femur (reconstructed from computerised tomography (CT) scans) (c.f. Figure 3.1). The joint capsule was created by extruding a solid wall from the proximal cut surface on the femur to the edges of the acetabular component.

To obtain the 2D geometry, a cross-sectional cut was made on the coronal plane, passing through the symmetric axis of the implant (c.f. Figure 3.2), and then this was transferred to the geometry modelling and meshing software GAMBIT (version 2.4.6, Ansys INC, Canonsburg, PA). A user specific code was developed in GAMBIT to automatically create gaps with the desired length (l) and width (w) between the bone and implant, and to separate capsule, gap and bone regions from each other. The

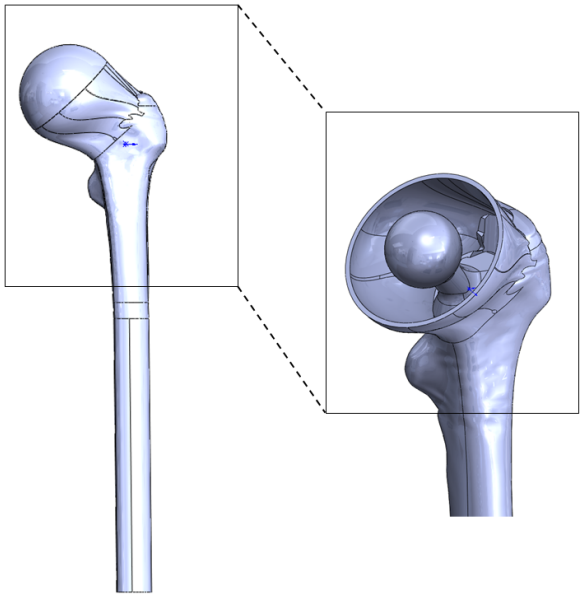

Figure 3.1: Anatomically derived 3D model of an implanted femur and the surrounding joint capsule.

schematic of a generated interfacial gap in communication with the joint capsule, and its interface with the periprosthetic bone can be seen Figure 3.2.

3.2.1.1 Gap dimensions

The choice of gap lengths in the current work was designed to cover the range in which radiolucent lines are seen along the femoral stem in radiographs [87] as discussed in section 2.4.2.2. Proximal gaps are represented by a short 5 mm gap and long gaps are represented by a 80 mm gap that nearly reaches the tip of the stem.

For the gap width, the upper limit of 500 μm was defined based on the study by Howard et al. [88] in which the threshold of 500 μm was chosen to detect the existence of interfacial gaps using Computer Tomography (CT) scans. The lower limit of 30 μm was fixed based on technical difficulties associated with the meshing process. Any narrower gap would result in very large aspect ratios between the length and width of the gap and, consequently, excessively large number of cells would be required. The computational cost of such models was particularly high when dynamic meshing was included to simulate implant motion.

3.2.2 Meshing the model

Another code was also written to mesh the generated models automatically. The gap region was meshed by structured quadrilateral cells whereas the rest of the model was meshed by unstructured quadrilateral cells using the 'pave' meshing scheme. Meshing the model required specification of many meshing parameters because of the very high

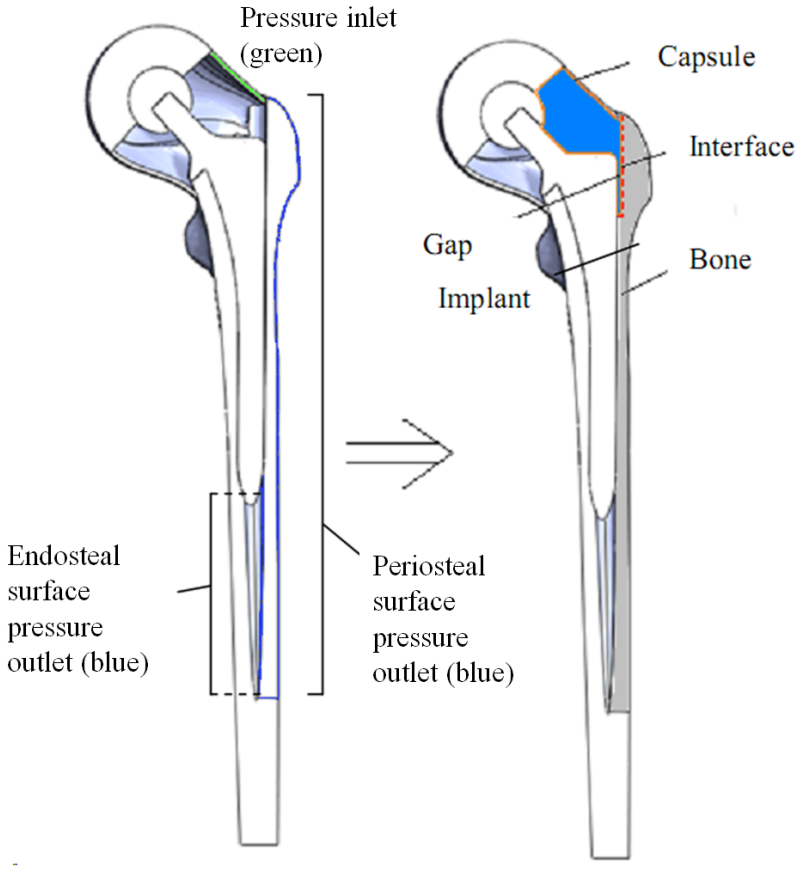

Figure 3.2: Cross-sectional cut of the 3D geometry that was employed to generate the 2D model. A gap in communication the joint capsule and its interface with the periprosthetic bone can be seen. The model boundary conditions as the capsule pressure inlet (in green) and periosteal and endosteal pressure outlets (in blue) can be seen.

aspect ratio between length, l, and width, w, as well as the dimensions of the gap itself with respect to the size of the entire model. All the implant walls and the fluid-porous interface were covered with boundary layer meshes. The meshed geometry of one of the models is shown in Figure 3.3. Details of the meshing process is further discussed in the model verification section (c.f. section 3.3).

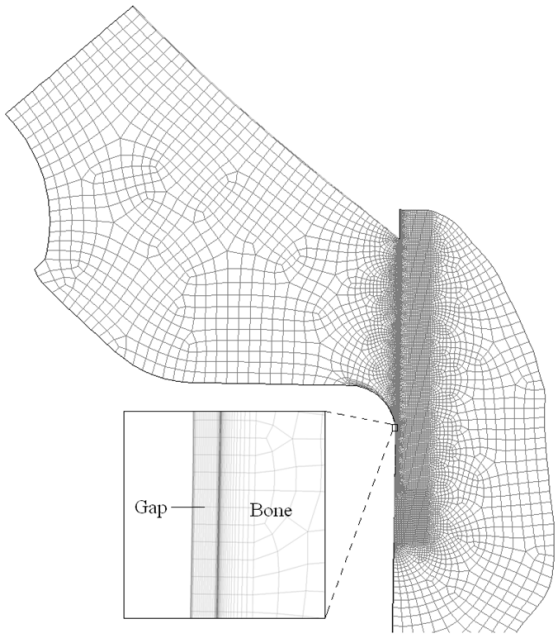

Figure 3.3: The meshed geometry for a 5mm length and 30 μm width gap to demonstrate an example of a meshed geometry. Models with different lengths and widths are meshed in the same manner. It can be seen that mesh resolution is much higher in the gap region and its surrounding bone where there are large flow gradients in the model.

3.2.3 Model constituents and their governing equations

The meshes were imported to the commercial CFD software Fluent (version 12.1.4, Ansys INC, Canonsburg, PA) in which the capsule and gap regions were modelled as fluid continua, the bone was represented as a porous medium and the implant wall was described as a moving rigid wall. The fluid flowing in the capsule, gap and the bone was modelled with the properties of liquid water with constant viscosity and density of 0.001 kg/ms and 998.2 kg/m^3, respectively. Based on arthrographic studies [78, 6] mentioned in section 2.4.1.4, it was observed that the contrast agent injected to the joint capsule immediately finds its way to the interfacial gaps and osteolytic lesions in communication with them. Therefore, it was assumed that the synovial fluid occupies the interfacial gaps and it can easily flow to the interface. It was not possible to model the situation in which the bone and implant are in contact, i.e. a completely closed gap. There always had to be an initial mesh for the gap at the interface to start the simulation. Laminar viscous flow was assumed to solve the Navier-Stokes equations

in these regions. The periprosthetic bone was described as a simple porous medium in which the fluid momentum loss was defined by Darcy's equation. This momentum loss, determined by the intrinsic permeability constant described in section 2.5.5, was added as a sink term to the Navier-Stokes equations:

$$\rho[\frac{\partial \mathbf{v}}{\partial t} + \mathbf{v}.\nabla\mathbf{v}] = -\nabla P + \nabla.(\mu\nabla\mathbf{v}) - (\frac{\mu}{k})\mathbf{v} \tag{3.1}$$

where, $\mathbf{v}$ is the fluid velocity (m/s), ρ is the fluid density (kg/m^3), t is time (s), P is the fluid pressure (Pa), μ is the dynamic fluid viscosity (kg/m.s) and k is the porous medium permeability (m^2).

The approach to calculate the intrinsic permeability of the periprosthetic bone is described in section 3.2.5.

3.2.4 Solver setups in Fluent

Table 3.1 shows the setup for the simulations. The default Fluent under-relaxation factors for convergence were used. The pressure-based solver uses a solution algorithm where the governing equations are solved sequentially. Because the governing equations are nonlinear and coupled, the solution loop must be carried out iteratively in order to obtain a converged numerical solution. Second order discretization was used for momentum for more accurate solutions and Standard pressure discretization was employed since it is the method recommended by Fluent for models with porous media [115]. Pressure-velocity coupling was achieved by the SIMPLE algorithm which uses a relationship between velocity and pressure corrections to enforce mass conservation and to obtain the pressure field.

Table 3.1: Simulation and solver setups in Fluent.

Simulation Methods	Scheme
Solver	Pressure based
Pressure-velocity coupling	SIMPLE
Spatial discretization (gradient)	Least square cell based
Spatial discretization (pressure)	Standard
Spatial discretization (momentum)	Second order upwind
Viscous model	Laminar

3.2.5 Effective permeability of the periprosthetic tissue

As mentioned in section 2.5.9, the hydraulic resistance of the whole bone system surrounding a gap cannot be represented by permeability measurements in the literature mentioned in section 2.5.3 since they are carried out only on individual specimens

from cancellous bone without marrow and the local soft tissue or from specimens of cortical bone without the periosteal layer. However, there is one study from Simkin et al. [114] in which a hydrostatic resistance in a whole bone system is established by injecting saline into a intact humerus as well as a cube of cancellous bone with marrow in place which was cut out from the humerus. This experiment presents the hydrostatic resistance of the system as the slope of a graph plotting injection pressure against fluid flow rate into the system. However, this hydrostatic resistance does not have the same definition of the permeability defined in the literature and used in the Fluent CFD software employed here. To obtain a realistic value, a simple 3D CFD model was developed resembling a part of Simkin et al. [114] experiment in which they injected saline into a cube of cancellous bone with marrow in place (c.f. section 2.5.9).

The geometry and the boundary conditions of the model are shown in Figure 3.4. Since the geometry is symmetric only one fourth of it was modelled. The dimensions are taken from [114] and pressure boundaries were defined as those in the experiment; an inlet pressure at the tip of the needle and outlet pressures on the outer surfaces of the surrounding bone except the top side which is covered by chondral bone. This chondral bone and the needle wall are represented by solid walls. A mesh convergence study based on fluid velocity was carried out to establish an appropriate mesh with sufficient resolution in areas of high velocity gradient. This mesh consisted of unstructured hexahedral cells. The needle solid wall was covered by boundary layers and the mesh near the inlet, where high velocity gradients were observed, had a higher resolution (c.f. Figure 3.4). The solid wall at end of the needle, where pressure inlet was defined, had a curved interface with the surrounding porous bone for easier meshing. A verification study showed no more than 5% variation in fluid velocity around near the inlet for finer meshes (c.f. Figure 3.4).

The model was run with different permeability values ranging from 1×10^{-8} to 1×10^{-18} m^2. For each permeability value the mass flow rate from the needle to the model was recorded at different pressures similarly to the experimental procedures and compared to the experimental values presented in Figure 2.23.

Figure 3.6 shows hydraulic resistance, calculated as the slope of pressure vs. mass flow rate, for experiments on humeral cube and whole humerus (c.f. Figure 3.4), and computed values at different permeabilities. The figure shows only the computed values for permeabilities that were close to the experimental values. It can be seen that, while the permeability value of $\alpha = 7.12 \times 10^{-14}$ m^2 yields similar results for the humeral cube, the permeability, $\alpha = 1.00 \times 10^{-14}$ m^2, represent the increased hydraulic resistance in the whole humerus caused by the presence of the cortical shell. Therefore, the value of $\alpha = 1.00 \times 10^{-14}$ m^2 was deemed to be a suitable representative value to use for further simulations. This value is between the lower and upper limits of reported permeabilities mentioned in section 2.5.3 and accounts for the extra resistance that

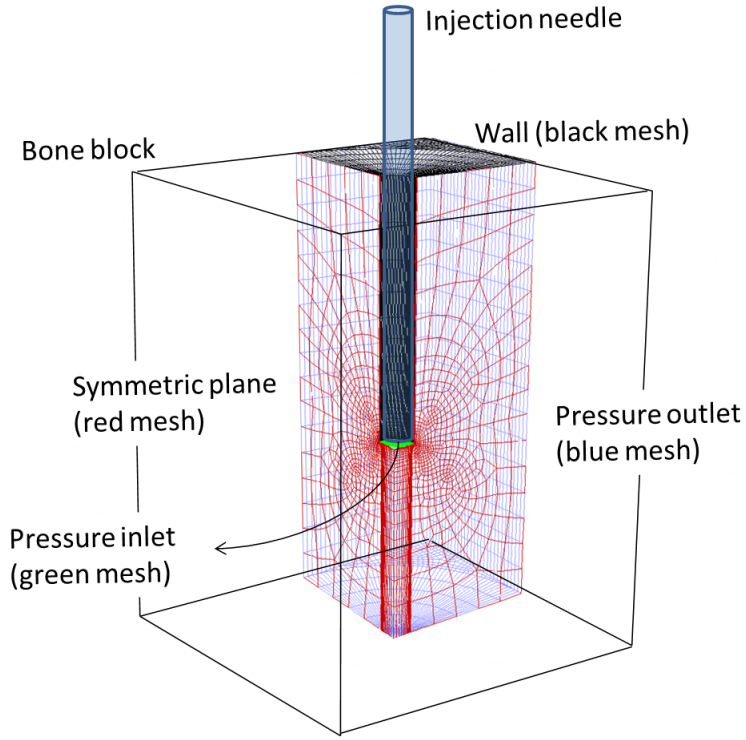

Figure 3.4: 3D model constructed based on the Simkin et al. [114] model. The mesh and the boundary conditions of the model are shown. Since the geometry is symmetric only one fourth of it (shown inside the box representing the whole cube) was modelled

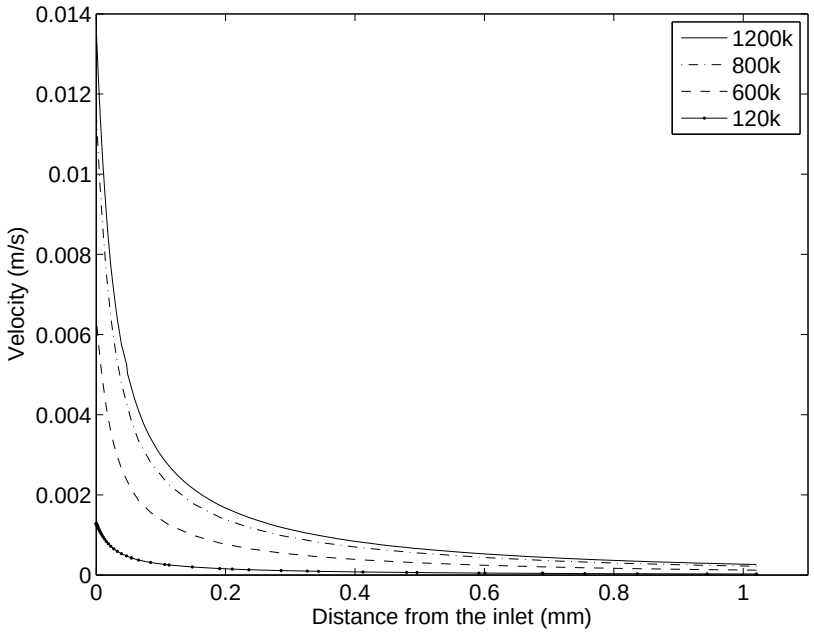

Figure 3.5: Plot of velocity at a profile line located around near the inlet region where velocity gradient is large. The figure shows that there is less than 5% variation in velocity between 1200k and 800k meshes.

bone marrow (the residing soft tissue) and the cortical shell may exert on the flow.

This value was further verified by carrying out simulations on the models used in the current study with permeabilities ranging from 1×10^{-8} m^2 to 1×10^{-20} m^2. It was seen that with a permeability of 1×10^{-14} m^2 fluid velocities in the bone ranged from a few μm/s to a few mm/s depending on gap dimensions and capsular pressure. The scale of fluid velocities obtained seemed the most plausible relative to those obtained at other permeability values when compared with velocities of blood flow in the vasculature of long bones, ranging from 1.5 mm/s in arterioles to 100 μm/s in venules [116]. Since a major route for the fluid to drain out of the system is the vascular system leaving the bone from the periosteal surface [97, 98], these values provide a reasonable base for comparison. However, validation of this value is not possible since no studies have been found in the literature that directly measure fluid velocities within the bone under fluid pressure. This permeability value was also verified by models with particles developed in Chapter 5. In this verification study, particles were tracked in the bone with different permeability values. In these models it was observed that permeability outside the range of 0.5×10^{-14} m^2 and 5×10^{-15} m^2 results in unrealistic flow and accumulation of particles in the bone and gap region. For example, permeabilities of 1×10^{-13} m^2 and larger result in penetration of particles to the periosteal surface before they even reach the bottom of a short gap of 5 mm. Also, permeability values of 5×10^{-15} m^2 and smaller result in no penetration of particles into the bone. Both of these cases seem unrealistic since the literature shows that particles can migrate to the bottom of the gaps at distal regions through interfacial gaps [47, 53] and they also penetrate into the bone tissue even several millimetres away from the interface [61].

3.2.6 Boundary conditions

As mentioned in section 2.4.1.3, high pressures in the joint capsule are generated as a result of joint motion or physical loadings in the presence of excessive fluid effusion to the capsule and/or synovitis. Joint motion or physical loadings may increase the pressure by causing volumetric changes in the capsule as a result of tension and stretching in the capsular wall [77]. However, there is a lack of detail in the literature concerning capsular volumetric changes and its relation to the pressure and it was decided to exclude this factor form the models. As a first attempt to model capsular pressure, fluid pressure inside the capsule was generated by a pressure inlet boundary defined on the soft tissue wall of the capsule (c.f. Figure 3.2). This assumption limits the model in predicting the volumetric changes in the capsule and any flow that it may cause within the capsule. However, it should be noted that in both cases of excessive effusion, where the capsule wall is stretched to its maximum elastic length, and synovitis where the capsule wall lacks flexibility, the volumetric change may be small and negligible. In

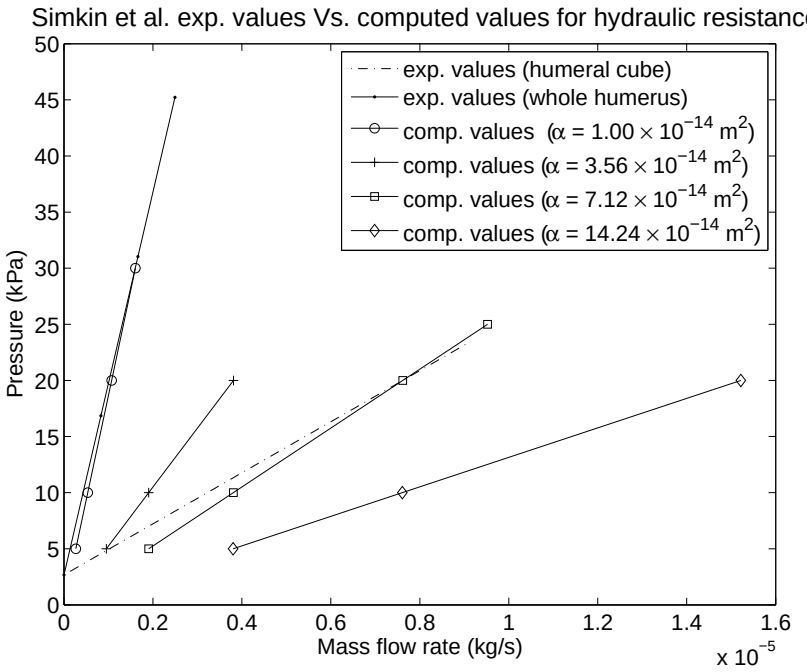

Figure 3.6: Hydraulic resistance represented as the slope of pressure vs. mass flow rate for experimental values obtained from Simkin et al. [114] and computed values from a model resembling their experiment. It can be seen that the permeability value of $\alpha = 7.12 \times 10^{-14}$ m^2 produces similar results for the humeral cube and the permeability value of $\alpha = 1.00 \times 10^{-14}$ m^2 can represent the increased hydraulic resistance in the whole humerus caused by presence of the cortical shell.

light of the findings described in section 2.4.1.2, high and low capsular pressures are defined as 60 and 1 kPa, respectively. The high pressure corresponds to capsular pressures at loading conditions such as stair climbing and the low pressure of 1 kPa was assumed to represent the case of a non-problematic replaced joint in which capsular pressure does not change during physical activity.

The pressure over the porous bone region was assumed to be zero with respect to the capsule (i.e. 0 kPa). This was achieved by defining a pressure outlet on the endosteal and periosteal surfaces of the bone (c.f. Figure 3.2). Zero pressure on the surface of the bone has also been used in other studies [95, 46]. In reality, these surfaces are not entirely open to the fluid flow. The flow may leave the bone only from orifices penetrated by the vascular and lymphatic systems. To investigate the influence of this fact on our model, case studies were setup in which endosteal and periosteal walls were divided into very small sections. Simulations in which only a specific number of these sections allowed fluid drainage were carried out. However no significant differences were observed in the behaviour of the model in all cases.

3.2.7 Implant motion

The displacements of the gap in the proximal lateral region were based on micromotion studies mentioned in section 2.4.2.4. It was shown that the proximal micromotion results in separation between the implant and bone and, therefore, leads to gap opening. Based on those studies a range between 30 μm to 300 μm was chosen for gap opening. As mentioned in section 2.4.2.1 a gait cycle lasts for approximately 1 second. However, dominant axial forces acting on the stem of an implant during a gait cycle reach their maximum value in approximately 0.1s at the beginning of the cycle, and then, after a period of small variation, drop to their original value in around 0.2 s at the end of the cycle [85]. In the current study, the implant motion was displacement-driven and it was assumed that an interfacial gap opens in the first 0.1s, when dominant forces reach their maximum value, and closes in the last 0.1s of the gait cycle when forces are removed from the implant. Therefore, the gait cycle was truncated and simplified to a cosine wave (c.f. Figure 3.7) with a period of T = 0.2 s representing only the instances in which dominant axial forces act upon the implant to open and close the gap. To describe this motion in Fluent, the entire wall representing the implant and its adjacent boundary layer in the model was set to an angular motion pivoting around the bottom of the gap (c.f. Figure 3.8) using a user defined function (UDF) written in C. The angular velocity (rads/s) was defined by

$$\omega = \Omega \sin(\frac{2\pi}{T}t) \tag{3.2}$$

where, Ω is the function amplitude that was adjusted every time for gaps with differing lengths l to generate the desired displacement d at the gap entrance, and T was the truncated gate period. Figure 3.7 shows the velocity and displacement profiles of the implant at the gap entrance when Ω was adjusted for a 300 μm gap opening. Since there is a very large aspect ratio between the gap opening d, and gap length l, the displacement in the y direction can be neglected.

3.3 Verification studies

A verification analysis has been carried out to ensure the solutions are accurate. Preliminary models showed that large variation in the flow velocity occurs in the gap region and its surrounding bone, which are the regions of interest for the current work. For this reason, the mesh refinement studies were focused in these regions. However, because of the large aspect ratios between the width and length of the gap the number of cells in the gap region can be large, particularly for a long gap of 80 mm in which the aspect ratio can be more than 1:2500. Any mesh refinement in these regions, which extend along the entire length of the gap, results in an exponential increase in the total

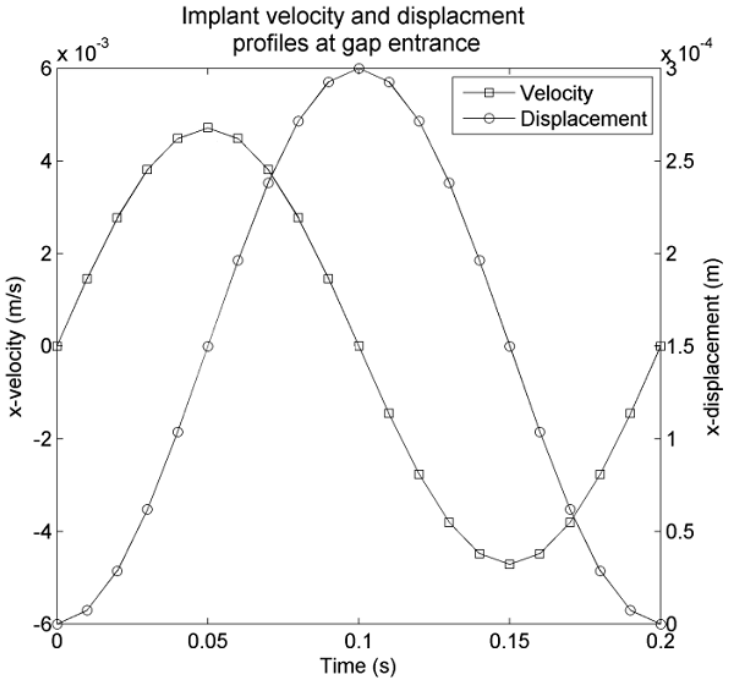

Figure 3.7: Transitional velocity and displacement of the implant in the x direction as a result of the angular motion around the tip of the gap for 300 μm opening. It can be seen that when velocity reaches zero, the gap is open to its maximum displacement and closes as the velocity turns negative.

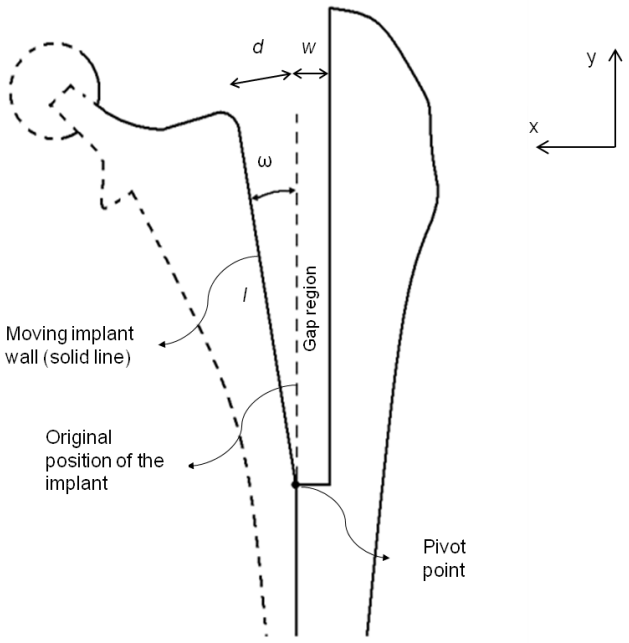

Figure 3.8: Schematic of the implant angular motion around the pivot point at the bottom of the gap (not to scale). The displacement and the size of the gap are exaggerated for demonstration purposes. l and w are the gap length and width respectively, d is the amount of gap opening at the entrance and ω is the angular velocity of the implant.

number of cells. This imposes a computational and memory usage limit on the mesh refinement of the models. Therefore, it was not possible to verify whether further increase in mesh resolution in the gap region could result in a more adequately accurate solution in a full-size model. For this reason, a reduced-size model which only included a small region of the gap at the entrance (30 μm $\times$ 1 mm) and its surrounding bone (1 mm $\times$ 1 mm), where maximum fluid velocity occurs, was generated (c.f. Figure 3.9). This enabled the mesh to be refined further than what is possible in the full size models. The reduced-sized model also eased the process of varying meshing parameters such as core mesh size and boundary layer size without the need of adjusting the entire model for such variations, which was a complex and time consuming process.

The boundary conditions for this reduced-size model were pressure profiles taken from the full size model with the finest possible mesh resolution at the cut surfaces, where it was isolated from the full size model (c.f. Figure 3.9). For a model to be considered converged the momentum and mass residuals had to reach a constant average level.

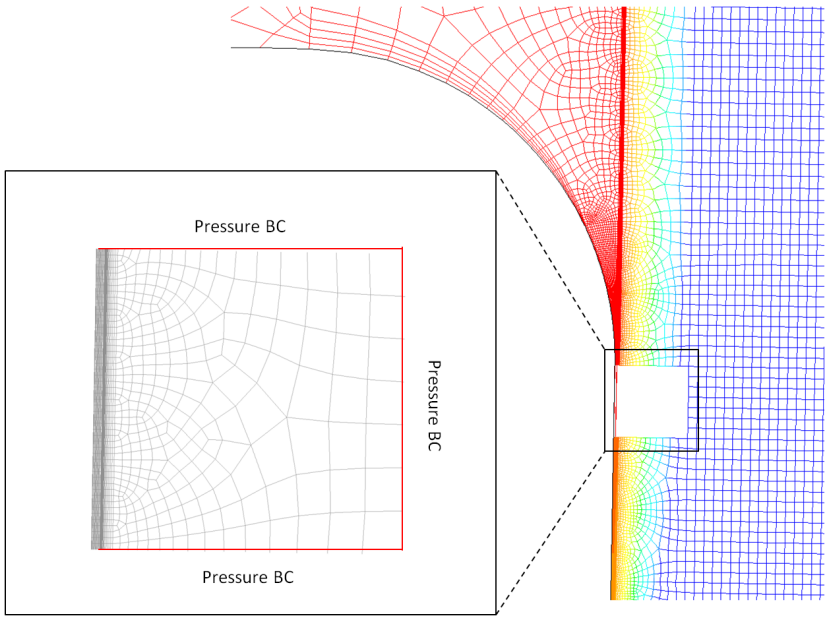

Figure 3.9: Reduced-size model isolated from the full size model. The pressure profile of the surrounding region was used as the boundary condition for the reduced-sized model.

3.3.1 Full-size model mesh verification

For the complete model, the following mesh parameters were varied to determine the affect on the solution: boundary layer resolution on the implant wall in the capsule and gap regions, boundary layer resolution at gap-bone and capsule-bone interfaces on both fluid (capsule and gap) and porous (bone) sides, and the resolution of the core

mesh in capsule, gap and bone regions. The strategy adopted to refine meshes was to approximately increase mesh resolution for each of these parameters in each refinement step to obtain an adequate resolution. This resulted in four mesh resolutions of 76 k, 149 k, 305 k and 1000 k for a geometry consisting of a 30 μm wide and 20 mm long gap.

All the convergence tests were based on velocity profiles at various regions of the model since velocity was the flow variable that showed the largest variation. These profiles included three vertical lines covering the width of the gap from the implant wall to the interface positioned at the entrance, middle and bottom of the gap (gap-ent, gap-mid and gap-bot profile lines, respectively), a vertical line extending from the interface 1.5 μm deep into the bone region (bone-int profile line), and fixed lines in the capsule and bone regions away from the gap region (capsule-line and bone-line, respectively) (c.f. Figure 3.10).

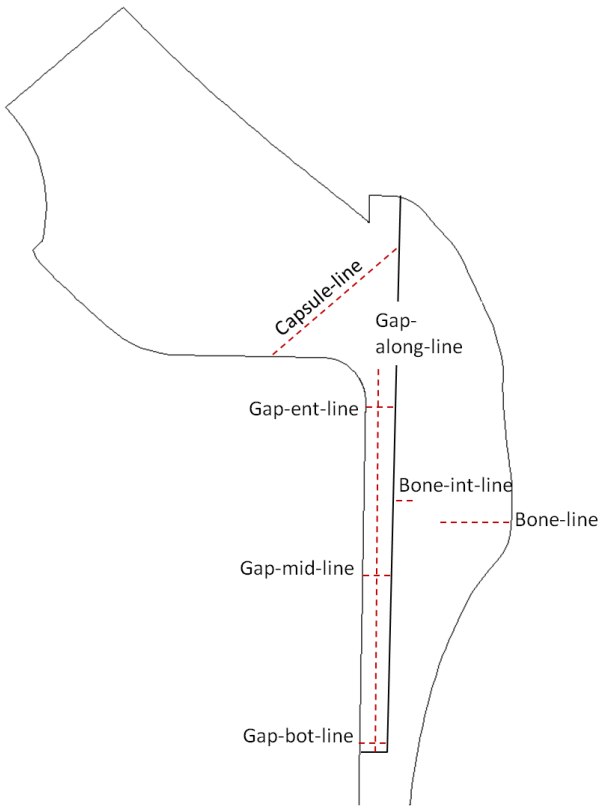

Figure 3.10: Profile line where the velocity measurements for mesh convergence studies are carried out. The schematic is not to scale and only approximate positions of the profile lines are demonstrated.

Velocities were only marginally sensitive to the mesh resolution along the length of the gap as shown in Figure 3.11. Velocity also varied slightly by changing the boundary layers and core mesh resolution in the gap region. Figure 3.12 shows the velocity profiles at the gap-ent profile line for full size model with different mesh resolutions. As can be seen, velocity is only slightly sensitive the mesh resolution along the width

of the gap. The same was observed for the profile lines gap-mid and gap-bot. The velocity measured at profile lines distant from the gap region (capsule-line and bone-line) showed no sensitivity to mesh resolution in those regions.

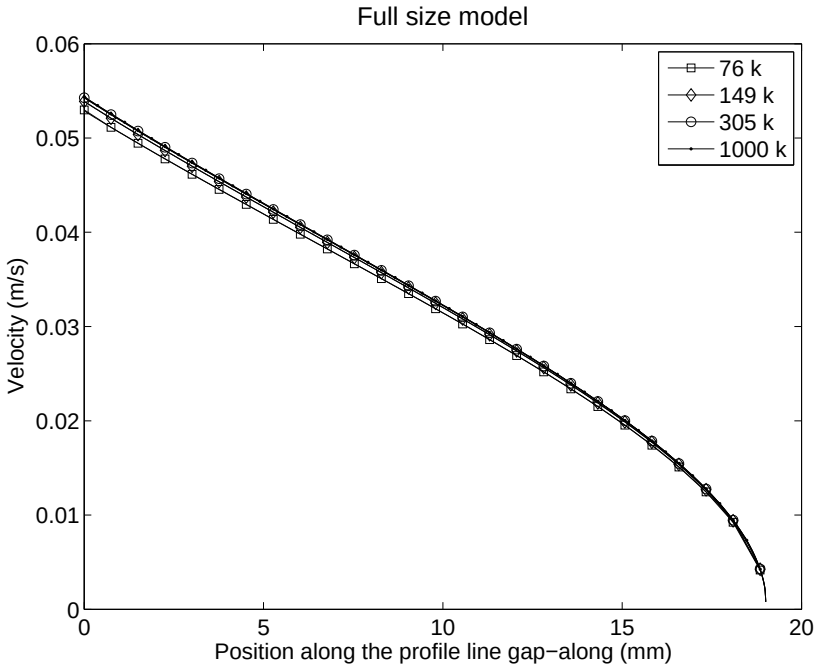

Figure 3.11: Velocity measurement at gap-along-line for the full size model with different mesh resolutions.

However, it was seen that the fluid velocity at the interface in the bone side varied significantly as the mesh resolution changed in this region (c.f. Figure 3.13). The width of the boundary layers in that region had a significant effect on the velocity measured on the profile line bone-int. Figure 3.13 shows that this change in velocity is not significant from the 305 k mesh to the 1000 k mesh. However, this was checked further using the reduced-size model with finer meshes.

3.3.2 Reduced-size model mesh verification

To verify the adequacy of the mesh further and to ensure that a higher resolution of mesh does not change the solution, the reduced size model was used to produce very fine meshes at both the gap and the bone region with varying core and boundary layer resolutions. For the reduced-size model, the following parameters were varied to determine the effects on the obtained solutions: the core mesh size of the gap and bone regions, boundary layer resolution at the interface on both bone and gap sides as well as the boundary layer on the implant wall. The findings from the full size model were confirmed by this model and it was shown that the resolution of the boundary layer at the interface in the bone region was the most influential parameter and the

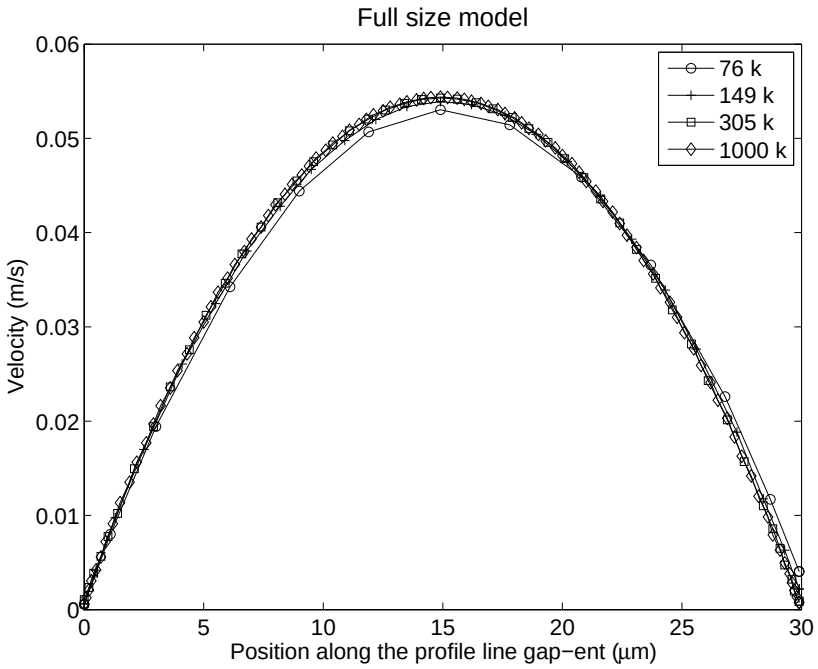

Figure 3.12: Velocity measurement at profile line gap-ent for the full size model with different mesh resolutions.

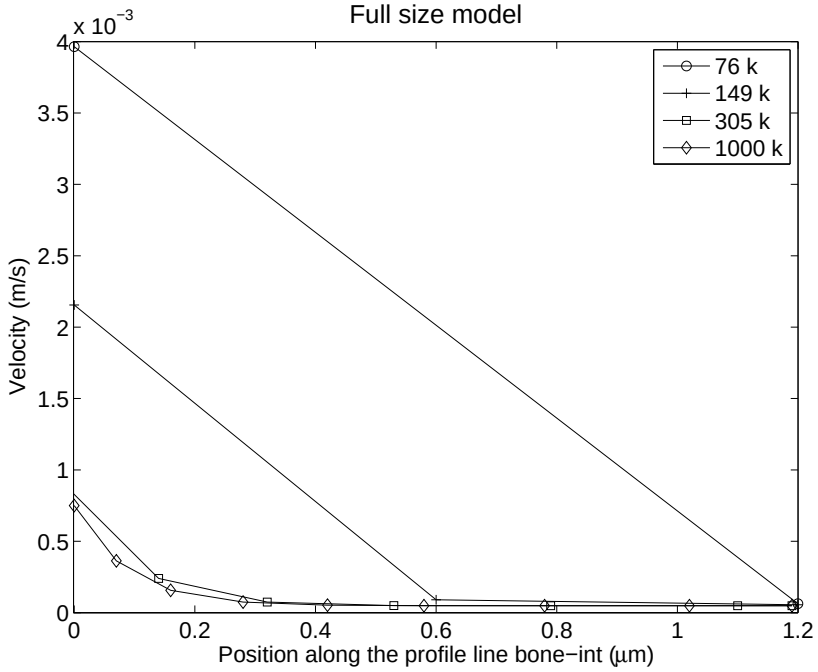

Figure 3.13: Velocity measurement at profile line bonr-int for the full size model with different mesh resolutions.

resolution of the core mesh in the gap and bone region did not change the solution, neither varying the resolution of the boundary layer at the interface on the gap side.

The parameter to change the mesh resolution at the interface on the bone side was the depth of the first layer of cells. The rate of growth of boundary layer cell size was kept constant at 1.2, thus, any change on the first cell layer would be reflected on other cell layers. Therefore, the mesh resolution imposed by boundary layer was only a function of the first layer cell depth. As can be seen in Figure 3.14, further refinement of the boundary layer in the reduced-sized model slightly changes the velocity profile and the change is not significant at boundary layer depth of 0.03 μm and below. Therefore, the mesh resolution imposed by first cell layer depth of 0.03 μm was chosen as an appropriate mesh resolution for the interface on the bone side and this cell depth was used in the full-size models.

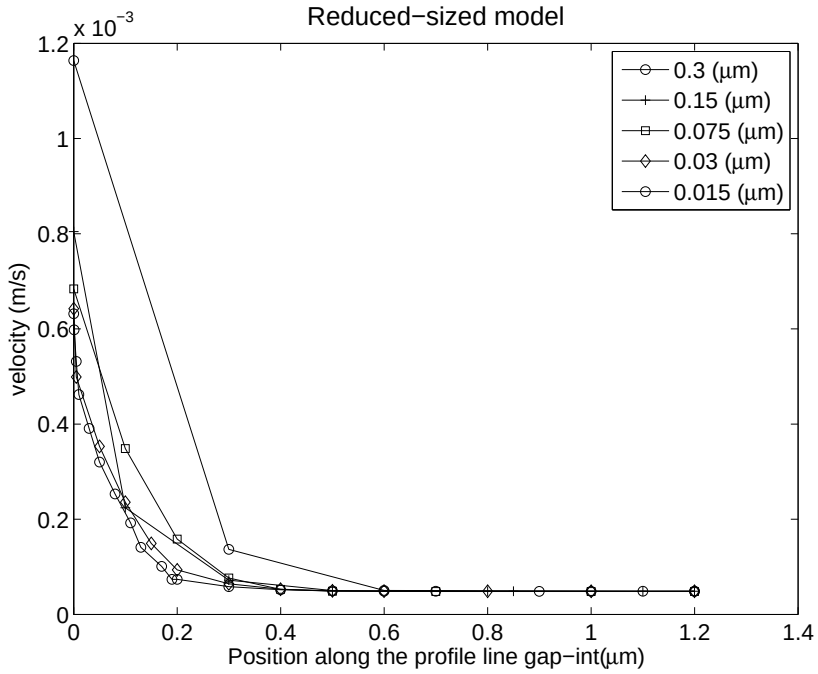

Figure 3.14: Velocity measurement at profile line bone-int for the reduced-size model with different mesh resolutions at the interface boundary layer. The legends show the depth of the first boundary layer. The growth rate was kept constant for all the meshes

3.4 The chosen mesh resolution

Mesh convergence studies from full size and reduced-sized models demonstrates that the 305 k mesh with an improved boundary layer resolution, corresponding to that of 0.03 μm depth for the first layer, shows less than 5% variation in fluid velocity in regions of high flow gradient. Therefore, meshing parameters for this mesh were deemed appropriate to produce adequate resolution for this study. All the selected

meshing parameters were scaled accordingly for geometries with different gap lengths and widths. Depending on the size of the gap, the number of cells ranged from 42,386 to 600,327.

3.5 Temporal convergence

The models incorporating the implant micromotion as a rigid body motion are transient and has to be solved through time. In Fluent, the rigid body is moved in each time-step and the magnitude of this movement is a function the time-step size. For example, if a gap has to open 30 μm within 0.1s (half a gait cycle), a time-step size of 0.002s opens the gap in 50 steps (0.1/0.002 = 50) while a time-step size of 0.01s opens the gap in only 10 steps (0.1/0.01 = 10). In this context, the time step has to be small enough to capture flow variation in time without increasing excessively computational costs. The solution and computational cost of models solved with time-step sizes of 0.01 s, 0.004 s, 0.002 s and 0.0002 s were studied. The residuals of mass and momentum had to reach 1e-7 in each time step for the solution to be considered converged. As an example, the computational times to run a model with a mesh resolution of 42k (gap width = 30 μm and gap length = 5 mm) for one gait cycle (gap opening of 300 μm) with different time-step sizes are shown in Table 3.2. To verify the effect of the time-step size on the solution, the corresponding velocity measurement after t = 0.05s (by this time the gap has opened 150 μm and has reached its maximum opening velocity) along gap-ent-line for each time-step size is shown in Figure 3.15. Table 3.2 shows that the computational cost is considerably less for time-step sizes of 0.002s, 0.004s and 0.01s in comparison to time-step size of 0.0002s. However, Figure 3.15 shows that the solutions for time-step sizes of 0.004s and 0.01s are less accurate than those of 0.002s and 0.0002s. Considering the accuracy of the results and the computational cost, the time step of 0.002 s showed sufficient accuracy (less than 5% variation compared to smaller time step of 0.0002 s) and minimum computational costs. The same phenomena were observed for other gap dimensions and displacements. This time step size is also appropriate for studies in which particles are injected to the models in each time step (c.f. Chapter 5). Therefore, it is the chosen time step for the models.

Table 3.2: Computational time to run a model with short gap for one gait cycle with a mesh resolution of 42k on a machine with Intel Xenon 2.00 GHz CPU and 8 GB of RAM.

Time-step (s)	Computational time (min)
0.0002	156
0.002	31
0.004	27
0.01	23

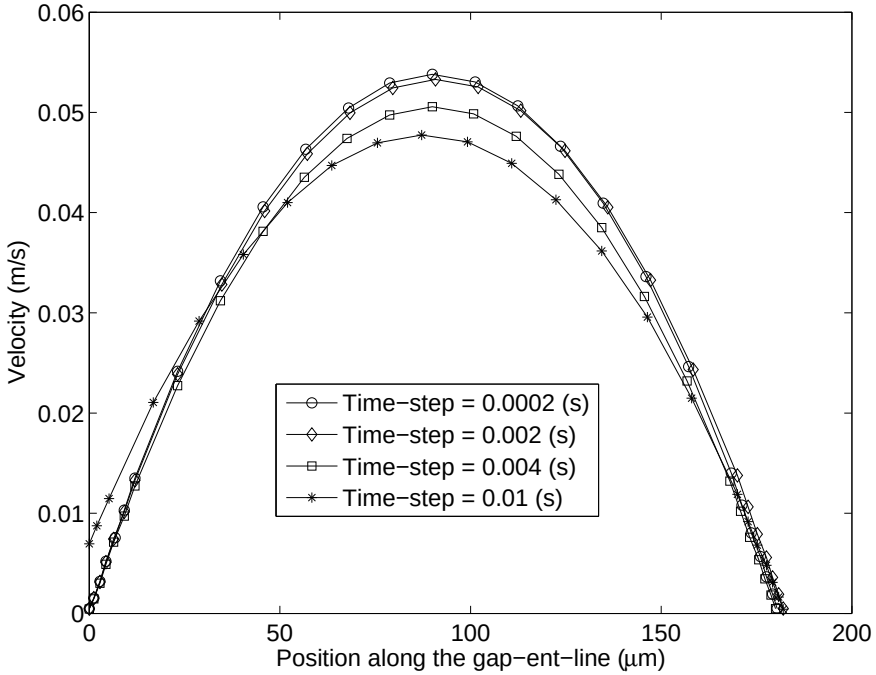

Figure 3.15: Velocity measurement at profile line gap-ent-line for different time steps when the gap is opening with maximum velocity. This figure shows the effect of time-step size on the solution after the model is run for t = 0.05 s.

Chapter 4

Periprosthetic flow modelling

4.1 Introduction

As mentioned in section 2.4, despite references to the 'pumping mechanism' and 'effective joint space' in the literature, there is no clear understanding of how capsular pressure, micromotion, gap location and dimensions or other additional factors may contribute to these mechanisms. Using the model developed in the previous chapter, this chapter investigates how these factors influence periprosthetic flow.

It is hypothesised that capsular pressure, gap dimensions, and the opening and closing motion of the gap during cyclic loadings of an implant can play a role in generating high fluid velocities and pressures as well as particle migration in both the gap region and its surrounding bone. The extent of the influence of each of these parameters on generating high fluid pressures and velocities in the gap and the surrounding bone is presented. It is important to emphasise that this work adopts a single fluid (with the adjacent bone having a single value of permeability which was calculated based on Simkin et al. experiment [114] in previous chapter) for simulating flow in the system. Although this is a gross approximation, simulations of this kind have not been performed before, and they provide the foundations for developing a better understanding of the causes of osteolysis.

4.2 Methods

The parameters varied in this study were capsular pressure p, gap width w, gap length l and gap displacement d. A parametric study of 16 models including extreme cases for these parameters was set up (Table1 4.1).

All simulations were first run in steady-state mode with no moving boundary and the steady-state solutions were then used to initiate the transient model with the moving implant boundary. Models were analysed by comparing the steady-state solutions

Table 4.1: Parameter definitions and ranges.

Varying parameter	Minimum	Maximum
Capsular pressure p (kPa)	1	60
gap length l (mm)	5	80
gap width w (μm)	30	500
gap displacement d (μm)	30	300

and transient solutions at times corresponding to fully closed gap (t = 0.0s), opening with maximum velocity (t = 0.05s), fully opened (t = 0.1), and closing with maximum velocity (t = 0.15), respectively (c.f. Figure 3.7). In each cycle, the model was solved in a hundred time steps of 0.002s (Δt) and the transient analysis was performed for two cycles. It was ensured that there was no change in the solution as the models were run for further cycles.

In the discussion that follows, the models are named according to the gap dimension and displacement in the following manner: Length l (mm), width w (μm) and displacement d (μm). For instance, a model named 80L-30W-300D is a model with dimensions of length 80 (mm), width 30 (μm) that experiences 300 (μm) of gap opening, where L, W and D denote gap length, width and displacement, respectively. Indeed, for steady state models where there is no gap displacement the third digit is replaced by zero, for instance 80L-30W-0D. All velocity and pressure measurements were carried out along 'bone', 'gap' and 'top-gap' profile lines shown in Figure 4.1. The profile line in the gap is situated in the middle of the gap width and extends from the entrance to the bottom of the gap. The profile line in the bone is situated in the bone adjacent to the gap region (1 μm away) and extends along the gap, terminating 5 mm below the bottom of the gap. Finally, the top-gap profile line is situated at the gap entrance along its width. Measurements were taken in the Cartesian coordinate system with x and y directions taking positive values in leftward and upward directions, respectively. The profile lines gap and top-gap, which are located in the gap region, are repositioned as the gap undergoes micromotion. The top-line extends and shrinks as the gap opens and closes, respectively, to cover the entire gap entrance. The upper end of the profile line gap moves in a manner that its position is always in middle of the gap width at the gap entrance while its bottom end is fixed in the middle of the gap width at the gap bottom. This ensures that this profile line is always located in the middle of the gap despite the micromotion. It is important to measure shear stresses at the gap-bone interface. However, Fluent does not provide capability to monitor shear stresses in regions other than solid walls. Therefore, in order to measure interface shear stresses, two profile lines parallel to the interface, one in the fluid side (gap region) and the other in the porous side (bone region) were generated and fluid velocities were recorded on these lines. Then, the shear stress in the direction of interest is calculated by the following

equation which defines shear stress:

$$\tau_n = \frac{\mu(\mathbf{u}_{f_n} - \mathbf{u}_{p_n})}{d}, \tag{4.1}$$

where, n is the numbering of the points along the profile lines where velocities are measured, d is the distance between the profile lines and $\mathbf{u}_{f_n}$ and $\mathbf{u}_{p_n}$ are the corresponding fluid velocities at each point in the fluid and porous sides, respectively.

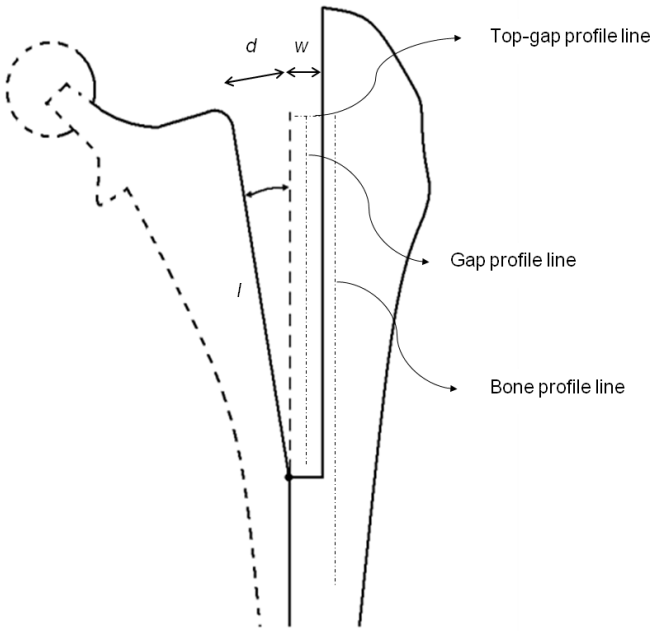

Figure 4.1: Schematic showing the bone, gap, and top-gap profile lines, along which the velocity and pressure measurements are taken.

Since all the variables were measured along the length of the gap, for easy comparison, the length of the gap is normalised for all the plots. It should be emphasised that since the bone profile line always extended 5 mm below the bottom of the gap regardless of the gap's length. Therefore, when it is normalised for a 80 mm length gap, the bottom of the gap is located at a normalised value of approximately 0.95, whereas for a 5 mm length gap the bottom of the gap is at the normalised value of 0.5. For easier interpretation of the figures, the top and bottom of the gap are marked on the x-axis.

4.3 Results

4.3.1 Steady state solutions

In general, in steady state, the pressure experienced in the gap and the surrounding bone is similar to the capsular pressure. Figure 4.2 illustrates this in the steady state

pressure contour for the 80L-500W-0D model (no micromotion included), where it can be seen that capsular pressure extends down the gap and into the surrounding bone. The only exception is the 80L-30W-0D model (the longest and narrowest gap) in which the capsular pressure does not penetrate the entire length of the gap and drops to approximately one fifth of the capsular pressure by the time the fluid reaches the bottom of the gap (c.f. Figure 4.3). In the same figure, a small drop in the pressure in the 5L-30W-0D model can also be seen. This drop in the pressure, which starts immediately at the entrance of the gap, seems to be mainly influenced by the gap width. The narrower the gap, the more resistance is exerted on the fluid flow. The pressure drop results in a corresponding increase in fluid velocity as seen in Figure 4.4.

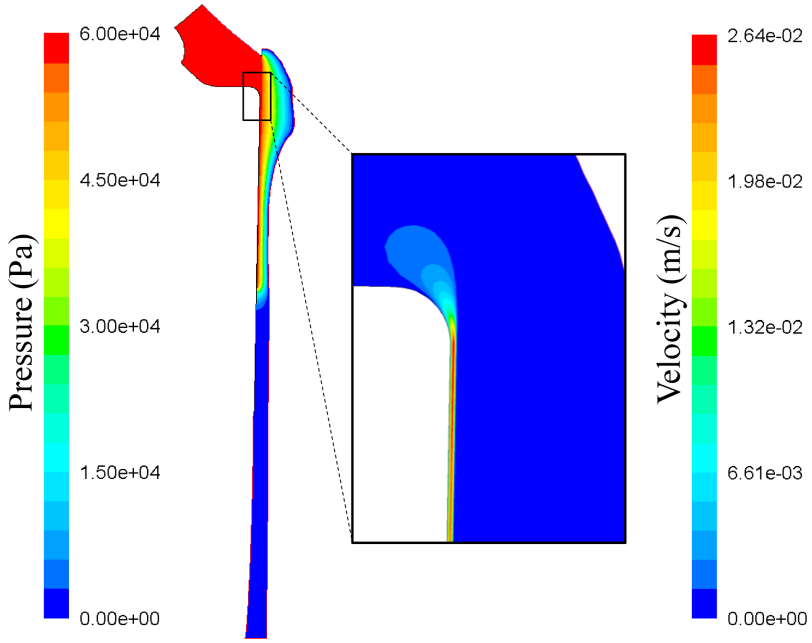

Figure 4.2: This figure shows pressure contour (left) along the gap and the corresponding fluid velocity contour (right) for the magnified region at the gap entrance for steady state solution of the 80L-500W-0D model at 60 kPa pressure. The extension of high capsular pressure down the gap and the flow of fluid to the gap region can be seen.

Reducing the capsular pressure from 60 kPa to 1 kPa induces a 60 fold decrease in fluid velocities and pressures measured along bone, gap and top-gap profile lines. Gap dimensions l and w, also influence the flow variables, although to a lesser extent. Figure 4.4 shows the effect of gap dimensions on fluid velocity on the gap profile line. Fluid flows into the gap in the negative y direction with maximum velocity occurring at the gap entrance (c.f. Figures 4.2 and 4.4). This high velocity then decreases as the fluid approaches the bottom of the gap. In the bone, as the fluid passes across the bone-gap interface, there is a shift towards the medial lateral direction in the flow and a significant decrease in velocity. In this region the velocity is of the order of a few

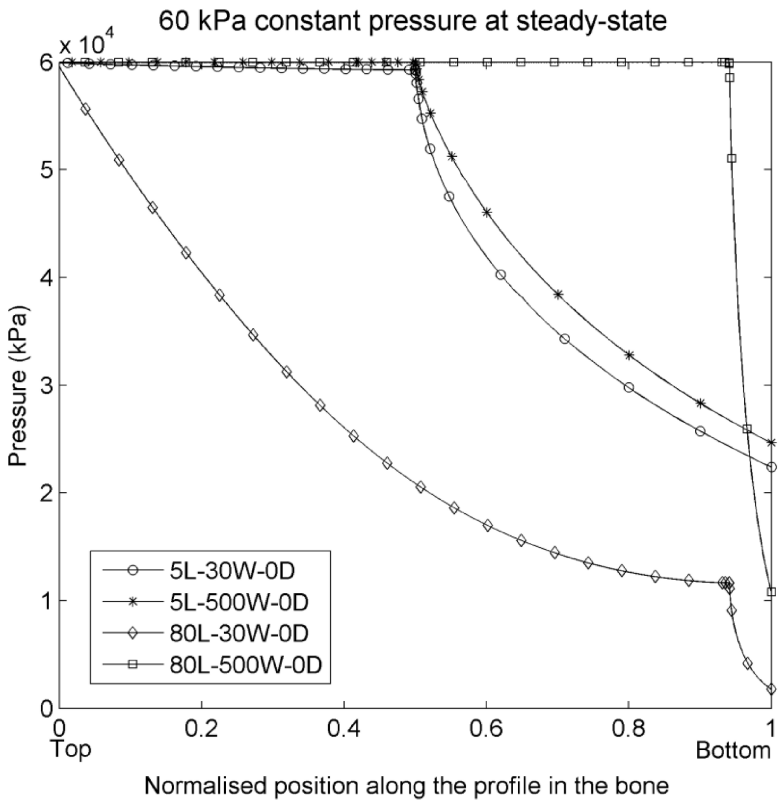

Figure 4.3: Pressure measurement along the bone profile line. Pressure drops up to five times from the capsular level for the longest and narrowest gap (80L-30W-0D) while it stays unchanged for all other models. Only four models are demonstrated here.

mm/s to μm/s depending on the gap dimensions and the capsular pressure. However, in all the models, as fluid crosses the gap-bone interface, there is always a sudden spike in fluid velocity (c.f. Figure 4.9 and 4.10) in the bone at the proximity of the bottom of the gap which, in some cases could be up to ten times larger than the fluid velocity in the neighbouring bone region. Along the gap-bone interface, relatively small amounts of the fluid flowing down the gap is driven to the bone by pressure gradients and diffusion effects, whereas at the gap bottom, the fluid is driven to the bone by the fluid momentum as there is no longer a path of least resistance for the fluid to flow to. This may explain the reason for the velocity spikes observed in the bone at the bottom of the gap. Notably, these velocity spikes are not affected as significantly by changes in gap dimensions in comparison to the capsular pressure and are primarily a function of capsular pressure. Figure 4.5 shows that three models with different gap dimensions at high capsular pressure and one model at low capsular pressure. At high pressure, the fluid spikes have the similar values for the 5L-30W-0D and 80L-500W-0D model and the magnitude of the fluid spike for the 5L-500W-0D model is still in the same order of magnitude as the 5L-30W-0D and 80L-500W-0D models. However, the figure shows that there is a significant decrease in the magnitude of the fluid spike when the pressure is reduced from 60 kPa to 1 kPa.

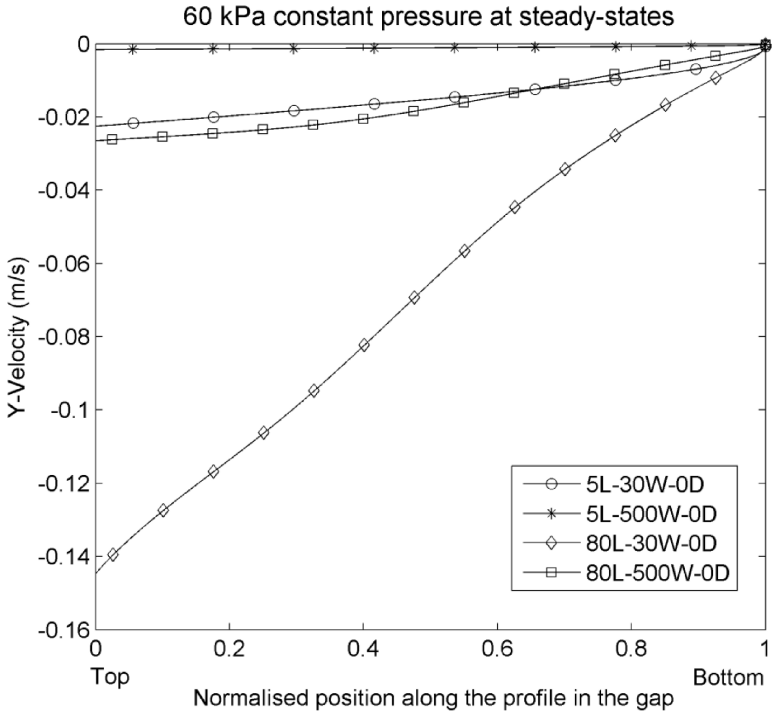

Figure 4.4: y velocity measured for different gap dimensions at gap profile line at steady state. It can be seen that changing gap dimension can induce over 16 times increase in fluid velocity in to the gap.

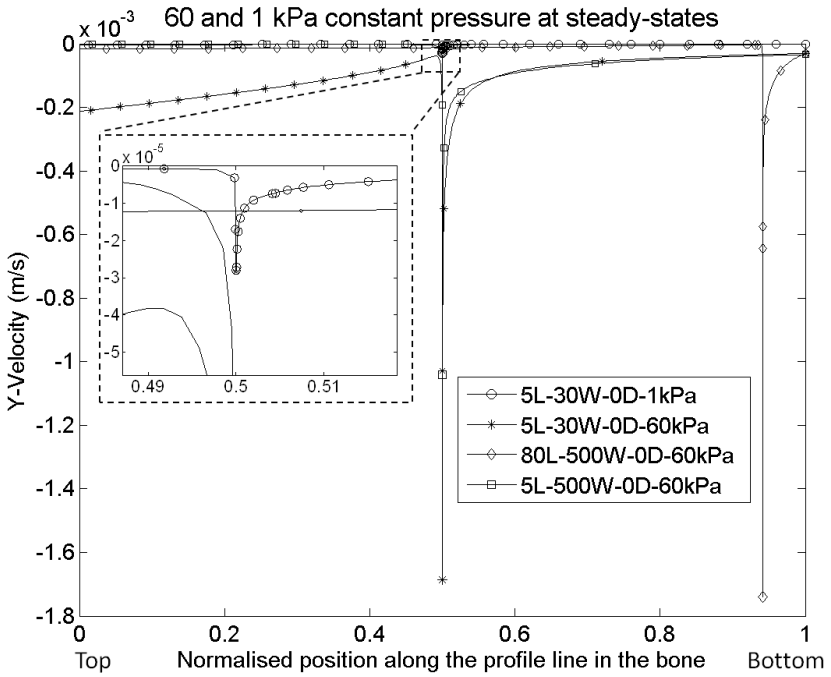

Figure 4.5: y velocity measured for different gap dimensions and pressures at gap profile line at steady state. It can be seen that, at high capsular pressure, the magnitude of fluid spikes remain in the same order of magnitude when gap dimension is changed while reducing the capsular pressure results in two orders of magnitude reduction in the velocity spikes.

4.3.2 Transient solution

In general, a pumping action of fluid being sucked in and pushed out of the gap is observed as the gap opens and closes during a cycle. Larger displacements cause higher fluid velocity in the gap region. In the low pressure models, where the flow to the gap region is small, a gap displacement causes considerable increases in fluid velocity compared to a constant gap, ranging from three to four orders of magnitude. This increase in flow velocity due to gap displacement in high pressure models, where the fluid is already pushed to the gap with high velocity as a result of high capsular pressure, is less pronounced (one to two orders of magnitude). This implies that the additive effect of micromotion in causing fluid pumping at high pressure is less significant compared to that at low pressure. It should be noted that despite the very large percentage increase in velocities, they still remain of the order of mm/s. While micromotion creates a pumping mechanism by generating significant fluid flow to the gap, it does not cause an increase in fluid pressure except for the very long and narrow gaps (80L-30W-30D and 80L-30W-300D models) in which micromotion as small as 30 μm can cause significant high fluid pressure fluctuations between 40 kPa and -40 kPa in opening and closing motions, respectively (c.f. Figure 4.6). This change in pressure is added to the already existing capsular pressure in both low and high pressure cases.

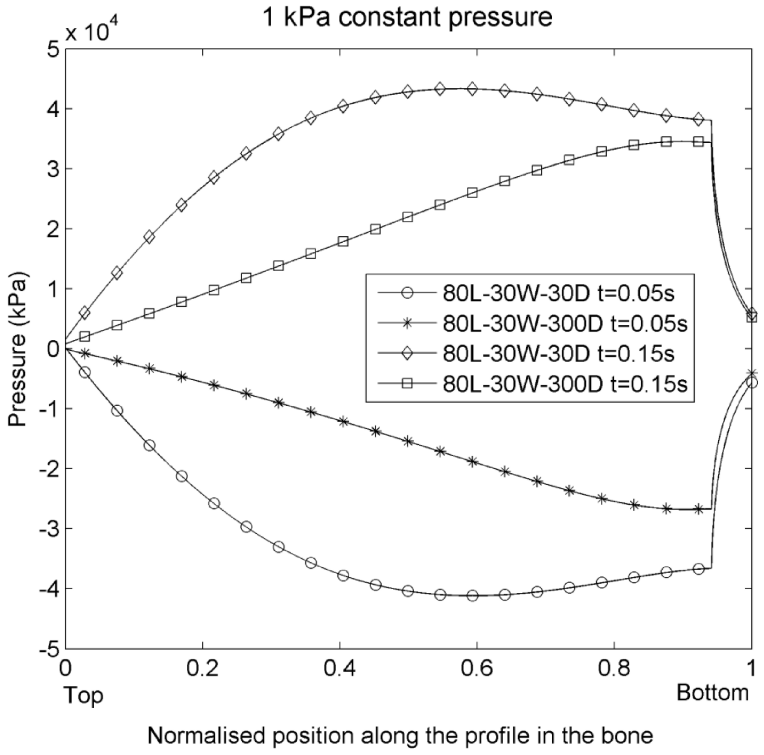

Figure 4.6: Gap displacement usually has no effect on the fluid pressure experienced by the bone adjacent to the gap. However, for the longest and narrowest gap even a small displacement as shown in this figure can cause pressure fluctuation up to 80 kPa.

In addition to hydrostatic pressure, the interfacial tissue is also subjected to shear stress caused by the fluid flowing in the gap region. However, Figure 4.7 show that shear stress on the interface along the gap is considerably less than the hydrostatic pressure experienced in that region. This is also the case for the a long and narrow gap in which fluid velocities are higher that other gap dimensions and displacements (c.f. Figure 4.8). This figure shows that shear stresses along the gap do not exceed a few Pascals.

Velocity spikes are only affected by gap displacement in the 80L-30W-30D and 80L-30W-300D models. At low pressures, these combinations of gap dimensions and displacement can increase the maximum velocity at the spikes by up to two orders of magnitude (c.f. Figure 4.9). Additionally, the flow direction in the spikes changes to positive for these models as the gap opens, which implies fluid suction from the bone tissue to the gap. In the high pressure models, the same behaviour is also observed. However, as seen in figure 4.10, only the 80L-30W-30D model creates a suction of fluid at the tip of the gap.

At low pressure, as the gap closes at t = 0.15s, almost all the fluid in the gap region changes direction and flows towards the top of the gap in all models apart from the 80L-30W-30D and 80L-30W-300D models. However, at high pressure (and in the

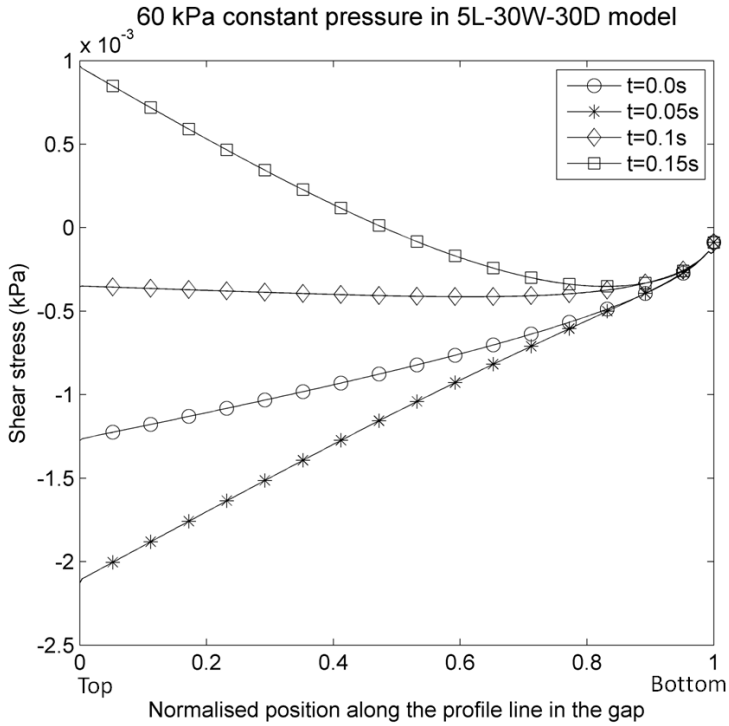

Figure 4.7: Shear stress along the gap at the gap-bone interface for the 5L-30W-30D model. It can be seen that the the shear stress experienced at the interface is considerably smaller than that of hydrostatic pressure.

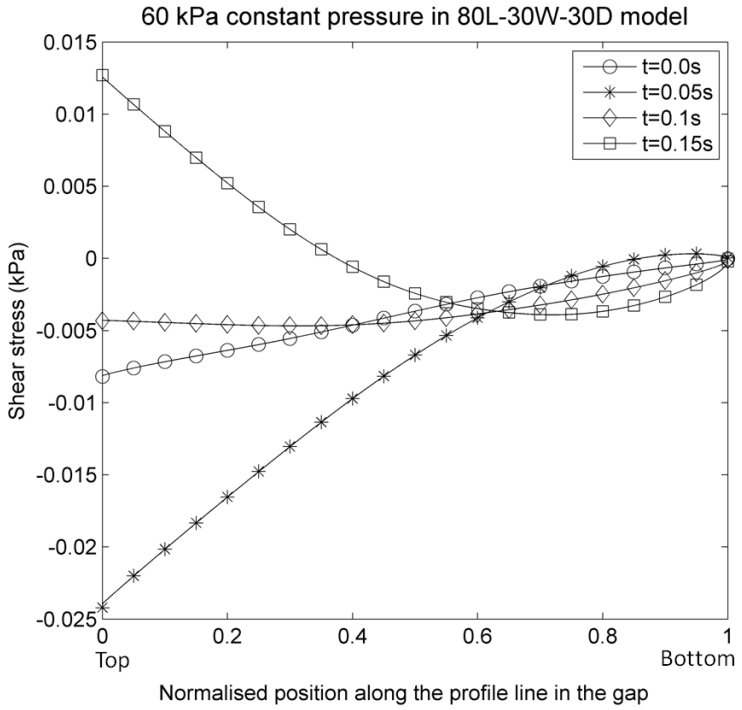

Figure 4.8: Shear stress along the gap at the gap-bone interface for the 80L-30W-30D model. Shear stress experienced at the interface is considerably smaller than that of hydrostatic pressure even for a very long and narrow gap in which interface tangential velocities are higher than other gap dimensions and displacements.

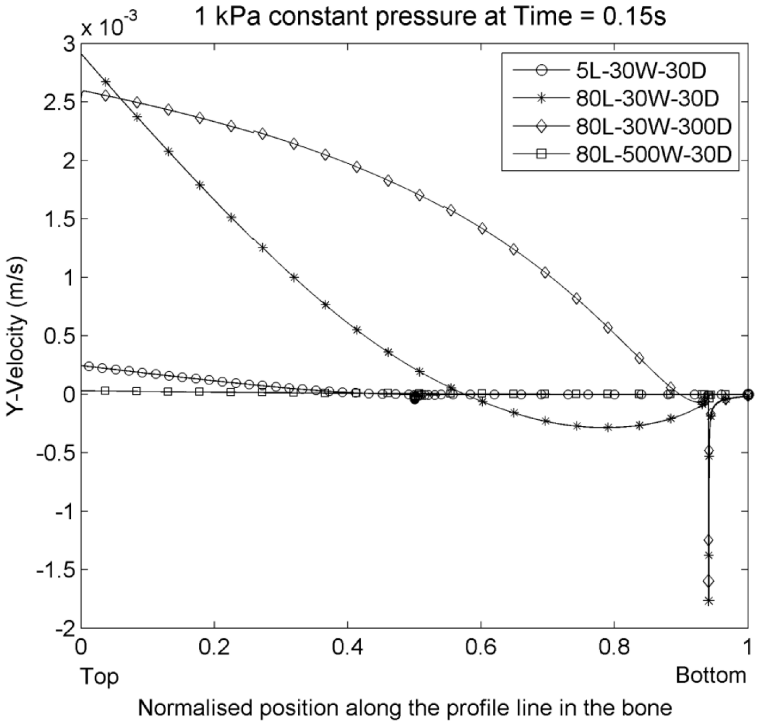

Figure 4.9: Very large velocity spikes caused by gap displacement in the 80L-30W-30D and 80L-30-300D models. All other models show no significant change in the velocity spike. Fluid spikes are located at bottom of the gap where fluid is pushed to the bone region by fluid momentum. For short gaps the bottom of the gap, and therefore, the fluid spike is at normalised location of 0.5, whereas for long gaps it is at normalised location of 0.95

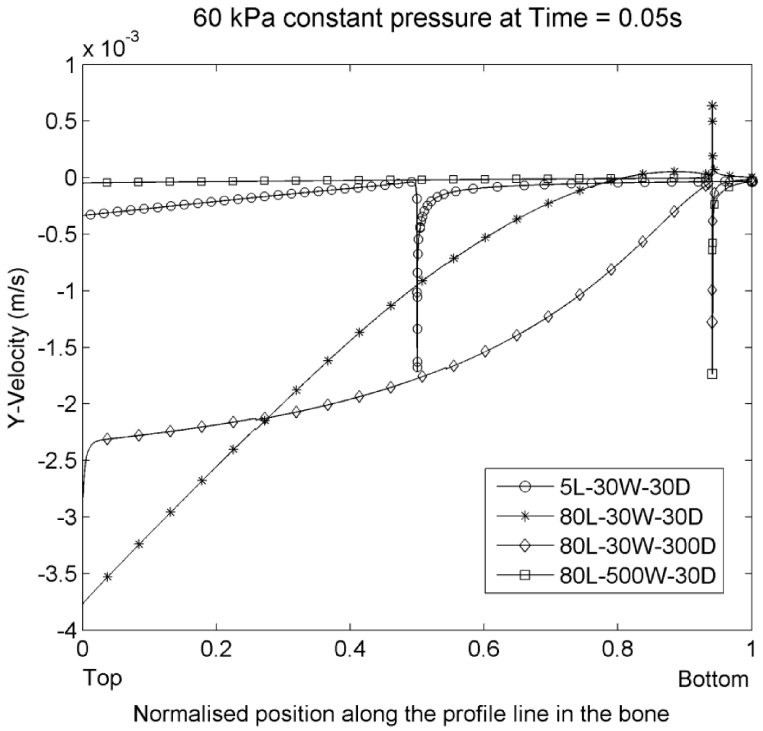

Figure 4.10: Velocity plot at bone profile line. It can be seen that 80L-30W-30D model shows suction of fluid from the bone to the gap as the spike is in the positive direction.For short gaps the bottom of the gap, and therefore, the fluid spike is at normalised location of 0.5, whereas for long gaps it is at normalised location of 0.95

80L-30W-30D and 80L-30W-300D low pressure models) the flow at the lower part of the gap does not change direction as the gap closes. In these regions, the fluid direction remains downwards. This generates a constant pumping of fluid to the lower part of the gap. This phenomenon is shown in Figure 4.11, where it can be seen that even at t=0.15s the velocities at the lower part of the gap are negative.

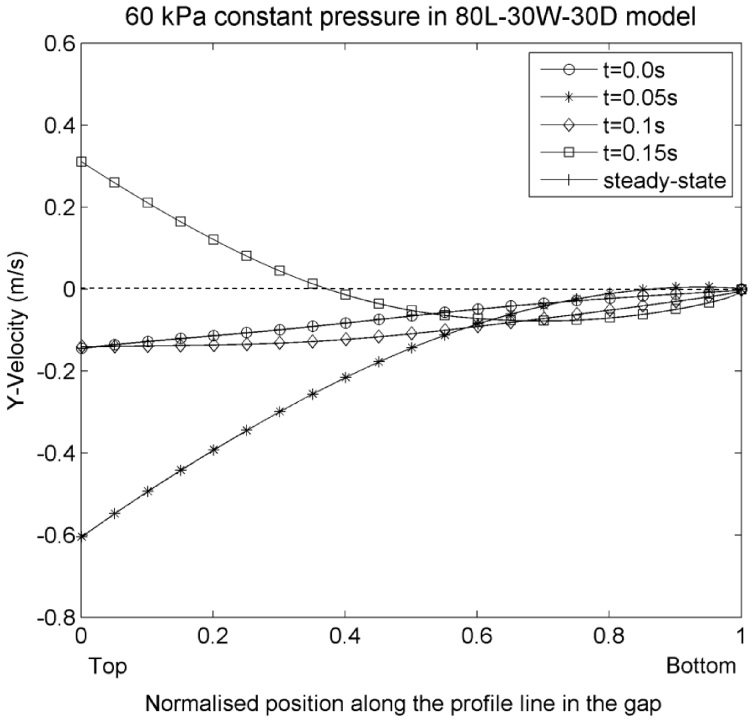

Figure 4.11: Velocity of fluid in the gap for the longest and narrowest gap with smallest displacement (80L-30W-30D) at different times during one cycle. It can be seen that even at t=0.15 when the gap is closing the velocity value is still negative meaning the fluid still flow down the gap.

4.4 Discussion

It has been hypothesised that high capsular pressure and/or implant micromotion can produce high pressure at the bone-implant interface and create a pumping mechanism that facilitates fluid transportation and wear particles migration into this region. However, the existence of such a mechanism is not directly evidenced in the literature, particularly for cementless implants.

The results of the current work have implications for each of the aseptic loosening theories. If high fluid velocity in the bone is assumed to be a crucial causative factor for osteolysis as suggested by Fahlgren et al. [39], then at high capsular pressure, the bone at the bottom of the gap is more prone to developing osteolytic lesions. However, as has been demonstrated, very long and narrow gaps are also capable of creating high

velocity flow in the bone along the length of the gap as well as its bottom even at low capsular pressure. The suction of fluid from the bone to the gap in these long and narrow gaps may also alter the composition of the local interstitial fluid. It has been shown that disturbance in the extracellular environment can affect osteoblast and osteoclast activities and result in bone resorption [45].

If high fluid pressure is assumed to play a key role in osteolysis development, then high capsular pressure in itself as well as micromotion of long and narrow gaps can be problematic since they can cause pressure fluctuations up to 80 kPa (c.f. Figure 4.6). McEvoy et al. [117], using cultured microphages, showed that pressures of 35 kPa can be biologically significant and result in production of cytokines which are involved in osteolysis generation. This threshold can be even lower (i.e., 17 kPa) in the presence of particles. In addition to hydrostatic pressure, shear stress may also play an important role in signalling bone cells for maintenance of bone structure. There is no study in the literature relating shear stress to osteolysis generation. However, it has been shown that osteocytes appear particularly sensitive to fluid shear stress. In vitro experiments show that shear stress of 0.2-6 Pa may alter osteocytes activities in producing cytokines which are involved in bone resorption and generation [44]. The shear stresses obtain in the current study are also in this range and may influence bone resorption and generation at the gap-bone interface, particularly at the bottom of the gap where fluid spikes are generation.

Assuming that the particles are the main cause of osteolysis, the models here suggest that they are more likely to accumulate in the bone at the bottom of the gap where the mass flow rate to the bone is higher than other regions because of the observed velocity spikes. Figure 4.11 also suggests that, at high capsular pressure, particles that reach the lower part of the gap are trapped in this region since the direction of the flow is always towards the bottom of the gap even when the gap closes, leaving this area more prone to particle-induced osteolysis. This may suggest that focal osteolytic lesions which contain large numbers of particles may develop at the bottom of interfacial gaps. This phenomenon can be supported by the fact that in radiographs, focal osteolytic lesions have always been observed to be contiguous with linear osteolytic lesions [87], which can facilitate a path for fluid and particles flow.

Robertsson et al. [75] suggested that capsular pressure is usually elevated with problematic hips. According to this statement, the findings of the current study may be able to explain that high capsular pressure could be the reason for the focal osteolysis that has been observed by Maloney et al. [34] in stable cementless femoral components in the absence of foreign material. It is reasonable to assume that the focal lesions that were located distally had developed at the end of gaps where high velocity fluid can be generated. This phenomenon can also be supported by the radiograph observations described above that focal osteolytic lesions are always contiguous with linear osteolytic

lesions.

The results suggest that the entire bone adjacent to the capsule and gap experiences high fluid pressure when the capsule is pressurised. The results show that in the absence of high capsular pressure when a very long and narrow gap undergoes displacement, most of the bone along the gap and particularly the lower region experience high fluid pressure (cf. Figure 4.6). Assuming high fluid pressure can cause bone resorption, this observation can explain the origins of linear osteolysis observed around many cementless implants. However, in vivo, high capsular pressure only rises in problematic replaced hips in which there is excessive fluid infusion or the joint capsule has lost its compliancy. Even in these problematic hips, high pressure is not usually sustained for a long period of time during a physical activity and it decreases as the loads are removed from the joint. This may reduce the likelihood of high-pressure-caused osteolysis. However, bone resorption in the greater trochanter region, in which our simulations show exposure to the high pressures, is not rare and there are many examples in the literature describing the existence of such osteolytic lesions [34, 35, 47, 32].

In the absence of the evidence in the literature regarding in vivo measurements of periprosthetic fluid pressure and flow, there was no direct validation for the models presented here. However, a fluid velocity of 17 mm/s in the pressurised bone in the model here is very close to the value of 20 mm/s estimated by Fahlgren et al. in rat bone pressurised to 90 kPa. The current model also exhibits the phenomenon observed by Bartlett et al. [76] , that the stem pump generates both negative and positive significant pressures under sinusoidal axial and torsional forces in a gait cycle. In addition, mean pressures of up 17 kPa generated at the implant-cement interface in their experiment was reasonably close to the high pressures generated as a result of gap micromotion here. It should be noted that the fluid used in their study was vegetable oil with a different viscosity than water and the gap micromotion was against the hard surface of the cement rather that of porous bone. Anthony et al. [84] showed that osteolytic lesions occurred in locations where there was a defect in the cement, and the joint fluid had access to the endosteal surface bone tissue. Pressure measurements in these periprosthetic lesions showed that 15° of passive flexion and extension could cause fluctuations in pressure up to 26 kPa. The pressure elevation could be a lot higher during physical activity. The current model also captures this periprosthetic pressure elevation as a result of high capsular pressure or micromotion.

Jayson et al. [41] showed that changes in intra-articular pressure were directly communicated to the cystic erosions in the bone space which suggest hydrostatic continuity with the joint space. This hydrostatic continuity was also observed here where high capsular pressure extended to the bone-implant interface.

4.5 Limitations

The models were developed in 2D as a first approximation and only the flow in gaps seen in radiographs of the coronal plane were of interest at this stage. In addition, it is believed that the dominant forces occur in the axial direction along the vertical axis of the stem which makes the coronal plane of more interest. Moreover, because of the high aspect ratio between the width and length of the gap, a 3D model would result in a very large number of computational cells that would be considerably more computationally expensive to handle in terms of both mesh generation and simulations. Nevertheless, as the gap shape and implant micromotion become more complex, the flow in other directions may become important, necessitating a 3D model for further investigation. Bone was modeled as a porous material, but in reality bone is poroelastic meaning that deformation of the bone can itself cause fluid flow in the tissue. However, it has been shown that in a poroelastic model of the bone under physiological loading the velocity generated even in a 'fibrous tissue with great amount of bone', is approximately 0.2 μm/s [95] which is at least ten times smaller than the smallest velocity measured in the bone in the vicinity of the gap in any of the models here. Therefore, it seems reasonable to neglect the deformation-induced flows in the current work.

The boundary conditions of the model were set as pressure inlet and outlet implying that the flow rate into and out of the model was adjusted to keep the pressure difference between the capsule and the bone tissue at the required level. Despite the fact that in reality infusion and drainage of fluid in the capsule and bone through the vascular and lymphatic systems is complex, the overall behaviour can still be represented by this set of boundary conditions. Moreover, in reality, pressure is elevated by excessive effusion of synovial fluid to the capsule and/or loss of capsule elasticity due to fibrosis [75]. Pressure can be elevated even further when the surrounding muscles and ligaments tighten the capsular cavity during physical activity [80]. Therefore, in the in vivo situation, high pressure can also be generated by a decrease in the volume of the capsule [82] rather than flow of fluid to the capsule. Any pressure increase due to volumetric shrinkage may relax to its initial value when the capsular volume returns to its original shape. This may create a mechanism that sucks back some of the fluid that has been transported to the bone and the interface gap. The current model does not have the capability to simulate this phenomenon. However, it can represent the case where high pressure is generated because of a rigid capsular wall or the case in which the capsule has been stretched to its maximum elastic volume because of the excessive infusion. Fluid drainage was modelled by a simple pressure outlet on the periosteal and endosteal surface of the bone. It seems that setting the pressure to zero at the outer surface of the bone in other studies [95, 46] has produced reasonable results and can still represent the overall behaviour of the complex biological drainage system.

It is arguable that gaps around an implant may be filled with fibrous tissue rather than synovial fluid. However it has been shown that micromotion-induced flows in fibrous tissue are incapable of pumping particles very far into the interface [63] and if migration of particles through this mechanism exists, it must be extremely slow [84]. The migration of particles to remote locations away from the joint capsule, where they are generated, suggest a path of least resistance along the interface for access of joint fluid. In addition, it has been observed that fluoroscopic contrast media is able to extend throughout the implant-bone interface immediately after its injection to the joint capsule in both cemented [6] and cementless [47] prostheses. Von Knoch et al. [64], studying successful implants from autopsy, also showed that fibrous tissue ingrowth to the porous surface appeared adequate to prevent distal particle migration, despite the lack of solid bony fixation. This evidence justifies the assumption that gaps may be filled with synovial fluid. Furthermore, there is no periprosthetic fibrous tissue in the gaps at early post-operative stages.

Lastly, the above model is incapable of modelling the situation in which an interfacial gap is completely closed. However, it is not unreasonable to suggest that very narrow gaps of 30 μm can reasonably represent this situation.

4.6 Conclusions

The model confirms the existence of a pumping mechanism originating from high capsular pressure and micromotion. The findings of this study suggest that capsular pressure may be the main driving force for high fluid pressure and flow in the bone surrounding the gap, while micromotion of only very long and narrow gaps can cause significant pressure and flow in the bone.

The results suggest the existence of velocity spikes in the bone region at the bottom of the gap. High capsular pressure is observed to be the main cause of these velocity spikes whereas, at low pressure, gap micromotion of only very long and narrow gaps can generate significant velocity spikes.

To conclude, the statement by Schmalzried et al. [3] that 'the primary factor in development of osteolysis is the access of joint fluid to bone' has to be re-emphasized. It is suggested that maximum attachment and contact between the bone and implant has to be achieved to eliminate the effects of both capsular pressure and micromotion. Large areas of detachment may lead to long and narrow gaps which can be problematic even for very small micromotion and in the absence of high capsular pressure.

In this chapter, only periprosthetic fluid flows were the focus of the study and wear particle migration caused by such flows was not considered. In the next chapter, particles are added to the continuum flow and the factors influencing their migration and distribution in the periprosthetic tissue are investigated.

Chapter 5

Periprosthetic particle migration and distribution

5.1 Intoduction

Periprosthetic flow, as described in chapter 4, is not the only likely cause of osteolysis. Particles released from bearing surfaces to the effective joint space are also a likely cause of osteolysis. Therefore, it is of interest to investigate how particles penetrate and are distributed in the periprosthetic bone. In the current chapter, particles with a defined mass are introduced to the continuum system to study their migration. The geometry and the mesh are similar to those described in chapter 4. In addition to those models, a 40 mm gap is constructed to include a mid-range gap that terminates in Gruen zone 6 (c.f. Fig. 2.11). This provides a more definitive particle distribution around the stem, which facilitates a better comparison with clinical data.

5.2 Methods

5.2.1 Particle modelling

In these set of models particles are introduced by utilising the Discrete Phase Model (DPM) capability of the Fluent software. The DPM adds a second discrete phase to the continuous phase consisting of dispersed spherical particles. The volume fraction of the discrete phase is neglected and the motion of particles is simulated by solving equations of motion for particles as a discrete second phase in a Lagrangian reference frame of references. As the continuum fluid phase is treated by solving the standard Navier-Stokes equation, the particles are tracked through the calculated flow field by integrating Eqn. 5.1, which equates the force balance on the particle with the particle inertia:

$$\frac{du_p}{dt} = \frac{18\mu}{\rho_p d_p^2}\frac{C_D Re}{24}(u - u_p), \tag{5.1}$$

where, u is the fluid velocity in the continuum phase, u_p is the particle velocity, μ is the fluid viscosity, ρ_p is the particle material density, d_p is the particle diameter, Re is the particle relative Reynolds number and C_D is the drag coefficient.

Since the DPM model is described by an ordinary differential equation (ODE) (as opposed to the partial differential equations of continuous flow), Fluent utilises a separate numerical and discretization scheme to solve the OED every time particle positions are updated after each time step or flow iteration. Once the particle velocities are calculated from equation 5.1, the particle location is predicted by:

$$\frac{dx}{dt} = u_p \tag{5.2}$$

5.2.1.1 Particle drag forces

In the simulations developed in this chapter, it is assumed that there are no particle-to-particle interactions and the presence of the particles does not change the basic flow pattern. Therefore, when a particle is introduced to a stream of fluid the response of the particle depends only on the relative velocity of the particle and the fluid. This relative velocity in turn depends on the drag, which is the sole force acting on a particle. In Fluent the drag coefficient C_D for smooth spherical particles is calculated based on a study by Morsi and Alexander [118] who presented the following empirical formula that describes the drag coefficient for a particle at different Reynolds numbers (c.f. Figure 5.1).

$$C_D = \frac{K_1}{Re} + \frac{K_2}{Re^2} + K_3, \tag{5.3}$$

where, K_1, K_2 and K_3 are constants applied over several ranges of Re. However, since in the current study the flow velocity is small and laminar, and the particle Reynolds number is small, Eqn. 5.3 simplifies to Eqn. 5.4, as shown by the dashed line in Figure 5.1.

$$C_D = \frac{24}{Re} \tag{5.4}$$

5.2.2 Particle modelling in Fluent

The quantity exchanged between the continuum and discrete phases throughout the calculation is momentum. Momentum is transferred to particles as they pass through each control volume, and the effect of particles on the continuum is incorporated in

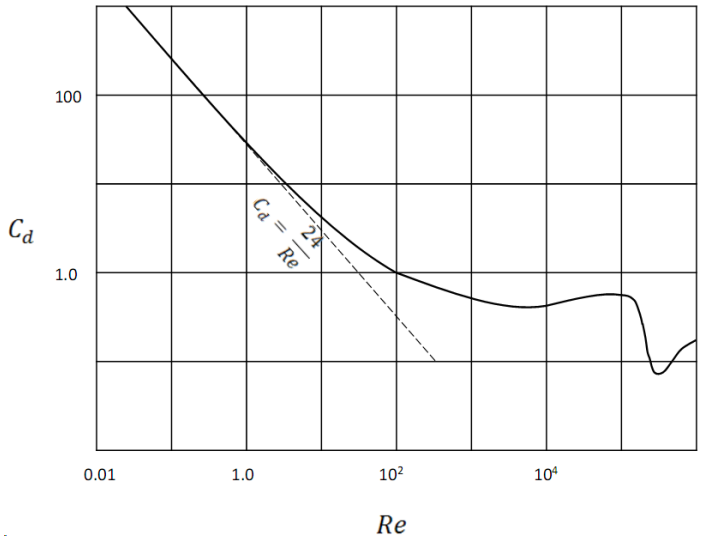

Figure 5.1: Drag coefficient for spherical particles against Reynolds number taken from Morsi et al. [118].

the model by a two-way coupling algorithm. This is achieved by alternately solving the discrete and continuous phase equations until the solutions in both phases have converged.

Particles are tracked unsteadily along with the continuous phase fluid flow. Discrete and continuous phase solutions are obtained in the following manner. The continuous phase flow field is solved prior to the introduction of the discrete phase, and then the discrete phase is introduced by calculating the particle trajectories for each discrete phase entity. Next, using the interphase exchange of momentum determined during the previous particle calculation, the continuous phase flow is recalculated and then the discrete phase trajectories in the modified continuous phase flow field are calculated. The latter steps are repeated until a converged solution is achieved in both phases. Once the converged solution is achieved, particle trajectories are calculated from Eqn. 5.1 and 5.2 and the particles are advanced to their new positions in the flow field at the end of a time step.

Fluent provides two parameter to control the accuracy of particle tracking integration. These parameters are 'tolerance factor' and 'maximum number of integration refinements'. Tolerance is the maximum relative error which has to be achieved by the tracking procedure and the maximum number of refinements is the maximum number of step size refinements in one single integration step. If this number is exceeded the integration is conducted with the last refined integration step size. In the current study, verification tests showed that the tolerance value below 1e-5 and the max number of refinement of above 20 did not alter particle positions and therefore these values were deemed appropriate to produce adequate accuracy for particle position in the domain.

It is computationally very expensive to track each individual particle in a particle

flow system. In order to reduce the computational time and memory usage, Fluent introduces particles into the model in packs of particles called 'parcels'. Each parcel contains a number of particles with the same properties including diameter, velocity and position. Instead of tracking each particle, Fluent tracks parcels. The behaviour of each parcel is determined by the behaviour of the particles inside.

5.2.3 Particle injections to the continuous field: location and the number per parcel

To reduce the computational cost of tracking particles, it was decided to introduce particles only at the gap entrance since the fate of particles in the capsule is not of interest in this study. Trial cases with particles present in the entire capsular region were carried out and it was observed that particles located remotely from the gap entrance hardly reached the gap and tracking them in the capsule would only lead to unnecessary computational cost. It was assumed that particles were evenly distributed throughout the synovial fluid and, therefore, any addition to the number of particles from bearing surfaces would result in new particles introduced at the gap entrance. In other words, particles are always available at the gap entrance. To simulate this situation and provide a continuous supply of particles to the model, particles were introduced to the continuous flow by means of injection points located at the gap entrance. New particles were injected to the flow in each time step.

A simple calculation on the result of an in vitro wear simulation on polyethylene-on-metal bearings by Shorez et al. [119] indicated that approximately 56,000 polyethylene particles are released to the joint capsule in each walking cycle, which results in approximately 6.7×10^{10} particles per year. Based on this figure, 560 particles were injected to the model in each time step which results in 56,000 particles for one cycle consisting of 100 time steps.

There are different ways to define injections in Fluent. The applicable injection options for the current study can be defined as either mesh dependent or mesh independent entities. While mesh independent injections provide flexibility over the location and the number of injection points, they are incapable of moving along with the dynamic meshing technique employed here. Mesh dependent injections can move and deform along with the dynamic mesh. However, the number and location of the injection points is defined by the mesh cell centroids. Consequently, this limits the number of injection points to the local mesh resolution. Once the mesh dependent injection is chosen, one way to increase the number of injection points in a location, which will be termed 'injection resolution' from this point, is to increase the local mesh resolution. However, for dynamic meshing to work in Fluent, the mesh at the gap and its entrance has to be a structured mesh, which means any change in the mesh resolution

at the gap entrance is reflected on the entire gap region. This significantly increases the total number of cells for the model and consequently the computational cost and, therefore, it is not a practical strategy to increase injection resolution. Another way to achieve a higher injection resolution is to increase the mesh area in which the injection points are located. It can be seen in Figure 5.2 that injection points can be defined on a line (entrance-line-1) resulting in 14 injection points, or on a surface (entrance-surface-1) resulting in 56 injection points or on two surfaces (entrance-surface-1 and entrance-surface-2) resulting in 112 injection points.

For ease of comparison and consistency between models, the total number of particles has to be constant. Therefore, as the injection resolution is increased, the number of particles in each parcel has to be decreased. To achieve the target value of 560 particles per time step, 14, 56 and 112 injection resolutions have to contain 40, 10 and 5 particles per parcel, respectively. Increasing the injection resolution from 14 to 56 and 112 leads to a significant increase in computational time and memory usage. A sensitivity analysis to injection resolution is carried out in section 5.3.3.

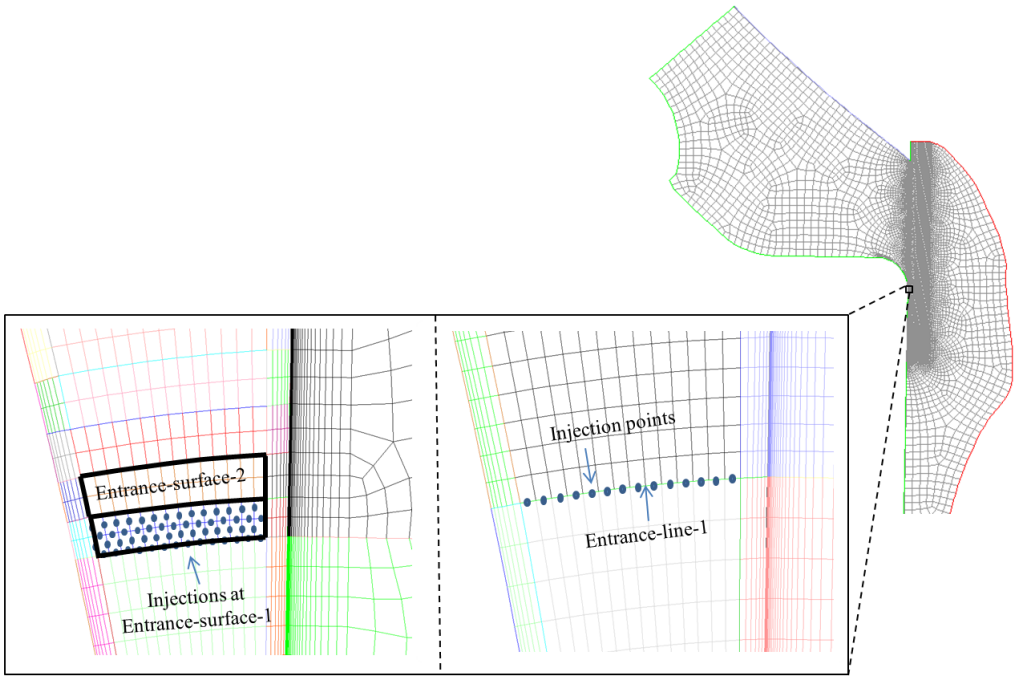

Figure 5.2: Mesh dependant injection points at the gap entrance. Injection can be defined on entrance-line-1, entrance-surface-1 and entrance-surface-2 resulting in 14. 56 and 112 densities, respectively.

5.2.4 Data processing

Postprocessing capabilities of Fluent are not adequate to produce the desired plots and data required for the current study. The region around the gap has to be discretised into equally spaced regions in which particles can be counted. Fluent is only capable

of producing contour plots of mass concentration of the discrete phase for each cell volume. These plots are highly dependent on the computational cell volumes which vary significantly around gap regions. To discretise periprosthetic bone into equally spaced regions, particle positions are exported from Fluent and postprocessing is carried out in MATLAB. User specific codes were written in MATLAB for data processing. Particles located in the bone region were separated from the rest and the space in the bone region was divided into 50 μm squares (c.f. Figure 5.5). These areas are termed 'measuring areas'. The number of particles were counted in each of these measuring areas. In addition, the gap length was normalised. However, this leads to distorted aspect ratios when the results are visualised, particularly for very long gaps with 80 mm length, in which the 50 μm squares appear elongated along the width of the gap. To better visualise the number of particles in these measuring areas (i.e. particle concentration) the results are presented in the shape of coloured 3D contour plots in which the y and x axes show particles position in the bone along the length and the width of the gap, respectively, and the z vertical axis shows the number of particles per 50 μm $\times$ 50 μm area. Figure 5.3 shows an example for a 3D plot generated for the 5L-30W-30D model ran at high capsular pressure.

As can be seen in Figure 5.3, the 3D contour plots contain many data points of regional concentration, which makes comparison between models difficult. To circumvent this problem, data is also presented in another form of plots called 'regional plots', an example of which is shown in Figure 5.4. In these plots the bone region containing particles along the gap is divided into five sub-regions (c.f. Figure 5.5). In each of these, the mean for particle concentrations obtained from the 3D contour plots is calculated. These mean values are depicted by square markers and the minimum and maximum concentrations occurring in each region are defined by the bottom and top edges of the boxes containing each of the data sets. On each box, the central line is the median of the data set. The difference between median and the mean value indicates how disperse that data set is.

However, by taking the mean value, important information about the presence of measuring areas with exceptionally high concentration values may be lost. To retain this information, when necessary, the number of measuring areas per region that are above the 90^{th} percentile of the data set, as a fraction of the total number of the measuring areas in that region is shown above each bar. The 90^{th} percentile is calculated for the whole data set of the measuring areas in the bone surrounding the gap and then, the number of measuring areas that have a value above the established 90^{th} percentile for a specific model is calculated for each region. For example, in Figure 5.4, the fractional value of 66/326 shown above the box in region one shows that 66 of the total 326 measuring areas in region one have a mean concentration value above the 90^{th} percentile of the data set.

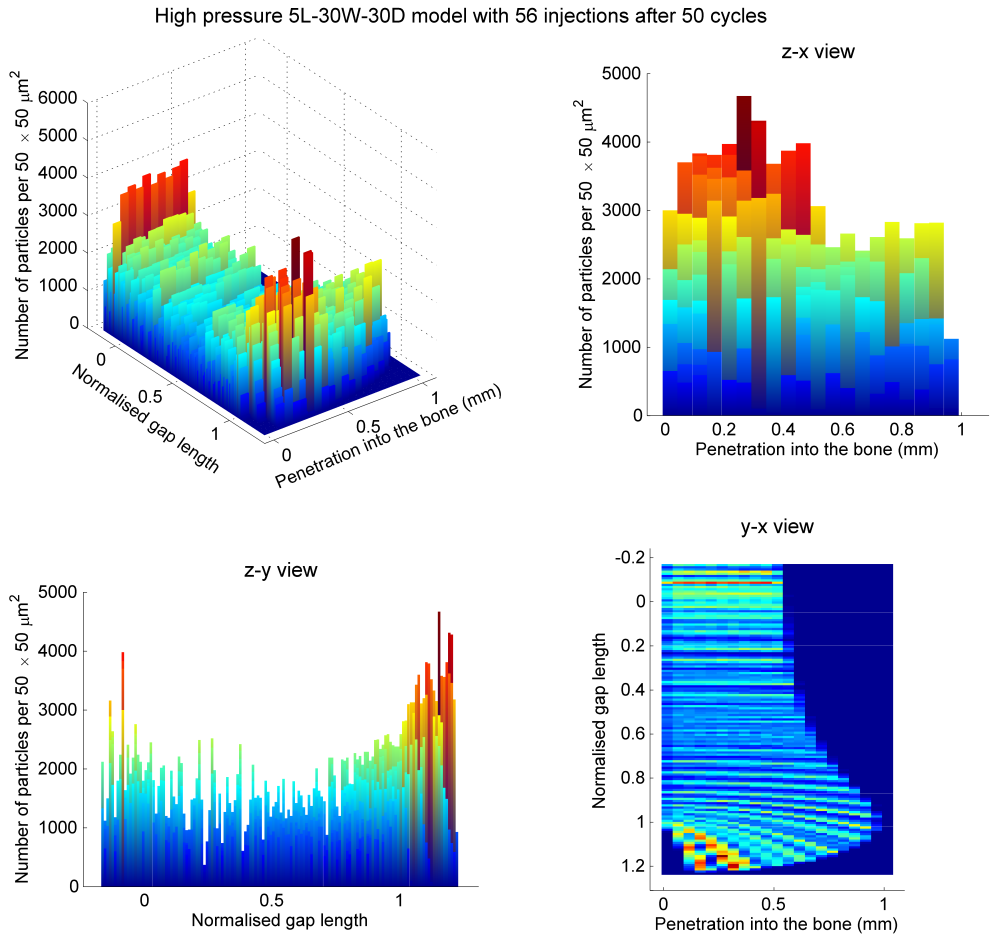

Figure 5.3: 3D contour plots from different views showing particle numbers per 50 × 50 μm^2 area and their penetration into the bone along width and length of the gap in the 5L-30W-30D model with high pressure and 56 injection points. High concentration at proximal and distal regions can be seen.

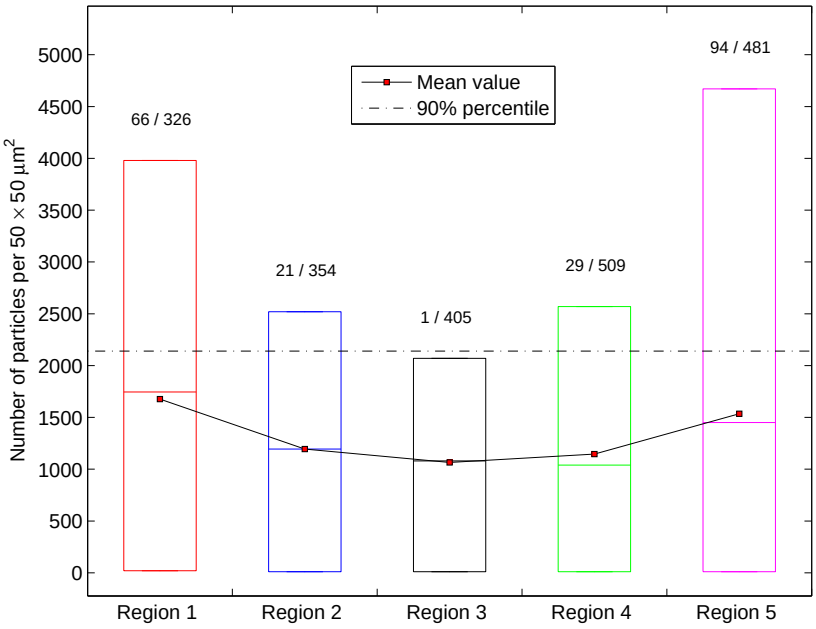

Figure 5.4: Regional plot of the particle concentration at different regions in the bone along the gap for the high pressure 5L-30W-30D model with 56 injections. The 90^{th} percentile is calculated based on the total particle number per measuring in the entire model. The mean value as well as the number of measuring areas above the 90^{th} percentile as a fraction of total number of measuring areas are shown above each box. The upper and lower edges of each box show the maximum and minimum concentrations.

Regional plots not only make it possible to compare particle concentration between different regions of a gap (for example distal and proximal regions), but they also make it possible to compare gaps with different dimensions and displacements. To establish whether two regions are significantly different, statistical analysis was carried out. The data comparison between different regions and models were performed using Kruskal-Wallis and multicomparison statistical tests [120]. Kruskal-Wallis tests, a nonparametric version of the classical one-way analysis of variance (ANOVA), were used since the data obtained for different regions did not fall into a normal distribution and, therefore, were not parametric. The statistical information obtained from the Kruskal-Wallis test was then used to perform a multicomparison test for pairwise comparison between different regions and models. Regions were significantly different if the p value was less than 0.05, i.e. a 95% confidence interval for the true difference of the medians. When the groups to be compared are more than two, applying an ordinary one to one test in which the alpha value, p, would apply to each comparison, the chance of incorrectly finding a significant difference would increase with the number of comparisons. The advantage of using a multiple comparison procedure over performing a test for one group against another is to provide an upper bound on the probability that any comparison is incorrectly found to be significant.

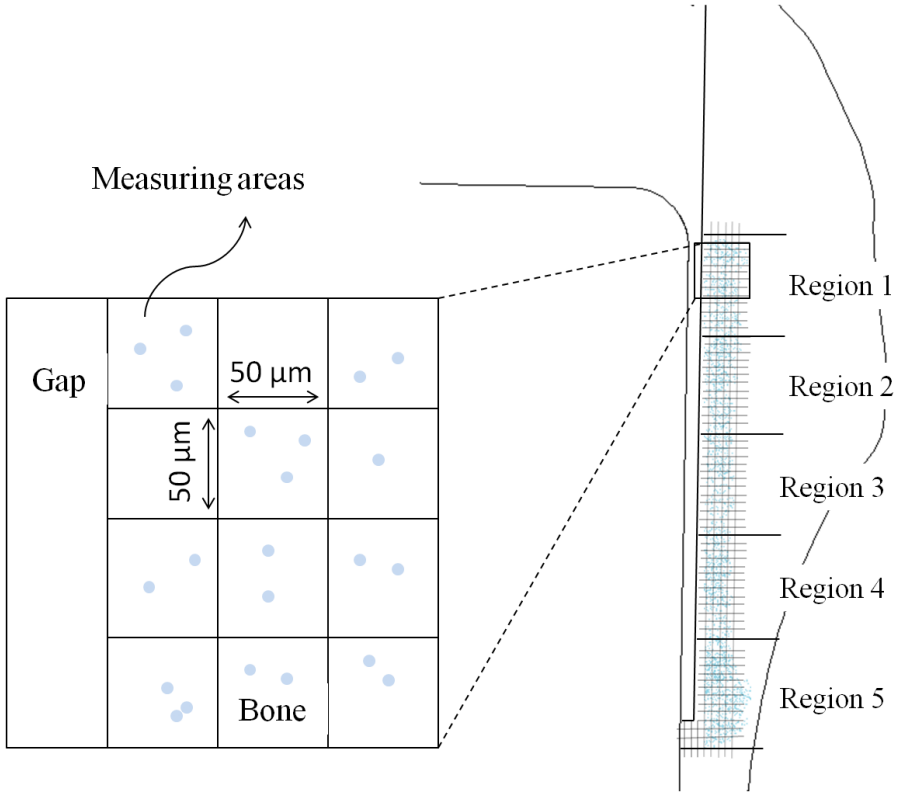

Figure 5.5: Regional division of the periprosthetic bone. The bone containing particles is divided into 5 equal regions which are used in regional plots. This figure also shows the 'measuring area' in which the particles are counted. This particle concentration is used for 3D contour plots

5.2.5 Simulation set-up

The parameters varied in the simulations in this chapter are show in Table 5.1. All the models were run for 50 gait cycles except the 5L-30D-30D model with 14 injections which was run for 200 cycles to study the temporal changes in particle distribution for longer periods. Because of high computational cost, only the 5L-3W-30D, 40L-3W-30D and 80L-3W-30D models were run with 56 injection points. A constant particle size of 1 μm was used in this study.

Table 5.1: Parameter definitions.

Varying parameter	Values tested
Capsular pressure p (kPa)	1 and 60
Gap length l (mm)	5, 40 and 80
Gap width w (μm)	30 and 500
Gap displacement d (μm)	30 and 300
Injection density	14, 56 and 112

5.3 Results

5.3.1 General observation

The models show that the particles injected to the fluid domain flow with the surrounding fluid. Their trajectories depend on the implant displacement and the initial locations of injections. Depending on gap dimensions and displacement, some particles flow into the gap and enter the surrounding bone at different regions along the gap and some are pushed away to the capsular region. An overview of the models shows that particle distribution and concentration in the bone region is influenced by injection resolution (i.e. the spacial coverage of injection points along the width of the gap), capsular pressure, gap dimensions and displacement. In the following sections the effect of each parameter is presented.

5.3.2 The effects of capsular pressure

Eight models with different gap dimensions and displacements explained in chapters 3 and 4 were run with particles at high (60 kPa) and low (1 kPa) capsular pressures. The percentage of particle accumulation in different regions of the model is presented in Table 5.2. At low pressure, no particles enter the bone region in models with short 5 mm gaps while in models with long 80 mm gaps, only up to 1.3 % of the total number of injected particles enter the bone at proximal regions. In contrast, at high pressure, depending on the gap dimension and displacement, up to 95% of particles accumulate

in the bone region which shows that capsular pressure is the main driving force that transports particles to the bone region.

Particles reside either in the gap, gap entrance, which is an extension of the joint capsule, or bone regions. Figure 5.6 shows how particles accumulate in these regions at low and high capsular pressures in the 5L-30W-3D model. At low pressure, as the number of cycles increases, particles number only increases in the gap entrance region and remains zero in other regions whereas, at high pressure, particles number increases significantly in the bone region and it remains constant in the gap and the entrance regions. In other words, this figure shows that, at low pressure, the majority of particles remain in the capsular region while at high pressure, the majority of them accumulate in periprosthetic bone. Despite the fact that particles do not enter the bone at low pressure, in some cases a large number of particles (for example, 23% for the low pressure 80L-30W-30D model) may still end up in the gap region.

Table 5.2 also shows that, at low pressure, the gap displacement does not generate enough driving force to transport particles into the bone region. In fact, large implant micromotion reduces particle accumulation in the bone region. Detailed analysis of particle accumulation and the effect of gap displacement are discussed in sections 5.3.5 and 5.3.7.

Table 5.2: Percentage of particle accumulation in the gap and periprosthetic bone regions at high and low capsular pressure.

Model name	Bone region		Gap region	
	Low	High	Low	High
5L-30W-30D	0%	95%	0.004%	3%
5L-30W-300D	0%	56%	0.05%	4%
5L-500W-30D	0%	49%	0%	40%
5L-500W-300D	0%	41%	12%	30%
80L-30W-30D	1.3%	94%	23%	5%
80L-30W-300D	0.4%	36%	0.45%	0.9%
80L-500W-30D	0%	58%	16%	40%
80L-500W-300D	0%	27%	6%	14%

5.3.3 Injection studies

Once injected, parcels destined to accumulate in the bone travel down the gap. In the meantime, because of high pressure and implant motion, they drift towards the gap-bone interface until they come into contact with it and enter the bone. A close look at the gap-bone interface shows that particles enter the bone regions at discrete intervals of defined trajectories. The number of entrance trajectories to the bone is proportional to the spacial resolution of injection points along the gap width (c.f. Figure. 5.7). Since

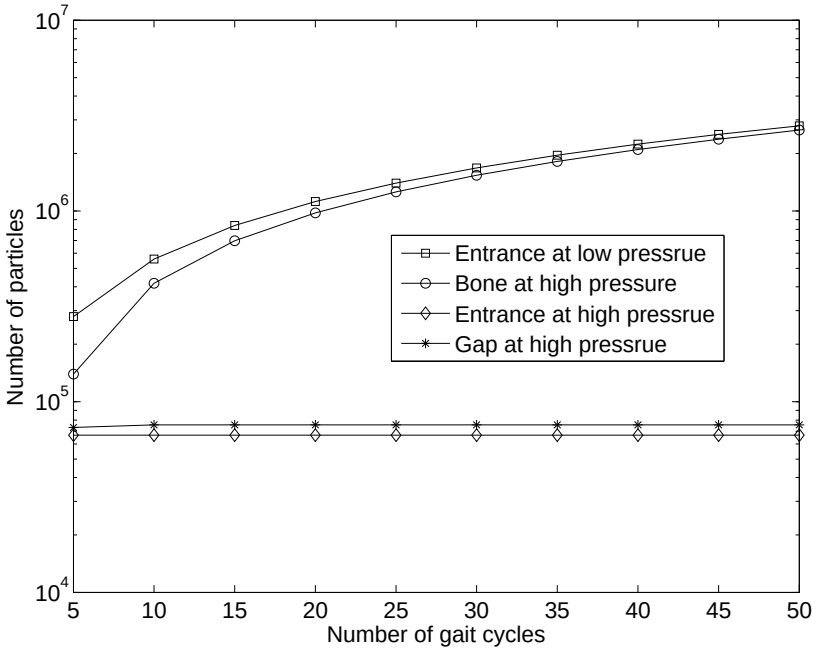

Figure 5.6: The plot showing particles number in the entrance, gap and bone regions of the 5L-30W-3D model as the number of cycles increases.

the number of particles in each parcel is different and inversely proportional to the number of injection points (parcels in models with smaller number of injection points contain larger number of particles), 'a clustering effect' is created. This phenomenon is demonstrated in Figure 5.7. It can be seen that the interface area covered by the trajectories of the injection points contains the same number of particles. However, the particle number in each measuring area (or the particle concentration) is smaller for a model with larger number of injection points. As a result, the higher the injection resolution, the more even is the particle distribution in the bone.

The distance between parcel trajectories at the gap-bone interface shown in Figure 5.7 is proportional to the gap length. In other words, parcels are distributed over a larger interface area in longer gaps and, therefore, the clustering effect is more pronounced for longer gaps. This manifests itself as high peak irregularities in associated 3D contour plots for longer gaps. Figure 5.8, which is a sectional view of the 3D plot shows how increasing the injection resolution can result in smoother distribution of parcels along the gap.

To verify the sensitivity of the results to the injection resolution, the 5L-30W-30D and 80L-30W-30D models were run with 14, 56 and 112 injections points. Figures 5.9 and 5.10 show how mean and maximum particle concentration is affected by changing the injection resolution. It can be seen that in both models the mean and maximum particle concentration are larger for 14 injections points. This difference is, however, less pronounced for mean values. Maximum concentration at different regions in the bone, particularly at proximal and distal regions (regions one and five) with 14 injec-

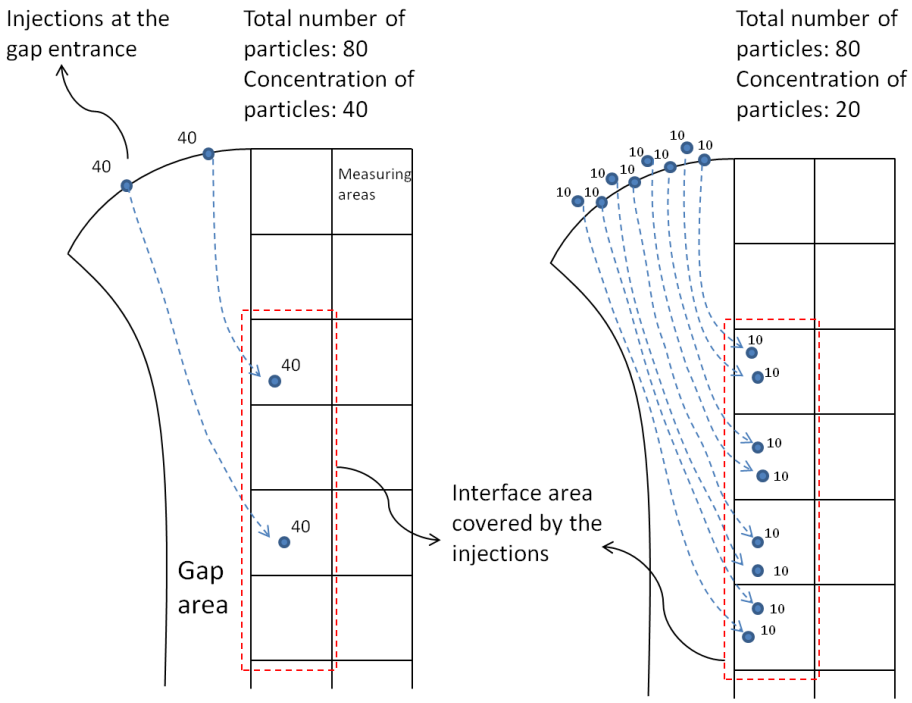

Figure 5.7: Schematic of particle trajectories for different injection densities. For the same interface area covered by the injected particles, particle concentration is different, whereas the total number of particles is the same. This results in the 'clustering effects' explained in the test. The trajectories are shown in this figure by simple curves for demonstration purposes. These trajectories have more complex curves in the simulations.

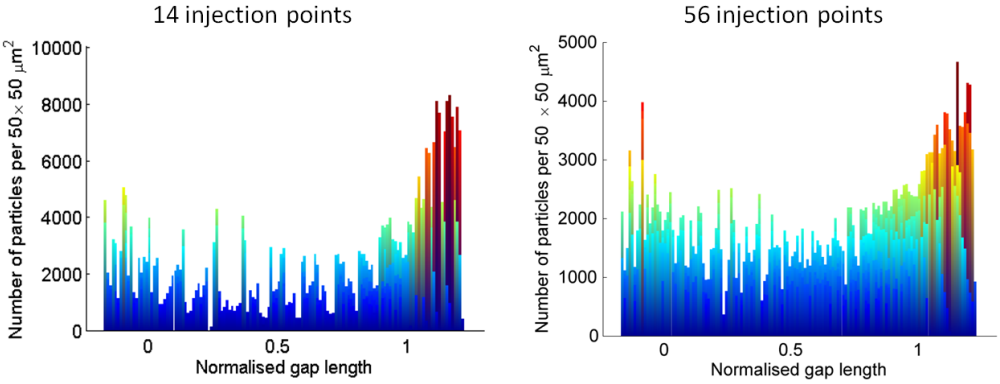

Figure 5.8: Manifestation of clustering effects in 3D contour plots for different injections.

tion points can be twice as large as those with 56 and 112 injections. This difference is likely to results from the clustering effect explained in Figure 5.7. Mean and maximum particle concentrations for 56 and 112 injection points appear to be similar in these figures. To confirm this, multicomparison statistical tests are performed to compare data for each bone region. The tests reveal that the models with 56 and 112 injections produce similar results. However, while results from models with 14 injections are quantitatively different from the models with 56 and 112 injections, they are not qualitatively different from the models with 56 and 112 injections. In all the models with different injections points the overall pattern of particle distribution throughout the bone, gap and capsule regions is similar. This means that while models with 14 injections may overestimate particle concentration, they still can represent qualitative results predicting the overall particle distribution in the bone.

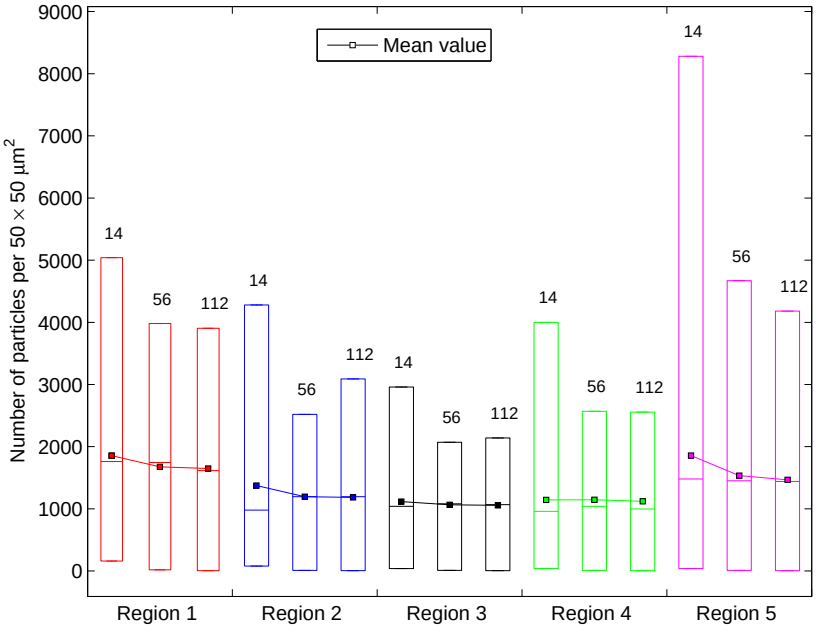

Figure 5.9: Regional plot of the particle concentration at different regions in the bone along the gap for the high pressure 5L-30W-30D model with 14, 56 and 112 injections.

5.3.4 Temporal variation in particle distribution in bone

Figure 5.11 demonstrates how the mean and maximum particle distribution changes for the 5L-30W-30D model in different bone regions as the model is run up to 200 cycles. Most notably, the mean value and maximum particle concentration in bone regions four and five significantly increase as the model is run up to 200 cycles. In addition, the rate of particle accumulation is higher in bone region five in comparison with region four. This suggests that if the model was run for further cycles, the difference in particle concentration between proximal and distal regions of the gap may increase even further. A similar phenomenon is observed for the model with a long gap; however, the rate

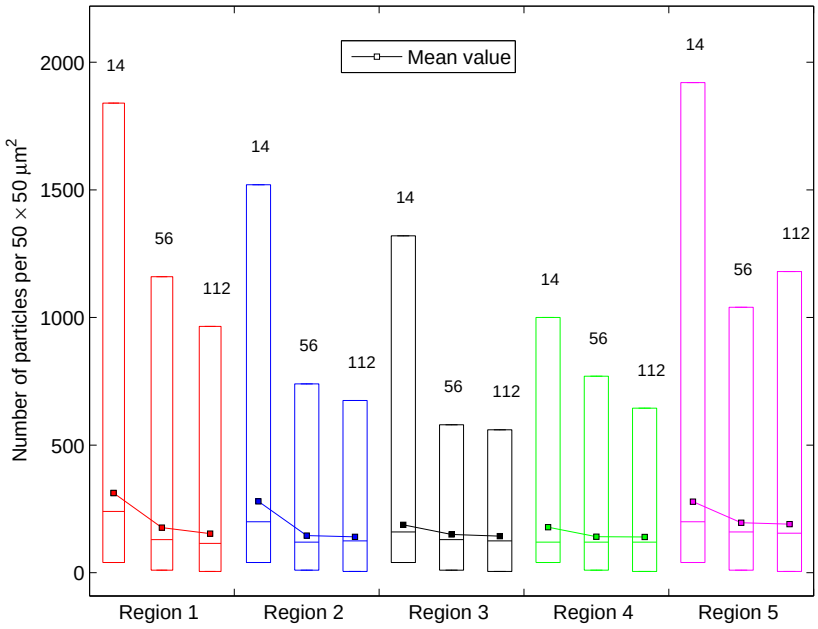

Figure 5.10: Regional plot of the particle concentration at different regions in the bone along the gap for the high pressure 80L-30W-30D model with 14, 56 and 112 injections.

of particle accumulation at the bottom of the gap (region five) is lower than the short gap shown in Figure 5.11.

5.3.5 Regional accumulation of particles

3D contour plots of particle concentration for the high pressure 5L-30W-30D model with 56 injection points after 50 cycles is shown with different views for ease of interpretations in Figure 5.12. It can be seen that particle concentration is considerably larger at the top and bottom of the gap. The y-x view shows that not only is the particle concentration large at the bottom of the gap, but the depth of particle penetration is also larger in this region creating a balloon shape distribution at the bottom of the gap resembling that of osteolytic lesions seen in radiographs. The regional plot corresponding to this 3D contour plot is shown in Figure 5.13. The mean values of particle concentration at distal and proximal regions are approximately 37% larger than the mid-gap region. However, in these regions there are a number of measuring areas with excessively high concentrations which may have a clinical significance for causing conditions for osteolysis generation. To assess the extent by which each bone region is influenced by these high concentration regions, the number of any measuring areas that contain more particles than the 90^{th} percentile value as a fraction of the total number of measuring areas in each bone region is shown above each box. Despite similar mean and maximum concentrations between region one and five, the number of high concentration measuring areas above the 90^{th} percentile is larger in bone region five. The number of high concentration measuring areas above the 90^{th} percentile is

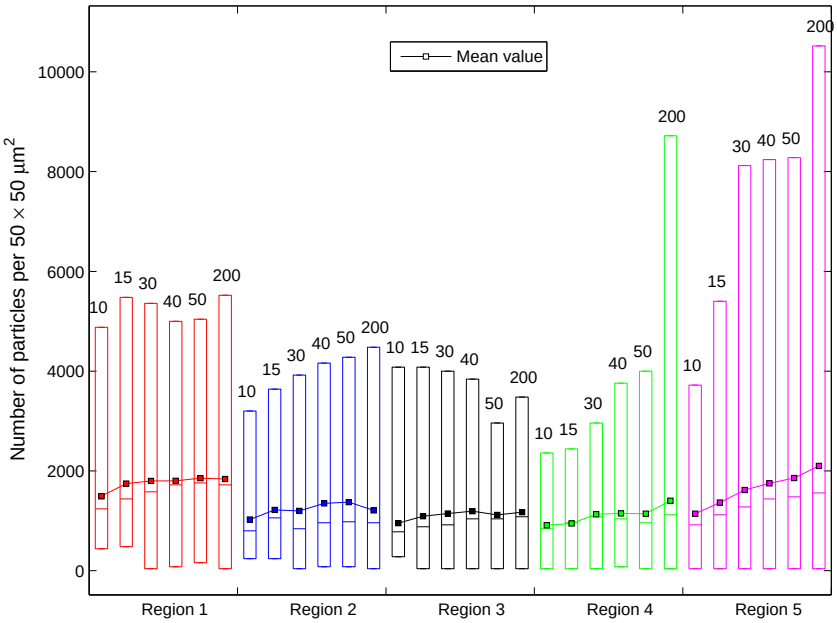

Figure 5.11: Regional plots of the particle concentration at different regions in the bone along the gap for the high pressure 5L-30W-30D model with 14 injection points after 10, 15, 30, 40, 50 and 200 cycles. Significant increase of particle concentration can be seen at region five (gap bottom) after 200 cycles while in other regions particle concentration remains approximately constant.

minimal in the mid gap region.

Quantitatively, the 3D contour plot and regional plot of the 40L-30W-30D model, which are shown in Appendix B (Figure B.1 and B.2) demonstrate similar particle distribution to the 5L-30W-30D throughout the bone. The corresponding regional plot shows that a number of high concentration measuring areas above the 90^{th} percentile also occur in regions five. However, the mean particle concentration value is only approximately 23% higher than that of the mid region. Figure 5.14 shows that, in a very long gap (80 mm), maximum penetration of particles into the bone occurs in the mid gap region and is approximately 0.6 mm deep (this is in contrast to the 5 mm and 40 mm gaps in which maximum particle penetration occurs in distal regions with values of 1 mm and 1.18 mm, respectively). The corresponding regional plot (c.f. Figure 5.15) shows that the mean value of particle concentration at the bottom of the gap is higher than that of top of the gap by 15% percent. Figure 5.15 also shows that peak concentrations which are above the 90^{th} percentile still exist and its higher for region five.

In summary, the results show that particle concentration is higher in distal and proximal regions of periprosthetic tissue after 50 cycles. However, proximal regions contain more measuring areas with excessively high concentrations.

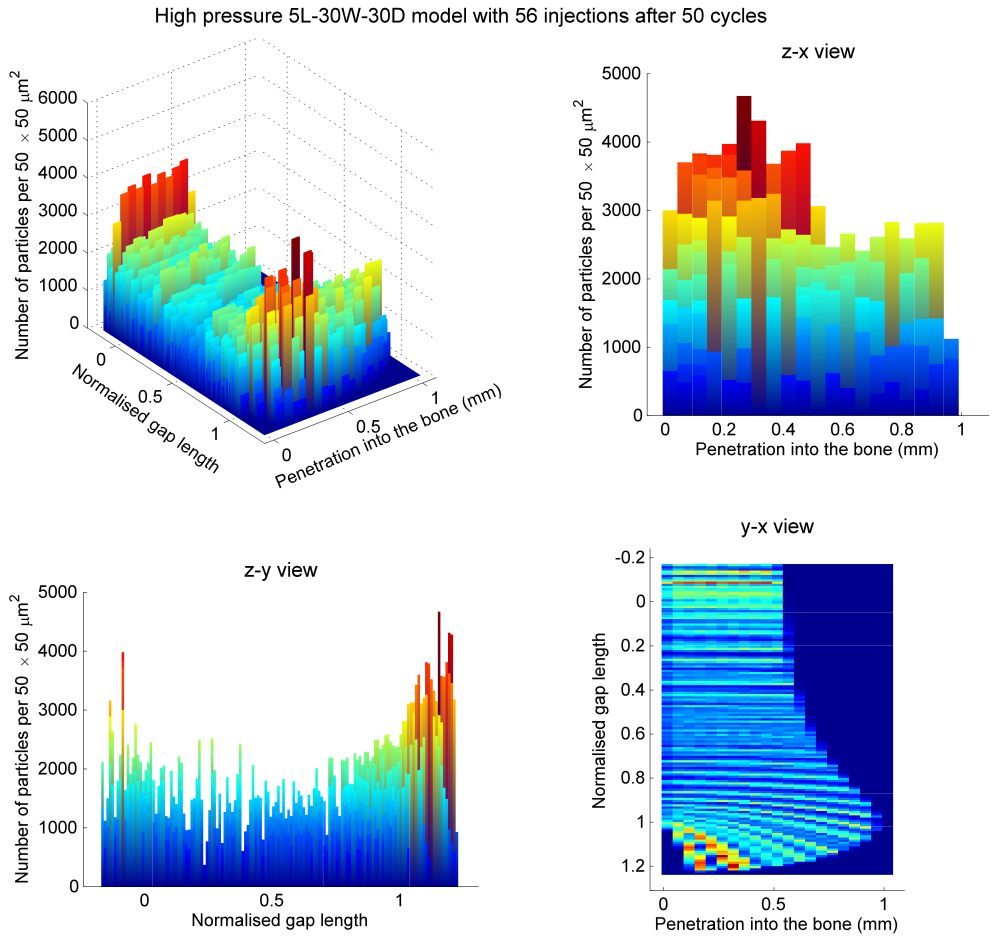

Figure 5.12: 3D contour plots from different views showing particles number per 50 × 50 μm^2 area and their penetration into the bone along width and length of the gap in the 5L-30D-30D model with high pressure and 56 injections. High concentration at proximal and distal regions can be seen.

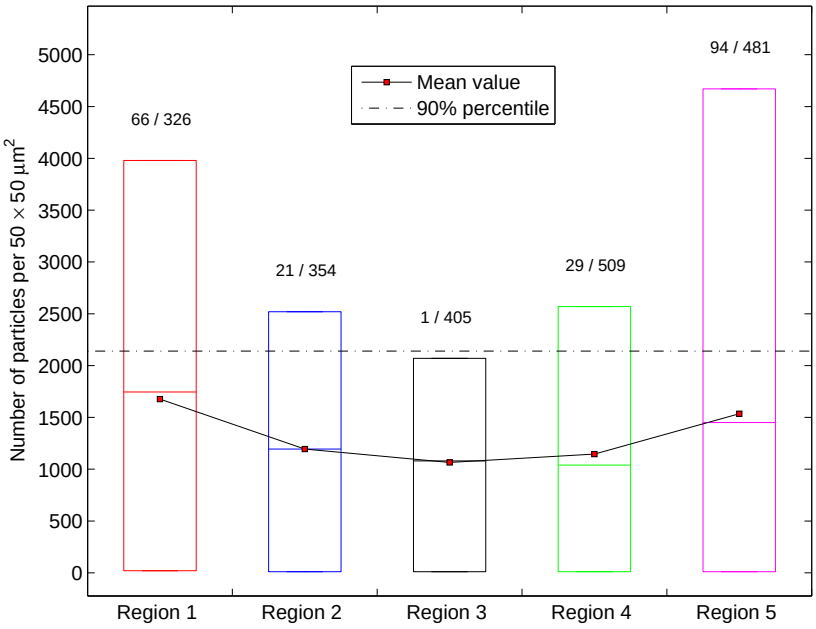

Figure 5.13: Regional plot of the particle concentration at different regions in the bone along the gap for the high pressure 5L-30W-30D model 56 injections. The 90^{th} percentile is calculated based on the total particle number per measuring in the entire model. The mean value as well as the number of measuring areas above the 90^{th} percentile as a fraction of total number of measuring areas are shown above each box.

5.3.6 The effect of gap dimensions

The regional plots for 5L-30W-30D, 40L-30W-30D and 80L-30W-30D are shown in Figure 5.16. The concentration of particles in the bone surrounding a shorter gap is generally higher than a longer gap. Mean concentration for the 5 mm gap is approximately six and ten times larger than the 40 mm and 80 mm gaps, respectively. The width of the gap also influences the particle concentration in the bone regions. For example, in the 5L-500W-30D model, the total number of particles in the bone region is half of that in the 5L-30W-30D model (c.f. Table 5.2), possibly as a result of a slower flow rate of fluid to the bone and the larger volume of the gap accommodating more particles than a narrower gap.

5.3.7 The effect of gap displacement

Gap displacement has a considerable influence on the regional distribution of the particles. Figure 5.17 shows the 3D contour plot of particles for the 5L-30W-300D model with high capsular pressure. It can be seen that high particle concentrations are no longer present at the bottom of the gap. This can be interpreted more easily in the corresponding regional plot in which the 5L-30W-30D and 5L-30W-300D models are compared (c.f. Figure 5.18). A large gap micromotion of 300 μm causes an average reduction of approximately 50% in the mean value of particle concentration. Qualita-

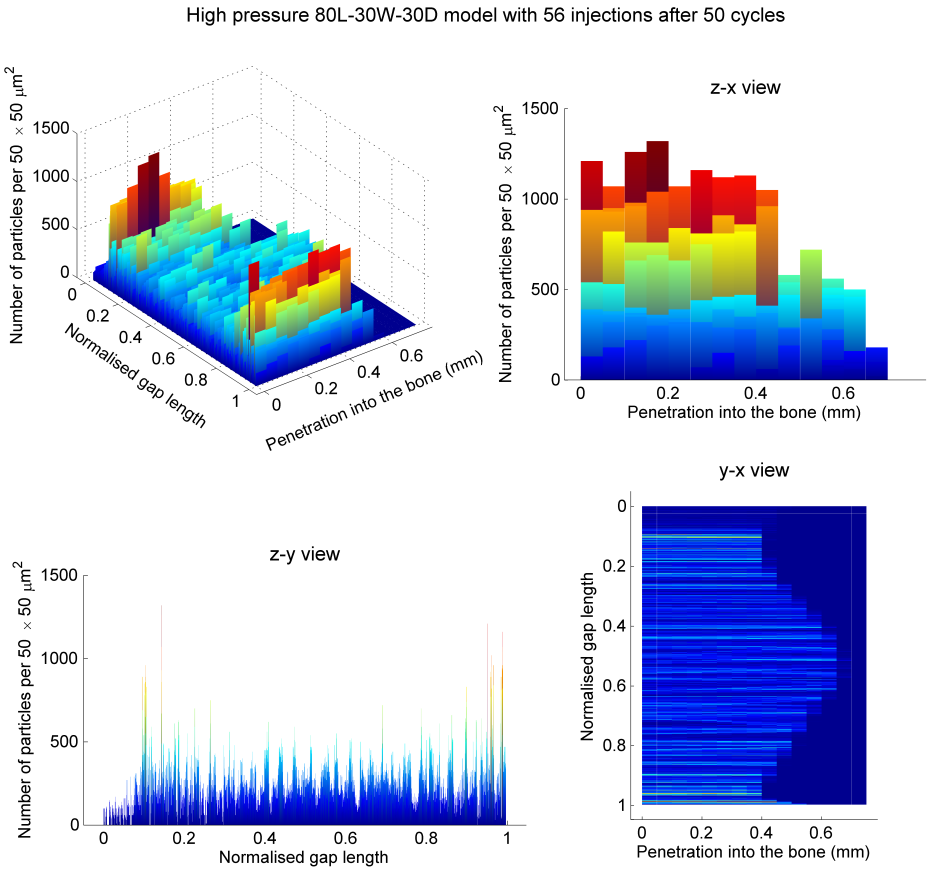

Figure 5.14: Particle numbers per 50 × 50 μm^2 area and their penetration into the bone along width and length of the gap in the 80L-30D-30D model with high pressure and 56 injections. High concentration at proximal and distal regions can be seen.

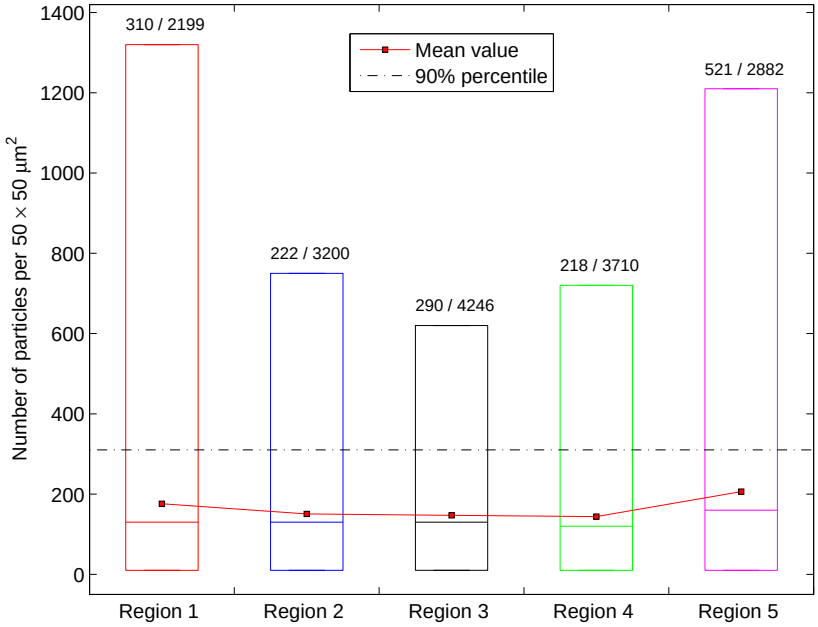

Figure 5.15: Regional plot of the particle concentration at different regions in the bone along the gap for the high pressure 80L-30W-30D model with 56 injections. The 90^{th} percentile is calculated based on the total particle number per measuring in the entire model

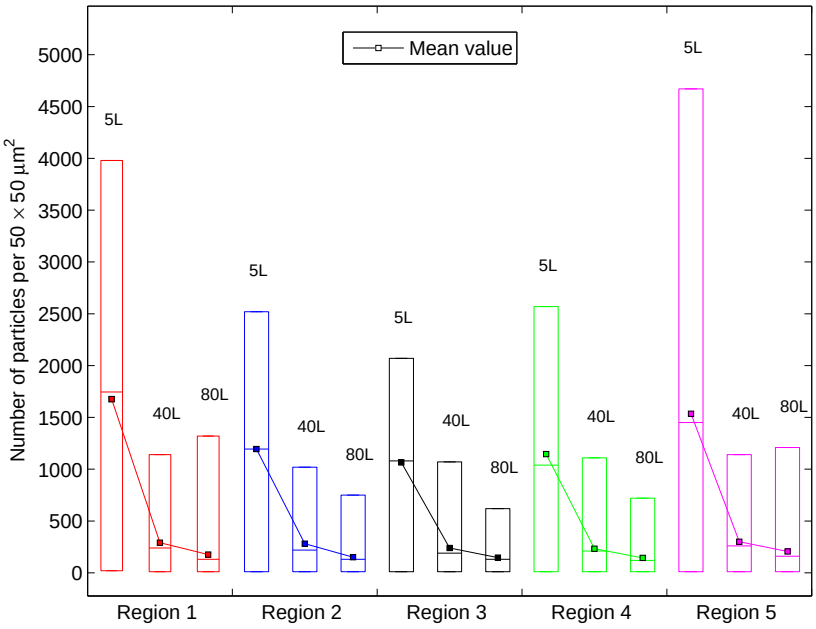

Figure 5.16: Regional plot of the particle concentration at different regions in the bone along the gap for the high pressure 5L-30W-30D, 40L-30W-30D and 80L-30W-30D models with 56 injections. Particle concentration decreases as the gap length increases.

tively, a similar displacement effect is observed for the longer and wider gaps (5L-500W-300D and 80L-30W-300D models). Observations on models with large gap micromotion shows that gap displacement pumps the particles out of the gap region. In other words, gap displacement generates a pumping-out rather than a sucking-in action. This subsequently reduces the number of particles accumulating in the bone. This pumping action is more pronounce for long 80 mm gaps. Table 5.2 shows that a 300 μm gap displacement causes a 39% reduction in the total number of particles in the bone in a short gap, while the same gap micromotion causes a 58% reduction in a long gap. The pumped-out particles flow to the capsular region. Since the force pumping out the particles is greater in the long gaps, they travel a longer distance in the capsule and some particles may reach regions in the capsule far from their injection points. Although micromotion reduces the particle concentrations in the bone, the distance that the particles penetrate into the bone is not affected and penetration distance is still primarily a function of capsular pressure.

At low pressure, the effect of displacement is not clear because the models are not run for long enough for the particles to reach the bottom of the gap. To accelerate the process, particles were injected directly at the bottom of the gap. When compared to the particles in higher regions in the gap, it was seen that particles enter the surrounding bone at the bottom of the long gap. This particle accumulation is considerably lower compared to high pressure models and therefore can be neglected. At low pressures, implant motion pumps the majority of the particles injected at the gap entrance

out of the gap region to the capsular region and, therefore, induces minimal particle penetration into the gap region.

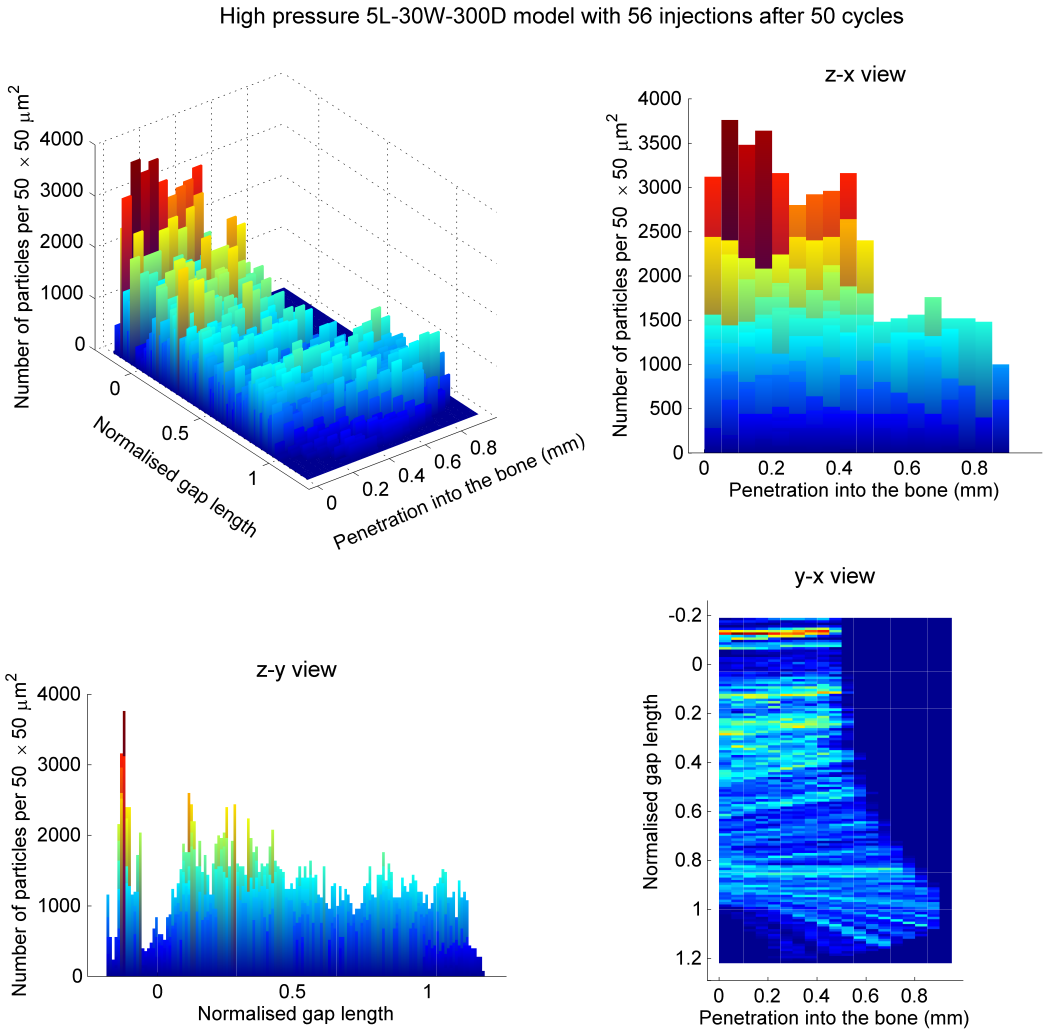

Figure 5.17: Particles number per 50 × 50 μm^2 area and their penetration into the bone along width and length of the gap in the 5L-30D-300D model with high pressure and 14 injections. A considerable reduction in the particle concentration at the bottom of the gap as a result of large micromotion can be seen.

5.4 Discussion

How polyethylene particles migrate away from a joint capsule is poorly understood. Models developed in the current study provide a means to better understand this phenomenon. Eight models described in chapters 3 and 4 in addition to the 40L-30W-30D model were run at low and high pressures with particles injected at the gap entrance. Since postprocessing capabilities in Fluent are not appropriate for analysing the results, postprocessing tools were developed in MATLAB to better interpret and understand the mechanisms influencing particle migration in periprosthetic tissue. These tools

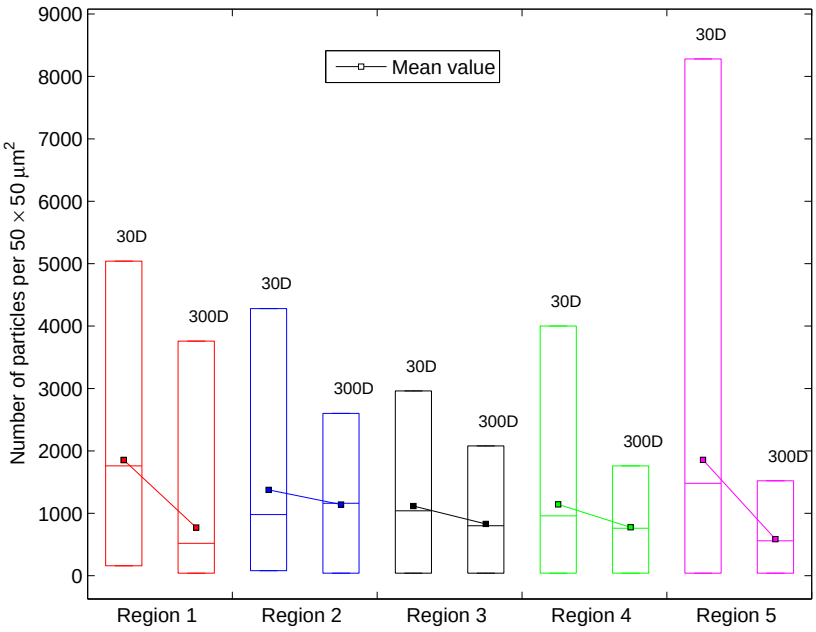

Figure 5.18: Regional plot of the particle concentration at different regions in the bone along the gap for the high pressure 5L-30W-30D and 3L-30W-300D models with 14 injections. Particle concentration decreases as a result of large implant micromotion.

include 3D contour and regional plots. The former counts particles in equally spaced regions of the periprosthetic bone and the latter uses the data obtained from 3D contours to facilitate means by which different models and bone regions could be analysed and compared. The effect of parameters including capsular pressure, injection resolution, gap dimensions and micromotion on periprosthetic particle migration were studied.

Injection points

For ease of comparison, the models were set up in a manner that the total number of particles injected to the system would always remain the same, which means a lower injection resolutions contains higher numbers of particles and vice versa. While this keeps the total number of particles constant, it influences particle concentration in the bone since the dispersion of particles in the bone region is a function of injection resolution. This phenomenon was termed the 'clustering effect' and is shown schematically in Figure 5.7. It was described that injection resolution could be increased only within allowable limits imposed by the number of mesh cells at the gap entrance. The results show that there is no significant difference between 56 and 112 injection locations. This is due to the fact that particles injected at entrance surface 2 follow approximately the same trajectory as those injected at entrance surface 1 (c.f. Figure 5.2) since their injection points are approximately located on the same vertical line. Therefore, they migrate to the same region in the bone. Also, the measuring areas are not small enough

to capture any difference in the position of particles injected from different injection surfaces. In other words, particles released from entrance surface 1 and entrance surface 2 end up very close to each other and they fall in the same measuring area in the bone. Therefore, 56 injection points results in the lowest achievable dispersion of particles and is used for the studies in Chapter 6. However, changes in injection resolution, at least in the range used here (14, 56 and 112), do not affect the qualitative behaviour of the particles. Therefore, models run with lower resolution of 14 injection points can still provide reasonable results for qualitative comparison at a lower computational cost.

Continuity of particle release

Particles were released in each time step at the gap entrance, just above where the gap starts. This ensured the availability of new particles at the gap entrance continuously throughout a gait cycle. This injection strategy was based on the assumption that a large number of particles have already been released to and evenly distributed in the joint fluid after a sufficient period of time, postoperatively. Although the postoperative time for sufficient numbers of particles to be generated depends on many parameters such as the rate of wear generation, it has been shown that osteolysis commonly appears at twelve to sixty six months [29], postoperatively. This period can be considered as the time when the particle concentration in the joint fluid is adequate to cause bone resorption through a constant supply of particles to the interface bone. The models developed in the current study attempt to represent this situation.

Gap communication with the joint capsule

Hydraulic communication between the interface and the joint capsule is demonstrated by Anthony et al. [84] who showed that arthroscopy contrast material injected to the hip capsule penetrates into the interfacial lytic lesions after 45 minutes of walking. This leakage of the joint fluid to the lesions was also confirmed during revision surgery. Similar communication between interfacial gap and joint capsule is demonstrated by Cone et al. and Hendrix et al. [78, 6]. Schmalzried et al. [47] also showed that in some of the problematic cementless implants in which torque-testing had shown that the prosthesis was rigidly fixed and histological examination revealed ingrowth of bone, the contrast medium flowed rapidly and extensively in the bone-metal interface. The above clinical observations support the assumptions that joint fluid has access to the bone-implant interface.

The assumption is also that joint fluid is the carrier of particles to the endosteal bone through interfacial gaps. However, another explanation for particle migration is transportation through the interfacial fibrous tissue, a constituent of periprosthetic

tissue in THRs that is not present in the current study. However, it has been shown that when the interface is surrounded by a stable fibrous tissue, the implant may still function perfectly [121] and particles do not penetrate to the distal regions of the interface [64]. In addition, it has been shown that micromotion-induced flows in fibrous tissue are incapable of pumping particles very far into the interface [63] and if migration of particles through this mechanism exists, it must be extremely slow [84]. Including fibrous tissue at the interface in the models as a material with a higher permeability than bone, particles can migrate the interface at a much slower rate, but probably not at a sufficient rate to create conditions for osteolysis.

Capsular pressure

During physiological loading, interfacial gaps are subject to extreme hydraulic capsular pressures [78]. In natural hips, when the joint is under load, the joint capsules deforms and increases its volume to accommodate elevated pressure caused by the physiological loading and the excess of synovial fluid is driven to the iliopsoas bursa. However in THRs these mechanisms are not often present. Tarasevicius et al. [82] has shown that high pressures are associated with low capsular elasticity which means joint fluid has nowhere to flow other than to interface gaps. The models in the current study show that high capsular pressures may be the main driving force for pumping particles into the bone region. It is shown that, in the presence of hydraulic communication between the capsule and the endosteal surface, up to 95% of the available particles at the gap entrance find their way into the periprosthetic bone tissue. Indeed, lower capsular pressure results in a lower rate of particle accumulation in the bone. Clinically, it has been shown by Hendrix et al. [6] that a significant relationship exists between implant loosening and the penetration of contrast material, equivalent to particle laden synovial fluid, into the interface because of high capsular pressure. This relationship is likely to be the result of capsular pressure pumping wear particles to the interface, as shown in the models here. Robertsson et al. [75] also suggested that it is very likely that capsular pressure functions as a pump that distributes particle-containing joint fluid through the path of least resistance of an interfacial gap. Flow of tracer particles to the bone under fluid pressure for 10 minutes, which is a relatively comparable time frame to the period of time represented by 50 cycles here, has also been observed by Fahlgren et al. [39]. The models show that at low (neutral) pressure, particles hardly enter the bone region although displacement of very long and narrow gaps (80L-30W-30D and 80L-30W-30D models) results in a small percentage of particle penetration into the bone. The effect of displacement in these models is discussed later in this section.

The significance of capsular pressure in osteolysis generation may also be confirmed by the clinical observation that focal osteolysis occurs more frequently in younger patients [32]. Indeed, younger patients are more active, and as a result, high pressures

may be more frequently generated in their joint capsule. Consequently, more particles may be pumped into the interface which leads to a higher prevalence of osteolysis. Zicat et al. [32] demonstrated that focal and larger lesions tend to develop in younger patients and Goddard and Gosling [79] showed that capsular pressure my be higher in young patients with problematic joints.

Despite the fact that, at low pressure, particles do not penetrate the bone significantly, up to 23% of available particles at the entrance find their way in the gap region in long gaps with small displacement (c.f. Table 5.2). These particles are located adjacent to the interfacial bone and may be transported to the bone by other means such as cellular or lymphatic transportation and trigger long term bone resorption. They also may cause production of cytokines that induce bone resorption.

The models here show that, under constant 60 kPa pressure, particles penetrate into the bone region up to a depth 1.5 mm after 50 cycles. However, it should be noted that high pressure does not normally remain constantly high and varies in physiological conditions. While constant high pressure helps to accelerate the process of particle migration in an affordable computational time, it may overestimate particle penetration during 50 cycles. Pressure variation may also lead to a phase difference between cyclic capsular pressure and the micromotion of the gap. Additional studies which included phases differences of $\frac{\pi}{2}$, π and $\frac{3\pi}{2}$ between a varying pressure (0 to 60 kPa during a gait cycle) and gap micromotion, showed that the phase difference did not change particle concentration and distribution significantly since capsular pressure was still the dominant driving force for particle penetration into the bone. Since flow remained laminar for a model run with cyclic pressure, including a pressure variation only reduced particle penetration into the bone and the overall behaviour of the model remained unchanged. In addition, the effect of the physical presence of the bone matrix solid phase which may lead to particle clogging at the interface is not included. These may explain why particle penetration is overestimated here. In fact, the next chapter includes these effect in the simulations.

Another factor to be considered is the phase difference between

Particle migration

In the current study, models produce results that may be comparable to clinical observations. Penetration of particles deep into the periprosthetic bone has been observed. Bauer et al. [20] mentioned that biopsies obtained several millimetres away from the implant membrane contain particles. Willert et al. [35] also observed that particles entered the interface and infiltrate marrow cavities of cancellous bone as well as the Haversian canals of cortical bone. The depth of particle penetration seen in the models is comparable to the finding of Bobyn et al. [122] who observed that the injected polyethylene debris (1×10^8 particles twice a week) penetrated the intratrabecular

spaces approximately 2 mm after 10 weeks of injection followed by 10 weeks of rest. Lalor et al. [60] also observed migration of particles to the periprosthetic bone marrow at a comparable time of 4 weeks when polyethylene particles were injected into an implanted rabbit joint. However, capsular pressure, micromotion and the number of cycles are not known in these studies.

Despite the predominant downward flow in the gap region, the results show that particles constantly enter the bone along the entire gap-bone interface and flow in lateral direction. This correlates well with clinical observations in radiographic examination in which osteolytic radiolucent lines extend along the edges of the stem. Histological examination of such cases demonstrate the existence of polyethylene particles along the stem in these regions [56, 122, 64, 29]. Also, Zicat et al. [32] has shown that osteolysis caused by particles appears to extend away from the bone-implant interface which is agreement with the lateral direction of particle flow seen here.

The distal direction of particle flow in the gap shows that it is only in the presence of an interfacial gap that particles flow to the distal regions, which is a common observation in cementless implants with smooth surfaces. It has been shown that in the absence of access to the bone along the edge of a stem, particles do not tend to accumulate along the interface or migrate to distal regions [65, 122]. Another indication for the necessity of an interfacial gap for distal particle migration is evident in stable cemented prosthesis, in which the interface is sealed by the bone cement. It has been shown that, in these implants, osteolysis appears only as small and focal lesions along the interface where there is a defect in the cement [123]. This shows that in the absence of interfacial gaps particles do not accumulate at the interface. Furthermore, particle concentration is significantly higher at the interface in cementless implants, which are more prone to develop interfacial gaps, compared to those that are cemented as shown by Hirakawa et al. [124].

Particle distribution and osteolysis

Despite the fact that particles enter the bone along the entire gap, simulations here show that the penetration is generally larger at the gap bottom, which creates a balloon shape distribution at the gap bottom resembling focal osteolysis seen in radiographs (c.f. Figure 5.19). The results also show that particle concentration in periprosthetic bone in proximal and distal regions is higher than other regions after 50 cycles. However, the number of measuring areas with high concentration is more at the bottom of the gap. In addition, while high concentration reaches a quasi steady state in the proximal region after 30 cycles, particle concentration constantly increases at the bottom of the gap. This phenomenon was confirmed by running some of the models up to 200 cycles. The reason for this may lie in the presence of high velocity spikes at the bottom of the gaps described in the previous chapter (c.f section 4.3.1), which generates a velocity

gradient across the bone in this region. As particles enter the bone, their velocity decreases significantly. Then, they travel through the porous bone with approximately a constant velocity. Since particle velocity is relatively constant, the number of particles entering and leaving a measuring area is the same. This results in a constant number of particles in a measuring area at any instance in time. However, this phenomenon does not occur in the bone around the bottom of the gap due to the presence of the velocity spikes. The number of particles entering the measuring areas at the bottom of the gap is more than the number of particles leaving these regions because of the velocity gradient across the bone in the vicinity of the gap bottom. This results in particle accumulation at this region.

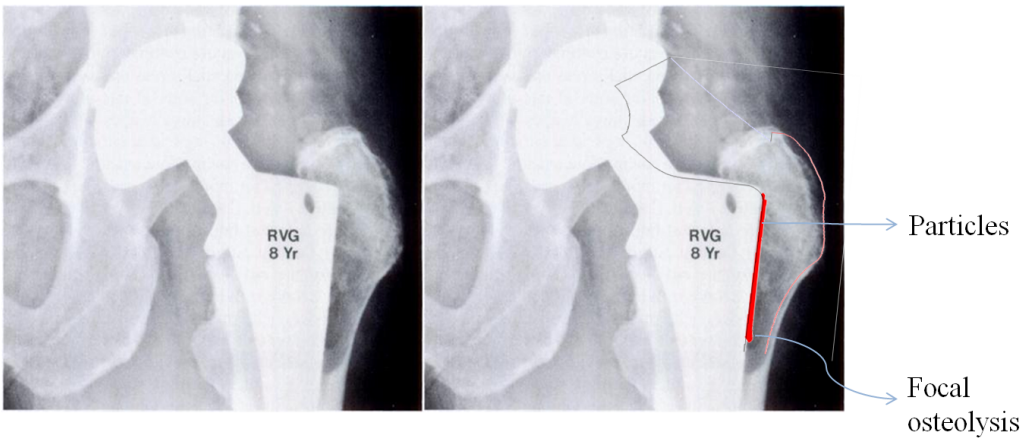

Figure 5.19: Particle distribution obtained from the 40L-30W-30D model superimposed on a radiograph of a linear-focal osteolytic lesion obtained by Zicat et al. [32].

The presence of polyethylene particles in periprosthetic bone has been reported in many studies [34, 35, 47, 84, 53, 61]. However, there is no study in the literature describing the pattern of particle distribution around the interface, particularly around interfacial gaps. The models here suggest that particles are mainly distributed and accumulate at distal regions around a gap. These regions, therefore, may be exposed to a higher risk of osteolysis generation because of increasing particle concentrations. The bottom of the gaps with lengths of 5 mm, 40 mm and 80 mm are located in Gruen zone one(seven), two(six) and three(five), respectively. The likelihood of osteolysis in these regions is shown in Figure 2.11 where it can be seen that in the presence of a route for particle migration at the interface (smooth surfaces of the stem), osteolysis is more likely to develop in lower zones of two(six) and three(five) (c.f. Figure 2.11). This may be in accordance with the observation here that particles accumulate at the distal regions of the gap. In the absence of interface access, as shown by Von Knoch et al. [64], osteolytic lesions may only develop in grater trochanter above the shoulder of the prostheses and/or in the upper Gruen zone one and seven which are represented by the short gaps in the current study.

The results show that in the long gaps the particle concentration is not as high is shorter gaps. However, it has been shown that particle concentration at the bottom of the gap increases as the model is run for more cycles. It is possible that in long gaps the particle concentration reaches the critical threshold for osteolysis at the bottom of the gap after more cycles, which is a very likely scenario considering the fact that an implant experiences millions of cycles through its lifespan. As mentioned earlier, the effect of porosity is not included. Having these effects included, higher concentrations may have been reached in the longer gaps, which may exceed the critical threshold of osteolysis. It is also shown that the concentration of particles is approximately 14% higher in focal osteolysis compared to linear osteolysis [53]. The models show similar results for the 80 mm long gap in which the mean concentration of particles is 15% higher at the bottom of the gap, where focal osteolysis is likely to occur. This difference in mean concentration between the gap bottom and mid-gap regions increases to 23% and 37% for 40 mm and 5 mm gaps, respectively. Assuming that the particle concentration reaches the critical threshold at some postoperative time, these values show that for all gap lengths, linear osteolysis may develop along the gap while bottom regions may turn to focal ostelysis. This process may be faster and more pronounced for shorter gaps due to higher particle concentrations. In addition, measuring areas with concentration above the 90^{th} percentile are greater in number in long 40 mm and 80 mm gaps. These may also lead to conditions for very small regions of osteolysis to develop along the implant edge that may join one another over a long period of time to form linear osteolysis.

Gap micromotion

Contrary to the general belief that implant micromotion can act as a pumping mechanism to transport particles to the bone-implant interface [76], the models in the current study show that micromotion appears to push the particles out of the interfacial gaps. This effect is more pronounced for longer gaps. It can be seen in Table 5.2 that, at high pressure, there is a 41% and 62% reduction in the total number of particles in the bone in the 5L-30W-300D and 80L-30W-300D models, respectively, as a result of a large micromotion of 300 μm. This may be caused by the fact that larger implant displacement exerts a larger force on the fluid in the gap region to overcome the force generated by the capsular pressure. At low pressure, as the gap opens, particles are drawn to the gap. As the gap closes, the majority of particles are pushed to the capsular region. However, some particles remain in the gap region and travel further down the gap as the implant undergoes further gait cycles. The particle that migrate towards the bottom of the gap are no longer pushed out by the implant micromotion. They are rather pushed further down the gap and to the bone region. This is shown in Figure 4.11 in the previous chapter, where it can be seen that in the lower gap regions the

fluid continuously flows down the gap and into the bone even when the gap is closing. However, an implant undergoes millions of cycles during its time in vivo so, long and narrow gaps may lead to particle accumulation at the bottom of the gap at low capsular pressure. This may cause the appearance of osteolysis even in joints that do not experience high pressures. However, the rate of particle accumulation is much lower in these cases.

5.5 Limitations

There are certain limitations associated with this 2D study that have to be considered while interpreting the results. In 3D, interfacial gaps have more complex geometries and displacements. For instance, a wedge shaped interfacial gap with its tip pointing distally may be significantly more efficient to transport particles to the gap bottom. Linear osteolysis may not appear in the these gaps because of the large surface area along which the particles may disperse whereas focal osteolysis may appear rapidly. As mentioned earlier, the presence of bone matrix as an obstacle to particle flow is not included in these set of models. In addition, as bone is resorbed, a larger space which may be filled with fluid or fibrous tissue is produced, encouraging more joint fluid and wear particles to flow into that location, which fuels additional bone resorption. This may change the pattern of particle distribution and osteolysis in the periprosthetic bone. Particle clogging in the solid matrix and increases in periprosthetic tissue permeability because of osteolysis are incorporated in the simulations in the next chapter.

Particles are modelled as spherical and inert with a constant size. In reality, however, wear particles have a variety of shapes and sizes. Considering these parameters is outside the scope of the current work. Further analysis is required to study the effect of these parameters on the flow of joint fluid and periprosthetic particle distribution.

5.6 Conclusions

It has been shown that capsular pressure is the main driving force for particle migration to periprosthetic tissue. Although cellular transport of particles has not been considered, hydraulic transfer appears to play an important role in particle migration to the bone. Implant micromotion acts to pump out particles rather than sucking them into the interfacial gaps, except in long gaps in which, even at low pressure, particles that made it to the bottom region migrate to the bone tissue as a result of micromotion. The models show that the type and degree of potential osteolysis sites depends on the initial dimension of the interfacial gaps. Focal osteolysis is more likely to develop at the bottom of the gaps where particle concentration is generally higher. In contrast, the potential for linear osteolysis to develop is higher along the gaps. It was also shown

that particle concentration is higher in shorter gaps leading to conditions for earlier development of osteolysis along them. Finally, for osteolysis to develop in distal regions, a constant supply of particles, as well as an access route to the endosteal bone must be available.

Chapter 6

Periprosthetic particle clogging and tissue permeability variation

6.1 Introduction

In the previous chapter, the migration of wear particles to periprosthetic tissue at the gap interface was studied. However, particle entrapment and clogging in the periprosthetic tissue were not considered. Data from the literature indicates the existence of such mechanisms. Based on autopsy studies, it has been shown that particles from the primary implantation stayed in the tissue for up to three months after revision [61]. This indicates that particles do not flow continuously with the fluid phase, but become trapped in the periprosthetic tissue. From a clinical perspective, the effect of particle clogging and entrapment in the periprosthetic tissue may become significant in long term, when the number of accumulated particles in the tissue becomes large enough to reduce tissue porosity resulting in a change in local tissue permeability, and osteolysis generation.

The first aim of this chapter is to devise methods to simulate particle clogging in long postoperative periods and to investigate the parameters influencing the resultant particle distribution and concentration. The second aim is to simulate permeability increases, representing fibrous tissue occupying the osteolytic lesions, in the periprosthetic tissue due to high particle concentration and to investigate parameters influencing its development. Increase in tissue permeability representing the generation of the fibrous tissue and its effect on the periprosthetic fluid flow may provide a means to better understand osteolysis generation and progression throughout time.

6.2 Methods

6.2.1 Clinical parameters

6.2.1.1 The rate of wear generation and the degree of particle access to the interface

The rate of wear generation depends on many parameters such as patient activity, the femoral head size, relative position between the head and cup etc. Dowd et al. [52] observed a forty-fold variability in wear rates between patients. By measuring the penetration of the stem head into the acetabular cup, they observed that the rate of wear generation during ten years, was linear for most of the cases. However, they also observed cases with bimodal wear rates consisting of two apparent linear segments (c.f. Fig. 6.1). These nonlinear cases were usually accompanied by the presence of non-polyethylene particles, otherwise known as third-body wear particles, released from the implant porous bed to the joint capsule. The release of these third-body particles is more likely for cementless implants which have a porous surface for fixation. The mechanical failure of this porous surface leads to wear debris release to the system. Third body particles may enter the space between the bearing surfaces, cause scratches and increase the surface roughness of the femoral head. Increased roughness of the femoral head may dramatically accelerate the rate of wear generation [125]. Damage to the femoral head is common and was found on 89% of fifty-four cobalt-chromium alloy heads after postoperative periods ranging from eight months to nineteen years [126]. Similarly, in an analysis of retrieved Charnley femoral components, 76% of seventy-one stainless steel heads had an average surface roughness greater than that of the time of implantation.

The rate of wear measured by the head penetration into the cup may overestimate wear generation in early postoperative periods because much of the initial head penetration is due to creep rather than the actual wear of the bearing material [28]. This may question the linearity in wear rate observed by Dowd et al. [52], who based their observation on the head penetration. Additionally, there is an initial conformity between bearing surfaces, which leads to lower contact stresses and consequently a lower rate of wear in early postoperative years [127]. At the later postoperative stage this conformity may disappear by inconsistent wearing of the cup, which may result in higher rates of wear.

Apart from the rate of release of particles to the system, the degree of particle access to the interface tissue through a gap also plays an important role. Some gaps may exist from the early postoperative stages and widen to provide a greater access at later stages, or some may appear some time after the implantation for various reasons including mechanical failure or fatigue at the interface and become larger as time

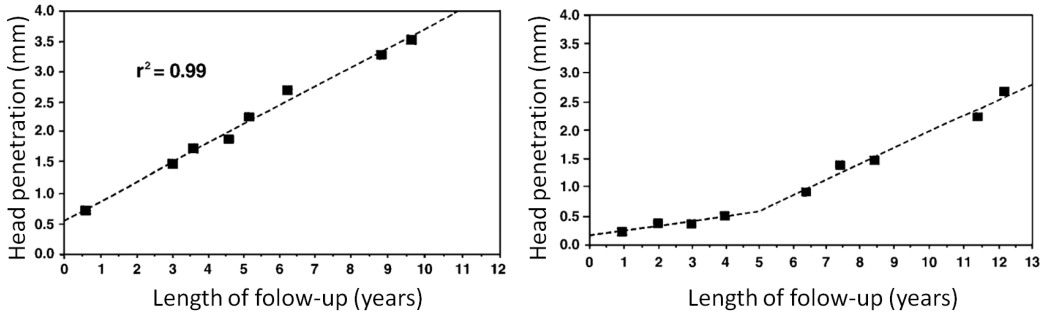

Figure 6.1: Rate of wear in 10 postoperative years. Wear release into the system can be linear or nonlinear [52]

elapses.

The above explanation may show that the rate of wear generation or its access to the tissue may vary for individual. To present this variation, different rates of particle release into the models are employed. This is explained in section 6.2.2.

6.2.1.2 Osteolysis threshold

A detailed explanation about the biological threshold for the onset of osteolysis in terms of the particle number was given in section 2.3.5.3. In the following sections the osteolysis threshold is referred to as os_t. The defined osteolysis thresholds in the literature have to be converted to an appropriate parameter that can be used in the current simulations.

In studies in which the particles in the fibrous tissue, occupying osteolytic lesions, are counted and the osteolysis threshold is established, the data is presented in terms of the particle number per gram of tissue. The wet weight of the tissue is measured first and the specimen containing the particles is digested in a solution. The particles in the suspension are then filtered and counted under Scanning Electron Microscopy (SEM). The results are then presented as particle concentration with units of number of particles per 1 gram of tissue. To make this value appropriate for the current study, the particle concentration has to be presented in terms of tissue volume. For example, for a threshold value of $os_t = 1 \times 10^9$, one gram of periprosthetic tissue contains one billion particles. Assuming a consistent particle distribution throughout the tissue and a density of 1500 kg/m^3 for periprosthetic tissue, 1 g of periprosthetic tissue consists of a cube with a volume of 6.667 $\times 10^{-7}$ m^3 and dimensions of approximately 8.7 $\times$ 8.7 $\times$ 8.7 mm in which the one billion particles are evenly distributed. However, it is possible to calculate the threshold for smaller volumes of tissue using linear interpolation. For example, this threshold reduces to 750 particles for a cube with dimensions of 10 $\times$ 10 $\times$ 50 μm as shown in Figure 6.2.

By assuming a depth of 50 μm for the model (same dimension as the measuring areas described in the previous chapter), it is possible to use linear interpolation to calculate

the corresponding osteolysis threshold for each of the cell volumes in the model. This is achieved by developing a user defined function (UDF) which was incorporated in the simulations. If the number of particles in a volume cell rises above the specified threshold defined by os_t then the UDF instructs Fluent to assign a permeability value of fibrous tissue (1×10^{-11} m^2 [95]) to that computational cell, thus simulating the effect of osteolysis.

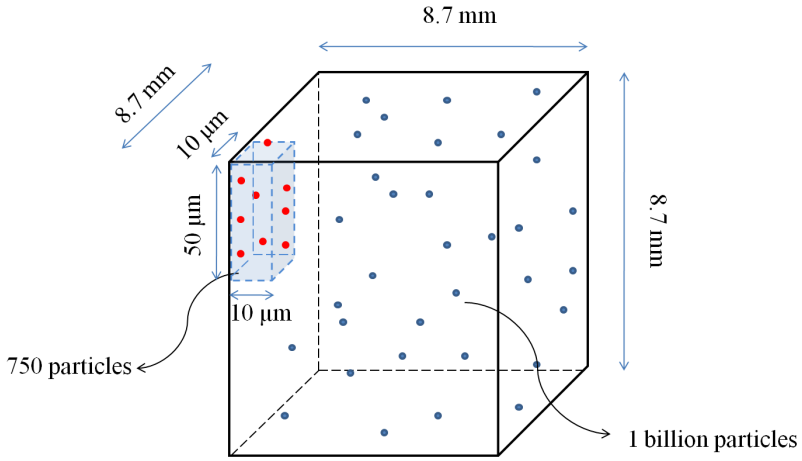

Figure 6.2: Particle concentration in the bone

6.2.2 Scaling factor to simulate long term postoperative periods

As mentioned earlier, billions of particles are released from bearing surfaces and accumulate in periprosthetic tissue during postoperative years. It has been shown that this large number of particles can accumulate over years in small regions containing only one gram of tissue [54]. The number of particles released during ten seconds of simulation time in the models developed for the previous chapter is significantly less than that which is released in the effective joint space during postoperative years. For instance, for a normally functioning implant, approximately 6.67 billion particles are released into the system during each postoperative year while during the simulation time of 10 seconds only 2.8 million particles (280000 parcels) in total are injected in a model. Injecting such a large number of particles to simulate long term postoperative periods is beyond the current computational capabilities. To circumvent this problem, a parameter called 'scaling factor' (s_{f_y}) is implemented to artificially multiply the number of particles that are released in the model during the practical simulation time of ten seconds to a target number appropriate for a particular postoperative year. The subscript y in s_{f_y} shows the intended postoperative year to be simulated where y can be 1, 2, 3 ... 16. For example, s_{f_1} indicates that the number of particles is scaled for the period of one postoperative year. Using this approach, it is possible to mimic a

long period of postoperative time using a practical simulation time of 10 seconds. This is demonstrated in Figure 6.3 where it can be seen how the real number of injected particles in the model is scaled to a desired number of particles during a simulation.

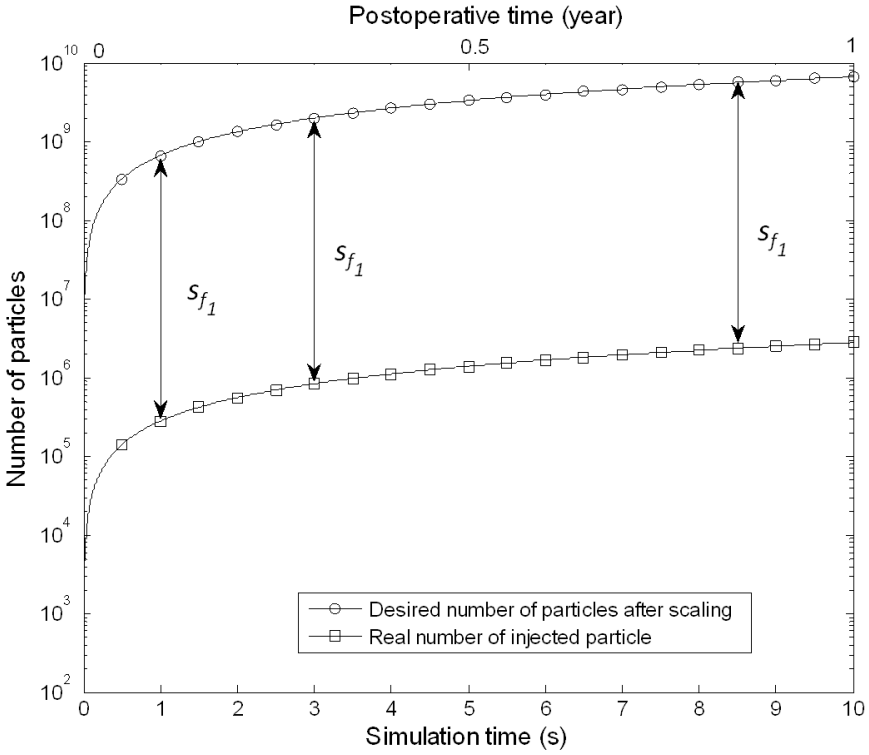

Figure 6.3: Example shows scaling factor, s_{f_1}, scales the real number of particles in the model to the desired number of particles. Lower x axis shows the simulation time and the upper x axis shows the postoperative time.

It was shown in Chapter 5 that at least 30 cycles are required to reach a quasi-state equilibrium for particle distribution and concentration in the bone. Ideally, every time the number of particles is scaled by the scaling factor s_{f_y}, the models should run until a new equilibrium is reached before the particle number is scaled again. However, this requires a significant computational time which is beyond the capabilities available for the current study. However, to circumvent this problem, particles number is scaled in small intervals of simulation time step ($\Delta t = 0.02s$) throughout a simulation. Although equilibrium is not achieved every time particles number is scaled by using this approach, the models can still provide a first approximation for the overall effect of particles on clogging the periprosthetic tissue and fibrous tissue generation.

If it is assumed that ten seconds of simulation time represents a period between implantation and a particular postoperative time, the number of particles has to be scaled according to the postoperative time that is represented by the simulation time at each instance. In addition, the rate of wear generation may change over postoperative time and is not necessarily linear. To represent these phenomena mathematically, s_{f_y} is defined as a polynomial function of the simulation time and its power degree represents

the degree of wear generation nonlinearity (c.f. Figure 6.4). If the desired number of particles at a particular postoperative time (t) is defined by $Np_d(t)$, the real number of particles that has been injected to the model by that time by $Np_{inj}(t)$, the final desirable number of particles that has to be achieved by the end of simulation by Np_f, the scaling factor by $s_{f_y}(t)$ and the degree of the scaling factor by p_d then,

$$Np_d(t) = s_{f_y}(t)^{p_d}.Np_{inj}(t). \tag{6.1}$$

Since the practical run time for the simulations in this study is ten seconds, the boundaries for the above function has to be set such that the total number of particles after scaling reaches the final target value. Therefore, the following criteria has to be satisfied:

$$Np_f = \int_0^{10s} Np_{inj}(t).s_{f_y}(t)^{p_d}dt \tag{6.2}$$

The realisation of the above equations is shown in Figures 6.4 and 6.5 which are plotted for the case of ten years of postoperative time. Figure 6.4 shows how the polynomial degree (p_d) affects the linearity of wear generation in the models. Regardless of the degree of the polynomial, the final number of particles in the model reached by the tenth year is always the same and set by the value of Np_f. Figure 6.5 shows the instantaneous scaling number during the simulation time for different polynomial degrees. For linear wear generation ($p_d = 1$) the scaling number is constant form the beginning of the simulation. For larger values of p_d it increases from zero to the desired number. p_d values greater than one produce a relatively slow rate of increase in particles number at first, which then increases by the end of simulation. In other words, the plots showing cases with p_d larger than one in Figure 6.4, have a smaller slope at the beginning of a simulation which increases by time. Throughout the text, $p_d = 1$ is referred to as higher wear generation rates and $p_d = 2$ and 4 represent slower rates, respectively.

In summary, the above approach can be used to induce different wear generation rates representative of a realistic postoperative time.

6.2.3 Particle clogging model and clogging factor (c_f)

Flow of particles through a porous medium is a complex phenomenon because of various mechanisms involved. Two types of particle clogging have been defined. Mechanical clogging for large particles (diameter $>$ 30 μm), and a physicochemical filtration for small particles (diameter about 1 μm). For mean particle size (1 μm $<$ diameter $<$ 30 μm), which is the focus of the current study, both mechanical and physicochemical phenomena [128] are in effect. When particles flow through a porous medium, they are

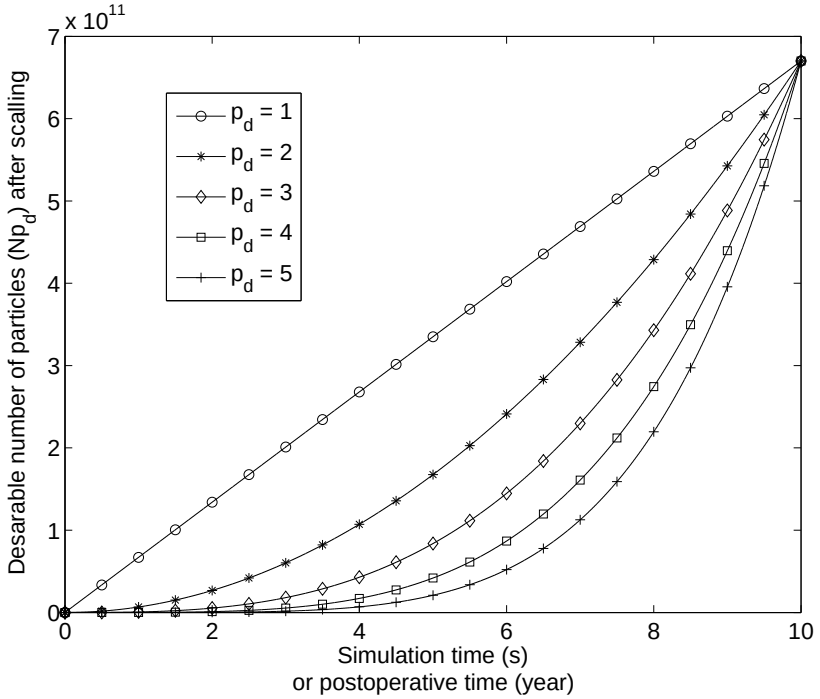

Figure 6.4: Variation of particle number during a simulation for ten postoperative years with different polynomial degrees . The final value of Np_f that is reached in all five cases is 6.67 $\times 10^{11}$, which is the final number of particles released into the system after 10 years.

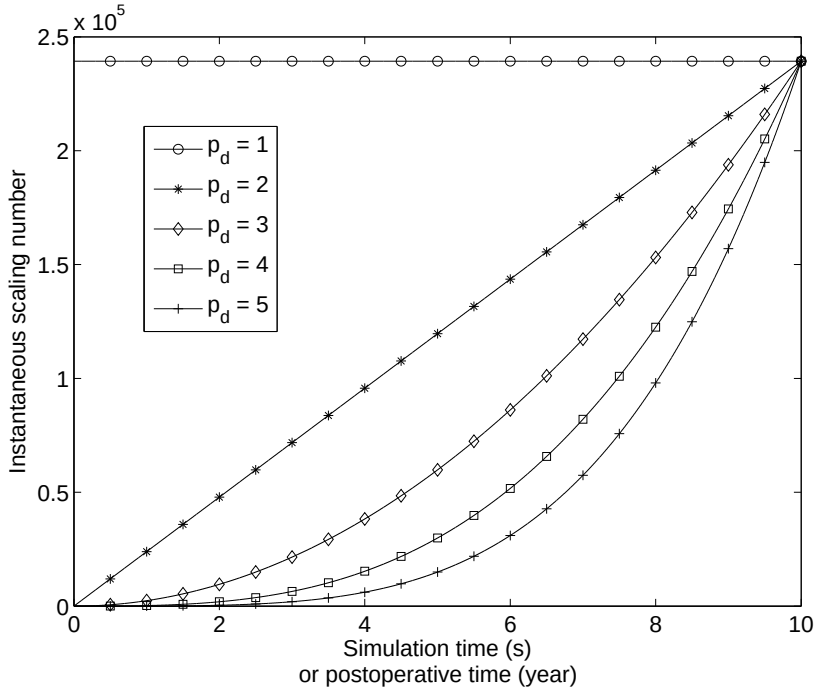

Figure 6.5: Variation of scaling number during a simulation for different polynomial degrees. Scaling number remains constant when $p_d = 1$.

brought into contact with possible retention sites; they stop there or are carried away by the stream. The following scenarios may occur in this process: contact of particles with the retention sites; fixing of particles on the sites, and eventually, the breaking away of previously retained particles. In the case of periprosthetic tissue, it is possible to consider different parameters which describe the elementary processes of clogging and de-clogging. Retention sites that may stop particles include periprosthetic immobile soft tissue and trabecular bone crevices and surfaces. These sites may be smaller smaller than the size of the particles. There may also be retention forces. The fluid pressure may hold an immobilised particle against a porous opening. Particles may also remain in place by friction. Surface forces including the Van der Waals forces, which are always attractive, the electrical forces (electrostatic or electrokinetic) which are either attractive or repulsive according to the physicochemical conditions of the suspension may also play a role. In addition, it is known that giant cells tend to accommodate and immobilise a large number of particles inside them [67], which may be considered as another clogging mechanism. Some of the entrapped particles may also be captured by the flow shear stress and start migrating again or they may be carried away by the vascular drainage system. This creates a scenario in which particles are continuously deposited on and broken away from periprosthetic tissue (c.f Figure. 6.6).

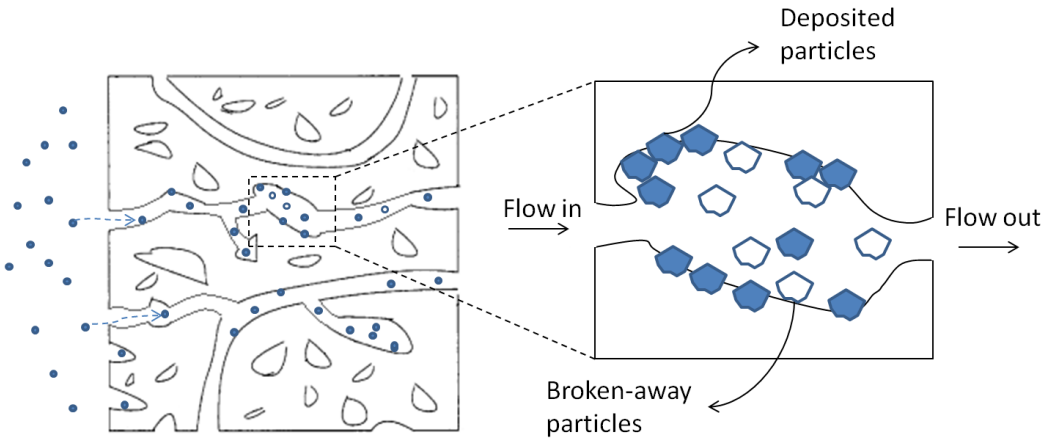

Figure 6.6: Schematic representing particle clogging in a porous medium. Some particles are deposited on the solid matrix of the porous medium while some previously deposited particles are broken away from the solid matrix and carried away by the flow.

Simulating each of the above mechanisms is not possible because of the complexity and the fact that there is no data available in the literature describing them for periprosthetic tissue. However, it is possible to represent their overall effects by a clogging parameter. This parameter may define the degree or the probability of the particles being trapped or stopped in the periprosthetic tissue.

There are two restrictions in defining and implementing such a parameter in the models in the current study. Firstly, such a parameter defining particle deposition

in porous media cannot be incorporated in the currently available theoretical models in Fluent. Secondly, there is no data defining particle clogging or similar properties for periprosthetic tissue. To circumvent the first restriction, a code was written in C and incorporated to Fluent as a UDF. In this code Fluent is instructed to tag particle parcels by a randomly generated number between zero and one in each time step as the particles are injected to the continuum field. This provides an identification number for each parcel. Then Fluent is instructed to loop through all the parcels and detect those particles in the bone region and assign a zero velocity to those particles that have been assigned a tag in a certain range. For instance, it is possible to instruct Fluent to stop particles which are tagged with a number less than 0.9 in each time step. This means that throughout the simulation, 90% of the particle are stopped in the bone region in each time step. This forced zero velocity simulates the entrapment of particles in porous obstacles. This approach makes it possible to control the percentage of particles that clog the bone region. The parameter that defines the percentage of stopped particles is called clogging factor (c_f). c_f values can range from 0% (no clogging) to 100% (a complete blockage to particles). A sensitivity analysis for c_f values is carried out in section 6.3.2.

To circumvent the second restriction, an empirical approach is adopted. In this approach the clinical observation of particle distribution pattern at the interface is used as a criteria for choosing an appropriate clogging factor. Bobyn et al. [122] described such a distribution by stating that particles were confined almost entirely to the membrane adjacent to the implant when there is a continuous supply of particles. The largest particle quantities are located in the membrane adjacent to the implant and extend along the entire interface and the smaller quantities of particles are located further from this membrane in trabecular spaces. No particles are observed within intratrabecular spaces in regions further than approximately 2 mm away from the implant. In other retrieval studies in which periprosthetic particles were analysed and counted, the specimens containing billions of particles were taken from regions just adjacent to the implant [124, 129]. These observations show that the majority of particles have a tendency to accumulate in close proximity of the interface. On the other hand, particles are also observed several millimetres away from the bone implant interface [53], which indicates that, despite the existence of obstacles, a small number of particles may still find their way deep into the periprosthetic tissue. Linear radiolucent lines, which indicate the presence of osteolysis and particles, normally do not extend more than 4 mm [130] which shows that migration of particles into the tissue is limited. All the above observations indicate that particle concentration is highest in close proximity of the interface and decreases further from the interface. Such a phenomenon is also seen in particle filtration studies in geological material [131]. Many studies have been reported in the literature addressing particle entrapment in

the soil and other material [128]. However, applicability of these studies is limited to particular cases considered. There is no such a study relevant to the bone-marrow system surrounding an implant. In summary, the clinical observation of higher particle concentration and accumulation in close proximity to the interface and lower particle concentration and accumulation at distant regions from the interface is used as a criteria to choose an appropriate value for c_f. The process of choosing the appropriate c_f for the current study is discussed section 6.3.2.2.

6.2.4 Particle-porosity relationship

As particles clog and accumulate in periprosthetic tissue over numerous postoperative years the tissue porosity and, therefore, its permeability tends to reduce. Thus, changes caused to the local permeability in regions containing particles becomes a function of the number of residing particles in that region. As explained in section 2.5.8, bone permeability k can be described as a function of its porosity, ϕ. For bone, this relationship is described by the Kozeny-Carmen model.

Porosity is the ratio between the void volume and the entire volume of a continuum element. As particles enter and clog the pores of periprosthetic tissue, the porosity and permeability of the material are reduced. Therefore, the new porosity, ϕ_{new}, as the result of particle accumulation is a function of initial porosity ϕ_0 and the volume occupied by the instantaneous number of particles V_p in a cell volume, c_v:

$$\phi_{new} = \phi_0 - \frac{V_p}{c_v}. \tag{6.3}$$

In the above equation, the total volume of particles is effectively subtracted from the void volume and a new value for the porosity is calculated. Therefore, a new permeability can be calculated based on the new porosity, ϕ_{new}, using the Kozeny-Carmen model described in section 2.5.8:

$$k_{new} = \frac{c\phi_{new}^{\alpha}}{S_v(\phi_{new})^2}, \tag{6.4}$$

where c and α are correlation coefficients, and $S_v(\phi_{new})$ is the bone specific surface function [101].

To simulate this phenomenon in Fluent, a UDF was written to identify those cells in the bone region containing particles, and to implement changes in the permeability in each cell volume at each time step using the above equations.

6.2.5 Varying parameters in simulations

To simulate particle clogging in long term postoperative periods and to investigate how the clinical parameters influencing the resultant particle distribution and concentration,

the parameters shown in Table 6.1 were varied in the specified ranges. The main focus is on models run with $s_{f_{10}}$ since ten years is the postoperative time intended to be simulated in this chapter. However, some simulations were run with s_{f_y} representative of postoperative periods other than ten years to establish sensitivity of the results to the length of the simulated postoperative period. To reduce the computational costs and also to only focus on the effect of the mentioned parameters, only the 5L-30W-30D high pressure model is used in this chapter. The simulations are transient and the boundary conditions and gap displacement are similar to that described in Chapter 3. The injection of particles and the number of cycles (56 injection points and 10s of simulation time consisting of 50 cycles) are similar to that described in the Chapter 5.

Table 6.1: Parameter definitions and ranges.

Varying parameter	Minimum	Maximum
Scaling factor (s_{f_y})	$y = 1$	$y = 16$
Polynomial degree of scaling factor (p_d)	1	4
Clogging factor (c_f) (%)	0	90
Osteolysis threshold (os_t) (particles number per gram of tissue)	5×10^8	1×10^{12}

6.3 Results

6.3.1 General observation

In general, the results discussed in details below show that particle distribution and concentration in periprosthetic tissue is significantly influenced by the value of clogging factor (c_f). An approach has been adapted to determine the value of clogging factor (c_f) for a given scaling factor (s_{f_y}) such that the distribution of particles closely represent clinical observations. The rate of wear generation represented by the polynomial degree of s_{f_y} also has an effect on particle distribution in the periprosthetic tissue. In the models simulating permeability increase representative of fibrous tissue generation, osteolysis threshold (os_t) and the polynomial degree (p_d) (also referred to as the rate of wear generation) play a combined role in determining the extent and onset of permeability increase (also termed as fibrous tissue generation) in postoperative years. For the ease of comparison in the following sections, the particle concentrations are represented by the actual number of particles in the model and not the number of particles after scaling.

6.3.2 Sensitivity to clogging factor (c_f)

6.3.2.1 The sole effect of c_f

The clogging factor (c_f) determines the percentage of particles that are stopped by the periprosthetic tissue solid phase (c.f. section 6.2.3). To investigate the effect of c_f, models with c_f values of 0%, 30%, 50%, 70% and 90% were run. Figure 6.7 shows that this parameter (when no permeability change is included) only affects the depth of penetration and concentration. However, the overall particle distribution which is characterised by relatively high particle concentration at the gap entrance and bottom remains unchanged. As c_f increases from 0% to 90% there is a linear reduction in particle penetration depth, approximately. However, Figure 6.8 shows that particle concentration in all five interface regions increases exponentially as c_f increases from 0% to 90%. An inspection on particle positions along the interface shows that, as the depth of penetration decreases, particles are packed more closely to each other resulting in higher concentrations. This increase in particle concentration may affect the periprosthetic flow and the particle distribution when changes in permeability during postoperative periods are included in the models. This phenomenon is discussed in the next section.

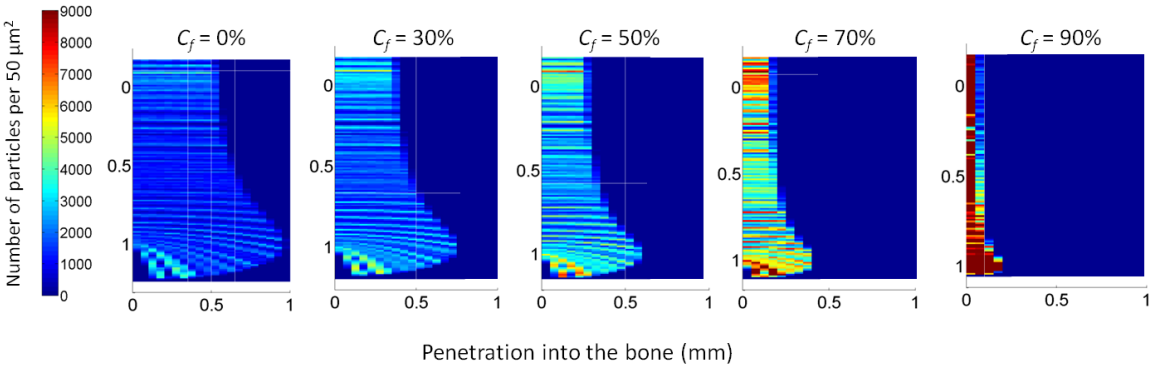

Figure 6.7: Contour plots showing particle concentration for models run with c_f values of 0% 30%, 50% and 90% when no permeability change is included. c_f influences the depth of penetration and subsequently the particle concentration in the periprosthetic tissue.

6.3.2.2 The combined effect of c_f and s_{f_y}

As mentioned earlier, there is no data available in the literature describing particle clogging (in terms of its probability or rate) in periprosthetic tissue. Therefore, the criteria to choose an appropriate c_f was based on clinical observations, which is referred to as 'clinical criteria' in the following text. Models with scaling factors representing one to sixteen years in conjunction with different values of c_f were run. The results

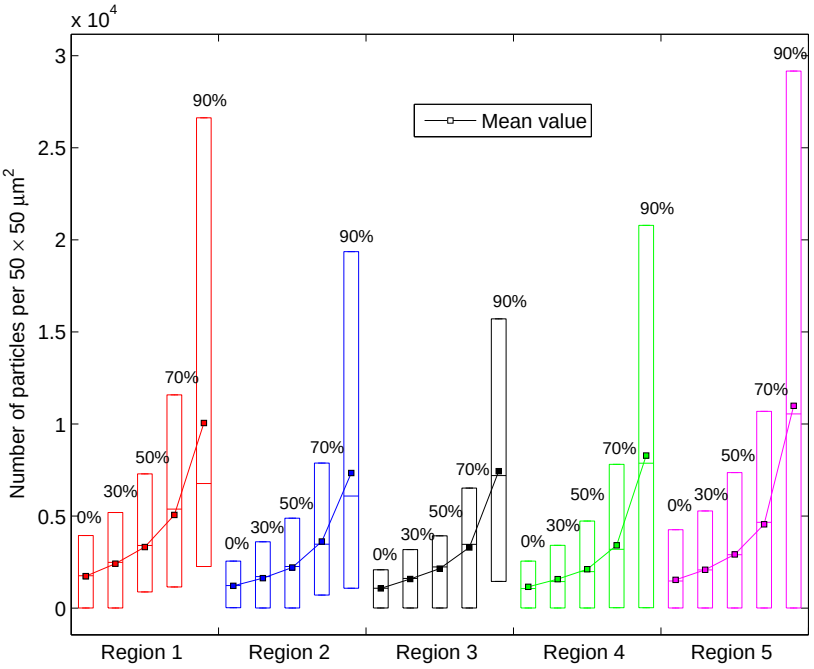

Figure 6.8: Regional plot of the particle concentration in different regions in the bone along the gap for models run with c_f values of 0% 30%, 50% and 90% when there no permeability change is included. Increasing the value of c_f causes an exponential increase in the mean particle concentration in all periprosthetic tissue regions. The maximum particle concentration also increases accordingly.

show that for a given s_{f_y} (y = 1,2 ... 16), c_f plays a defining role in determining the periprosthetic particle distribution. The overall observation is that, for a given postoperative year represented by y, for the particle distribution at the interface tissue to satisfy the clinical criteria, the value of c_f has to be empirically adjusted for that particular postoperative period. The overall trend is that, as y decreases, the c_f must increase for the models to be confined within the clinical criteria. For instance, for particle distribution to resemble clinical observation, a higher value of c_f is required for $y = 1$, when compared to a model run with $y = 10$. A detailed analysis for the relationship between s_{f_y} and c_f for the case of $y = 10$ is presented here since the purpose of this chapter is to model a postoperative time up to ten years.

The contour plots of particle concentration and distribution for the models with c_f values of 0%, 30%, 50%, 70% and 90% and $s_{f_{10}}$ are shown in Figure 6.9. For $c_f > 50\%$, particle penetration is effectively blocked and a few particles penetrate the bone beyond 50 μm from the interface. In other words, particles only accumulate at the gap interface. On the other hand, for $c_f < 50\%$ deep particle penetration into the bone is possible. However, particle concentration throughout the tissue for most of the regions remains unchanged (c.f. 0% and 30% cases in Figure 6.9). In other words, there is no particle accumulation at close proximity of the interface in these cases. To better demonstrate this, plots showing particle concentration along a profile line located in the mid-gap

region perpendicular to the interface for c_f values of 0%, 30% and 50% are shown in Figure 6.10. The plots for c_f values of 70%, 90% are not shown since there is no significant particle penetration to be measured for these values. This figure shows that, it is only when the value of $c_f = 50\%$ that a gradual decrease in particle concentration occurs. Lower values produce an approximately constant particle concentration along this profile line. Therefore, it is possible to conclude that the c_f value of 50% may be able simulate the aforementioned clinical criteria for the postoperative period of ten years. This value was thus employed for the rest of the simulations in this chapter.

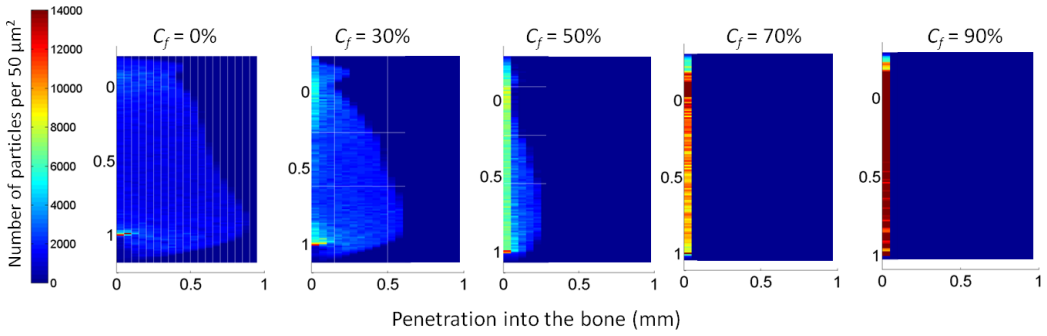

Figure 6.9: Contour plots showing particle concentration and distribution for c_f values of 0% 30%, 50% and 90% when the simulation intends to represent a postoperative time of ten years.The clinical criteria is best presented by the c_f value of 50%.

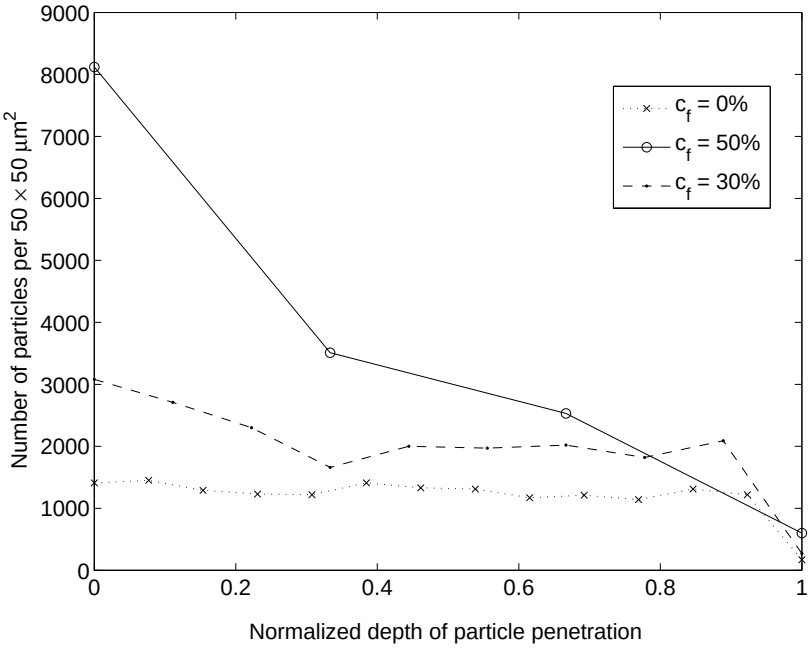

Figure 6.10: Particle concentration along a profile line which is located in the mid-gap region. This profile line is perpendicular to the interface and extends to up to the regions of farthest particle penetration. For ease of comparison its length is normalised. A gradual decrease in particle concentration occurs for $c_f = 50\%$.

6.3.3 The effect of the scaling factor (s_{f_y}) polynomial degree (p_d) on periprosthetic particle distribution and flow

6.3.3.1 Interfacial permeability change due to particle clogging

As particles clog the interface tissue during postoperative years, they may reduce the local permeability of the tissue. How this reduction occurs, depends on the rate of wear and the degree of particle access to an interfacial gap. The rate of wear generation or the degree of particle access can be presented by the sacling factor polynomial degree p_d. Figure 6.11 a, b and c show how changes in permeability evolves for p_d values of one, two and four, respectively. In the first postoperative year only polynomial degree of one results in noticeable reduction in permeability of the interface tissue. This reduction can be up to three orders of magnitude. However, the regions affected only extend to a small depth. As the model is run further in time, Figure 6.11 (a) shows that permeability reduction is always more pronounced in regions closer to the interface. This is also the case for $p_d = 2$ and $p_d = 4$ in those postoperative years in which a reduction in the permeability starts appearing. For $p_d = 2$, the permeability change starts appearing between the second and third postoperative years. This change, however, only occurs at the bottom of the gap initially and it is only at later postoperative years (between years six and eight) that it develops along the interface. By the tenth year a significant reduction in permeability along the interface with further development at the bottom of the gap can be seen. For polynomial degree of four, reduction in permeability similarly occurs at the gap bottom initially, but at later postoperative stage (sixth year). It then develops along the entire interface. For the polynomial degree of four, however, regions experiencing permeability reduction are located deeper into the periprosthetic tissue by the tenth year. This is more pronounced at the bottom of the gap in particular. Comparing the three polynomial degree cases presented here, it can be seen that a constant scaling number, which is induced by $p_d = 1$ (c.f. Figure 6.5) results in a greater and an earlier permeability reduction. The effects of these patterns of permeability change on periprosthetic particle concentration and distribution is presented in the following section.

6.3.3.2 Interfacial particle distribution after particle clogging

Figure 6.12 a, b and c show the variation of particle distribution and concentration for $p_d = 1, 2$ and 4. In the early postoperative years, there is no significant difference between these cases. At later stages, however, this figure shows that as the polynomial degree increases, the depth of particle penetration also increases. This means that higher initial rates of wear generation clog the interface at early stages and inhibits the following particles from penetrating deeper into the bone. At a constant wear

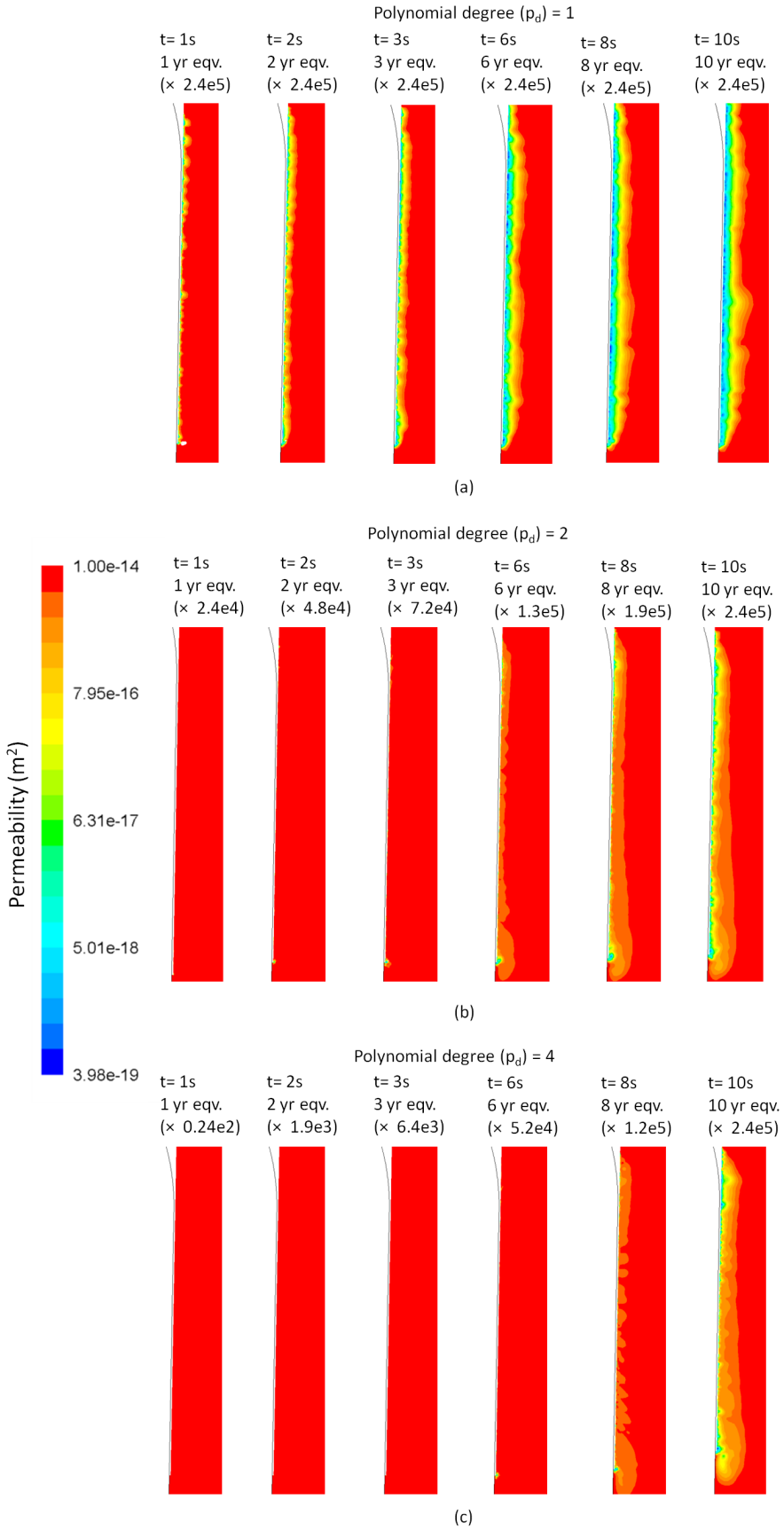

Figure 6.11: Contour plots showing permeability change at the interface tissue for $p_d = 1, 2$ and 4. The plots show how reduction in permeability progresses into the interface tissue as time elapses.

generation ($p_d = 1$) particle concentration is higher at the bottom of the gap in the early postoperative years (until the sixth year). However, at later stages, particle accumulation becomes pronounced also in other interfacial regions.

Figure 6.12 b and c show that particle concentration remains higher at the gap entrance and bottom during all the postoperative years. This is more clearly evident in Figure 6.13 where regional plots for particle concentration at the tenth postoperative year are shown. However, for the case of $p_d = 2$, it can be seen that, by the tenth postoperative year high concentration is about to appear along the entire interface similar to that of observed in the case of $p_d = 1$ in the tenth year (c.f. Figure 6.12 a). Running the model with $p_d = 2$ for further time confirmed this trend. The average concentration is higher in all the regions for $p_d = 1$, whereas it remains approximately the same for the $p_d = 2$ and $p_d = 4$ (c.f. Figure 6.13).

A common feature seen in all the simulations is the significantly higher number of particles in regions adjacent to the gap bottom. This is also evident in Figure 6.13 where maximum concentrations are significantly higher in region five. Significantly, the location of this highly concentrated measuring area coincides with regions where fluid spikes were observed in Chapter 4.

6.3.3.3 Interfacial fluid velocity and pressure

The presence of particles and the subsequent reduction in permeability affect the fluid velocity in the gap and periprosthetic tissue adjacent to the gap. However, change in pressure is not significant in these regions. Figures 6.14, 6.15 and 6.16 show velocity measurements along the gap and bone profile lines, described in Chapter 4, throughout the simulation time for the case run with $p_d = 1$. Figure 6.14 shows that there is no significant change in the fluid velocities in the gap up to the third postoperative year except for regions experiencing negative velocity (downward flow) during gap closing motion (shown with square legend). It can be seen that the region located below zero at early postoperative years is shifted above zero (upward flow). This shift to velocities above zero indicates that part of the fluid which was previously (early postoperative years) flowing into the bone even during gap closing motion no longer enters the bone. In other words, in late postoperative years, when the interface tissue is clogged significantly, most of particle carrying fluid which enters the gap region leaves this region without flowing significantly to the bone into. In addition, between the sixth and tenth postoperative years, there is a significant reduction in velocity magnitudes at instances in which the gap is not in motion (fully open and closed). These reductions in velocity between zero and ten postoperative years are 90% and 91% for open and closed gap, respectively. However, the change is 25% reduction and 24% increase when the gap is opening and closing, respectively. Similar phenomenon can be seen in the x direction in Figure 6.15. This figure shows that by the eighth

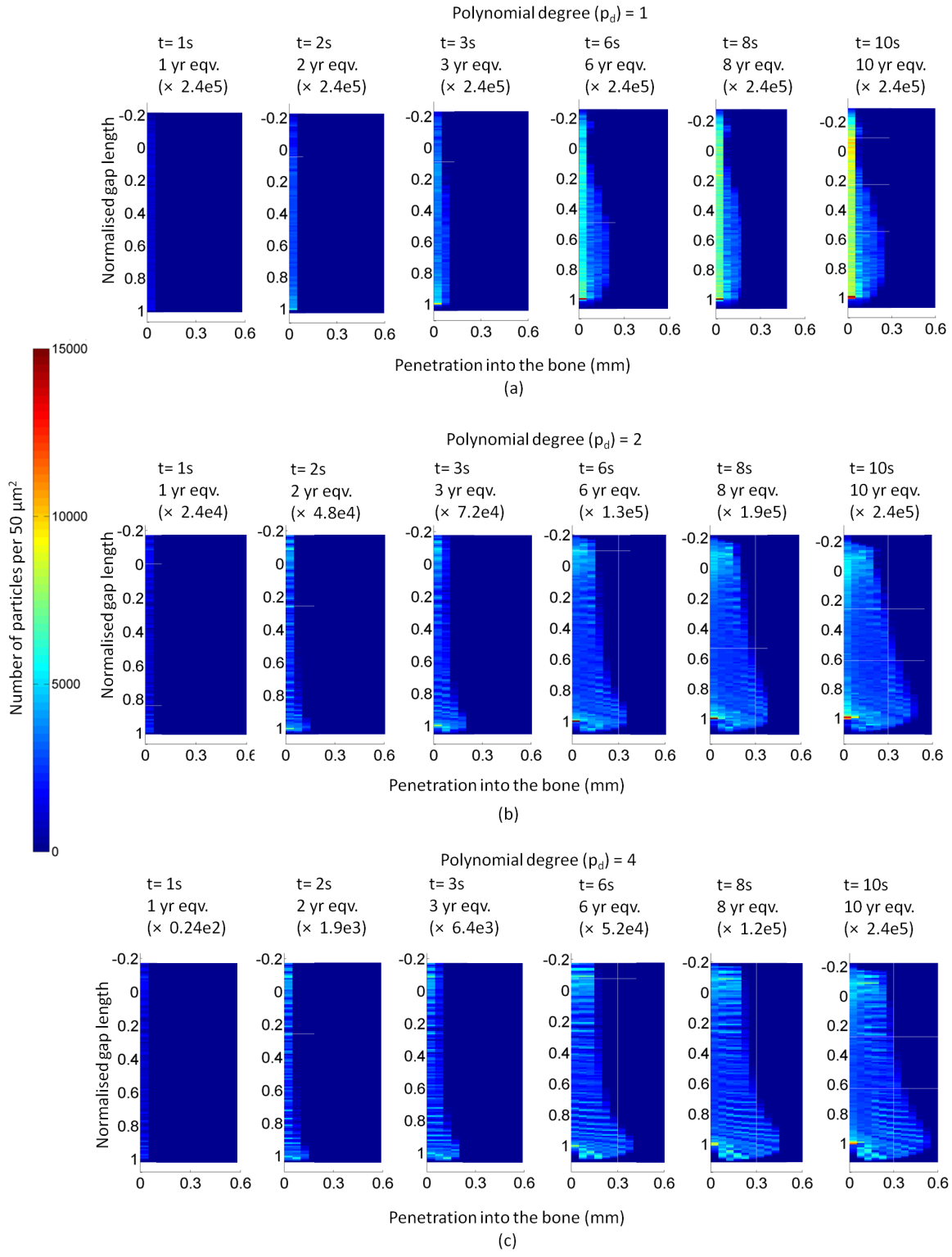

Figure 6.12: Contour plots showing particle concentrations for models with $p_d = 1, 2$ and 4. Plots show the changes in particle distribution and concentration as the simulations progress in time.

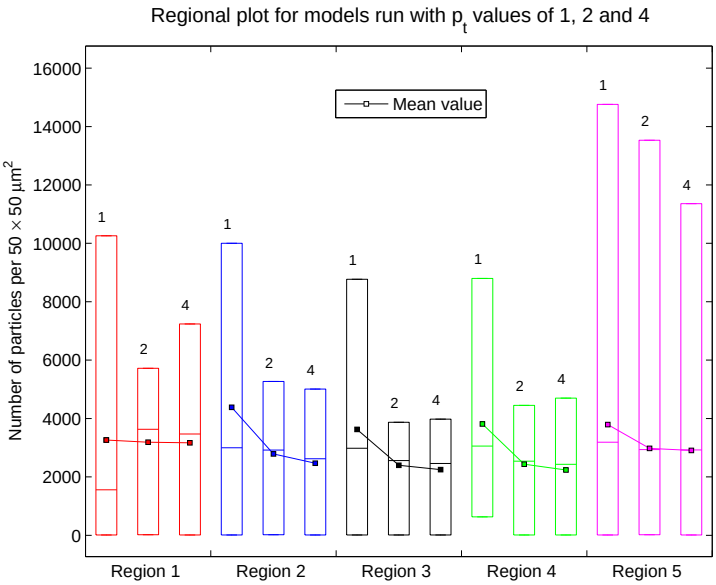

Figure 6.13: Regional plots showing the mean and maximum particle concentrations for a model representing ten postoperative year with $p_d = 1, 2$ and 4. High rare of wear generation cause an increase in both mean and maximum particle concentrations in the periprosthetic tissue. There is no significant change between cases run with $p_d = 1$ and 2.

postoperative year when the interface tissue is significantly clogged, fluid velocities are also similar in the x direction along the gap in both opening and closing motions. This observation indicates that, in long postoperative time, despite the fact that fluid velocities generated by micromotion remain high, the overall effect of micromotion in pumping particles into the periprosthetic tissue is not significant since most of the fluid carrying particles leaves the gap regions when gap closes. The mentioned effects are less pronounced for other cases of polynomial degree of two and four (no plot presented here). For $p_d = 2$, the reduction in velocity between zero and the tenth postoperative years is 39% and 43% for open and closed positions, respectively. This reduction for the time when gap is opening is only 11%. For $p_d = 4$, the reduction in velocity between zero and the tenth postoperative year is 26% and 28% for open and closed positions, respectively. This reduction for the time when gap is opening is only 7%. There is almost no change in velocity for gap closing instances for both p_d value of two and four.

These changes in fluid velocity in the gap region have direct effects on the flow in the periprosthetic tissue. Figure 6.16 shows a significant change in the magnitude of fluid spikes. The fluid spike increases 254% by the third postoperative year in comparison to its initial value at zero postoperative year. There is a reduction in the sixth year and again an increase in the eighth year. The velocity spike finally reduces to 60% of its initial value at the zero postoperative year by the tenth postoperative year. These changes in the magnitude of velocity spikes can be explained by a close inspection at the local particle distribution and permeability at the bottom of the gap. Significant

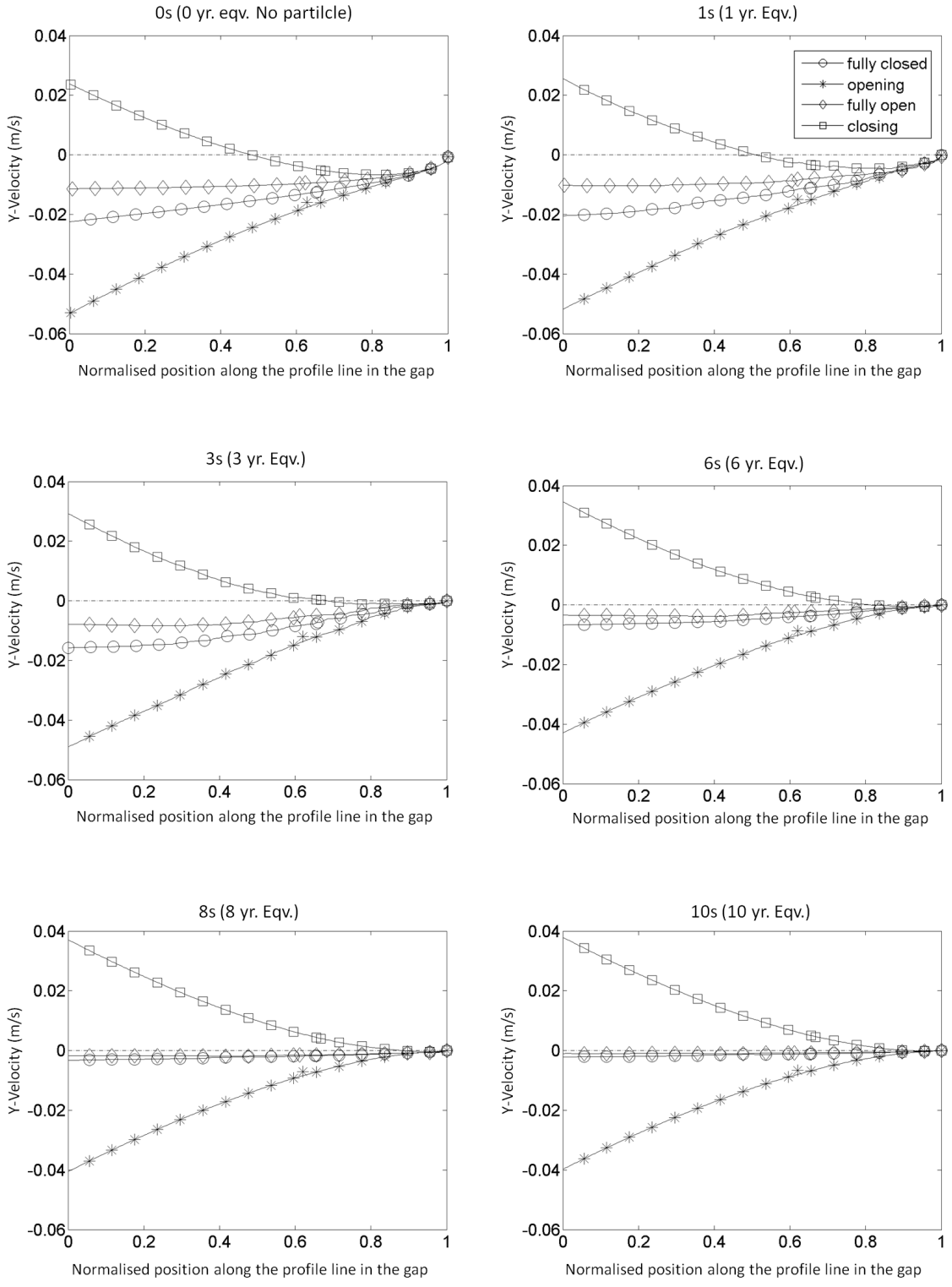

Figure 6.14: Velocity plots for the gap profile line in different postoperative periods. The effect of particle clogging on the these velocities can be observed. The figure shows that there is no significant change in the fluid velocities in the gap initially except for regions experiencing negative velocity (downward flow) during gap closing motion (shown with square legend). However, at later stages, there is a significant reduction in velocity magnitudes at instances in which the gap is not in motion.

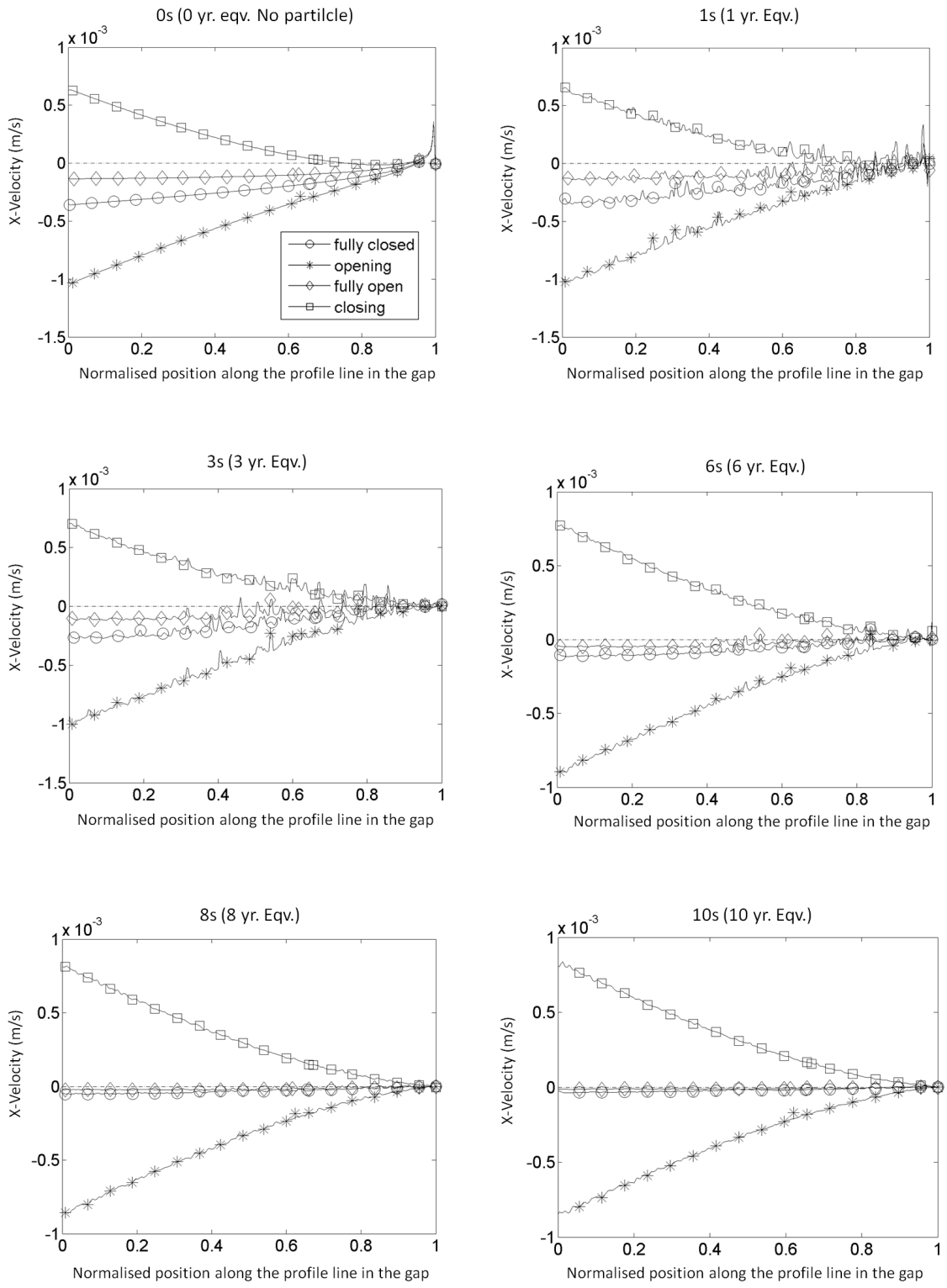

Figure 6.15: Velocity plots in the x direction for the gap profile line in different postoperative periods. The effect of particle clogging on the these velocities can be observed. The figure shows that there is no significant change in the fluid velocities in the gap initially expect appearance of fluctuations caused by particles clogging reducing the permeability at the discrete regions of their entrance to the bone. The velocities are also larger when the gap is opening. However, at later stages, fluid velocity in the x direction are similar when the gap is in closing and opening motion.

increases in the fluid spikes occurs when the gap bottom is only partially clogged by particles. This partial clogging and reduction in permeability leaves local regions and paths with least resistance into which fluid flows with higher velocities. As particles are constantly flowing and as the stopping mechanism is random, the area of the clogged region may vary over time, as does the magnitude of the fluid spikes. However, it can be seen that by the tenth year the entire gap bottom is evenly clogged and, therefore, there is a significant reduction (60%) in the velocity spike. The same can be observed for polynomial degrees of two and four. However, increase in spikes appears after the sixth postoperative year and remains until the tenth year since the bottom region is not fully and evenly clogged.

6.3.4 Permeability increase simulations

The results in this section show that the model is capable of simulating bone replacement by fibrous tissue (represented by permeability increase) as a function of particle concentration at the periprosthetic tissue. Simulations with osteolysis threshold ranging between 5×10^8 and 1×10^{12} particles per gram of tissue were run for ten postoperative years with different wear generation rates (p_d = 1, 2 and 4).

6.3.4.1 The effect of osteolysis threshold (os_t)

Figure 6.17 demonstrates periprosthetic regions experiencing increased permeability. These regions are referred to as fibrous tissue in this figure, which appear to have a grain-shaped pattern. This feature is due to particle injection resolution and the fact that particle enter the bone through discrete and distinguishable paths. This figure shows the threshold for osteolysis has a direct impact on the extent of fibrous tissue expansion. Lower values of os_t result in a greater area of bone experiencing increased permeability (fibrous tissue). In cases run with $os_t = 5 \times 10^8$ and 1×10^9 particles per gram of tissue, permeability increase is not significant in the first operative year (not shown here). The increase in permeability stars appearing from the second postoperative year and then it progresses through bone tissue as time elapses. By the tenth postoperative year, it has penetrated the bone approximately 0.6 mm in regions located along the gap and approximately 1.5 mm in regions located at the bottom of the gap (c.f. Figures 6.17 a and b). The most pronounced feature of these cases is the excessive expansion of increased permeability (fibrous tissue) at the bottom of the gap which may resemble focal osteolysis observed clinically. Comparing its expansion along the interface with that of the bottom of the gap throughout time, indicates that its the rate of progression is greater at the bottom of the gap compared to other regions

For $os_t = 1 \times 10^{10}$ particles per gram of tissue, increase in tissue permeability around the gap is not observed until the third postoperative year. By the sixth year, only

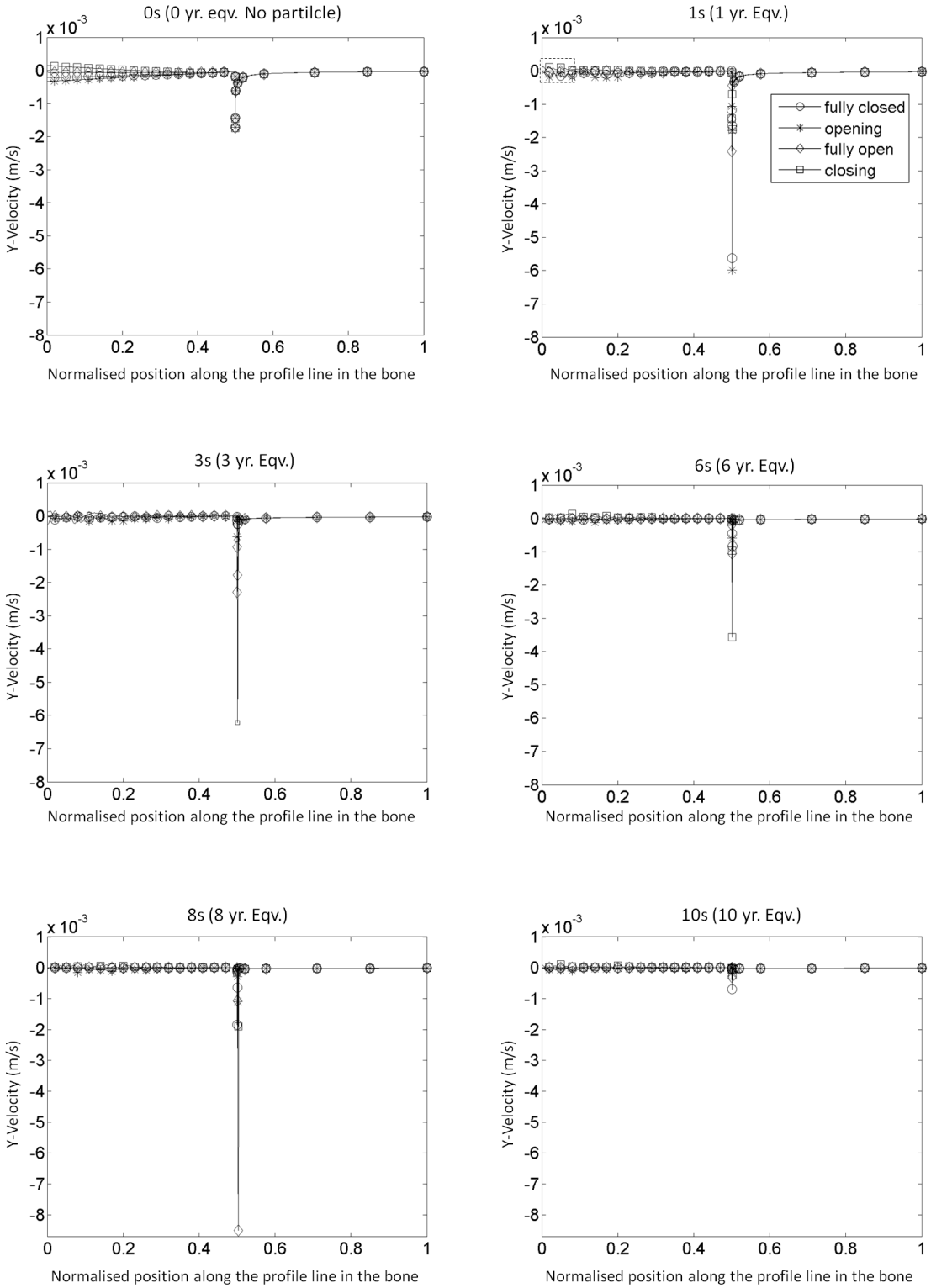

Figure 6.16: Velocity plots for bone profile line. It can be seen that velocity spikes still occur at the bottom of the gap. However, their magnitudes vary over time.

small regions of bone located at the gap entrance and bottom experience an increase in permeability. It is only by the tenth year that distinctive regions with increased permeability (fibrous tissue) are observed. The pattern of permeability increase tends to be linear in this case. As os_t increases to 5×10^{10} particles per gram of tissue and any value above, no increase in permeability occurs in the model and only a permeability reduction is observed a a result of particle clogging the periprosthetic tissue.

In summary, the results show that there is a relationship between the osteolysis threshold and the temporal and regional development fibrous tissue.

The periprosthetic fibrous tissue generation has a direct impact on particle transport. Contour plots of particle concentration and distribution for four os_t values are shown in Figure 6.18 for a model with $p_d = 2$. Comparing this figure with Figure 6.17, shows that regions in which bone is replaced by fibrous tissue there is an excessive particle penetration. Particles penetrate further into the bone through distinguishable paths of least resistance generated by the fibrous tissue. Since particles are distributed over a larger area, the concentration of particles is, in general, lower than the cases in which permeability increase is not included. As the rate of fibrous tissue generation is, generally, faster at the bottom of the gap, the rate of particles entering this region is also faster compared to other regions.

6.3.4.2 The effect of wear generation rates (p_d)

Figure 6.19 shows regions with increased permeability in the tenth postoperative year for different combinations of wear generation rates (p_d = 1, 2 and 4) and osteolysis thresholds ($os_t = 1 \times 10^9$ and 1×10^{10} particles per gram of tissue). It can be seen that for a lower os_t value, permeability increase occurs in all wear generation rates and it has a focal shape at the bottom of the gap. However, the rate of wear generation has a more significant effect for the higher value of os_t. $p_d = 1$ leads to an expanded region with increased permeability at the bottom of the gap while wear generations of p_d = 2 and 4, which represent initial lower rates, lead to a linear pattern of permeability increase along the gap.

Inspecting the temporal development of each case presented in Figure 6.19, shows that, similar to the case for $p_d = 2$, increase in permeability starts developing by the second postoperative year for $p_d = 1$. However, there is no sign of permeability increase until the eighth postoperative year for the case with $p_d = 4$. For this case, an increase in wear generation rate towards the end of simulation leads to a rapid increase in permeability at the interface which has a linear pattern. These findings demonstrate that the rate of wear generation and the os_t play a synergistic role in temporal and regional increase in permeability.

The corresponding particle concentration and distribution for different combinations of wear generation rates and osteolysis thresholds is shown in Figure 6.20. This

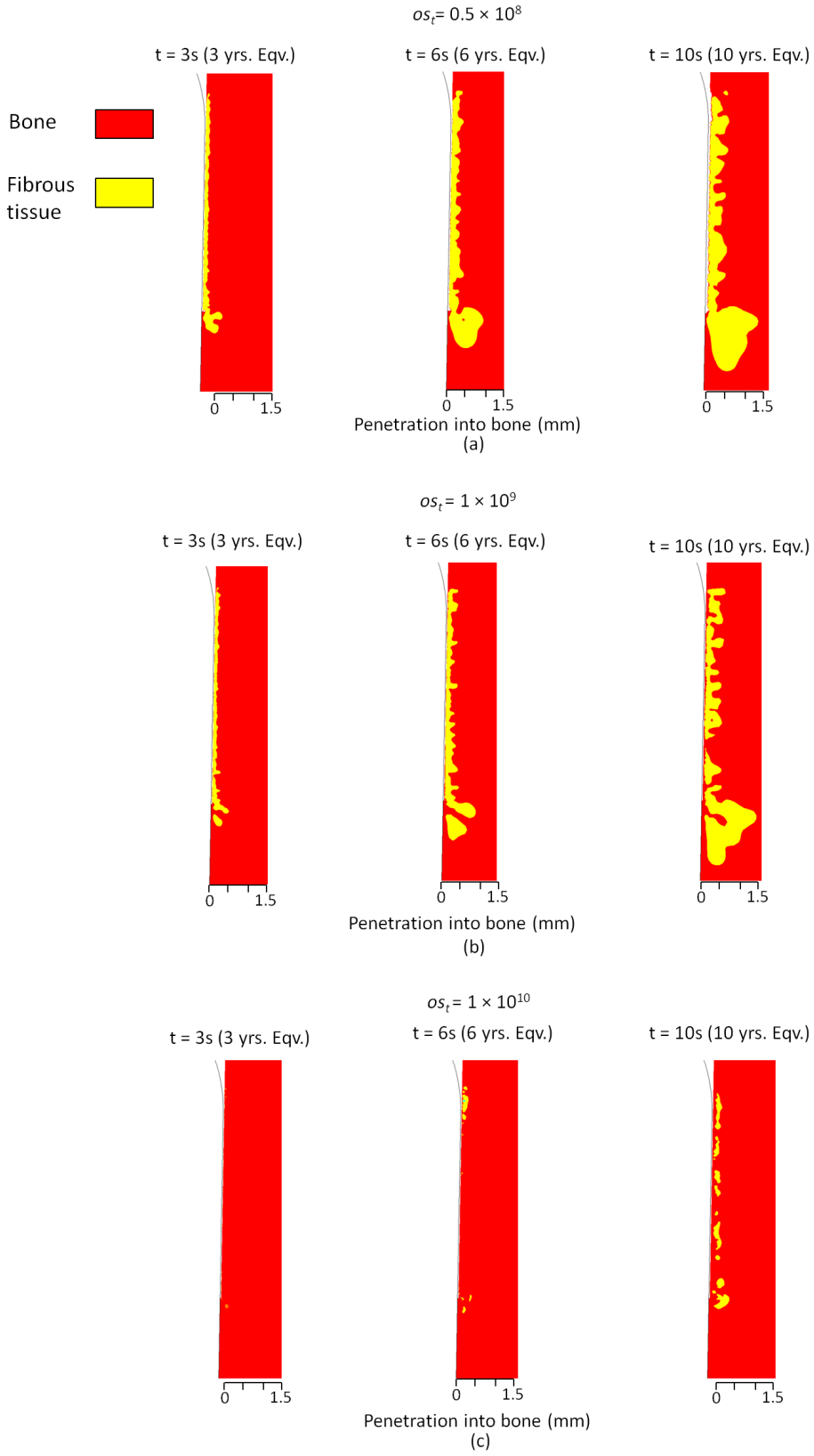

Figure 6.17: Permeability plots which represent fibrous tissue generation at the interface for different values of os_t. Regions with permeability of fibrous tissue ($k = 1 \times 10^{-11}$) and permeability of bone ($k > 1 \times 10^{-14}$) are shown. Fibrous tissue patterns tend to take a focal shape for a lower os_t and tend to be more linear for higher os_t.

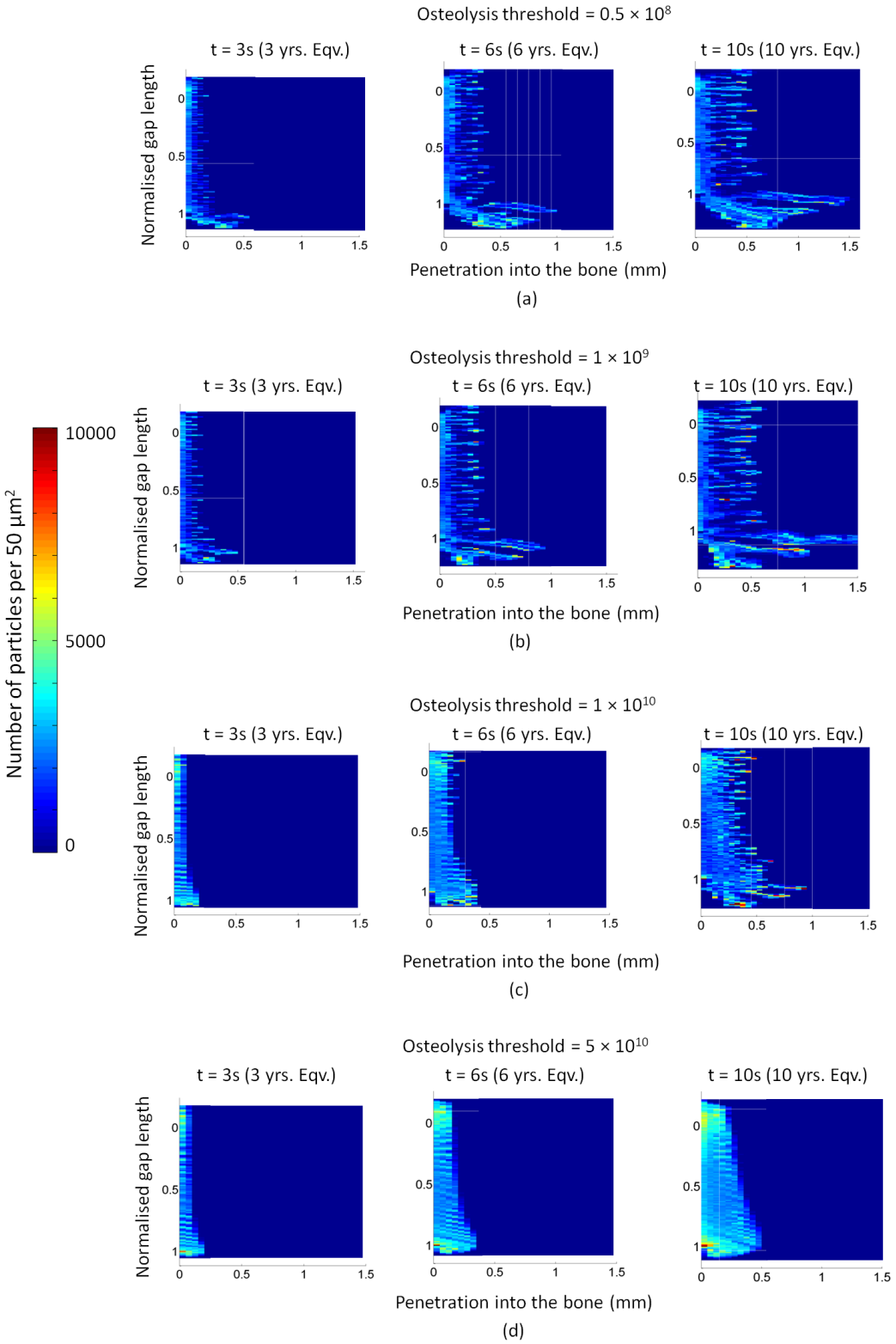

Figure 6.18: Particle concentration and distribution in models simulating osteolysis generation with different values of os_t. Particles penetrate further into the bone through distinguishable paths of least resistance generated by the fibrous tissue.

figure shows that particle penetration is larger at the bottom of the gap for all cases run with os_t=1×10^9 particles per gram of tissue and for the case of high wear generation rates ($p_d = 1$) and os_t=1×10^{10} particles per gram of tissue. Despite the fact that the region experiencing increased permeability at the bottom of the gap is smaller for the case of high wear generation rates ($p_d = 1$) and os_t=1×10^{10} compared to the cases with os_t=1×10^9, it can be seen that particles still penetrate farther into tissue at the bottom of the gap in this case, although the depth of penetration is smaller compared to cases presented in Figure 6.20 a.

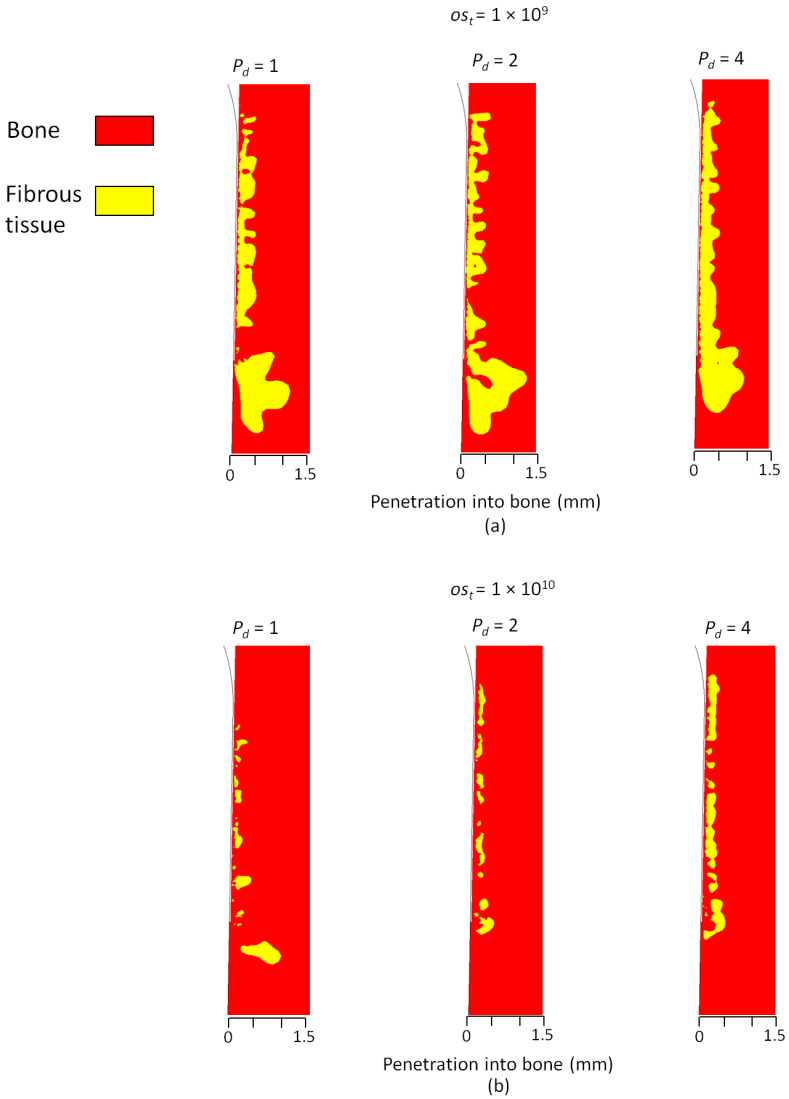

Figure 6.19: Permeability plots which represent fibrous tissue generation at the interface for different values of p_d and os_t. Regions with permeability of fibrous tissue ($k = 1 \times 10^{-11}$) and permeability of bone ($k > 1 \times 10^{-14}$) are shown.

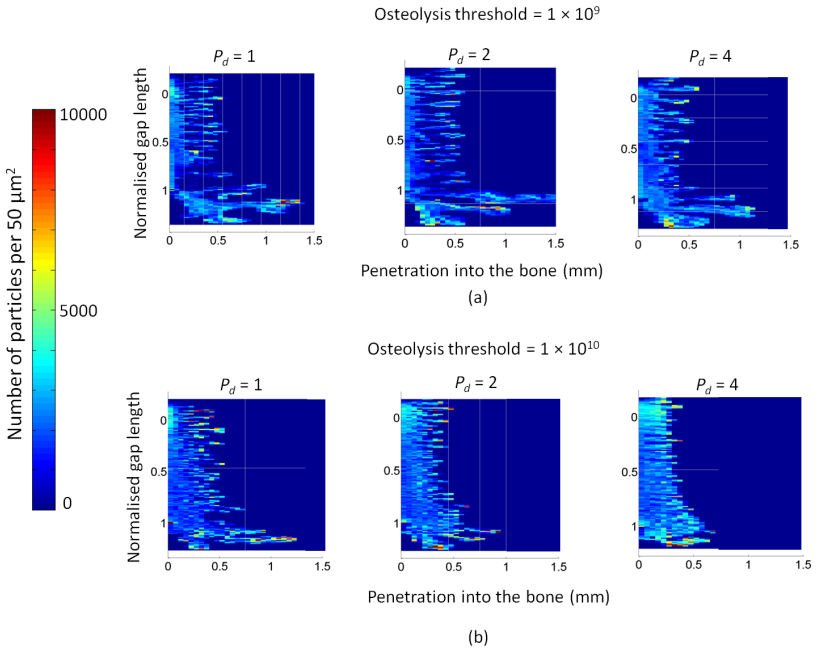

Figure 6.20: Particle concentration and distribution in models simulating osteolysis generation with values of $os_t = 1 \times 10^9$ and 1×10^{10} and $p_d = 1, 2$ and 4 in the tenth postoperative year.

6.3.4.3 Fluid velocity and flow in osteolytic tissue

Despite generation of fibrous tissue along and at the bottom of the gap, the velocity plots along the bone profile line (shown in Appendix B Figure B.3) demonstrate the presence of fluid spikes at the bottom of the gap. However, the magnitude of the fluid spike reduces 50% in early postoperative years (until the sixth year) and increase up to 100% at later postoperative years. The important observation is that the fluid spikes which appears to act as a pump, still exist at the bottom of a gap surrounded by regions with increased permeability. The increase in its magnitude at late postoperative stages may lead to a more pronounced pumping action.

6.4 Discussion

The effect of particle clogging on particle accumulation and fibrous tissue generation in the periprosthetic tissue may be not be significant in short-term periods such as those modelled in chapter 5. Therefore, the focus of this chapter has been on long-term postoperative periods. The high capsular pressure 5L-30W-30D model was run with settings developed to simulate particle clogging and increase in permeability (representing fibrous tissue) in the periprosthetic tissue along an interfacial gap. Such simulations have not been carried out before.

Realistic simulation of particle clogging in a porous medium is beyond the current capabilities of the CFD Fluent software. Therefore, the following parameters and settings were developed and incorporated within the Fluent software in the form of user defined functions (UDF). (i) Scaling factor (s_f) which artificially increases the number of particles during the transient simulation time to a desired number representative of a particular postoperative year, (ii) Polynomial degree of the scaling factor (p_d) which describes the rate (or linearity) of wear generation during postoperative years, (iii) Clogging factor (c_f) which determines the appropriate percentage of particle being stopped at each time step and (iv) Osteolysis threshold (os_t) that determines the particle concentration in which the periprosthetic tissue turns into fibrous tissue. A UDF was also developed that was capable of changing the porous medium permeability in each volume cell according the instantaneous number of particles residing in that cell. This UDF, counted the number of particles after scaling and used the Carmen-Kozeny model to calculate the changes in tissue permeability because of the porosity change caused by particle accumulation. The UDF also changed the cell permeability to that of fibrous tissue once particle concentration was above the osteolysis threshold. The focus of the case studies presented in this chapter was based on ten postoperative years since this was the period in which osteolysis is observed in the majority of failed cementless implants.

Particle number scaling and clogging

The physical effect of $s_{f_{10}}$ in the model is on the volume of particles occupying the periprosthetic tissue porosity. A sensitivity analysis showed that the values of c_f and s_{f_y} are interrelated. In other words, depending on the postoperative period represented by s_{f_y}, the value of c_f has to be empirically adjusted for the model to behave realistically to generate regions of high particle accumulation in the proximity of the implant akin to clinically observed data and shapes of osteolysis. Basing the adjustment of c_f on clinical observations was the only available option for determining c_f due to the lack of data in the literature and limited access to the discrete phase model (DPM) solver in Fluent. The clinical criteria considered in the current work is also observed in other

porous materials. It has been shown that particle concentration and permeability reduction are pronounced at the inlet interface of a porous medium and they diminish by moving away from it [131].

It was shown that the appropriate value for c_f to simulate ten year postoperative period was 50%. The correlation between c_f and s_{f_y} may be explained by the time period presented within each time step for different postoperative periods presented by of $s_{f_{10}}$. The percentage of particles being stopped in each time step is determined by c_f and the duration of the real postoperative time compressed in each time steps is determined by the length of time presented by s_{f_y}. For example, in a simulation for $s_{f_{10}}$, compressed in the transient simulation time of ten seconds (discretised into 5000 time steps), each time step represents 0.71 days (17 hours). This means that particles are stopped and the permeability changes are calculated and implemented every 17 postoperative hour. However, for s_{f_1}, simulated in transient time of ten seconds, the particles are stopped and the permeability change is calculated and implemented every 1.7 hours (365 days divided by 5000 time steps). This shows that for shorter periods represented by s_{f_y}, the effect of c_f remains in place for a shorter postoperative time. To compensate for this, a larger value of c_f maybe required to induce a permeability reduction more frequently to obtain a particle distribution that fulfils the clinical criteria.

Particle distribution and wear rate

The results show that there is a complementary relationship between particle concentration and the reduction of permeability. An increase in particle concentration leads to a reduction in the permeability of a region, which in turn stops more particles as they flow into that region. In other words, those regions experiencing more pronounced reduction in permeability tend to accommodate increasingly more particles as time elapses. This phenomenon is particularly evident at the bottom of the gap, where a reduction in permeability initially starts. This leads to a common feature in all models; the existence of measuring areas adjacent to the gap bottom which contains significantly higher numbers of particles. An inspection on the models shows that the location of these measuring areas corresponds to those regions at the bottom of the gap where the reduction in permeability first start to appear in early postoperative stages. Fluid spikes are also located in those regions. Although small in area, this highly particle laden region may become a frontier for accelerated osteolysis progression and generation. After the appearance of fibrous tissue with high permeability in this region, the fluid spikes, which appeared to have a larger magnitude in regions with increased permeability, may pump more particles to the region causing more extensive permeability increase. In addition, high concentrations of particles in these or any other interfacial region, may impair the drainage system by blocking the blood or

lymphatic vessels and exacerbate the situation further. It has been suggested that high concentration of wear particle may cause blockage of lymphatic capillaries. This blockage may also be a cause for edema and inflammatory conditions leading to osteolysis [71].

The results representing particle clogging only, show that particles may have higher concentration at the gap entrance and bottom initially. However, mean particle concentration along the entire interface may increase to approximately the same level as those at the entrance and a the bottom eventually as particles clog the entire interface. This occurs earlier for higher initial wear generation rates ($p_d = 1$) compared to lower initial generation rates ($p_d = 2$ and 4). The overall particle distribution is also affected by the rate of wear generation in the joint during ten postoperative years. Despite the fact that the final number of particles reached by the end of simulation is the same, faster initial wear generation rates ($p_d = 1$) results in higher particle concentration. This may be a result of earlier clogging of the interface tissue which creates conditions for further particle accumulation and subsequently higher concentration at regions closer to the interface. The results indicate that, at slower initial wear generation rates, it is more likely to find particles in the deeper interfacial tissues. Deeper penetration means that particles are distributed over a larger area. Due to lower concentrations these regions may be less prone to experience osteolysis generation. Although the total number of particles entering the system is the same for all wear generation rates in the current study, the results show that the likelihood of conditions leading to osteolysis is less for larger values of p_d. In fact, models that include permeability increase to represent fibrous tissue generation in the osteolytic lesions, show that the regions with increased permeability expand into periprosthetic tissue to a lesser degree for $p_d = 4$.

The instantaneous scaling number, determined by the polynomial degree of the scaling factor, magnifies the volumetric effect of particles in each parcel throughout the simulation time. The degree of magnification is particularly high from the beginning of the simulation for the cases run with $p_d = 1$. This means that each parcel entering the periprosthetic tissue at each instance contains a large number of particles. However, in reality, particles entrance and deposition at the interface tissue is a gradual process. Therefore, changes in tissue permeability is also a gradual process and may be insignificant initially. This leaves a higher chance for particles entering the tissue at early stages to penetrate deeper into the tissue. For this reason, the depth of particle penetration may be underestimated in the current work. This magnification may be most influential for higher wear generation rates ($p_d = 1$) in which the scaling number is high from the beginning of the simulation, and least influential for lowest wear generation rate ($p_d = 4$) in which the scaling number is low at first and then gradually starts increasing.

Fluid velocity

Velocity measurements in the gap and bone regions show that fluid velocity in these regions is effected by particle accumulation in the tissue. This effect is more pronounced when the gap is in motionless state and the capsular pressure is the only effective fluid pumping force. This observation indicates that, in long postoperative time, despite the fact that micromotion still generates high velocities in the gap region, it generates insignificant particle pumping into into the periprosthetic tissue since most of the fluid that enters the gap region during opening motion leaves this region when gap closes. However, as shown in Figure 6.15, when particles significantly clog the interface tissue, micromotion still generates large velocities in positive x direction (towards the interface) at the gap entrance This may generate a mechanism which pushes particles into the bone more pronouncedly at the gap entrance when the effect of capsular pressure is reduces because of clogging. In fact, the model with $s_{f_{10}}$ and $p_d = 1$ was run for 100 more cycles and it was seen that particle concentration became increasingly high at the gap entrance where the influence of gap micromotion on the fluid flow in the bone is the most. The clinical implication for this observation is that if osteolysis threshold is high for an individual, the excessive particle accumulation at the gap entrance may lead to osteolysis generation at the gap entrance first rather than at the gap bottom. However, the more likely scenario is that osteolysis has already been generated before such phenomena occur. It was also shown that particle accumulation may increase the magnitude of fluid spikes at the bottom of the gap. If fluid velocity influences osteolysis, then particle accumulation may indirectly facilitate osteolysis generation, particularly at earlier postoperative years when the tissue is not yet significantly clogged. This may place the bottom region of the gap at a higher risk of osteolysis generation.

Permeability increase: representative of osteolytic fibrous tissue

The models show how progressive increase in tissue permeability may provide a pathway for particles to penetrate deep into the tissue, and how, in turn, a constant supply of particles causes further expansion of regions with increased permeability representative of the fibrous tissue in osteolytic lesions. As particles enter a region, clogging and permeability reduction occurs. This leads to further particle entrapment in that region resulting in high particle concentrations. Once the osteolysis threshold is reached, tissue permeability increases to that of fibrous tissue causing more particles to flow to that region. The flow of particles leads to particle clogging and high concentrations in that region again until the osteolysis threshold is reached. This loop is repeated as regions with increased permeability (fibrous tissue) penetrate into periprosthetic bone.

The pattern of fibrous tissue observed in the this chapter is in agreement with the prediction of the results from Chapter 5 in that linear fibrous tissue occupying

osteolytic lesions potentially occurs along the interface gaps while osteolytic fibrous tissue expansion occurs at the bottom of the gap. The higher rate of fibrous tissue expansion at the bottom of the gap indicates the significance of the fluid spikes in pumping increasing number of particles to the lower regions of the gap.

The pattern of particle penetration seen in the current study is similar to that described by Schmalzried et al. [47]. They observed that fibrous tissue stroma running like a stream through the periprosthetic tissues providing channels or routes for particle penetration which leads to expansion of the effective joint space. They suggested that the difference between focal and linear osteolysis may be related to the concentration and distribution of particles in the periprosthetic tissue. This phenomenon is observed in the models in the current study. The permeability increase seen in the current simulation is similar to that observed by Willert et al. [35]. They observed that the fibrous connective tissue around the stem was completely occupied by foreign body giant cells and polyethylene fragments. This fibrous tissue infiltrated the marrow cavities of cancellous bone in addition to the haversian canals of the cortical bone. They stated that the presence of osteolysis in a region was directly related to the amount of particles in that region. Furthermore, the models here show that conditions for osteolysis generally start to appear between the second and third postoperative years. This temporal prediction is in accordance with clinical appearance time of osteolysis as explained in section 2.3.2. The critical osteolysis threshold values have been described to be between 1×10^9 [55] and 1×10^{10} [54] per gram of tissue. The results also show that the conditions for osteolysis progression changes in the vicinity of the these thresholds. This behaviour in the model can be considered as one possible explanation of the model following clinical data.

Osteolysis threshold and wear generation rates

It has been shown that there is a relationship between the rate of wear generation - indicated by the penetration of the stem head into the acetabular cup - and the occurrence of osteolysis [52]. However, there is no study showing a detailed temporal and regional relationship between osteolysis and changes in wear rate in postoperative years. The current work may provide insight for temporal and regional characteristics of particle distribution and permeability increase (leading to osteolysis) in terms of wear generation rates. As described before in section 2.3.5.3, there are patients with high rates of wear generation who show no signs of osteolysis. One possible explanation for this phenomenon is that their biological sensitivity to particles in these patients is less, i.e. higher osteolysis threshold. This implies that osteolysis thresholds may vary for individuals. In fact, Ise et al. [57] observed a correlation between the ratio of osteolysis in radiographic images and patient sensitivity to polyethylene particles. They showed that, the point at which osteolysis occurs and the speed of its development

varied in each individual. The speed of progression was faster for patients who were more sensitive to polyethylene particles. The results also show that os_t, which may represent the degree of biological sensitivity, plays an important role on the temporal and regional progression of osteolysis.

For cases with $os_t < 1 \times 10^{10}$ particles per gram of tissue, regions experiencing increased permeability produce a focal pattern at the gap bottom for all wear generation rates. For cases with $os_t = 1 \times 10^{10}$, lower wear generation rates ($p_d = 2$ and 4) lead to linear pattern of permeability increase while higher wear generation rates (p_d =1) still causes a focal expansion of increased permeability at the bottom of the gap. Regardless of wear generation rates, the extent of penetration of the regions with increased permeability (representative of fibrous tissue thickness) is smaller for $os_t = 1 \times 10^{10}$ compared to lower value of os_t. At values larger than 5 $\times 10^{10}$ particles per gram of tissue, no increase in permeability is induced. These observations suggest that there is synergistic effect between osteolysis threshold and the rate of wear generation and may explain why there is only linear osteolysis in some patients while in others, focal osteolysis is also observed if particles are account for the main cause of osteolysis.

The number of particles generated considered in the current work is for a normal functioning implant, which is at a lower limit of wear generation. Not all the generated particles enter or have access to interfacial gaps. Estimating the exact number of particles flowing into an interfacial gap, which depends on many factors such as the number of gaps, the extent and volume of the effective joint space etc, is difficult. It is possible that, in reality, less particles than generated have access to a gap. On the other hand, it has been shown that the wear generation in problematic THRs can be seventy fold more than normally functioning implants [52], which sets the upper limit of wear generation. Therefore, it is possible to assume that the number of particles injected into the gap region in the current work is in the realistic range of particle access to the interface between the lower and the upper limits. The number of particles that have access to the interface may influence the temporal characteristics of particle clogging and the extent of permeability increase, but it does not influence the results qualitatively.

6.5 Limitations

The results of the current model should be interpreted taking into consideration that long term postoperative periods are compressed to a short transient simulation time. This implies that flow conditions in the system are assumed to be unchanging during the postoperative period. In other words, the transient changes in each cycle in periprosthetic flows and pressures are neglected. Each particle parcel injected and micromotion experienced in each computational cycle are representative of many par-

ticles and gait cycles experienced by an implant in reality. However, with the current computational power it is difficult to include more micromotion cycles in the model.

As mentioned in section 2.3.5.8, there are drainage mechanisms to clear some of the particles from the periprosthetic tissue. However, no drainage mechanism is included in the current work. Despite the existence of such mechanisms, a large number of particles accumulate at the interface. This shows the insufficiency of this mechanism to clear significant number of particles from the tissue. Therefore, models run without such mechanisms may still represent the in vivo conditions.

Particles are modelled with a constant size. In reality, however, there is a distribution of particle size in the effective joint space. Considering this parameters is outside the scope of the current work and further analysis is required to study its effect on periprosthetic particle clogging and distribution.

The case studies presented in this chapter only include short gaps with small displacement. As particle mean concentration is less for longer gaps (as shown in Chapter 5), tissue clogging and permeability reduction may be less. Therefore, conditions for osteolysis development may be generated later compared to shorter gaps. Also, large gap displacements are not included in the simulations in this chapter. However, in Chapter 5, it was shown that for large gap displacements, a large portion of injected particles do not flow to the interface gap and particle concentration remains lower in the bottom region compared to the gap entrance regions. This may show that in these gaps conditions for fibrous tissue generation may develop at later stages and it may initiate from the gap entrance.

6.6 Conclusions

It has been shown that the permeability of interface tissue is reduced by particle clogging. This reduction in permeability causes increased particle accumulation in the tissues in the stem proximity, which in turn leads to reduction in fluid flow velocities in the region. As time elapses, particle concentrations become higher than the osteolytic threshold, which leads to an increase in tissue permeability (to that of fibrous tissue) in regions with high particle concentrations.

In general, for lower osteolysis thresholds increase in permeability progresses faster at the bottom of the gap which results in regions with increased permeability taking a linear pattern along the interface and a focal pattern at the bottom of an interfacial gap. Higher osteolysis thresholds, generally, result in linear pattern of increased permeability except for the cases with high wear generation rates in which a focal pattern at the bottom of the gap can still be seen.

Chapter 7

Conclusions and future work

7.1 Conclusions

In Chapter 2, the causes of implant failure were discussed and it was shown that, periprosthetic bone loss, otherwise known as osteolysis, played an important role in implant failure. It was shown that high pressures/velocities and the presence of polyethylene particles in the periprosthetic tissue are considered as the main causes of osteolysis generation, and capsular pressure and implant micromotion are postulated as the main contributors to cause high pressure/velocity generation and particles migration in the periprosthetic tissue. It was also shown that, the existence of gaps at the bone-implant interface may facilitate high pressure/velocity transmission and particle migration to the interface tissue. However, these mechanisms are only postulated theories in the literature. No reported study has been found in the literature that investigates how capsular pressure, micromotion or gap dimensions contribute to high pressure/velocity generation, particle migration and osteolysis generation in periprosthetic tissue. Also no study has been found showing the extent of the role played by each of these mechanisms, or of the influence of other parameters. The current study attempts to elucidate the factors causing or influencing periprosthetic flows of fluid and particles and the subsequent osteolysis generation by means of computational methods.

The main contributions of this thesis are:

- A mathematical model has been setup and verified for the modelling of:
  - Periprosthetic fluid flow in interfacial gaps and the adjacent tissue.
  - Particle migration to periprosthetic tissue.
  - Particle clogging in periprosthetic tissue in long postoperative periods.
  - Increase in periprosthetic tissue permeability representative of fibrous tissue residing in osteolytic lesions.

- Simulations confirm the existence of a pumping mechanism and show high joint capsular pressure may be:
  - The main driving force for high fluid pressure and flow in the gap and the surrounding bone.
  - The main factor influencing the magnitude of velocity spikes observed in the bone region at the bottom of the gap.
  - The main driving force for particle migration to the periprosthetic tissue.
- Simulations show the existence of velocity spikes in the bone region at the bottom of the gap. The velocity spikes:
  - Are generated due to blockage to the fluid flow in the gap bottom region.
  - Can be considered a potential cause for osteolysis caused by large fluid velocities.
  - Appear to cause high particle concentrations at the bottom of an interfacial gap by pumping more particles to that region.
  - May cause faster expansion of fibrous tissue at the bottom of the gap.
- Simulations show that implant micromotion may be secondary to the capsular pressure in influencing periprosthetic flow:
  - Micromotion of only very long and narrow gaps can cause significant pressures in the bone and influence the magnitude of fluid spikes.
  - Implant micromotion pumps out, rather than sucks in the particles to the interfacial gaps
- Simulations incorporating particle clogging show that:
  - Wear particles in long term postoperative periods may clog the interface tissue and reduce its permeability which, in turn, causes increasing particle accumulation at the stem proximity, particularly in the bottom region.
- Simulations incorporating particle clogging and increased permeability to represent fibrous tissue in osteolytic lesions show that:
  - As periprosthetic tissue permeability is increased, a larger sink is produced, encouraging more flow into that region. Thus, more particles can penetrate the bone leading to repeatedly progressive clogging and potential for further expansion of fibrous tissue.

  - The rate of expansion of fibrous tissue is larger at the bottom of the gap at high wear generation rates and/or low osteolysis thresholds which resembles focal osteolytic lesions observed clinically.
  - Higher osteolysis threshold in conjunction with lower rates of wear generation can lead to a linear pattern of fibrous tissue generation in periprosthetic tissue.

- Other contributions of the current study are:
  - Establishment of a permeability value representing the whole bone-marrow system surrounding an implant.
  - Development of an algorithm that can be used to simulate particle clogging and permeability change in Fluent.

7.2 Future work

The current study can be extended in various ways to gain a more in-depth insight into periprosthetic flows and particle migration. Extending the model into 3D will enable the investigation of the effect of different gap shapes and geometries. It will also make it possible to incorporate realistic loading mechanisms which include torques and sliding motions. The periprosthetic tissue can be presented as a poroelastic material which can simulate the effect of bone tissue deformation and pressure build-up when the capsular pressure and physiological loadings are applied. The joint capsule can also be represented by a deformable body in which the effect of volumetric changes in causing joint fluid flows and high pressures could be incorporated. The drainage mechanisms can be incorporated as a mechanism that removes particles from the system. This could prove to be a powerful tool to study the effect of the degree of particle drainage on the temporal and regional particle accumulation and osteolysis development. Many patients who have THR, experience osteoporosis, which is a condition in which bone mineral density is reduced and bone microarchitecture deteriorates, or stress shielding (see section 2.2.4.2) at some time after implantation. In these conditions, periprosthetic permeability may increase significantly. This may have an influence on wear accumulation and osteolysis generation. In the future models, implementing these porosity and permeability variations may provide a better understanding of osteolysis generation in patients with these conditions.

The simulations carried out in this Chapter 6 are based on an adapted constant c_f value for a constant scaling number representative of ten postoperative years. For nonlinear wear generations rates in which the scaling number is varying in time, a more appropriate c_f which is a function of the instantaneous scaling number may

better simulate the clogging mechanism. In addition, using such a c_f, it is possible to carry out detailed analysis exploring the effect of varying the period of time represented by the scaling factor within a particular simulation time. Further analysis could be carried out to establish a time varying c_f.

In the current study, a constant particle size is employed, whereas in reality there is a distribution of particle sizes dispersed in the effective joint space. The future models could study the effect of a heterogeneous particle size distribution on tissue clogging and fibrous tissue generation with consideration of biologically active size ranges described in section 2.3.5.3.

In addition to fibrous tissue generated by particles, the simulations can also include models which define osteolysis generation as a function of fluid velocity and pressure. These models have already been developed in the literature [46]. This provides a more in-depth insight on the synergistic effect of fluid pressure and particles in causing osteolysis. The osteolysis simulation methods developed in the current study may be used in conjunction with models of different implant designs to establish likely regions for osteolysis development for that particular design. This could be a powerful tool to predict the long term performance of a particular design.

Finally, there is a lack of information on the regional pattern and extent of osteolysis and particle distribution in periprosthetic tissue in the literature. Information gained from clinical and retrieval studies is necessary to better understand the nature of osteolysis generation and progression, and subsequent implant loosening and failure. In addition, experimental methods can be used to validate the simulations developed for the current study. The experimental tools may consist of a chamber of pressurised fluid and an implanted cadaveric or animal bone with a gap at the interface. Such a system could be mounted on a hip motion simulating or mechanical testing machine. Then, it may be possible to track particles and record fluid velocities and pressures in such a system using transducers and particle tracking velocimetry methods. Until such information and tools are available, the methods and simulations developed in the current work, and those improvements suggested in this section, provide a powerful tool to better understand the nature of osteolysis and implant loosening.

Appendix A

List of Publications

- Alidousti, H. and Taylor, M. and Bressloff, N.W. Do Capsular Pressure and Implant Motion Interact to Cause High Pressure in the Periprosthetic Bone in Total Hip Replacement? *Journal of Biomechanical Engineering*, 133:121001, 2011.
- Alidousti, H. and Taylor, M. and Bressloff, N.W. Do Capsular Pressure and Implant Motion Interact to Cause High Pressure in the Periprosthetic Bone in Total Hip Replacement? Orthopaedic Research Society (ORS) Annual Meeting. February 2012, San Francisco.

Appendix B

Results not shown in the main text

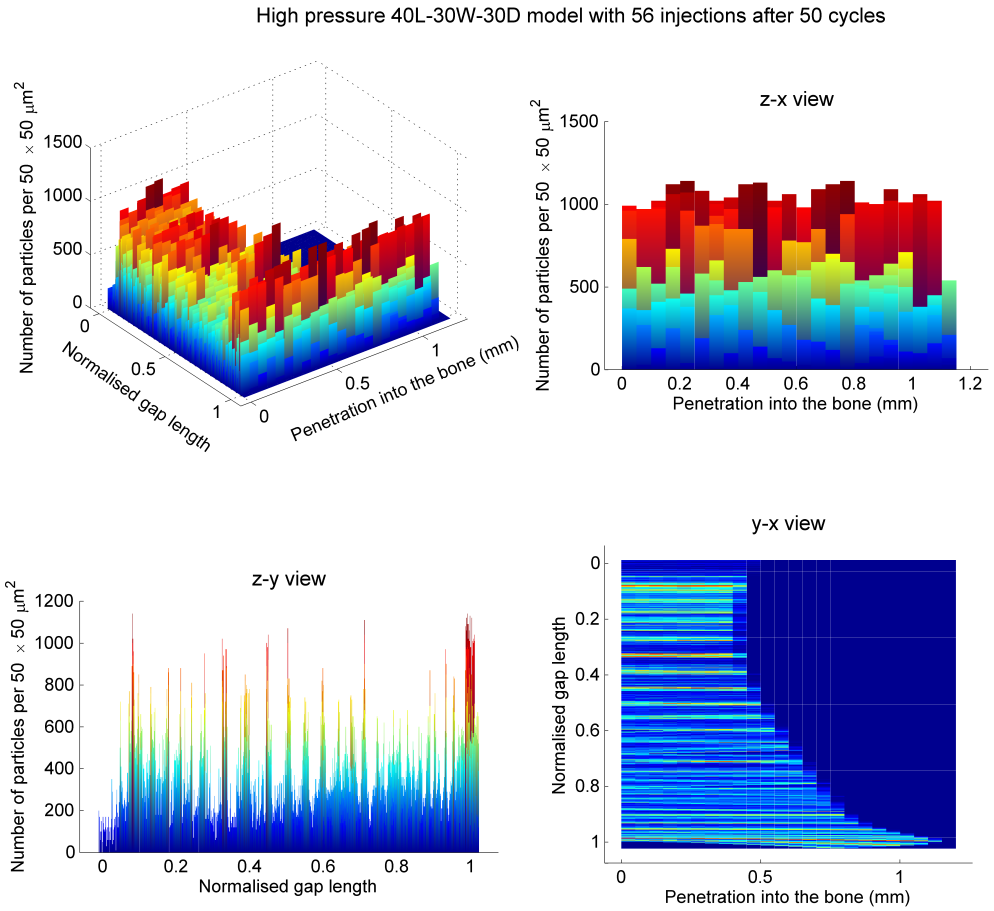

Figure B.1: 3D contour plots from different views showing particles number per 50 × 50 μm^2 area and their penetration into the bone along width and length of the gap in the 40L-30D-30D model with high pressure and 56 injections. High concentration at proximal and distal regions can be seen.

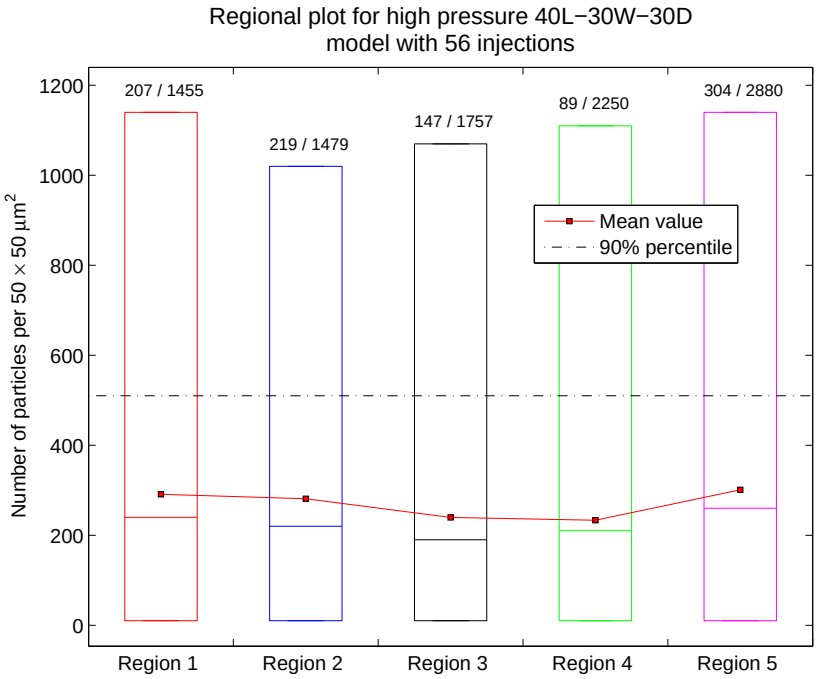

Figure B.2: Regional plot of the particle concentration at different regions in the bone along the gap for the high pressure 40L-30W-30D model 56 injections. The 90^{th} percentile is calculated based on the total particle number per measuring in the entire model. The mean value as well as the number of measuring areas above the 90^{th} percentile as a fraction of total number of measuring areas are shown above each box.

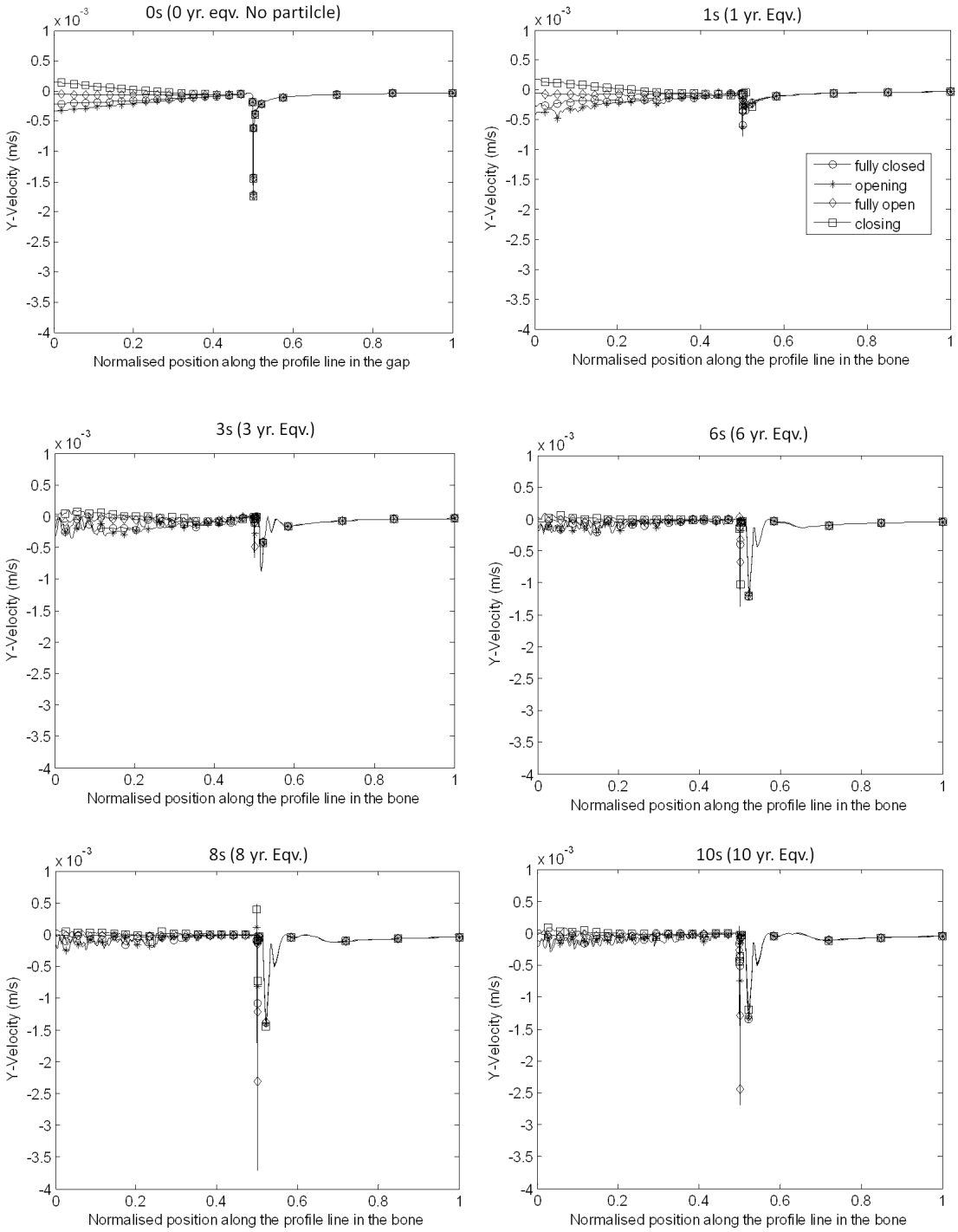

Figure B.3: Velocity plots for the bone profile line in different postoperative periods. The effect of particle clogging and increase in permeability due to fibrous tissue generation on the these velocities can be observed. The figure shows that velocity spikes still occur at the bottom of the gap. However, their magnitudes vary over time.

References

[1] National Joint Registry for England and Wales. 6th annal report njr. Technical report, 2009.

[2] R. L. Drake, W. Vogl, and A. W. M. Mitchell. *Gray's Anatomy for Student.* Elsevier, 2005.

[3] T. P. Schmalzried, K. H. Akizuki, A. N. Fedenko, and J. Mirra. The role of access of joint fluid to bone in periarticular osteolysis - a report of four cases. *Journal of Bone and Joint Surgery-American Volume*, 79A(3):447–452, 1997.

[4] E.N. Marieb and K. Hoehn. *Human anatomy & physiology.* Pearson Education, 2007.

[5] H. Wingstrand, A. Wingstrand, and P. Krantz. Intracapsular and atmospheric-pressure in the dynamics and stability of the hip - a biomechanical study. *Acta Orthopaedica Scandinavica*, 61(3):231–235, 1990.

[6] R. W. Hendrix, R. L. Wixson, N. A. Rana, and L. F. Rogers. Arthrography after total hip arthroplasty: a modified technique used in the diagnosis of pain. *Radiology*, 148(3):647–52, 1983.

[7] Swedish Hip Arthroplasty Register. Annual report,. 2007.

[8] J. M. Cuckler and R. C. Rhoad. Alternatives to hip, knee, and ankle total joint arthroplasty. *Curr Opin Rheumatol*, 3(1):81–7, 1991.

[9] P. F. Gomez and J. A. Morcuende. Early attempts at hip arthroplasty–1700s to 1950s. *Iowa Orthop J*, 25:25–9, 2005.

[10] Swedish Hip Arthroplasty Register. Annual report (shortened version), 2008.

[11] K. J. Messick, M. A. Miller, L. A. Damron, A. Race, M. T. Clarke, and K. A. Mann. Vacuum-mixing cement does not decrease overall porosity in cemented femoral stems: an in vitro laboratory investigation. *J Bone Joint Surg Br*, 89(8):1115–21, 2007.

[12] M. R. Dayton, S. J. Incavo, D. L. Churchill, J. A. Uroskie, and B. D. Beynnon. Effects of early and late stage cement intrusion into cancellous bone. *Clin Orthop Relat Res*, (405):39–45, 2002.

[13] M. Chandler, R. S. Kowalski, N. D. Watkins, A. Briscoe, and A. M. New. Cementing techniques in hip resurfacing. *Proc Inst Mech Eng H*, 220(2):321–31, 2006.

[14] L. Cristofolini, P. Erani, P. Savigni, T. Grupp, O. Thies, and M. Viceconti. Increased long-term failure risk associated with excessively thin cement mantle in cemented hip arthroplasty: a comparative in vitro study. *Clin Biomech (Bristol, Avon)*, 22(4):410–21, 2007.

[15] J. L. Gilbert. Complexity in modeling of residual stresses and strains during polymerization of bone cement: effects of conversion, constraint, heat transfer, and viscoelastic property changes. *J Biomed Mater Res A*, 79(4):999–1014, 2006.

[16] I. D. Learmonth, C. Young, and C. Rorabeck. The operation of the century: total hip replacement. *Lancet*, 370(9597):1508–19, 2007.

[17] T. P. Schmalzried. Why total hip resurfacing. *J Arthroplasty*, 22(7 Suppl 3):57–60, 2007.

[18] Y. Watanabe, N. Shiba, S. Matsuo, F. Higuchi, Y. Tagawa, and A. Inoue. Biomechanical study of the resurfacing hip arthroplasty: finite element analysis of the femoral component. *J Arthroplasty*, 15(4):505–11, 2000.

[19] R. Huiskes. Failed innovation in total hip replacement. diagnosis and proposals for a cure. *Acta Orthop Scand*, 64(6):699–716, 1993.

[20] T. W. Bauer and J. Schils. The pathology of total joint arthroplasty.ii. mechanisms of implant failure. *Skeletal Radiol*, 28(9):483–97, 1999.

[21] J. Wolff. The law of bone remodeling. translated by maquet p and furlong r, 1986.

[22] I. Oh and W. H. Harris. Proximal strain distribution in the loaded femur. an in vitro comparison of the distributions in the intact femur and after insertion of different hip-replacement femoral components. *J Bone Joint Surg Am*, 60(1):75–85, 1978.

[23] C. A. Engh, T. F. McGovern, J. D. Bobyn, and W. H. Harris. A quantitative evaluation of periprosthetic bone-remodeling after cementless total hip arthroplasty. *J Bone Joint Surg Am*, 74(7):1009–20, 1992.

[24] A. H. Glassman, J. D. Bobyn, and M. Tanzer. New femoral designs: do they influence stress shielding? *Clin Orthop Relat Res*, 453:64–74, 2006.

[25] M. A. Freeman. Radiolucent lines: a question of nomenclature. *Journal of Arthroplasty*, 14(1):1–2, 1999.

[26] L. Linder, L. Lindberg, and K.E. Carlsson. Aseptic loosening of hip prostheses a histologic and enzyme histochemical study. *Clinical Orthopaedics and Related Research*, 175:93, 1983.

[27] W. H. Harris, A. L. Schiller, J. M. Scholler, R. A. Freiberg, and R. Scott. Extensive localized bone resorption in the femur following total hip replacement. *J Bone Joint Surg Am*, 58(5):612–8, 1976.

[28] T. P. Schmalzried and J. J. Callaghan. Wear in total hip and knee replacements. *J Bone Joint Surg Am*, 81(1):115–36, 1999.

[29] M. Tanzer, W. J. Maloney, M. Jasty, and W. H. Harris. The progression of femoral cortical osteolysis in association with total hip-arthroplasty without cement. *Journal of Bone and Joint Surgery-American Volume*, 74A(3):404–410, 1992.

[30] W. J. Donnelly, A. Kobayashi, M. A. R. Freeman, T. W. Chin, H. Yeo, M. West, and G. Scott. Radiological and survival comparison of four methods of fixation of a proximal femoral stem. *Journal of Bone and Joint Surgery-British Volume*, 79(3):351, 1997.

[31] W. J. Maloney, M. Jasty, A. Rosenberg, and W. H. Harris. Bone lysis in well-fixed cemented femoral components. *Journal of Bone and Joint Surgery-British Volume*, 72(6):966–970, 1990.

[32] B. Zicat, C. A. Engh, and E. Gokcen. Patterns of osteolysis around total hip components inserted with and without cement. *Journal of Bone and Joint Surgery-American Volume*, 77A(3):432–439, 1995.

[33] T.A. GRUEN, G.M. MCNEICE, and H.C. AMSTUTZ. " modes of failure" of cemented stem-type femoral components: a radiographic analysis of loosening. *Clinical orthopaedics and related research*, 141:17, 1979.

[34] W. J. Maloney, M. Jasty, W. H. Harris, J. O. Galante, and J. J. Callaghan. Endosteal erosion in association with stable uncemented femoral components. *Journal of Bone and Joint Surgery*, 72A(7):1025–1034, 1990.

[35] H. G. Willert, H. Bertram, and G. H. Buchhorn. Osteolysis in alloarthroplasty of the hip - the role of ultra-high-molecular-weight polyethylene wear particles. *Clinical Orthopaedics and Related Research*, (258):95–107, 1990.

[36] H.M. Van Der Vis, P. Aspenberg, R.K. Marti, W. Tigchelaar, CJ Van Noorden, et al. Fluid pressure causes bone resorption in a rabbit model of prosthetic loosening. *Clinical orthopaedics and related research*, (350):201, 1998.

[37] H.M. vander Vis, P.A. Berg, R. de Kleine, W. Tigchelaar, and C.J.F. van Noorden. Short periods of oscillating fluid pressure directed at a titanium-bone interface in rabbits lead to bone lysis. *Acta Orthopaedica*, 69(1):5–10, 1998.

[38] R. Skripitz and P. Aspenberg. Pressure-induced periprosthetic osteolysis: A rat model. *Journal of Orthopaedic Research*, 18(3):481–484, 2000.

[39] A. Fahlgren, M. P. G. Bostrom, X. Yang, L. Johansson, U. Edlund, F. Agholme, and P. Aspenberg. Fluid pressure and flow as a cause of bone resorption. *Acta Orthopaedica*, 81(4):508–516, 2010.

[40] J. W. Landells. The bone cysts of osteoarthritis. *J Bone Joint Surg Br*, 35-B(4):643–9, 1953.

[41] M. I. V. Jayson, Rubenste.D, and A. S. J. Dixon. Intra-articular pressure and rheumatoid geodes (bone-cysts). *Annals of the Rheumatic Diseases*, 29(5):496–8, 1970.

[42] H.D. Huddleston. Femoral lysis after cemented hip arthroplasty. *The Journal of arthroplasty*, 3(4):285–297, 1988.

[43] C.C. Arnoldi. Vascular aspects of degenerative joint disorders. a synthesis. *Acta orthopaedica Scandinavica. Supplementum*, 261:1, 1994.

[44] S. C. Cowin. Mechanosensation and fluid transport in living bone. *Journal of Musculoskeletal and Neuronal Interactions*, 2(3):256–260, 2002.

[45] A. Carano, P.H. Schlesinger, N.A. Athanasou, S.L. Teitelbaum, and H.C. Blair. Acid and base effects on avian osteoclast activity. *American Journal of Physiology-Cell Physiology*, 264(3):C694–C701, 1993.

[46] L. Johansson, U. Edlund, A. Fahlgren, and P. Aspenberg. Bone resorption induced by fluid flow. *Journal of Biomechanical Engineering-Transactions of the Asme*, 131(9):094505 (1–5), 2009.

[47] T. P. Schmalzried, M. Jasty, and W. H. Harris. Periprosthetic bone loss in total hip arthroplasty. polyethylene wear debris and the concept of the effective joint space. *Journal of Bone and Joint Surgery-American Volume*, 74(6):849–63, 1992.

[48] T. P. Schmalzried, E. S. Szuszczewicz, M. R. Northfield, K. H. Akizuki, R. E. Frankel, G. Belcher, and H. C. Amstutz. Quantitative assessment of walking activity after total hip or knee replacement. *J Bone Joint Surg Am*, 80(1):54–9, 1998.

[49] M. Jasty, D. D. Goetz, C. R. Bragdon, K. R. Lee, A. E. Hanson, J. R. Elder, and W. H. Harris. Wear of polyethylene acetabular components in total hip arthroplasty - an analysis of one hundred and twenty-eight components retrieved at autopsy or revision operations. *Journal of Bone and Joint Surgery-American Volume*, 79A(3):349–358, 1997.

[50] C. J. Sychterz, K. H. Moon, Y. Hashimoto, K. M. Terefenko, C. A. Engh, and T. W. Bauer. Wear polyethylene cups in total hip arthroplasty - a study of specimens retrieved post mortem. *Journal of Bone and Joint Surgery-American Volume*, 78A(8):1193–1200, 1996.

[51] K. F. Orishimo, A. M. Claus, C. J. Sychterz, and C. A. Engh. Relationship between polyethylene wear and osteolysis in hips with a second-generation porous-coated cementless cup after seven years of follow-up. *J Bone Joint Surg Am*, 85-A(6):1095–9, 2003.

[52] J. E. Dowd, C. J. Sychterz, A. M. Young, and C. A. Engh. Characterization of long-term femoral-head-penetration rates. association with and prediction of osteolysis. *J Bone Joint Surg Am*, 82-A(8):1102–7, 2000.

[53] P. A. Revell, N. Alsaffar, and A. Kobayashi. Biological reaction to debris in relation to joint prostheses. *Proceedings of the Institution of Mechanical Engineers Part H-Journal of Engineering in Medicine*, 211(2):187–197, 1997.

[54] A. Kobayashi, M. A. R. Freeman, W. Bonfield, Y. Kadoya, T. Yamac, N. AlSaffar, G. Scott, and P. A. Revell. Number of polyethylene particles and osteolysis in total joint replacements - a quantitative study using a tissue-digestion method. *Journal of Bone and Joint Surgery-British Volume*, 79B(5):844–848, 1997.

[55] A. P. D. Elfick, S. M. Green, S. Krikler, and A. Unsworth. The nature and dissemination of uhmwpe wear debris retrieved from periprosthetic tissue of thr. *Journal of Biomedical Materials Research Part A*, 65A(1):95–108, 2003.

[56] H. Koseki, T. Matsumoto, S. Ito, H. Doukawa, H. Enomoto, and H. Shindo. Analysis of polyethylene particles isolated from periprosthetic tissue of loosened hip arthroplasty and comparison with radiographic appearance. *Journal of Orthopaedic Science*, 10(3):284–290, 2005.

[57] K. Ise, K. Kawanabe, T. Matsusaki, M. Shimizu, E. Onishi, and T. Nakamura. Patient sensitivity to polyethylene particles with cemented total hip arthroplasty. *J Arthroplasty*, 22(7):966–73, 2007.

[58] T. R. Green, J. Fisher, M. Stone, B. M. Wroblewski, and E. Ingham. Polyethylene particles of a 'critical size' are necessary for the induction of cytokines by macrophages in vitro. *Biomaterials*, 19(24):2297–302, 1998.

[59] E. B. Benz, M. Federman, J. J. Godleski, B. E. Bierbaum, T. S. Thornhill, and M. Spector. Transmission electron microscopy of intracellular particles of polyethylene from joint replacement prostheses: size distribution and cellular response. *Biomaterials*, 22(21):2835–42, 2001.

[60] P. A. Lalor, R. Namba, S. L. Mitchell, J. Bearcroff, N. Beals, C. B. Sledge, and M. Spector. Migration of polyethylene particles around stable implants in an animal model. *Journal of long-term effects of medical implants*, 9(4):261, 1999.

[61] P. Massin, D. Chappard, B. Flautre, and P. Hardouin. Migration of polyethylene particles around nonloosened cemented femoral components from a total hip arthroplasty-an autopsy study. *J Biomed Mater Res B Appl Biomater*, 69(2):205–15, 2004.

[62] J. D. Bobyn, R. M. Pilliar, H. U. Cameron, and G. C. Weatherly. Osteogenic phenomena across endosteal bone-implant spaces with porous surfaced intramedullary implants. *Acta Orthop Scand*, 52(2):145–53, 1981.

[63] X. Yuan, L. Ryd, and R. Huiskes. Wear particle diffusion and tissue differentiation in tka implant fibrous interfaces. *Journal of Biomechanics*, 33(10):1279–1286, 2000.

[64] M. von Knoch, C. A. Engh, C. J. Sychterz, C. A. Engh, and H. G. Willert. Migration of polyethylene wear debris in one type of uncemented femoral component with circumferential porous coating - an autopsy study of 5 femurs. *Journal of Arthroplasty*, 15(1):72–78, 2000.

[65] M. J. Coathup, J. Blackburn, A. E. Goodship, J. L. Cunningham, T. Smith, and G. W. Blunn. Role of hydroxyapatite coating in resisting wear particle migration and osteolysis around acetabular components. *Biomaterials*, 26(19):4161–9, 2005.

[66] J. D. Mabrey, A. Afsar-Keshmiri, G. A. McClung, M. A. Pember, T. M. Wooldridge, and C. M. Agrawal. Comparison of uhmwpe particles in synovial fluid and tissues from failed tha. *Journal of Biomedical Materials Research*, 58(2):196–202, 2001.

[67] E. Zolotarevova, G. Entlicher, E. Pavlova, M. Slouf, D. Pokorny, F. Vesely, J. Gallo, and A. Sosna. Distribution of polyethylene wear particles and bone fragments in periprosthetic tissue around total hip joint replacements. *Acta Biomaterialia*, 6(9):3595–3600, 2010.

[68] K. J. Kim, Y. Kobayashi, and T. Itoh. Osteolysis model with continuous infusion of polyethylene particles. *Clin Orthop Relat Res*, (352):46–52, 1998.

[69] J. Noble, A. G. Jones, M. A. Davies, C. B. Sledge, R. I. Kramer, and E. Livni. Leakage of radioactive particle-systems from a synovial joint studied with a gamma-camera - its application to radiation synovectomy. *Journal of Bone and Joint Surgery-American Volume*, 65(3):381–389, 1983.

[70] R. M. Urban, J. J. Jacobs, M. J. Tomlinson, J. Gavrilovic, J. Black, and M. Peoc'h. Dissemination of wear particles to the liver, spleen, and abdominal lymph nodes of patients with hip or knee replacement. *Journal of Bone and Joint Surgery-American Volume*, 82A(4):457–477, 2000.

[71] G. Jell, D. Kerjaschki, P. Revell, and N. Al-Saffar. Lymphangiogenesis in the bone-implant interface of orthopedic implants: importance and consequence. *Journal of Biomedical Materials Research Part A*, 77A(1):119–127, 2006.

[72] J. Edwards, E. Schulze, A. Sabokbar, H. Gordon-Andrews, D. Jackson, and N. A. Athanasou. Absence of lymphatics at the bone-implant interface: implications for periprosthetic osteolysis. *Acta Orthop*, 79(2):289–94, 2008.

[73] P. Aspenberg and P. Herbertsson. Periprosthetic bone resorption. particles versus movement. *J Bone Joint Surg Br*, 78(4):641–6, 1996.

[74] F. H. R. De Man, W. Tigchelaar, R. K. Marti, C. J. F. Van Noorden, and H. M. Van Der Vis. Effects of mechanical compression of a fibrous tissue interface on bone with or without high-density polyethylene particles in a rabbit model of prosthetic loosening. *Journal of Bone and Joint Surgery-American Volume*, 87A(7):1522–1533, 2005.

[75] O. Robertsson, H. Wingstrand, U. Kesteris, K. Jonsson, and R. Onnerfalt. Intracapsular pressure and loosening of hip prostheses - preoperative measurements in 18 hips. *Acta Orthopaedica Scandinavica*, 68(3):231–234, 1997.

[76] G. E. Bartlett, D. J. Beard, D. W. Murray, and H. S. Gill. The femoral stem pump in cemented hip arthroplasty: An in vitro model. *Medical Engineering & Physics*, 30(8):1042–1048, 2008.

[77] H. Wingstrand and A. Wingstrand. Biomechanics of the hip joint capsule - a mathematical model and clinical implications. *Clinical Biomechanics*, 12(5):273–280, 1997.

[78] R. O. Cone, N. Yaru, D. Resnick, D. Gershuni, and J. Guerra. Intracapsular pressure monitoring during arthrographic evaluation of painful hip prostheses. *American Journal of Roentgenology*, 141(5):885–889, 1983.

[79] N. J. Goddard and P. T. Gosling. Intra-articular fluid pressure and pain in osteoarthritis of the hip. *J Bone Joint Surg Br*, 70(1):52–5, 1988.

[80] J. Vegter. The influence of joint posture on intraarticular pressure - a study of transient synovitis and perthes-disease. *Journal of Bone and Joint Surgery-British Volume*, 69(1):71–74, 1987.

[81] G. C. Lloyd-Roberts. The role of capsular changes in osteoarthritis of the hip joint. *Journal of Bone and Joint Surgery-British Volume*, 35(4):627, 1953.

[82] S. Tarasevicius, U. Kesteris, A. Gelmanas, A. Smailys, and H. Wingstrand. Intracapsular pressure and elasticity of the hip joint capsule in osteoarthritis. *Journal of Arthroplasty*, 22(4):596–600, 2007.

[83] R. Soto-Hall, L.H. Johnson, and R.A. Johnson. Variations in the intra-articular pressure of the hip joint in injury and disease a probable factor in avascular necrosis. *The Journal of Bone and Joint Surgery (American)*, 46(3):509–516, 1964.

[84] P. P. Anthony, G. A. Gie, C. R. Howie, and R. S. M. Ling. Localized endosteal bone lysis in relation to the femoral components of cemented total hip arthroplasties. *Journal of Bone and Joint Surgery-British Volume*, 72(6):971–979, 1990.

[85] G. Bergmann, G. Deuretzbacher, M. Heller, F. Graichen, A. Rohlmann, J. Strauss, and G. N. Duda. Hip contact forces and gait patterns from routine activities. *Journal of Biomechanics*, 34(7):859–871, 2001.

[86] MO Heller, G. Bergmann, J.P. Kassi, L. Claes, NP Haas, and GN Duda. Determination of muscle loading at the hip joint for use in pre-clinical testing. *Journal of biomechanics*, 38(5):1155–1163, 2005.

[87] H. Iwaki, G. Scott, and M. A. R. Freeman. The natural history and significance of radiolucent lines at a cemented fomoral interface. *Journal of Bone and Joint Surgery. British Volume*, 84B(4):550–555, 2002.

[88] J.L. Howard, A.J. Hui, R.B. Bourne, R.W. McCalden, S.J. MacDonald, and C.H. Rorabeck. A quantitative analysis of bone support comparing cementless tapered and distal fixation total hip replacements1. *The Journal of arthroplasty*, 19(3):266–273, 2004.

[89] Y. Park, H. Shin, D. Choi, C. Albert, and Y. S. Yoon. Primary stability of cementless stem in tha improved with reduced interfacial gaps. *Journal of Biomechanical Engineering.Transactions of the Asme*, 130(2), 2008.

[90] S. Glyn-Jones, K. Polgar, J. Hicks, DW Murray, and HS Gill. Rsa-measured inducible micromotion and interface modeling with finite element methods. *Clinical Orthopaedics and Related Research*, 448:98, 2006.

[91] M.R. Abdul-Kadir and N. Kamsah. Interface micromotion of cementless hip stems in simulated hip arthroplasty. *American Journal of Applied Sciences*, pages 1682–1689, 2009.

[92] D.W. Burke, D.O. O'Connor, E.B. Zalenski, M. Jasty, and W.H. Harris. Micromotion of cemented and uncemented femoral components. *Journal of Bone and Joint Surgery-British Volume*, 73(1):33, 1991.

[93] M. K. Harman, A. Toni, L. Cristofolini, and M. Viceconti. Initial stability of uncemented hip stems: an in-vitro protocol to measure torsional interface motion. *Medical engineering & physics*, 17(3):163–171, 1995.

[94] W. S. S Jee. Integrated bone tissue physiology: anatomy and physiology. *Bone mechanics handbook*, pages 1–1, 2001.

[95] P. J. Prendergast, R. Huiskes, and K. Soballe. Biophysical stimuli on cells during tissue differentiation at implant interfaces. *Journal of Biomechanics*, 30(6):539–548, 1997.

[96] M. Brookes. *The blood supply of bone*. Butterworth & Co, 1971.

[97] M. A. Churchill, M. Brookes, and J. D. Spencer. The blood supply of the greater trochanter. *J Bone Joint Surg Br*, 74(2):272–4, 1992.

[98] G. Bridgeman and M. Brookes. Blood supply to the human femoral diaphysis in youth and senescence. *J Anat*, 188 (Pt 3):611–21, 1996.

[99] F. W. Rhinelander. Circulation in bone. *The biochemistry and physiology of bone*, 2:1–77, 1972.

[100] D.R. Carter. Mechanical loading history and skeletal biology. *Journal of biomechanics*, 20(11-12):1095–1109, 1987.

[101] Y.P. Arramon and E. A. Nauman. The intrinsic permeability of cancellous bone. In S.C Cowin, editor, *Bone mechanics*. Informa Healthcare, New York, second edition, 2000.

[102] S. C. Cowin. Bone poroelasticity. In S.C Cowin, editor, *Bone biomechanics handbook*, pages 23–1 23–31. CRC Press, 2nd edition, 2000.

[103] JD Bryant, T. David, PH Gaskell, S. King, and G. Lond. Rheology of bovine bone marrow. *ARCHIVE: Proceedings of the Institution of Mechanical Engineers, Part H: Journal of Engineering in Medicine 1989-1996 (vols 203-210)*, 203(28):71–75, 1989.

[104] S. C. Cowin. The plumbing of long bones. In M. Cerrolaza, G. MartÃŋnez, M. DoblarÃľ, and B. Calvo, editors, *Computational bioengineering: current trends and applications*, pages 45–67. Imperial College Press, 2004.

[105] D. Zhang, S. Weinbaum, and S. C. Cowin. Estimates of the peak pressures in bone pore water. *Journal of Biomechanical Engineering.Transactions of the Asme*, 120(6):697–703, 1998.

[106] M. J. Grimm and J. L. Williams. Measurements of permeability in human calcaneal trabecular bone. *J Biomech*, 30(7):743–5, 1997.

[107] M. S. Thompson, G. Flivik, R. Juliusson, A. Odgaard, and L. Ryd. A comparison of structural and mechanical properties in cancellous bone from the femoral head and acetabulum. *Proceedings of the Institution of Mechanical Engineers. Part H, Journal of Engineering in Medicine*, 218(H6):425–429, 2004.

[108] E. A. Nauman, K. E. Fong, and T. M. Keaveny. Dependence of intertrabecular permeability on flow direction and anatomic site. *Ann Biomed Eng*, 27(4):517–24, 1999.

[109] PW Hui, PC Leung, and A. Sher. Fluid conductance of cancellous bone graft as a predictor for graft-host interface healing. *Journal of biomechanics*, 29(1):123–132, 1996.

[110] S.S. Kohles, J.B. Roberts, M.L. Upton, C.G. Wilson, L.J. Bonassar, and A.L. Schlichting. Direct perfusion measurements of cancellous bone anisotropic permeability* 1. *Journal of Biomechanics*, 34(9):1197–1202, 2001.

[111] M. Pakula, F. Padilla, P. Laugier, and M. Kaczmarek. Application of biot's theory to ultrasonic characterization of human cancellous bones: Determination of structural, material, and mechanical properties. *Journal of the Acoustical Society of America*, 123(4):2415–2423, 2008.

[112] G. Li, J. T. Bronk, K. N. An, and P. J. Kelly. Permeability of cortical bone of canine tibiae. *Microvascular Research*, 34(3):302–310, 1987.

[113] T.H. Smit, J.M. Huyghe, and S.C. Cowin. Estimation of the poroelastic parameters of cortical bone. *Journal of biomechanics*, 35(6):829–835, 2002.

[114] P.A. Simkin, C.C. Pickerell, and W.J. Wallis. Hydraulic resistance in bones of the canine shoulder. *Journal of biomechanics*, 18(9):657–659, 1985.

[115] Fluent manual. Section 18.4.1. ansys inc, canonsburg, pa. 2009.

[116] P. J. Kelly. Anatomy, physiology, and pathology of the blood supply of bones. *J Bone Joint Surg Am*, 50(4):766–83, 1968.

[117] A. McEvoy, M. Jeyam, G. Ferrier, C. E. Evans, and J. G. Andrew. Synergistic effect of particles and cyclic pressure on cytokine production in human monocyte/macrophages: proposed role in periprosthetic osteolysis. *Bone*, 30(1):171–7, 2002.

[118] S.J. Morsi and A.J. Alexander. An investigation of particle trajectories in two-phase flow systems. *Journal of Fluid Mechanics*, 55(2):193–208, 1972.

[119] J. P. Shorez, T. S. Harding, P. J. Atkinson, and N. Walter. Alteration of the amount and morphology of wear particles by the addition of loading profile transitions during artificial hip wear testing. *Proceedings of the Institution of Mechanical Engineers Part H-Journal of Engineering in Medicine*, 222(H6):865–875, 2008.

[120] D.A. Wolfe and M. Hollander. Nonparametric statistical methods. *Nonparametric statistical methods*, 1973.

[121] V.L. Fornasier and H.U. Cameron. The femoral stem/cement interface in total hip replacement. *Clinical Orthopaedics and Related Research*, 116:248, 1976.

[122] J. D. Bobyn, J. J. Jacobs, M. Tanzer, R. M. Urban, R. Aribindi, D. R. Sumner, T. M. Turner, and C. E. Brooks. The susceptibility of smooth implant surfaces to periimplant fibrosis and migration of polyethylene wear debris. *Clinical Orthopaedics and Related Research*, (311):21–39, 1995.

[123] R. D. Mulroy Jr and W. H. Harris. The effect of improved cementing techniques on component loosening in total hip replacement. an 11-year radiographic review. *Journal of Bone and Joint Surgery-British Volume*, 72(5):757, 1990.

[124] K. Hirakawa, T. W. Bauer, B. N. Stulberg, A. H. Wilde, and M. Secic. Characterization and comparison of wear debris from failed total hip implants of different types. *Journal of Bone and Joint Surgery-American Volume*, 78A(8):1235–1243, 1996.

[125] J. Fisher, P. Firkins, EA Reeves, JL Hailey, and GH Isaac. The influence of scratches to metallic counterfaces on the wear of ultra-high molecular weight polyethylene. *Proceedings of the Institution of Mechanical Engineers, Part H: Journal of Engineering in Medicine*, 209(4):263–264, 1995.

[126] M. Jasty, CR Bragdon, K. Lee, A. Hanson, and WH Harris. Surface damage to cobalt-chrome femoral head prostheses. *Journal of Bone and Joint Surgery-British Volume*, 76(1):73, 1994.

[127] PSM Barbour, DC Barton, and J. Fisher. The influence of contact stress on the wear of uhmwpe for total replacement hip prostheses. *Wear*, 181:250–257, 1995.

[128] J. P. Herzig, D.M. Leclerc, and P. L. Goff. Flow of suspensions through porous medi Ůapplication to deep filtration. *Industrial and Engineering Chemistry*, 62(5):8–35, 1970.

[129] K.J. Margevicius, T.W. Bauer, J.T. McMahon, S.A. Brown, K. Merritt, et al. Isolation and characterization of debris in membranes around total joint prostheses. *The Journal of bone and joint surgery. American volume*, 76(11):1664, 1994.

[130] L. M. Kwong, M. Jasty, R. D. Mulroy, W. J. Maloney, C. Bragdon, and W. H. Harris. The histology of the radiolucent line. *Journal of Bone and Joint Surgery-British Volume*, 74(1):67, 1992.

[131] F. Civan, R. M. Knapp, and H. A. Ohen. Alternation of permeability by fine particle processes. *Journal of Petroleum Science and Engineering*, 3:65–79, 1989.